UNIVERSITY OF OKLAHOMA

GRADUATE COLLEGE

Split ends (*spen*), A TRANSCRIPTIONAL REGULATOR, INHIBITS MYOSIN ACTIVITY TO REGULATE NEURONAL REMODELING DURING METAMORPHOSIS

A DISSERTATION

SUBMITTED TO THE GRADUATE FACULTY

in partial fulfillment of the requirements for the

Degree of

DOCTOR OF PHILOSOPHY

By

TAO ZHAO
Norman, Oklahoma
2011

Split ends (*spen*), A TRANSCRIPTIONAL REGULATOR, INHIBITS MYOSIN ACTIVITY TO REGULATE NEURONAL REMODELING DURING METAMORPHOSIS

A DISSERTATION APPROVED FOR THE
DEPARTMENT OF ZOOLOGY

BY

Dr. Randy Hewes, Chair

Dr. David Durica

Dr. David McCauley

Dr. Richard Broughton

Dr. Leonidas Tsiokas

To my dear mother. May her soul rest in perfect peace.

ACKNOWLEDGEMENTS

I would like to thank all people who have helped and inspired me during my doctoral study.

I am heartily thankful to my supervisor, Randy Hewes, for his generous encouragement, guidance and support throughout my study at the University of Oklahoma. He is like my older brother and a wise and reverenced friend, always thinking the best for me, giving me help whenever needed. His patience and optimism have made my research life a smooth and pleasant experience.

Dr. Durica, Dr. McCauley, Dr. Broughton, and Dr. Tsiokas, deserve special thanks as my thesis committee members and advisors, for all the suggestions and comments during my study. I owe Kathleen McAdams and Elizabeth Moran, for their selfless help in my research.

My deepest gratitude goes to my family for their unflagging love and support throughout my life. My parents have spared no effort to help take care of my baby and do the housework. Tingting, my wife, my best friend and partner, has been sharing my every happiness and sadness. Her dedication, love, and persistent confidence in me have fueled me to chase my goal. Finally, I really want to say thank you to my little Sophia, as you have brought so much joy to my life.

TABLE OF CONTENTS

LIST OF FIGURES

LIST OF TABLES

ABSTRACT

Split ends (*spen*), a transcriptional regulator, inhibits myosin activity to regulate neuronal remodeling during metamorphosis

By Tao Zhao

Animal neurons dynamically change their morphologies in response to steroid hormone signaling to adapt to changing environments. The molecular mechanisms underlying animal neuronal remodeling, however, remain largely unknown. Metamorphosis is an important developmental stage in insects when crawling and feeding larvae transform into reproductive and flying adults. During this period, many insect larval neurons undergo dramatic morphological and functional alterations. These neuronal changes are regulated by a arthropod-specific steroid hormone, 20-hydroxyecdysone (ecdysone). Research on the metamorphic remodeling of insect neurons, has provided insights into the general neuronal remodeling process. During the early stage of metamorphosis, the larval neurons prune their projections and then grow out adult-specific neurites. A group of *Drosophila melanogaster* (fruit fly) neuroendocrine cells, the crustacean cardioactive peptide (CCAP) neurons, experiences metamorphic remodeling, and I used these neurons to dissect the molecular mechanisms controlling this process. The CCAP neurons mainly produce two neuropeptides, CCAP and bursicon, to control insect molting-related behaviors, ecdysis and wing expansion. Functional disruption of the CCAP neuron remodeling leads to defective wing expansion in adults. In a genetic screen, thousands of genes were mis- or overexpressed in the CCAP neurons. The genes that produced strong wing expansion defects were identified. Fourteen of the

identified genes specifically inhibited the outgrowth of adult-specific neurites during metamorphic remodeling. One of these, *split ends* (*spen*) was selected to identify the molecular pathways affected by its overexpression. I performed a deficiency modifier screen to identify mutations that modify the outgrowth defects induced by *spen*. A mutation of *Mbs*, the gene encoding the Myosin binding subunit, moderately suppressed the outgrowth defects. Since *Mbs* negatively regulates myosin II activity, the results suggested that *spen* overexpressin suppressed myosin II activity. Another myosin-modulating signaling pathway, Rac1-PAK, was also tested to confirm the observations. The Rac1-PAK signaling pathway positively regulates myosin II function, and this pathway suppressed the neurite outgrowth defects induced by *spen* overexpression. Furthermore, down-regulation of *spen* activity strongly rescued the wing expansion and neurite growth defects resulting from disrupted Rac1-PAK signaling. These results strongly support a model in which *spen* functions antagonistically with myosin II to regulate neuronal outgrowth during metamorphosis.

CHAPTER 1

Insect metamorphic neuronal remodeling: the roles of ecdysone signaling and the cytoskeleton system

Neurons dynamically change their morphologies and activities

After terminal differentiation, neurons remain plastic and may undergo dynamic changes in their morphologies to accommodate new functions or activities. For example, in the brains of adult male vertebrates, gonadal hormones, specifically androgens, modify the synapses of mature neurons to masculinize the nervous system for certain behaviors (COOKE *et al.* 1998). Learning and memory formation are also accompanied by the rewiring of neurite projections and synapses of cortical neurons to increase memory storage capacity (CHKLOVSKII *et al.* 2004; HOLTMAAT and SVOBODA 2009).

Besides sexual differentiation and learning and memory, a variety of external and internal factors also contribute to the structural rearrangement of neurons, or "neuronal remodeling". These factors include brain injury (KADISH and VAN GROEN 2002; STEWARD 1982), changes in temperature (ZHONG and WU 2004), puberty (ZEHR *et al.* 2006), and chronic stress (SOUSA *et al.* 2008). Steroid hormones can perform a critical role in the regulation of neuronal morphological changes. For instance, low doses of estrogen significantly diminish axonal spouting after entorhinal cortex lesions

in the mouse (KADISH and VAN GROEN 2002). In other cases, the effects of steroid hormone can be transient and rapid. For example, estradiol treatement of cultured cortical neurons rapidly and transiently increases spine density, and this is followed by temporary formation of silent synapses (SRIVASTAVA *et al.* 2008). In each of these systems, the relevant molecular machinery downstream of steroid hormones in remodeling remains largely unknown.

Neuronal remodeling of insect neurons during metamorphosis

The remodeling of the neurons of holometabolous insects has provided an excellent model to study steroid-controlled neuronal remodeling. These events occur during a specific developmental stage called "metamorphosis", when the vermiform, feeding larvae transform into walking, flying, and reproductive adults. James Truman and others have spent many years investigating the metamorphic changes of the larval neurons in *Manduca sexta* and *Drosophila melanogaster* (LEVINE and TRUMAN 1982; TRUMAN 1984; TRUMAN 1992b; TRUMAN 1996). Unnecessary larval neurons are deleted through programmed cell death (CHOI *et al.* 2006; TRUMAN 1984; TRUMAN 1992b; TRUMAN 1996; TRUMAN *et al.* 1994; WEEKS 2003), whereas other larval neurons, undergo metamorphic remodeling. Typically, the later group of larval neurons displays two phases of morphological changes: initial selective pruning of larval neurites, followed by outgrowth and elaboration of a morphologically and functionally distinct adult-specific arbor. The adult-specific projection pattern, which is often coupled with altered physiological characteristics, subserves functions that are tailored for the adult.

All the changes observed during neuronal metamorphosis appear to be coordinated by changes in the circulating titer of the insect steroid molting hormone, 20-hydroxyecdysone (referred to as ecdysone) (THUMMEL 2001). The ecdysone level increases and decreases (a pulse) to control the initiation of metamorphosis and the transitions between successive metamorphic stages. Ecdysone signaling executes its functions through binding to and activating its nuclear receptor, ecdysone receptor (EcR). Together with its dimerization partner, ultraspiracle (USP), the activated EcR then binds to the promoters of downstream genes and triggers transcriptional changes, yielding different physiological events. Numerous studies have demonstrated that ecdysone signaling plays an essential role in metamorphic remodeling. Nevertheless, the downstream pathways affected by ecdysone signaling, as well as the connections between the ecdysone signaling pathway and other pathways involved in neuronal remodeling, remain largely unknown.

Ecdysone signaling regulates metamorphic neuronal remodeling

The holometabolous insect life cycle comprises four stages: embryo, larva, pupa, and adult. After hatching from the eggs, *D. melanogaster* embryos develop for around 24 hours and become first instar larvae. Then under the regulation of ecdysone signaling, the larva experiences two molts to enter into the second instar larva and the third instar larva, respectivley. At the end of the final larval stage, a pulse of ecdysone initiates metamorphosis. The larva stops eating and crawls around until giving itself to the substrate and becoming an immobile white prepupa. As the white prepupa darkens its body color into brownish, the ecdysone titer decreases to a trough level (TALBOT *et*

al. 1993; THUMMEL 2001; TRUMAN *et al.* 1994). During the prepupal stage, many larval tissues/organs undergo programmed cell death, e.g., larval midgut. Then, there is another small ecdysone pulse, which triggers eversion of head structures and elongation of the wings and legs. These morphogenetic events are produced in part by stereotyped ecdysis behaviors, also called "head eversion". After head eversion, the animal is a pupa that begins the development of adult-specific tissues and organs until the completion of metamorphosis. During pupal development, the ecdysone titer displays the largest and most prolonged surge and then falls at the end of metamorphosis. After metamorphosis, the new adult emerges from the pupal case, crawls around, and then perches and initiates wing expansion behaviors that expand the folded, thick wing tissues into thin, membrane-like wings.

The external cuticle, or exoskeleton, does not increase in size during a given stage of the life cycle. During every transition between two developmental stages, insects experience "molting", in which they form a new, larger or differently shaped cuticle inside the old one and then shed the old cuticle. The behaviors of periodic shedding of the old cuticle are called "ecdysis". For example, aroung 12 hours after pupariation, the fly prepupa undergoes "pupal ecdysis", during which it sheds the larval cutile, everts its head structure, and expands its wings and legs (THUMMEL 2001). Ecdysis is coordinated by the declining ecdysone titer at the end of each developmental stage, and it acts through a hierarchical cascade of neuropeptides and peptide hormones to trigger the behaviors (BAKER *et al.* 1999; CLARK *et al.* 2004a; ZHAO *et al.* 2008). The current model of the hierarchy includes the activation of the endocrine inka cells, which produce ecdysis-triggering hormone (ETH). ETH stimulates the secretion of additional

peptide hormones, including eclosion hormone (EH) and crustacean cardioactive peptide (CCAP). Together with other neuropeptides, these peptide hormones regulate ecdysis behaviors (BAKER *et al.* 1999; CLARK *et al.* 2004a; KIM *et al.* 2006). Disruptions in this hormonal regulation may lead to ecdysis defects. For example, flies without the CCAP-producing cells often failed to complete the pupal ecdysis, showing the phenotype of defective head eversion, (PARK *et al.* 2003). The defective pupae in these mutants often complete metamorphosis, but with partially or completely uneverted head and shortened legs (PARK *et al.* 2003; ZHAO *et al.* 2008).

Ecdysone signaling plays a critical role in controlling insect development through interacting with other hormonal signaling pathways. In addition to the dramatic titer changes during metamorphosis, ecdysone level boosts during mid-embryonic stage and each molting, indicating the actions of ecdysone throughout insect development. Much of the knowledge regarding ecdysone signaling pathway was obtained through studies on *Drosophila melanogaster* (BAKER *et al.* 1999; EWER *et al.* 1997; KOZLOVA and THUMMEL 2003; THUMMEL 2001), a powerful model organism for genetic and molecular analysis. There exist three isoforms of EcR in Drosophila genome, that are produced through alternative splicing: EcR-A, B1 and B2 (BENDER *et al.* 1997). These isoforms share a C- terminal portion, which includes the ligand- and DNA-binding domains, but they vary in the N-terminal sequences (BENDER *et al.* 1997). Without ligand binding, the nuclear receptor heterodimers function as transcriptional repressors, whereas the interaction of these receptors with ecdysone activates a genetic hierarchy (BROWN *et al.* 2006). The three EcR isoforms can perform different functions and contribute to the stage- and tissue-specific actions of ecdysone signaling. Mutations in

the common region of EcR are embryonic lethal while EcR-B1 mutants die during metamorphosis (BENDER *et al.* 1997). Temperature-sensitive rescue with wild type cDNAs of the EcR mutants confirmed the necessity of ecdysone signaling for hatching, molting, and initiation of metamorphosis (LI and BENDER 2000).

The EcR isoforms are expressed differentially in the central nervous system (CNS) during metamorphosis to coordinate neuronal remodeling. Truman *et al.* (TRUMAN *et al.* 1994) studied the expression of EcR-A and B1 in the Drosophila CNS using specific antibodies against the two receptors. Most larval neurons display high EcR-B1 expression at the onset of metamorphosis, and EcR-A expression predominates during the pupa-adult transformation in later metamorphosis. Heat-induced activation at the time of head eversion of either EcR-B isoforms can give rise to developmental arrest, indicating importance of timing and isoform in mediating EcR functions (SCHUBIGER *et al.* 2003). This is also consistent with the hypothesis that the EcR-B isoforms are involved in the pruning of larval neurites, which occurs early during metamorphosis, whereas EcR-A is more important for the growth of adult-specific projections at the later stages of metamorphosis (ROY *et al.* 2007; SCHUBIGER *et al.* 2003; SCHUBIGER *et al.* 1998; TRUMAN *et al.* 1994).

Genetic studies in Drosophila have added to our understanding of the roles of the different EcR isoforms in remodeling. Schubiger *et al.* (1998) studied flies carrying a null mutation in the common region shared by *EcR-B1* and -*B2*. Although most of the flies died during larval development, a small proportion survived until the prepupal/pupal transition. These *EcR-B* mutants displayed defective metamorphic

neuronal remodeling of a set of neuroendocrine cell, the Tv neurons, shown as retention of the larval projections, which are normally removed during the pruning process (SCHUBIGER *et al.* 1998). Further evidence came from a study of the γ neurons in the Drosophila mushroom body (LEE *et al.* 2000). *EcR-B1* is specifically expressed in the mushroom body γ neurons rather the α′/β′ neurons. Single γ neurons or a small subset of γ neurons containing null mutations in either *EcR-B1* or *usp* exhibited defects in pruning, shown as preserved larval projections throughout metamorphosis. Ecdysone signaling can also be disrupted by expression of dominant negative (DN) forms of EcR, which encode either a mutated form or a truncated form of EcR that can compete with wild type EcR at gene promoters (CHERBAS *et al.* 2003). Two commonly used EcR DN mutants EcR-F645A and EcR-W650A have point mutations in the conserved C-terminal helix of the ligand-binding domain of EcR (HU *et al.* 2003). EcR-F645A produces a mutated EcR with normal ligand- and DNA-binding capability but no transcriptional activation, whereas EcR-W650A can bind DNA but not ecdysone (HU *et al.* 2003). Kuo *et al.* (2005) used the two DN forms of EcR-B1 (EcR-B1-F645A and EcR-B1-W650A) to study the remodeling of a kind of peripheral sensory neuron, the class IV da (C4da) neurons. They found expression of either DN inhibited the normal pruning of the C4da neurons, *usp* mutations in the C4da neurons also showed similar defective pruning phenotypes.

During later metamorphosis, expression of the EcR dominant negatives can block normal growth of the adult-specific neurites. Brown *et al.* (2006) compared the consequences of expressing various dominant negative mutants of the three EcR isoforms and RNA interference (RNAi) constructs that target the common region in the

Tv neurons, a group of neuropeptide-producing cells. Four dominant negative proteins were used: EcR-B1-F645A and W650A, EcR-B2-W650A, and EcR-A-W650A. All these dominant negatives produced similar pruning defects when expressed in the Tv neurons, whereas only EcR-A-W650A and EcR-B1-W650A strongly inhibited the growth of the adult-specific neurites. Closer examination revealed that filopodia, which were associated with the initiation of neurite outgrowth, were strongly inhibited by the EcR-A- and EcR-B1-W650A mutants. Roy *et al.* (2007) obtained similar results after expressing EcR-B1-W650A in the serotonergic neuron in the Drosophila olfactory system. They also found reduced pruning and retention of larval neurite morphology into adulthood.

A few genes involved in regulation of ecdysone signaling have been implicated in metamorphic neuronal remodeling. For example, *Krüppel homolog 1* (*Kr-h1*) null mutants displayed severe ecdysone signaling-relevant developmental defects during prepupal/pupal transition, including pupal molting and programmed cell death in the larval salivary glands (PECASSE *et al.* 2000). The *Kr-h1* mutation also altered expression of several ecdysone primary-response genes, and *Kr-h1* expression itself was upregulated five fold by ecdysone in cultured salivary glands from wild-type larvae (BECK *et al.* 2005; PECASSE *et al.* 2000). Tzumin Lee's lab found that *Kr-h1* is expressed in the mushroom body neurons, but the expression level is precipitously reduced during the re-elaboration stage of remodeling (SHI *et al.* 2007). Overexpression of *Kr-h1* in the mushroom body neurons during the outgrowth of the adult-specific neurite arbor led to reduced outgrowth, while knockdown of *Kr-h1* expression can enhance the morphogenesis that is otherwise delayed by defective TGF-β signaling (SHI

et al. 2007). These observations indicate that *Kr-h1* is a negative regulator of neuronal morphogenesis (HEWES 2008). This lab also discovered that Baboon/dSmad2 TGF-β signaling regulates ecdysone signaling during metamorphosis to control neuronal remodeling (ZHENG *et al.* 2003). Mutations in *Baboon*, which encodes a *Drosophila* TGF-β/activin type I receptor, and in *dSmad2*, the downstream transcriptional effector of the signaling pathway, both inhibited the metamorphic pruning. Moreover, EcR-B1 expression depends on Baboon/dSmad2 signaling, and expression of EcR-B1 significantly restored the remodeling defects induced by the mutants. Therefore Baboon/dSmad2 signaling regulates neuronal remodeling at least in part by controlling EcR-B1 expression. Hoopfer *et al.* (2008) also showed that the gene *boule*, which encodes an RNA-binding protein, is downregulated during metamorphosis by ecdysone signaling in mushroom body γ neurons. Like *Kr-h1*, forced expression of *boule* in the γ neurons resulted in pruning defects. Thus, *boule* is a negative regulator of neuronal pruning during metamorphosis. *Broad Complex* (*BRC*) is among one of the primary response genes of ecdysone signaling. Consoulas *et al.* (CONSOULAS *et al.* 2005) showed that *BRC* is required by the outgrowth of the dendrites of Drosophila flight motoneurons MN1-MN4 during metamorphic remodeling. These reports all provide more insights into the control of metamorphic neuronal remodeling by ecdysone signaling.

Other cellular pathways involved in metamorphic remodeling

A lot of work has been dedicated to identifying additional molecular and cellular processes involved in neuronal pruning. These pruning-regulatory factors include the

ubiquitin-proteasome system (UPS) (KUO *et al.* 2005; KUO *et al.* 2006; LEE *et al.* 2009; WATTS *et al.* 2003), extracellular matrix metalloproteases (KUO *et al.* 2005), glial engulfment (AWASAKI and ITO 2004; AWASAKI *et al.* 2006; WATTS *et al.* 2004), and cell adhesion molecules (HEBBAR and FERNANDES 2005).

In contrast to the pruning process, only a few studies have been reported that explore the molecular mechanisms underlying the growth of adult-specific neurites. Some reports indicate that metamorphic pruning and neuronal electrical activity are both important for the establishment of the adult arbor during metamorphosis (HEBBAR and FERNANDES 2004; HEBBAR and FERNANDES 2005; WILLIAMS and TRUMAN 2004). Excepting this, our knowledge pertaining to the control of growth of adult arbors is limited to ecdysone signaling and some ecdysone-response genes (BROWN *et al.* 2006; CONSOULAS *et al.* 2005; ROY *et al.* 2007). Much more work is needed to determine how the ecdysone signaling pathway interacts with other signaling pathways to orchestrate the transition from pruning to outgrowth, and to guide the formation of a stereotyped adult-specific neuritic pattern.

Small Rho GTPases regulate neuronal growth through effects on the cytoskeleton

After the completion of mitosis, neurons begin to send out axons and dendrites in a stereotypic way, guided by a wide array of external and internal, long- and short-range cues. These morphogenetic events depend on changes in the cytoskeleton, which include important roles for actin, myosin protein complexes, and their interactions with the plasma membrane (LUO 2002). Neurite formation includes four aspects: initiation, growth, guidance, and branching. Initially, neurons send out many minor processes,

one of which will display rapid and persistent growth to become an axon. Bradke *et al.* (1999) took advantage of retrospective video microscopy and realized that the processes destined to develop into axons show a significant increase in actin dynamics and instability. Furthermore, they noticed that destabilization of the actin cytoskeleton of a single growth cone could convert an otherwise minor neurite into an axon-like process.

These findings are consistent with the consensus view of axonal growth or elongation as a dynamic and well-balanced process. Growing neurons send out preliminary buds to form extending axons or dendrites, at the ends of which are growth cones. Growth cones contain two types of important cellular structures, veil-like lamellipodia and several finger-like filopodia on top of the lamellipodia. Filopodia are composed of bundled F-actin fibers whereas Lamellipodia contain a cross-linked actin meshwork (LUO 2002). At the leading edge of a growth cone, actin monomers are polymerized into F-actin bundles. At the same time, in filopodia and lamellipodia there exists a constant retrograde flow of F-actins (LUO 2002). Therefore, growth cones display both assembly of actin monomers and back flow of F-actin filaments, which maintains the dynamic balance of actin turnover and ensures appropriate growth orientation (LUO 2002).

It is the myosin complex that provides motility to the backflow of F-actin. Treatment of myosin inhibitor on the growth cone significantly slowed the backflow (LIN *et al.* 1996). Through interactions with guidance cues, including attractant and repellent signals, the rate of actin depolymerization in the filopodia slows down to lead growth cone advancement in the correct direction (HUBER *et al.* 2003). Filopodia play an essential role in this guidance of axon growth. In the current model, filopodia

respond to attractive or repellant cues by showing either enhanced stabilization and expansion, or selective destabilization (LUO 2002). Therefore, the asymmetric presence of negative or positive cues at different points on a growth cone can determine the growth or elongation direction. Finally, axon branching is also closely tied to the cytoskeleton. Two types of axon branching, splitting of a growth cone and emerging of a new branch from the trunk of an axon, both depend on proper cytoskeleton dynamics. The latter is induced by local destabilization of the microtubule and actin cytoskeleton, followed by extension of a single filopodium (LUO 2002). Splitting of growth cone occurs when a myosin inhibitor is applied to the middle of the growth cone, actin bundles are disrupted at that location, and the growth cone is split into two, which then continue to grow independently (ZHOU *et al.* 2002).

Small Rho GTPases play essential roles in the morphogenesis of neurites. These small molecules (~200 amino acids long) belong to the Rho subfamily and are critical regulators of the myosin-actin cytoskeleton. Rho GTPases have two functional states: a GDP-bound inactive state and a GTP-bound active state (LUO 2000; LUO 2002). These molecules switch between the two states, which are controlled by the actions of two kinds of molecules: Guanine nucleotide exchange factors (GEFs) and GTPase activating proteins (GAPs). GEFs switch the GTPase from a GDP-bound state to a GTP-bound state, while GAPs do the reverse.

The best-studied Rho GTPases are Rac1, Cdc42, and Rho1. These three molecules regulate the cytoskeleton by affecting actin polymerization and myosin activity, both of which are essential for neuronal growth, pathfinding, and plasticity (HUBER *et al.* 2003; LUO 2002) (Figure 1-1). Rac1 and Cdc42 can both promote actin

polymerization through activation of target protein p21-activated kinase (PAK), via promoting its autophosphorylation (GOVEK *et al.* 2005). PAK then activates Lin-11, Isl-1, and Mec-3 kinase (LIMK), which inhibits Colifin, an actin-depolymerizing protein (GOVEK *et al.* 2005; NG and LUO 2004). Cdc42 can also activate Wiskott-Aldrich syndrome protein (WASP), which stimulates actin polymerization by interacting with the protein complex of actin-related proteins 2 and 3 (GOVEK *et al.* 2005). Therefore, Rac1 and Cdc42 both promote actin polymerization using partially independent pathways. Mutations in Rac1 and expression of Rac1 dominant negative, both disrupt axonal growth, pathfinding, and branching (NG *et al.* 2002). PAK mutations also showed similar neuronal defects as Rac1 mutations (NIKOLIC 2008). These mutant assays provide strong support for the roles played by Rac1-PAK signaling pathway in modulating neuronal growth.

In mammals, non-muscle myosin II, a motor component of the cytoskeleton, controls the bundling and flowing of F-actin, thereby modulating the growth of neurons (BROWN and BRIDGMAN 2004). Non-muscle myosin II is a hexamer composed of two myosin heavy chains (MHC), two myosin light chains (MLC), and two myosin regulatory light chains (MRLC) (KORN and HAMMER 1988) (Figure 1-1). Phosphorylation and dephosphorylation are the two key events in regulation of the activity of non-muscle myosin II. Phosphorylation of MRLC by the myosin regulatory light chain kinase (MLCK) enhances the activity of the myosin molecule, whereas dephosphorylation of MRLC by the myosin light chain phosphotase (MLCP) antagonizes the effects of MLCK (ALESSI *et al.* 1992). MLCP protein is a heterotrimer consisting of a catalytic subunit (PP1cδ), a 20-kDa protein, and the myosin binding

subunit (MBS) that targets MLCP to its substrates of MRLC for dephosphorylation (HARTSHORNE *et al.* 1998a) (Figure 1-1). The *Drosophila* genome also contains the genes encoding each of these proteins, and they show similar interactions. For example, like its mammal counterparts, *Drosophila* myosin binding subunit, encoded by the gene *Mbs*, regulates F-actin activity by mediating dephosphorylation activity through interactions with the fly MLCP (MIZUNO *et al.* 2002). The eye disc of *Mbs* mutants showed increased levels of phosphorylated fly MRLC protein, which is encoded by gene *spaghetti squash* (*sqh*), whereas reintroduction of wild type *Mbs* expression normalized MRLC phosphorylation (LEE and TREISMAN 2004a). In addition, expression of a *sqh* allele containing mutations at the conserved phosphorylation sites strongly suppressed the defects induced by *Mbs* mutation, strongly indicating that *Mbs* exerts its function through regulating the phosphorylation of MRLC (LEE and TREISMAN 2004a).

The activity of non-muscle myosin II is also tightly regulated by the Rho GTPases (Figure 1-1). Rho1 transmits cellular signals through phosphorylation and activation of the downstream protein Rho-Kinase (ROCk), thereby mediating further phosphorylation events (AMANO *et al.* 1996). ROCK regulates the activity of non-muscle myosin II mainly through two mechanisms. First, the ROCK protein directly phosphorylates MRLC. In *Drosophila*, genetic interactions and *in vitro* co-immunoprecipitation assay both supported this conclusion (MIZUNO *et al.* 1999; WINTER *et al.* 2001). On the other hand, ROCK can phosphorylate MBS to inhibit the dephosphorylation effects of MLCP, thereby indirectly activating MRLC (KAWANO *et al.* 1999; KIMURA *et al.* 1996a; MIZUNO *et al.* 1999). Genetic interactions observed in

fly mushroom body neurons supported these results (LEE and TREISMAN 2004a; TAN *et al.* 2003).

PAK can also affect myosin II activity. PAK can either promote myosin activity through direct phosphorylation of MRLC, or inhibit myosin function through phosphorylation of MLCK, thereby preventing phosphorylation of MRLC (GOVEK *et al.* 2005; LUO 2000) (Figure 1-1). Therefore, Rac1 may regulate myosin II activity through its effector PAK.

To date, there has been little or no work on the role of small Rho GTPases in regulating metamorphic neuronal remodeling through affects on the cytoskeleton dynamics. If they are important regulators of remodeling, how does ecdysone interact with these small GTPases? In this work, I have begun addressing these questions, and I found that at least two small Rho GTPases, Rac1 and Rho1, are both involved in the outgrowth of the adult-specific neurites during metamorphosis (Chapter 3).

The CCAP/bursicon neurons control ecdysis and wing expansion behavior and are an excellent model for studies of metamorphic neuronal remodeling

We have been using a group of Drosophila neuroendocrine cells to dissect the molecular mechanisms underlying the metamorphic remodeling of insect neurons. Neuroendocrine cells are neurons that are specialized for production, packaging, and secretion of neuropeptides and other hormones into the circulation. We are particularly interested in the crustacean cardioactive peptide (CCAP) neurons. This group of neuroendocrine cells produces at least two neuropeptides, CCAP and bursicon, that control ecdysis and wing expansion (BAKER *et al.* 1999; CLARK *et al.* 2004a; DEWEY *et*

al. 2004; KIM *et al.* 2006; LUAN *et al.* 2006b; PARK *et al.* 2003). The cells can be easily visualized by immunostaining for either CCAP or bursicon (LUAN *et al.* 2006a; PARK *et al.* 2003). At the onset of ecdysis, CCAP is released in response to the signals from ETH and EH and turns on the ecdysis motor program (PARK *et al.* 2003). Park *et al.* (PARK *et al.* 2003) expressed cell death genes specifically in the CCAP neurons to knockout (KO) the cells and observed the consequences. Most of the CCAP neuron KO flies survived the larval developmental stages with merely slight timing differences in ecdysis. In contrast, 90% of the CCAP neuron KO animals failed to complete pupal ecdysis and later died. During pupal ecdysis, flies evert the developing head structures from behind the larval mouthparts to a position at the front of the body. In addition, adult appendages such as legs and wings are extended to attain their full pupal length (PARK *et al.* 2003). The CCAP neuron KO flies showed partially everted or uneverted heads, and they failed to properly elongate the legs and wings.

The bursicon neuropeptide is a protein heterodimer comprising two subunits encoded by the genes *burs* and *pburs* (LUO *et al.* 2005). After adult eclosion (adult ecdysis) bursicon is released to trigger wing expansion and cuticle tanning and sclerotization. This process is usually completed within a couple of hours after eclosion (BAKER and TRUMAN 2002; DEWEY *et al.* 2004; LUAN *et al.* 2006a; ZHAO *et al.* 2008). Flies carrying mutations in either *burs* or the bursicon receptor gene, *rickets*, showed defects in wing expansion and cuticle tanning (BAKER and TRUMAN 2002; DEWEY *et al.* 2004).

Most bursicon expression is limited to the CCAP neurons. The 10% of the CCAP neuron KO flies that completed head eversion went on to complete metamorphosis. However, after adult eclosion, they exhibited unfolded wings and untanned cuticle (LUAN *et al.* 2006a; PARK *et al.* 2003; ZHAO *et al.* 2008). Importantly, both the head eversion and wing expansion defects can persist for a long time and are readily scored days later by visual examination of culture vials. Therefore, these two phenotypes can be ideally used in genetic analysis and large-scale genetic screens to identify genes involved in the development and functioning of Drosophila neurons (BANTIGNIES *et al.* 2000; LUAN *et al.* 2006a; PEABODY *et al.* 2009; ZHAO *et al.* 2008).

Many insect neuroendocrine cells undergo extensive metamorphic remodeling, providing excellent models to study the mechanisms underlying growth of adult-specific neurites (BROWN *et al.* 2006; SANTOS *et al.* 2006; SCHUBIGER *et al.* 1998; ZHAO *et al.* 2008). We found that the CCAP neurons undergo metamorphic remodeling as well (Chapter 2). The CCAP neurons begin pruning soon after the onset of metamorphosis, and pruning peaks around 12-15 hours after puparium formation (APF). Then the CCAP neurons start to grow out new neurites and form distinct, adult-specific projections (LUAN *et al.* 2006b; ZHAO *et al.* 2008). In addition, during metamorphic remodeling, the sizes of the somata in abdominal segments A1-A7 increase substantially. These cells also adopt a multiangular shape (ZHAO *et al.* 2008). In the periphery, compared with the unbranched larval peripheral axons with type III neuromuscular endings projecting into muscles 12 and 13, the adult-specific peripheral projections are much thicker, more varicose, and contain many strongly

immunoreactive, large neuropeptide boutons and high-order distal branches (ZHAO *et al.* 2008).

A gain-of-function screen identified genes involved in metamorphic neuronal remodeling

Since both CCAP neuron-controlled behaviors, head eversion (pupal ecdysis) and wing expansion, occur around metamorphosis (ZHAO *et al.* 2008), defects in these behaviors may reflect disrupted metamorphic changes of the CCAP neurons. In addition, by screening for factors that disrupt wing expansion while leaving head eversion intact, we can isolate processes that affect remodeling without impacting embryonic or larval development. Therefore, the CCAP/bursicon neurons provide an excellent system for uncovering genes specifically controlling neuronal metamorphic remodeling.

With this in mind, we carried out a large-scale, gain-of-function screen (Chapter 2) to identify genes that when misexpressed (overexpressed) in the CCAP/bursicon neurons are capable of interfering with the normal pupal ecdysis and/or wing expansion behavior. Among the 6 thousand loci tested we identified 29 that produced defects in wing expansion and/or head eversion when overexpressed in the CCAP neurons (ZHAO *et al.* 2008). These loci represented diverse pathways including insulin and epidermal growth factor signaling pathways, an ecdysteroid-response gene, *cabut*, and an ubiquitin-specific protease gene, *fat facets*, with known functions in neuronal development. Several additional genes, including the *mir310-313* microRNA cluster and two factors related to signaling by Myb-like proto-oncogenes, have not previously been implicated in steroid signaling or neuronal remodeling. Cellular analysis was also

carried out to examine the cellular phenotypes for the 29 loci. We found misexpression of *Patched-related* (*Ptr*) induced a neurite pathfinding defect, misexpression of the *mir310-313* microRNA cluster led to defective bursicon secretion without notable abnormal changes in adult cell morphology, and misexpression of 14 other genes resulted in loss of adult-specific neurites (ZHAO *et al.* 2008). I have performed follow-up studies on selected genes (below), and the others may serve as a resource for future work to dissect the genetic and molecular mechanism controlling metamorphic remodeling.

split ends (*spen*) regulates metamorphic neuronal remodeling

We were particularly interested in one of the lines indentified in the screen, *EP(2)2583*, which drives misexpression of a transcriptional regulator, *split ends* (*spen*). The SPEN protein is the founding member of a large, evolutionarily conserved family of proteins containing a C-terminal SPOC domain and N-terminal RRM motifs (ARIYOSHI and SCHWABE 2003). The RRM motifs can bind to DNA or RNA molecules while the SPOC domain is mainly responsible for protein-protein interactions. Between the two characteristic domains, SPEN proteins may have some other functional domains such as the nuclear localization sequences (NEWBERRY *et al.* 1999), the RGG domain that comprises repeated Gly-Gly dipeptides interspersed with Arg and aromatic residues and is involved RNA metabolism, and functioning of glutamine-rich regions (Poly Q) (WIELLETTE *et al.* 1999). The SPEN protein family is further subdivided into two subclasses based primarily on size.

spen genes have been found in a wide range of eukaryotic organisms from protista (SANCHEZ-PULIDO *et al.* 2004), plants (CHEN *et al.* 2007; SANCHEZ-PULIDO *et al.* 2004), invertebrates (KOLODZIEJ *et al.* 1995; LUDEWIG *et al.* 2004) to vertebrates (NEWBERRY *et al.* 1999; SHI *et al.* 2001). In *Drosophila*, there are two members of the family, with SPEN representing the large subclass and Spenito (NITO) representing the smaller subclass (JEMC and REBAY 2006). Both *spen* and *nito* are ubiquitously expressed in flies (CHANG *et al.* 2008). Drosophila *spen* encodes a transcript of 18 kb which can be translated into a very large 570 kDa protein product (WIELLETTE *et al.* 1999).

spen is interesting because it is a functionally essential gene involved in many cellular processes. *spen* loss-of-function mutants usually die during the embryonic stage with various developmental and physiological defects in infection-induced hemocyte differentiation (JIN *et al.* 2009; JIN *et al.* 2008), cell cycle regulation (LANE *et al.* 2000), and development of head-like sclerites (WIELLETTE *et al.* 1999). *spen* interacts with several important developmental pathways including the Notch signaling pathway (DOROQUEZ *et al.* 2007; JIN *et al.* 2009), the epithelial growth factor receptor (EGFR) signaling pathway (CHEN and REBAY 2000; DOROQUEZ *et al.* 2007; KUANG *et al.* 2000), the wingless signaling pathway (CHANG *et al.* 2008; KUANG *et al.* 2000; LIN *et al.* 2003), and the HOX pathway (WIELLETTE *et al.* 1999). Moreover, *spen* plays a significant role in directing development and functioning of neurons. *Drosophila* embryos lacking both zygotic and maternal *spen* showed altered number of many PNS and CNS cell types, as well as growth and guidance defects (KUANG *et al.* 2000). At later stages, *spen* is also required for the differentiation and proliferation of fly

photoreceptor cells (BRUMBY *et al.* 2004; DOROQUEZ *et al.* 2007; JEMC and REBAY 2006; LANE *et al.* 2000; LIN *et al.* 2003; MINDORFF *et al.* 2007; REBAY *et al.* 2000; STAEHLING-HAMPTON *et al.* 1999; THERRIEN *et al.* 2000). Despite these discoveries, little research on *spen* functions in neurons after puparium formation has been conducted.

Misexpression of *EP(2)2583* produced defects in two behaviors that require CCAP neuron function: wing expansion and pupal ecdysis (head eversion). At 29°, 100% of the adult flies had unexpanded wings (UEW), and 20% of the pupae displayed partially everted heads (ZHAO *et al.* 2008). Truncated forms of SPEN proteins, missing either one of the two characteristic functional domains, function as dominant negatives that antagonize the function of the wild type SPEN protein. For example, expression of a SPEN fragment missing the SPOC domain (referred to as *spenΔC*) in *Drosophila* photoreceptor cells and midline glia cells mimicked the effects of *spen* mutation (JEMC and REBAY 2006; KUANG *et al.* 2000). Expression of the C terminal amino acids 4540-5476 of SPEN protein (referred to as *spenΔN*), which contains the SPOC domain, also showed the similar dominant negative effects (KUANG *et al.* 2000).

In Chapter 3, I confirmed that *spen* is targeted by *EP(2)2583* and *spen* normally functions in the CCAP neurons. We noted overexpression of *spen* specifically interfered with the metamorphic remodeling of the CCAP neurons and the effects of *spen* could be suppressed by functional changes in the Egfr/Ras signaling pathway and some other transcriptional regulators. Finally, we carried out a genome-wide modifier screen to identify genes/pathways affected by *spen* overexpression in the CCAP neurons. The results of the screen implicated cellular processes or signaling pathways such as the

insulin/IGF signaling pathway, the actin-myosin cytoskeleton system, and the TBP-associated factor in the behavioral defects produced by *spen* overexpression. Cellular analysis of some of these genotypes showed effects of these pathways/processes on neuronal remodeling as well.

Both loss-of-function and gain-of-function manipulations of *spen* interfered with the outgrowth process during metamorphic remodeling of the CCAP/bursicon cells. Our results support a model in which *spen* is specifically involved in neuronal growth following the completion of pruning. Based on findings from the modifier screen, we investigated the role of Rho GTPases in controlling remodeling, and we found important roles for the small Rho GTPases Rac1 and Rho1, and including the Rac1 effector PAK. These genes displayed robust genetic interactions with *spen*, indicating that *spen* may interact with the small Rho GTPases to control neuron growth during metamorphosis. Furthermore, SPEN function has been connected with steroid hormone signaling. Expression of the human homolog of fly *spen*, *sharp*, is controlled by steroid hormone signaling (SHI *et al.* 2001). SHARP can also directly interact with steroid receptor to affect expression of downstream genes (SHI *et al.* 2001). In Drosophila, microarray assays indicated that *spen* expression is enhanced during the early metamorphosis stage (BECKSTEAD *et al.* 2005). Therefore, our findings point to a possible role of *spen* in mediating the effects of steroid hormone on neuronal remodeling through interactions with the small GTPases to control cytoskeleton dynamics.

Figure 1-1.— Signaling pathways from Rho, Rac, and Cdc42 to the regulation of actin polymerization and myosin II complex. See text for details. Abbreviation: ROCK: Rho associated coiled-coil containing kinase; PAK: p21 activated kinase; LIM-K: LIM domain containing kinase; WASP: Wiskott-Aldrich syndrome protein; MBS: myosin-binding subunit; MLCK: myosin light chain kinase; MRLC: myosin regulatory light chain. (Adapted from (HUBER *et al.* 2003; LUO 2002)).

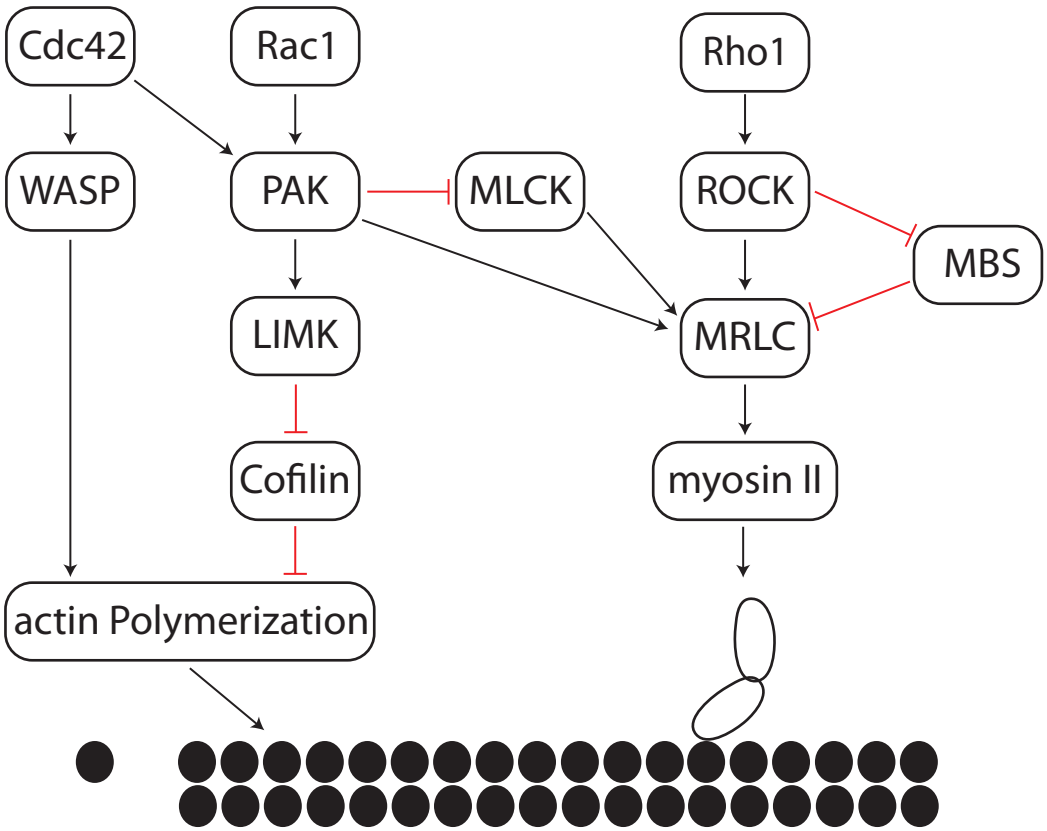
Cdc42
Rac1
Rho1
WASP
PAK
MLCK
ROCK
MBS
LIMK
MRLC
Cofilin
myosin II
actin Polymerization

CHAPTER 2

A Drosophila gain-of-function screen for candidate genes involved in steroid-dependent neuroendocrine cell remodeling

INTRODUCTION

Neurons display extensive morphological and functional changes after terminal differentiation. The resulting changes in neuronal activity shape nervous system homeostasis, seasonal and developmentally staged behavior, learning, and responses to stress, injury, and disease (ARANCIO and CHAO 2007; BURBACH *et al.* 2001; KARMARKAR and DAN 2006; NAVARRO *et al.* 2007; ROMEO and MCEWEN 2006; THIERY *et al.* 2002; VIAU 2002; ZITNANOVA *et al.* 2001). In recent years, exponential progress has been made toward understanding the molecular and cellular mechanisms underlying neuronal plasticity. However, the factors governing developmental remodeling in neuroendocrine systems remain poorly understood.

Metamorphosis of the insect nervous system involves extensive developmental reorganization. Differentiated larval neurons adopt one of two fates: programmed cell death or morphological remodeling (TRUMAN 1992b). The programmed cell death of many larval neurons occurs through autophagy or apoptosis (CHOI *et al.* 2006; WEEKS 2003). Neuronal remodeling involves the selective elimination of larval neurites and the outgrowth and elaboration of adult-specific projections (LEE *et al.* 2000; LEVINE and TRUMAN 1982). These events support the transformation of the insect from a vermiform larva that is devoted to feeding into an active adult with well-developed legs, wings, and sensory organs and complex reproductive behavior. Molting and

metamorphosis are coordinated by two families of hormones, the juvenile hormones and the ecdysteroids (NIJHOUT 1994). During metamorphosis, ecdysteroids act cell-autonomously to control neuronal cell fates (BROWN *et al.* 2006; LEE *et al.* 2000; ROBINOW *et al.* 1993) through evolutionarily conserved cellular mechanisms and signaling pathways (CHOI *et al.* 2006; DRAIZEN *et al.* 1999; HOOPFER *et al.* 2006; KINCH *et al.* 2003; WATTS *et al.* 2003).

Successful molt completion requires precise timing of ecdysis behaviors, which lead to shedding of the old cuticle. This is controlled, in part, by declining ecdysteroid levels that act through a hierarchical cascade of neuropeptides and peptide hormones to trigger the behaviors (EWER and REYNOLDS 2002). Intensive study over the past four decades has revealed many salient features of this hierarchy, although some components of the system remain to be identified. In the current model (EWER and REYNOLDS 2002), one of the first steps is activation of the endocrine Inka cells, which are located peripherally on the tracheae. In Drosophila, the Inka cells produce two related peptide hormones, referred to collectively as ecdysis triggering hormone (ETH). ETH stimulates the secretion of additional peptide hormones, including eclosion hormone (EH) and crustacean cardioactive peptide (CCAP). These and other neuropeptides contribute to the control of ecdysis behaviors (CLARK *et al.* 2004b; KIM *et al.* 2006). After ecdysis, some of the CCAP neurons are thought to secrete CCAP and additional neuropeptides to control post-ecdysis behaviors. These include bursicon, a heterodimeric neuropeptide hormone that controls wing expansion behaviors and cuticular sclerotization shortly after adult ecdysis.

The CCAP/bursicon neurons undergo substantial remodeling during the pupal stage (LUAN *et al.* 2006a). These changes likely underlie some of the differences following metamorphosis in the timing, pattern, and function of ecdysis and post-ecdysis behaviors. Many other neuropeptidergic cells with known or potential roles in the control of molting-related behaviors also undergo metamorphic remodeling (e.g., RIDDIFORD *et al.* 1994; SCHUBIGER *et al.* 1998). These changes are accessible for relatively high-throughput genetic screens. Although ecdysis and post-ecdysis behaviors are generally completed within a few minutes, the targeted ablation of the Drosophila CCAP/bursicon and EH neurons results in a variety of easily observable phenotypes that can be scored days later. These include failure to evert the adult head at pupal ecdysis and failure to expand the wings and sclerotize the adult cuticle (MCNABB *et al.* 1997; PARK *et al.* 2003). Similar phenotypes are produced through the targeted manipulation of cell signaling within these neurons (CHERBAS *et al.* 2003; HODGE *et al.* 2005; LUAN *et al.* 2006a; PARK *et al.* 2003).

Drosophila genetic mosaic methods provide powerful tools for the inhibition or stimulation of gene function in small numbers of neurons (down to the level of single cells) and at specific stages in development (LEE and LUO 1999; MCGUIRE *et al.* 2004). These tools allow the experimental manipulation of signaling pathways involved in metamorphic remodeling within the complex brain, where cells display the impact of these changes within the context of hormonal signals, metabolic and other microenvironmental cues, and other cellular interactions. Coupled with our detailed understanding of the neuroendocrine control of metamorphosis and molting behaviors, this system provides unique opportunities to perform unbiased genetic screens for novel

regulators of neuronal remodeling. However, genes that regulate nerve cell remodeling during metamorphosis are likely to also regulate the embryonic or larval development of neurons (temporal pleiotropy) or the development of other tissues (spatial pleiotropy). If these other functions are essential to the survival of embryos or larvae, then they will preclude the observation of loss-of-function (LOF) mutant phenotypes involving the disruption of neuropeptidergic cell metamorphosis. Gain-of-function (GOF) screening may overcome these problems of spatial and temporal pleiotropy and can also reveal gene functions even when other genes have redundant functions (RØRTH 1996; RØRTH *et al.* 1998). As a proof of principle, GOF screens in several other well-studied Drosophila developmental models have identified many genes with previously confirmed roles (ABDELILAH-SEYFRIED *et al.* 2000; KRAUT *et al.* 2001; MCGOVERN *et al.* 2003; PENA-RANGEL *et al.* 2002; RØRTH 1996; RØRTH *et al.* 1998; TSENG and HARIHARAN 2002). GOF screens also have resulted in the identification of several novel and important developmental regulators, thus confirming the utility of this approach for gene discovery (BRENNECKE *et al.* 2003; SHERWOOD *et al.* 2004; TELEMAN *et al.* 2005; TELEMAN *et al.* 2006).

Here, we performed a GOF screen to identify candidate regulators of ecdysteroid-dependent metamorphosis of neuropeptidergic cells. We first used the Gal4/UAS system to direct expression of several known cell signaling regulatory molecules to three different populations of neuropeptidergic cells. These experiments established the feasibility of this approach by demonstrating our ability to detect ecdysis and wing expansion defects in the progeny. We then used this method to perform a systematic GOF screen of 6,097 lines that provided neuropeptidergic cell-targeted

activation of randomly selected loci in the Drosophila genome. These experiments revealed at least 14 loci with putative functions in the formation or maintenance of adult-specific neurite projections during metamorphosis. Our screen also revealed the existence of additional, as yet unidentified, neuropeptidergic cells with critical roles in the signaling hierarchy controlling ecdysis and wing expansion.

MATERIALS AND METHODS

Stocks: Flies (*Drosophila melanogaster*) were cultured on standard cornmeal-yeast-agar media at 22-25°, and test crosses were performed at 29° unless otherwise noted. *EP* lines with insertions on the 2nd and 3rd chromosomes (RØRTH 1996; RØRTH *et al.* 1998) were obtained from the Szeged Drosophila stock center. *EP* lines with insertions on the X chromosome, and *EY*, *WH*, and *XP* lines (BELLEN *et al.* 2004) with insertions on chromosomes X-4 were obtained from the Bloomington Drosophila stock center. The Gal4 drivers used were *EH-Gal4* (*w*; P{GAL4-Eh.2.4}C21*; FBti0012534) (MCNABB *et al.* 1997), *c929-Gal4* (*w*; P{GawB}crc^{929}*; FBti0004282) (O'BRIEN and TAGHERT 1998), *386Y-Gal4* (*w*;; P{GAL4}386Y*; FBti0020938) (BANTIGNIES *et al.* 2000), and *CCAP-Gal4* (*y* w*; P{Ccap-GAL4.P}16*; FBti0037998) (PARK *et al.* 2003). Other lines were obtained from the Bloomington Drosophila Stock Center or were kindly provided by individual labs (Appendix1, Supplemental Table S1-1).

Insertion site analysis: Flanking DNA sequences for the target lines used in this screen were previously determined [*EP* and *EY* lines (ABDELILAH-SEYFRIED *et al.* 2000; BELLEN *et al.* 2004); *XP* and *WH* lines (THIBAULT *et al.* 2004)]. For each target line obtained through the GOF screening, we used the University of California, Santa Cruz (KAROLCHIK *et al.* 2003) and FlyBase (GRUMBLING *et al.* 2006) Genome Browsers and the BLASTN user service at the National Center for Biotechnology Information to identify transcripts near the insertion. We defined the putative target gene(s) as the first locus (loci) within 30 kb of the insertion site and in the same orientation (GOF) as the run-off transcript derived from the UAS sites in the target

element. We also identified loci that were in reverse orientation, within 5 kb of the insertion, and located closer to the insertion than any transcripts in the forward orientation, as potential mediators of LOF phenotypes (cf., ABDELILAH-SEYFRIED *et al.* 2000).

We used three criteria—phenocopy with UAS transgenes, induction of elevated immunostaining, or induction of *in situ* hybridization signals—to independently validate the identification of the misexpressed genes for selected GOF lines. The identifications of nine loci have been validated, including seven of the 17 loci included in our analysis of CCAP/bursicon cellular phenotypes (see supplemental Results and Discussion): *cabut* (*cbt*), *fat facets* (*faf*), *forkhead box sub-group O* (*foxo*), *miR-310-miR-313*, *miR-276a*, *miR-279, Myb-interacting protein 120* (*mip120*), *pointed* (*pnt*), and *split ends* (*spen*).

Immunochemistry and quantification: Immunostaining was performed on central nervous system (CNS) or whole animal fillet preparations obtained from wandering larvae, prepupae at the indicated times after puparium formation (APF), staged pupae (BAINBRIDGE and BOWNES 1981), or adults at the indicated times after eclosion. After dissection in calcium-free saline [182 mM KCl, 46 mM NaCl, 2.3 mM $MgCl_2.6H_2O$, 10 mM 2-Amino-2-(hydroxymethyl)propane-1,3-diol (Tris), pH=7.2], tissues were fixed for 1 hr at room temperature (RT) in either 4% paraformaldehyde (PFA) or 4% paraformaldehyde/7% picric acid (PFA-PA), and immunostaining was performed as described (HEWES *et al.* 2006; HEWES *et al.* 2003). We used antisera directed against the following proteins: CCAP (1:4000, PFA/PA) (PARK *et al.* 2003),

Bursicon α-subunit (1:5000, PFA/PA) (LUAN *et al.* 2006a), Green fluorescent protein (GFP) (1:500, PFA) (Invitrogen, Carlsbad, CA), Split ends (SPEN) (1:50, PFA) (CHEN and REBAY 2000), Myb-interacting protein 120 (MIP120) (1:1000, PFA) (LEWIS *et al.* 2004). Confocal *z*-series projections were obtained using an Olympus Fluoview FV500 microscope (Olympus, Center Valley, PA). Many of the grayscale images were inverted in Adobe Photoshop (San Jose, CA) for better visualization of fine cellular processes. Images of external structures were obtained on an Olympus SZX12 stereomicroscope with a SPOT RT camera and software (Diagnostic Instruments, Sterling Heights, MI). Photomontages of the images were obtained using Adobe Photoshop. Test and control preparations, and preparations in each developmental time series, were stained and imaged in parallel.

For quantification of the extent of neurite pruning and outgrowth during metamorphosis and of bursicon secretion in adult animals, we used the threshold function in Adobe Photoshop (with the same threshold for all images) to convert the background to white and all remaining pixels (neurites and somata) to black. Somata and any obvious artifacts were manually cut from the image, and then we obtained a count of the black pixels. For time points during which pruning and outgrowth overlapped, the extent of each was obtained by manually cutting away portions of the arbor and then re-counting the number of black pixels. We reported variances as standard errors (for means) or interquartile ranges (IQR, distance between the 75th percentile and the 25th percentile). Statistics were performed using NCSS-2001 software (NCSS, Kaysville, UT).

***In situ* hybridization with locked nucleic acid (LNA) probes:** We performed *in situ* hybridization using a protocol modified from Li and Carthew (2005) with digoxigenin (DIG)-labeled LNA probes (Exiqon, Woburn, MA). The probes and the modified protocol are described in the supplemental Materials and Methods. We obtained near infrared fluorescent images of the insoluble purple precipitate (McCauley and Bronner-Fraser 2006; Trinh *et al.* 2007) using a Zeiss Axio Imager Z1 system with an Hg arc lamp source, a 645–685 nm excitation band pass filter, and a 760-nm long pass emission filter. We also captured weak autofluorescence of the tissue with the fluorescein filters.

Expression patterns of the Gal4 drivers: We used four Gal4 lines—*EH-Gal4*, *CCAP-Gal4*, *c929-Gal4* [*dimmed-Gal4*; (Hewes *et al.* 2003)], and *386Y-Gal4*—to direct GOF element expression to peptidergic cells. These lines were chosen to target different populations of cells, some of which are known to control key aspects of ecdysis and wing expansion behaviors. Reporter gene expression in the *EH-Gal4* line is limited to just two CNS neurons, the ventromedial EH neurons (McNabb *et al.* 1997). The *CCAP-Gal4* driver is expressed specifically in ~35 pairs of neurons in the brain and ventral nerve cord (VNC) that produce CCAP and bursicon (Dewey *et al.* 2004; Luo *et al.* 2005; Park *et al.* 2003). The *c929-Gal4* driver is expressed in several peptidergic cell types, including 100-200 heterogeneous CNS neurons, intrinsic endocrine cells in the corpora cardiaca, the endocrine Inka cells, midgut cells, and peripheral nervous system (PNS) neurons. *c929-Gal4* also drives transgene expression in scattered locations in other tissues, including fat body, epithelial cells, and salivary glands

(HEWES *et al.* 2003). The *386Y-Gal4* element drives transgene expression in numerous CNS peptidergic neurons and in many peripheral endocrine cells, including the Inka cells (BANTIGNIES *et al.* 2000; TAGHERT *et al.* 2001). This driver produced the largest number of Gal4-positive neurons and secretory cells of the three lines used for this screen. All four lines yield strong transgene expression in peptidergic cells beginning in late embryos or early larvae and continuing through the adult stage (BANTIGNIES *et al.* 2000; HEWES *et al.* 2003; LUAN *et al.* 2006a; MCNABB *et al.* 1997; PARK *et al.* 2003; TAGHERT *et al.* 2001).

RESULTS

Overview of the GOF screen: We conducted a modular GOF screen in which we misexpressed native Drosophila genes in neuropeptidergic cells and examined the effects on neuropeptide-mediated developmental transitions. The screen was performed in three phases. In phase I, we examined whether gene GOF in these Gal4 patterns could produce defects in molting-related behaviors by crossing *EH-Gal4*, *c929-Gal4*, and *386Y-Gal4* to a collection of UAS lines controlling expression of cell signaling proteins. These included wild-type, dominant-negative, or constitutively active factors involved in cAMP signaling [*dunce* (*dnc*), *Cyclic-AMP response element binding protein B at 17A* (*CrebB-17A*), *Jun-related antigen* (*Jra*), *kayak* (*kay*)], Ca^{++} signaling [*Calmodulin* (*Cam*)], ecdysteroid action [*Ecdysone receptor* (*EcR*)], endocytosis [*shibire* (*shi*)], and electrical excitability [*Open rectifier K^+ channel 1* (*Ork1*)] (Appendix 1, Supplemental Table S1-1). Each of the Gal4 drivers produced molting or metamorphosis defects in combination with multiple UAS lines (Appendix 1, supplemental Table S1-2). The mutant phenotypes (Figure 2-1) included (1) larval lethality, often associated with a failure to properly shed the larval mouthparts (HEWES *et al.* 2000), (2) retention of larval characteristics following pupariation, (3) pupal lethality associated with a failure to properly evert the adult head and to fully extend the legs and wings (head eversion defects) (Figure 2-1C-D), (4) late pupal lethality associated with the completion of adult development [through stage P15(*i*) (BAINBRIDGE and BOWNES 1981)] and failure to eclose (pharate adult lethality), and (5) adults that displayed defective tanning of the cuticle and that partially or completely failed to expand their wings (Figure 2-1B). Similar phenotypes have previously been

reported following expression of wild type or dominant negative constructs with all four of the above Gal4 drivers (BANTIGNIES *et al.* 2000; CHERBAS *et al.* 2003; CLARK *et al.* 2004b; DEWEY *et al.* 2004; HODGE *et al.* 2005; KIM *et al.* 2006; LUAN *et al.* 2006a; MCNABB *et al.* 1997).

The behaviors leading to head eversion, adult eclosion, and adult wing expansion all occur during brief (<1 hr) periods (BAKER and TRUMAN 2002; PARK *et al.* 2003). However, the disruption of any of these events leads to morphological defects that can be easily scored days later by visual examination of culture vials. Therefore, we used these three events to detect genetic interactions in phases II and III of the screen. In phase II, we crossed *EH-Gal4*, *c929-Gal4*, and *386Y-Gal4* to a collection of 1808 *EP* lines, each with an insertion on the second or third chromosome. We obtained 16 lines that displayed head eversion, adult eclosion, or wing expansion defects with the *386Y-Gal4* driver. In contrast, the *c929-Gal4* driver yielded two lines (both of which also interacted with *386Y-Gal4*), and the *EH-Gal4* driver produced no hits in this phase of the screen (see supplemental Results and Discussion). Therefore, in phase III of the screen, we crossed *386Y-Gal4* only to a collection of 202 *EP* lines with insertions on the X chromosome and an additional set of 4,087 *EY*, *WH*, and *XP* lines with insertions on the X and all three autosomes. With the exception of *XP(3)d02595* (see below), lines that did not produce viable prepupae after two attempts were discarded and were not included in the above counts; we did not attempt to recover lines that may have produced mutant phenotypes that were restricted to larval ecdysis. In total (phases II and III combined), we obtained 57 out of 6097 lines (0.93%, representing 50 independent loci) that produced defects in head eversion, adult eclosion, or wing

expansion in the progeny when crossed to *386Y-Gal4*. One additional line (and locus), *XP(3)d02595*, produced larval lethality associated with defects in larval ecdysis. Because each of these mutant phenotypes occurs naturally at low frequencies in wild type stocks, we scored crosses as hits in the screen only when the defects occurred in at least 10% of the pupae or adults. These 57 lines, plus *XP(3)d02595*, were then crossed to two drivers, *c929-Gal4* and *CCAP-Gal4*, that produce Gal4 expression in subsets of the *386Y-Gal4* pattern. Only 14% (8 of 58) of the lines produced phenotypes when crossed to *c929-Gal4*, while 59% (34 of 58) of the lines did so with *CCAP-Gal4* (Table 2-1). Supplemental Table S1-3 lists the lines obtained in phases II and III of the screen, the distance and orientation of each insertion with respect to the reference sequence landmark, the genes targeted by these insertions, and the mutant phenotypes observed with each Gal4 driver.

The frequency of gene hits obtained in the screen was dependent upon the class of response element used. The rank order of effectiveness in generating phenotypes was *XP* > *EY* ≈ *EP* > *WH* (Table 2-1). These differences likely reflect multiple factors, including the difference in insertion site distributions obtained with *PiggyBac* (*WH*) versus *P* (*EP*, *EY*, and *XP*) elements (BELLEN *et al.* 2004), and the bidirectional (*XP*) versus unidirectional (*EP*, *EY*, and *WH*) orientation of transcription off of the different drivers. However, the frequencies of hits obtained also may have been skewed by the pre-selection of lines deposited into the stock centers (BELLEN *et al.* 2004; THIBAULT *et al.* 2004), and our results provide only a rough estimate of the relative effectiveness of these different elements in the screen.

Most of the insertions (52 out of the 55 in regions with known transcripts) were located within +1.0 kb to -7.0 kb of a confirmed transcriptional start site (EST or cDNA) or intron splice acceptor site (Figure 2-2). Thus, in most cases, the affected transcripts appear to be located within 7 kb of the insertion. In three lines [*EY(3)00681*, *EY(3)10546*, and *EY(3)13010*], the GOF phenotype may result from transcription over longer distances (approaching 25 kb). We obtained indirect support of this hypothesis through identification of two insertions, *EP(3)3523* and *EY(3)13010*, that are both upstream of the *miR-276a* locus. *EY(3)13010* is located ~23 kb further away (Appendix 1, Supplemental Table S1-3). Both insertions led to pharate adult lethality when crossed to *386Y-Gal4*, but only *EP(3)3523* produced wing expansion defects when crossed to *CCAP-Gal4*. Therefore, while both insertions may misexpress the same locus, the closer insertion appeared to produce a stronger gain-of-function phenotype, presumably through more efficient transcription of the nearer target. However, we cannot exclude the possibility that *EY(3)13010* produced a similar phenotype through GOF of a second, unannotated gene.

Metamorphosis of the CCAP/bursicon neurons: As a basis for determining the cellular consequences of neuropeptidergic cell overexpression of the genes obtained in the screen, we first characterized the morphology of control CCAP/bursicon neurons in larvae and in pupae at various stages of metamorphosis. We labeled the cells with either mCD8::GFP, a membrane linked fusion protein that provides excellent visualization of fine cellular processes (visualized directly or through anti-GFP immunostaining) (LEE and LUO 1999), or antisera recognizing CCAP and the bursicon

α-subunit (hereafter referred to as bursicon). Consistent with prior observations (DEWEY *et al.* 2004; LUO *et al.* 2005), in wandering third instar larvae, most elements of the CCAP/bursicon cell pattern were visible following anti-bursicon immunostaining (Figure 2-3A). This generally produced a much stronger signal than anti-CCAP immunostaining (Figure 2-3B). However, the MP neurons and their processes in the brain and ventral nerve cord (MPA and MLT; Figure 2-3B) were not stained with the anti-bursicon antiserum, although they were strongly CCAP immunoreactive (cf., DEWEY *et al.* 2004). With the exception of the brain DP neurons (which were weakly bursicon-positive and CCAP-negative), most of the CCAP- and bursicon-positive somata and neurites were also clearly visible after labeling with mCD8::GFP under control of the *CCAP-Gal4* driver (Figure 2-3C). Some of the finer processes were more intensely labeled with the anti-neuropeptide antisera then with mCD8::GFP (e.g., MPA in Figure 2-3B, C), presumably due to the concentration of secretory granules in portions of the arbor.

During metamorphosis, the CCAP/bursicon cells underwent substantial remodeling, resulting in an adult pattern of neuritic projections that was markedly different from the larval pattern (Figure 2-3D) (LUAN *et al.* 2006a). In order to track the fate of individual larval neurons and portions of the neurite arbor, we examined anti-bursicon and anti-GFP immunostaining on *CCAP-Gal4, UAS-mCD8::GFP* animals at various stages during metamorphosis: At 3 hr intervals for the first 24 hr APF, at 6 hr intervals for the period between 24 hr and 60 hr APF, and at 72 hr APF (Figure 2-4 and Appendix 1, Supplemental Figure S1-1). We could follow the neurons throughout metamorphosis—most of the larval CCAP/bursicon cells were retained—and we did not

observe the development of new cells with this marker during the 72 hr period APF. We first detected the loss of bursicon/GFP immunoreactive neurites in the thoracic and abdominal ganglia at 3 hr APF. The peak amount of pruning occurred from 12-15 hr APF, after which, the disappearance of larval neurites continued at a slower rate until ~30 hr APF. The first appearance of new, adult-specific projections occurred simultaneously with the latter stages of larval neurite pruning, and peak outgrowth occurred at 36-42 hr APF in the abdominal ganglia and at 48-54 hr APF in the thoracic ganglia. Outgrowth was essentially complete at 60 hr APF throughout the VNC.

In addition to the pruning back of larval neurites and outgrowth of new, adult-specific neurites, there were three other notable changes in the CCAP/bursicon cell pattern in the CNS during metamorphosis. First, the somata in abdominal segments A1-A7 more than doubled in diameter (Figure 2-4) and later became multi-angular in shape (not shown). Their orderly segmental arrangement was lost as they migrated or were pushed to new locations during the reorganization of the abdominal ganglia. Second, bursicon expression was turned off in 14 abdominal neurons. In larvae there was a pair of bursicon-immunoreactive neurons in each abdominal hemisegment. One cell in each pair was smaller and more weakly bursicon- (and CCAP-) immunoreactive. During the first 12-24 hr APF, these more weakly bursicon-positive neurons lost this epitope (Figure 2-4A and Appendix 1, Supplemental Figure S1-1), although they continued to express mCD8::GFP (Figure 2-4B). Third, a few CCAP/bursicon cells either died or turned off CCAP, bursicon, and *CCAP-Gal4* expression during metamorphosis. The most prominent example of this class of cells was the MP neurons (Figure 2-3), which were strongly CCAP-immunoreactive in larvae but undetectable shortly after head

eversion (data not shown).

In larvae, many of the CCAP/bursicon neurons in the VNC had efferent projections. We observed five pairs of unbranched axons that were weakly bursicon- and CCAP-immunoreactive and that projected to larval muscles 12 and 13 (HODGE *et al.* 2005). There they terminated in a few higher order branches with numerous strongly bursicon- and CCAP-immunoreactive type III endings (Appendix 1, Supplemental Figure 2-2, and data not shown). Up to three additional pairs of axons projected out through terminal abdominal nerves. These projections did not terminate on the body wall muscles and did not branch, although strongly bursicon- and CCAP-immunoreactive varicosities were present near the distal tips (see below, Figure 2-6B).

To determine the fate of the CCAP/bursicon efferents during metamorphosis, we performed anti-GFP immunostaining on *CCAP-Gal4, UAS-mCD8::GFP* animals (Appendix 1, Supplemental Figure S1-2). At 12-24 hr APF, the larval pattern of axons was still recognizable, although the peripheral terminals retracted back toward the CNS and lost most of the larval branches and boutons. We also observed axonal fragments that may have resulted from the severing of axons during pruning (see asterisk in Appendix 1, Supplemental Figure S1-2). By 30-36 hr APF, the larval efferents were gone in several preparations. At this time, we saw newly forming processes that were characterized by numerous small, branching fibers near the distal tips. By 42-48 hr APF, the adult pattern of tree-like projections and branches began to form, with 8 efferents projecting out a short distance through the thick medial abdominal nerve trunk and 3 pairs of efferents projecting out of the two or three adjacent nerves [Ab_1Nv, Ab_2Nv, and $AcNv_3$; (DEMEREC 1994)]. The peripheral projections also were thicker,

more varicose, and often terminated as a mass of multiple short, poorly organized, higher order distal branches. At 54 hr APF, the peripheral projections displayed a nearly complete adult pattern, with efferents that ramified into further, higher order branches as they extended further posteriorly to form a tree-like arbor. The efferents closer to the abdominal midline extended a long distance posteriorly before branching into the terminal abdominal nerves and forming large, strongly immunoreactive varicosities. The lateral efferents branched and formed strongly immunoreactive varicosities much closer to their exit points from the CNS.

Disrupted metamorphosis of the CCAP/bursicon neurons: Cell ablation experiments have shown that the CCAP/bursicon neurons are essential for head eversion behavior during pupal ecdysis as well as wing expansion and complete tanning of the adult cuticle after adult eclosion (PARK *et al.* 2003). However, for 70% of the lines that produced mutant phenotypes when trans-heterozygous with *CCAP-Gal4*, wing expansion defects were the only defects observed (Table 2-1, Appendix 1, Supplemental Table S1-3). Overall, 88% of the lines (versus 57% and 25% with *386Y-Gal4* and *c929-Gal4*, respectively) displayed wing expansion defects either alone or together with other mutant phenotypes. In contrast, only a third of the lines produced defects in pupal ecdysis when crossed to *CCAP-Gal4*. Thus, the GOF of many of these genes may have selectively disrupted the reorganization of the CCAP/bursicon neurons during metamorphosis [whereas the cell ablations of Park *et al.* (2003) disrupted both pupal and adult functions]. To test this hypothesis, we examined anti-CCAP and anti-bursicon immunostaining and expression of mCD8::GFP (using direct fluorescence) in

wandering third instar larvae and in stage P14 pharate adults. In order to maximize our ability to detect cellular phenotypes, we focused the analysis on insertions representing the 16 loci that produced the strongest wing expansion defects when misexpressed with *CCAP-Gal4*. In addition, we analyzed the effect of directly driving the *foxo* gene, which produced stronger wing expansion defects than the original insertion [*EY(3)11248*] upstream of the *foxo* locus. We performed most of the crosses at 29° (in parallel with crosses to the wild type stock, Oregon R, as controls).

The results of these experiments are described in supplemental Table S1-4. The responses of the CCAP/bursicon cells to the GOF of these 17 genes fell into at least three distinct classes: (I) gross defects in axonal pathfinding that were evident in both the larval and adult stages, (II) selective loss of adult-specific neurites, often associated with neuronal degeneration, and (III) defective bursicon secretion in adults without obvious defects in neuron morphology. Except for the first class, the GOF of these loci (in heterozygous animals) either had no effect on the larval morphology of the CCAP/bursicon neurons or resulted in very modest cellular defects, while the adult morphology was often profoundly disrupted. For any given line the changes in cellular morphology were not a good predictor of the external phenotypes observed (and *vice versa*). Nevertheless, these results were consistent overall with the trend toward greater disruption of adult wing expansion and tanning than of pupal head eversion behaviors.

In addition to the above insertion-specific effects, we observed a generalized response to transgene expression in the CCAP/bursicon neurons. For most insertions, we observed 30-50% lower expression of CCAP, bursicon, and mCD8::GFP in most somata, central neurites, and peripheral projections at both the wandering third instar

and P14 pharate adult stages (the VA neurons, and their dorsal efferent projections, were one notable exception). We also observed this generalized reduction in immunostaining of the CCAP/bursicon neurons when we crossed *CCAP-Gal4* to *UAS-GFP* alone, even though this cross did not produce significant lethality or wing expansion/tanning defects. Therefore, this effect appeared to be a global cellular response to transgenic protein expression, and we did not examine it further. Instead, we focused our analysis on examples of the three specific classes of GOF phenotypes.

Class I—Neurite pathfinding defects with *EP(2)2003* (*Ptr*): Of the 17 insertions that we examined, only one line, *EP(2)2003* [inserted upstream of *Patched-related* (*Ptr*)], produced widespread, gross defects in the CCAP/bursicon neuron pattern of dendritic and axonal projections (Appendix 1, Supplemental Table S1-4). Six other lines [*EP(2)2583*, *EP(2)2587*, *EP(3)3140*, *EP(3)3354*, *EP(3)3520*, *EY(2)04392*] produced subtle defects in small portions of the CNS arbor in larvae. However, in each of these cases, the larval projection pattern was mostly preserved.

With *Ptr* GOF, portions of the normal larval pattern of CNS projections, and most of the CCAP/bursicon somata, were present. However, some somata and neurites were missing. Only 30-50% of the normal efferents and ~75% of the bilateral pairs of somata in abdominal segments 1-7 (A1-A7) were visible. Many parts of the normal larval neuritic arbor were missing, often unilaterally [e.g., LB(A3) and LLT in Figure 2-5A′ and inset in Figure 2-5B′], or they were substantially scaled back in size and complexity [e.g., MA(A4) in Fig. 2-5A′]. Ectopic neurites were also observed. Thus, the effects of *Ptr* GOF on the morphology of the CCAP/bursicon neurons were likely

due to the disruption of neurite pathfinding. Similarly, *Ptr* produced striking defects in axonal and dendritic pathfinding during metamorphosis, leading to the bilaterally asymmetric loss of major portions of the normal neuritic arbor and the formation of ectopic neurites throughout the pharate adult CNS (Appendix 1, Supplemental Table S1-4, Figure 2-5C).

Previous work has shown that these neurons are essential for successful completion of head eversion during ecdysis from the larval to the pupal stage (PARK *et al.* 2003). Remarkably, despite the severe defects in larval CCAP/bursicon neuron morphology resulting from *Ptr* GOF, head eversion in heterozygous *CCAP-Gal4, EP(2)2003* animals occurred normally (Appendix 1, Supplemental Table S1-3). These results show that heterozygous *CCAP-Gal4, EP(2)2003* animals retained enough CCAP/bursicon, and enough larval CCAP/bursicon neuron connectivity, to allow normal functioning of the neuropeptidergic signaling hierarchy controlling pupal ecdysis behavior. In contrast, the adult function of the CCAP/bursicon neurons in controlling wing expansion was not preserved.

Class II—Loss of adult-specific neurites: Of the 17 lines examined for cellular changes following GOF with the CCAP-Gal4 driver, 14 displayed the loss of some or all adult-specific neurite projections. This group comprises *EP(2)2237*, *EP(2)2583*, *EP(3)3140*, *EP(3)3520*, *EY(X)10575*, *EY(2)04392*, *EY(2)05304*, *EY(3)00559*, *EY(3)00146*, *XP(2)d07339*, *XP(3)d00809*, *XP(3)d02595*, *XP(3)d04253*, and *UAS-foxo*, which was substituted for *EY(3)11248* (Appendix 1, Supplemental Table S1-4). In each case, we detected only minor morphological changes in the CCAP/bursicon cells in

larvae. These changes may have been physiologically significant, particularly when the gene dosage was increased (when more lines displayed head eversion defects). Nevertheless, the disruption of remodeling of the CCAP/bursicon neurons during metamorphosis (or the failure to retain adult projections) was the predominant phenotype for lines that produced defects in wing expansion or ecdysis when crossed to *CCAP-Gal4*.

We examined one insertion, *EP(2)2237*, to determine whether adult-specific neurites were lost through a pruning defect, an outgrowth defect, or atrophy. *EP(2)2237* is located immediately 5′ of the *cbt* C2H2 type zinc finger transcription factor, and overexpression of a *cbt* cDNA phenocopied *EP(2)2237* expression in the eye disc and wing disc (S. MUNOZ-DESCALZO, PERSONAL COMMUNICATION). In wandering third instar larvae, the morphology of the CCAP/bursicon neurons was largely unchanged following *cbt* GOF with *EP(2)2237* (Appendix 1, Supplemental Table S1-4; Figure 2-6A-B), except that we observed fewer and smaller boutons at the peripheral endings. In contrast, we observed severe defects at the P14 pharate adult stage (Appendix 1, Supplemental Table S1-4; Figure 2-6C-D), including the loss of many central neurites and efferent projections, with the remaining efferents displaying substantially fewer/shorter branches and large varicosities (Figure 2-6D′). In addition, we observed the loss of 1-6 of the 14 abdominal bursicon neurons [the B_{AG} cells, (LUAN *et al.* 2006a)]. The remaining B_{AG} somata were reduced in diameter and either intensely immunoreactive or only very weakly immunostained (Figure 2-6C′ and data not shown).

To determine whether these defects were due to either a failure of the CCAP/bursicon neurons to remodel or cellular atrophy after remodeling, we crossed

CCAP-Gal4, UAS-mCD8::GFP flies to *EP(2)2237* and performed anti-GFP immunostaining on whole animal fillets and isolated CNSs at 18, 30, 42, 54, 60 hr APF (Figure 2-6E-H). In control *CCAP-Gal4, UAS-mCD8::GFP/+* pupae at 18 hr, we observed numerous thick, anteriorly and posteriorly directed projections from the LB (Figure 2-6E) that appeared to set down the future location of an adult-specific axon tract located approximately 5 μm to each side of the CNS midline (Figure 2-6F). While these projections were also present following *cbt* GOF, they were shorter and less numerous (Figure 2-6E′). These differences persisted at later stages. In the controls at 30 hr, the central neurite projections were finer and much more numerous, and the abdominal arbor displayed a more adult-like pattern. At 42 hr, the neurite tracts were thicker and more varicose. By 54 hr, the adult abdominal longitudinal axon tracts were well-formed, and there were many thin neurite projections extending into the neuropile (Figure 2-6F). In contrast, following *cbt* GOF, the new projections retained their thick, meandering, blunt-ended appearance throughout this period and were still individually discernable even at 54 hr (Figure 2-6F′). Although the adult abdominal longitudinal axon tracts were visible, much of the finer abdominal neuritic arbor failed to form.

cbt GOF also resulted in defects in formation of the peripheral arbor. At 18 hr (*n*=7), the efferents in the control pupae remained long with accumulated material at the distal endings. The pattern was similar in *CCAP-Gal4, UAS-mCD8::GFP/EP(2)2237* pupae, but the efferents were finer and had less distal end material. At 30 hr (*n*=5), these differences were retained. However, there were fewer efferents visible in both genotypes, and many appeared to have pruned back to the CNS (Figure 2-6G). By 42 hr (*n*=7), all of the larval efferents were gone, and new projections were visible

extending from the CNS. In the control pupae, these projections began to acquire a more varicose appearance and terminated in a loosely associated network of finer branches, while the *cbt* GOF efferents were thinner and less varicose and terminated in fewer branches. At 54 hr (*n*=7) and 60 hr (*n*=3), the *cbt*-expressing efferents were short, with only a few small branches, while the control efferents formed a nearly complete adult arbor (Figure 2-6H). Thus, in both the CNS and the periphery, *cbt* GOF led to an arrest in the remodeling of the CCAP/bursicon neurons at an early stage of neurite outgrowth.

Among the 14 lines displaying the loss of some or all adult-specific neurites in pharate adults, there were differences in the phenotypes that suggest the presence of multiple different underlying mechanisms. In addition to *EP(2)2237*, six other insertions [*EP(2)2583*, *EY(X)10575*, *EY(3)00559*, *EY(3)11248/UAS-foxo*, *XP(2)d07339*, *XP(3)d02595*] displayed the loss of many central neurites and efferents, which in all of the lines except *XP(2)d07339* was accompanied by a reduced number of bursicon-immunoreactive B_{AG} (and LSE) neuron somata. In some genotypes, a subset of the observed B_{AG} somata were very small and weakly immunoreactive (Figure 2-7), and a few appeared to be fragmented. We observed a similar reduction in soma number by examining GFP fluorescence in pupae expressing *UAS-mCD8::GFP* in parallel with the gain-of-function transgenes (data not shown). While we cannot exclude the down-regulation of bursicon, CCAP, and *CCAP-Gal4* expression in the missing neurons as the cause of the apparent loss of cells, these results are consistent with cell death. Thus, neuronal degeneration often appeared to accompany, or follow, the loss of adult-specific neurites.

A second group of five lines [*EP(3)3140*, *EP(3)3520*, *EY(2)5304*, *XP(3)d00809*, *XP(3)d04253*] displayed similar losses of adult-specific neurites and loss of a few CCAP/bursicon neuron somata when crossed to *CCAP-Gal4*. The efferent projections displayed either failure or reduced capacity to form *en passant* varicosities and higher order branches. *EP(3)3140*, for example, produced efferents lacking most branches and large varicosities and ending in large, strongly bursicon-immunoreactive club-shaped endings. Thus, the GOF of these loci appeared to disrupt the accumulation of secretory material at neuroendocrine release sites.

Two insertions produced other phenotypes (Appendix 1, Supplemental Table S1-4). *EY(2)04392* displayed a loss of adult-specific neurites that was limited to the brain, subesophageal, and thoracic arbor in the CNS. *EY(3)00146* displayed weak immunostaining or loss of many central neurites and efferents, but the number of bursicon-immunoreactive anterior B_{AG} (B_{AG}^{a}) somata was increased from 8 to ~18. This was not accompanied by an increase in the number of somata labeled with *UAS-mCD8::GFP* (data not shown). In wild type animals, the number of bursicon-immunoreactive abdominal neurons decreases from 28 to 14 during metamorphosis (compare the anti-bursicon staining to the CD8::GFP signal in Figure 2-4). Taken together, these results show that *EY(3)00146* blocked the downregulation of bursicon expression in 14 abdominal neurons during metamorphosis.

Class III—Defective bursicon secretion without gross changes in adult cell morphology: Two insertions, *EP(2)2587* and *EP(3)3354*, produced moderate to strong, highly penetrant wing expansion defects when crossed to *CCAP-Gal4* without affecting

the gross morphology of the CCAP/bursicon neurons in pharate adults (Appendix 1, Supplemental Table S1-4). Both *EP(2)2587* and *EP(3)*3354 appear to drive the expression of microRNAs that all belong to the same family. *EP(2)2587* [along with two other insertions obtained in the screen, *EP(2)2586* and *EP(2)2356*] is inserted directly upstream of a cluster of four microRNAs, *miR-310-miR-313* (Appendix 1, Supplemental Table S1-3). Of the four microRNAs in the *miR-310-miR-313* cluster, *miR-310* is the furthest downstream of the *EP(2)2587*. We confirmed the overexpression of this microRNA cluster in wandering stage *CCAP-Gal4/EP(2)2587* larvae by *in situ* hybridization with LNA probes to *miR-310* (Figure 2-8A; *n*=8), *miR-312*, and *miR-313* (data not shown). In *CCAP-Gal4/+* control CNS, we observed a weak stripe of expression of *miR-310*, *miR-312*, and *miR-313* near the presumptive optic lobes (data not shown).

EP(3)3354 is inserted directly upstream of the putative transcription factor, *jing interacting gene regulatory 1 (jigr1)*. There are also two nearby microRNAs. *miR-92a* is located ~9 kb downstream, in an intron of *jigr1*, and *miR-92b* is ~14 kb downstream, 1 kb beyond the 3′ end of the *jigr1* gene. Interestingly, *miR-92a*, *miR-92b*, and *miR-310-miR-313* are closely related (ARAVIN *et al.* 2003; LEAMAN *et al.* 2005) and share many of the same predicted target mRNAs (ENRIGHT *et al.* 2003; GRUN *et al.* 2005; RAJEWSKY and SOCCI 2004; STARK *et al.* 2003). Thus, we hypothesize that *EP(2)2587* and *EP(3)3354* affect the CCAP/bursicon neurons through inhibition of common loci. Both insertions produced similar phenotypes, although the behavioral defects elicited with *EP(2)2587* were stronger than with *EP(3)3354*.

The failure of *EP(2)2587* and *EP(3)3354* to affect the morphology of the CCAP/bursicon neurons led us to ask whether the secretion of bursicon was affected. In Drosophila, bursicon activity appears in the blood within the first 20 min after eclosion (BAKER and TRUMAN 2002; LUAN *et al.* 2006a). In control *CCAP-Gal4/+* flies at 22-23°, the median times until wing expansion were 23 min after eclosion (AE) in females (*n*=26, IQR=18) and 12 min AE in males (*n*=23, IQR=9). Although the sexual dimorphism in the time to wing expansion was statistically significant (*P*=0.000048; Mann-Whitney U), all but one of the animals of either sex initiated wing expansion within 50 min AE (one female took 473 min). In the tobacco hornworm, *Manduca sexta*, the secretion of bursicon is accompanied by an ~80% depletion of the hormone from the neuroendocrine release sites in the transverse nerve (TAGHERT and TRUMAN 1982; TRUMAN 1973), and bursicon bioactivity in the hemolymph of both *M. sexta* and blowflies peaks within 1 hr of eclosion (FRAENKEL and HSIAO 1965; REYNOLDS *et al.* 1979). Thus, we expected to be able to detect bursicon secretion through an immunofluorescence assay, as we and others have done previously to detect robust secretion of CCAP, EH, and ETH (CLARK *et al.* 2004b; EWER *et al.* 1997; HEWES and TRUMAN 1991; MCNABB *et al.* 1997). We performed anti-bursicon immunostaining on fillet dissections of Drosophila adults staged at either 0 hr or 1 hr AE at 25°. We collected the flies without anesthesia to preclude anesthesia-induced behavioral changes. In control *CCAP-Gal4/+* flies, we observed a 73% depletion in the intensity of anti-bursicon immunostaining over this period [Figure 2-8B (upper panels), C]. In wild type animals, there was a concomitant depletion of CCAP and PHM immunoreactivity at this time (data not shown). Taken together with the earlier bioassay data (BAKER and

TRUMAN 2002), these results are consistent with the regulated neuroendocrine secretion of neuropeptides and other secretory granule contents from the peripheral projections of the CCAP/bursicon neurons within 1 hr AE.

When we examined *CCAP-Gal4/EP(2)2587* flies, which at this temperature (25°) displayed 100% unexpanded wings, we observed two changes in the anti-bursicon immunostaining [Figure 2-8B (lower panels), C]. First, the baseline levels of bursicon immunoreactivity were lower than in the *CCAP-Gal4/+* controls, consistent with the generalized 30-50% decrease in bursicon, CCAP, and mCD8::GFP levels in most lines expressing transgenes in the CCAP/bursicon neurons (see above). Second, there was no depletion of bursicon immunoreactivity during the 1 hr AE in *CCAP-Gal4/EP(2)2587* flies. Thus, the GOF of *miR-310-miR-313* in the CCAP/bursicon neurons inhibited bursicon secretion after eclosion. This inhibition may have resulted from direct disruption of the secretory apparatus in the CCAP/bursicon efferents. Alternatively, *miR-310-miR-313* could have altered the electrical activity (or synaptic efficacy) of neurons within the CCAP/bursicon cell population that may provide synaptic input to the subset of neurons with neuroendocrine projections.

Critical window for the *miR-310-miR-313* GOF phenotype: *EP(2)2587* expression did not perturb head eversion, even in homozygous *CCAP-Gal4, EP(2)2587* animals. This result was in contrast to the apparent dosage sensitive disruption of head eversion for a few other lines, including *EP(2)2003*, *EP(2)2237*, and *EP(2)2583* (data not shown). Thus, the effects of *miR-310-miR-313* GOF appeared to be strictly limited to adult-specific functions of the CCAP/bursicon neurons. This could have resulted

from an acute block in the expression of one or more proteins required for exocytosis or for trans-synaptic activation of the CCAP/bursicon neurons. Alternatively, *miR-310-miR-313* may have altered the earlier development of these cells. To test these hypotheses, we used the TARGET system (McGuire *et al.* 2003) to determine the critical period for the disruption of wing expansion by *miR-310-miR-313* expression in neuropeptidergic cells. We generated a fly line containing *386Y-Gal4* and the *tubulinP-Gal80^{ts}* transgene, which provides ubiquitous expression of a temperature-sensitive Gal80 protein (McGuire *et al.* 2003), and crossed these flies to *EP(2)2587*. Gal80^{ts} binds to Gal4 at permissive temperatures (18–22°) and represses Gal4 transcriptional activity. We observed normal wing expansion in ~100% of *tubP-Gal80^{ts}/EP(2)2587; 386Y-Gal4/+* animals raised throughout development. The inhibition by Gal80^{ts} is released at restrictive temperatures (27.5–30°), and when raised throughout development at 30°, 100% of *tubP-Gal80^{ts}/EP(2)2587; 386Y-Gal4/+* flies failed to inflate their wings.

To determine the critical period for *miR-310-miR-313* expression, we then conducted temperature shift experiments. We collected eggs for 24 hr at either 19° or 30°. Groups of animals then were shifted up or down to the other temperature at daily intervals until the adults emerged. After eclosion, we measured the percentage of adults displaying partially or completely uninflated wings (Figure 2-8D). When the temperature was shifted down (30° to 19°), *miR-310-miR-313* was expressed early and then repressed after the temperature shift. If *miR-310-miR-313* expression was repressed before a critical window opened, then animals would be able to expand their wings. Conversely, when the temperature was shifted up (19° to 30°), *miR-310-miR-*

313 was expressed after the temperature shift. If this occurred after a critical window closed, then animals would be able to expand their wings. Therefore, we defined the opening and closing times for the critical window as the times at which the respective shift down and shift up curves each crossed the 50% mark for animals with uninflated wings. These results show that *miR-310-miR-313* expression was effective in blocking wing expansion when the animals were at the restrictive temperature, 30°, between 6.5 and 8 days of age. The curve for timing the onset of the critical window (shift down) displayed a rapid exponential rise that sharply delineated the onset of sensitivity of the CCAP/bursicon cells to *miR-310-miR-313* expression.

The time for the close of the critical window (shift-up) was less well defined. In the control experiments by McGuire et al (2004), the repression of control transcript expression after shifting to 19° was half-maximal at 15 hr and complete by 36 hr. A similar slow decline likely accounts for the greater variability and shallower curve for the shift-up tests in Figure 2-8D. When we examined the stage of development of *tubP-Gal80^{ts}/EP(2)2587; 386Y-Gal4/+* animals after 8.7d at 19°, 71% of the animals were wandering third instar stage larvae, and the rest were feeding stage third instar larvae (*n*=105). If the offset of *miR-310-miR-313* occurred roughly 8-30 hr after the animals were shifted to 19°, then most of these animals would have been in the early stages of pupal development. Therefore, we conclude that the critical window for the effects of *miR-310-miR-313* GOF on the ability of the CCAP/bursicon neurons to secrete bursicon coincides with the first half to middle third of metamorphosis.

DISCUSSION

Analysis of steroid-dependent neuroendocrine cell remodeling through GOF screening:

We screened 6,097 randomly inserted GOF transposon insertions and identified 30 lines (29 unique loci) that produced wing expansion defects and 5 lines (3 loci) that produced pupal lethality (two with head eversion or eclosion defects) when crossed to the *CCAP-Gal4* driver. We also identified 19 loci that produced head eversion, eclosion, or wing expansion defects when expressed with the much broader neuropeptidergic cell driver, *386Y-Gal4*, but not *CCAP-Gal4*. These results point to the existence of one or more undefined neuropeptidergic cell types in the *386Y-Gal4* pattern with important roles in the control of head eversion, eclosion, and wing expansion behaviors (Appendix 1, Supplemental Results and Discussion). Our phenotypic analysis of 17 of the loci that produced the most severe wing expansion defects with *CCAP-Gal4* suggests functions for these genes in axonal pathfinding, development of competence for developmentally timed neuropeptide secretion, outgrowth of adult-specific neurite projections, neuropeptide expression, and neuronal maintenance. The other lines obtained in the screen revealed several additional genes with putative roles in neuroendocrine cell remodeling.

Combined with LOF data, GOF screens have proven to be an effective method for identification of genes involved in the development of many tissues (ABDELILAH-SEYFRIED *et al.* 2000; BRENNECKE *et al.* 2003; KRAUT *et al.* 2001; MCGOVERN *et al.* 2003; PENA-RANGEL *et al.* 2002; RØRTH 1996; RØRTH *et al.* 1998; SHERWOOD *et al.* 2004; TELEMAN *et al.* 2005; TELEMAN *et al.* 2006; TSENG and HARIHARAN 2002). However, this method also poses special concerns that are not usually encountered with

traditional LOF screens. For example, some genes produce phenotypes in cells in which they are not normally expressed. In many cases, these phenotypes are complementary to LOF phenotypes in other cells, and they are therefore useful for defining gene functions (e.g., ALLAN *et al.* 2003; HEWES *et al.* 2006; HEWES *et al.* 2003). Alternatively, GOF phenotypes may arise from abnormal protein-protein interactions or through the activation of cellular homeostasis machinery, such as the unfolded protein response (RYOO and STELLER 2007). In future studies, it will be important to map the normal expression patterns of these genes and test for complementary LOF phenotypes in order to identify factors that 1) control remodeling of the CCAP/bursicon during metamorphosis, and 2) regulate more general aspects of steroid-dependent neuronal plasticity. Nevertheless, our phenotypic analysis and other published studies provide several insights into their possible functions. Below, we describe a few of the putative associations among these genes.

MicroRNAs: GOF screens have proven to be effective for identifying functions of microRNAs, which are 20-22 nucleotide non-coding RNAs that assume diverse gene regulatory roles (KLOOSTERMAN and PLASTERK 2006). Hundreds of microRNA genes have been identified through computational prediction and experimental verification (BEREZIKOV *et al.* 2006), yet relatively few microRNA functions have been identified. In this study, we isolated 6 insertions, out of a total of 58 (10%), that drove expression of three different microRNA loci. In other published GOF screens, these 6 insertions produced developmental phenotypes involving regulation of cell growth, differentiation, or apoptosis in the eye imaginal disc, adult dorsal thorax and external sensory organs,

and motor axon guidance and synaptogenesis in embryos and larvae (ABDELILAH-SEYFRIED *et al.* 2000; KRAUT *et al.* 2001; MULLER *et al.* 2005; PENA-RANGEL *et al.* 2002; TSENG and HARIHARAN 2002). Other similar screens led to the discovery of microRNAs involved in tissue growth and energy homeostasis (BRENNECKE *et al.* 2003; TELEMAN *et al.* 2006). Thus, coupled with target prediction, LOF experiments, and mapping of microRNA expression patterns, GOF screening provides an additional tool for systematic examination of microRNA function.

The GOF phenotypes obtained with microRNAs in our screen likely result from the repression of unidentified mRNAs that are normally expressed in the CCAP/bursicon neurons. It will be of interest to determine the identity of these target mRNAs and whether the repression by the microRNAs occurs normally in other cells, or in the CCAP/bursicon neurons at other stages during development. Through *in situ* hybridization of wandering third instar larval CNS, we detected weak, heterogeneous expression of *miR-279* in the VNC (data not shown) and of *miR-310*, *miR-312*, and *miR-313* in the brain (see Results). Therefore, these microRNAs may be involved in the developmental regulation of certain CNS neurons. In a previous study, *miR-311* and *miR-313* were shown to play significant roles in embryonic nervous system development (LEAMAN *et al.* 2005). Interestingly, the *miR-310-miR-313* cluster, and the closely related microRNAs, *miR-92a* and *miR-92b*, were strongly expressed in embryos and then less abundant at later stages (ARAVIN *et al.* 2003; SEMPERE *et al.* 2003). For some of these microRNAs, significant down-regulation occurred near the embryo-larval and larval-pupal transitions. Our observation of a critical period for *miR-310-miR-313* action during early metamorphosis suggests that the upregulation of some

of their target mRNAs was required for the CCAP/bursicon cells to acquire competence to secrete bursicon after eclosion.

Growth factor signaling: Several of the genes identified in our screen are involved in signaling by growth factors. Two of the genes, *foxo* and *Insulin-like receptor* (*InR*), encode components of the insulin signaling pathway. In mammals, multiple forkhead O (FoxO) subfamily transcription factors play important roles in the regulation of neuronal apoptotic death in the context of low level insulin signaling (BARTHELEMY *et al.* 2004; BISWAS *et al.* 2007; GILLEY *et al.* 2003; SORIANO *et al.* 2006). In Drosophila, *foxo* is the only FoxO subfamily member in the genome, and it has been shown to mediate apoptosis in retinal neurons (LUO *et al.* 2007). Here, we found that *foxo* overexpression resulted in evident neurodegenerative phenotypes: reduced and fragmented neurites, reduced cell sizes, and loss of neuronal somata. Interestingly, overexpression of *InR* by *EY(3)00681* in the *386Y-Gal4* pattern also produced pharate lethality. Based on these results, we are currently examining the role of insulin signaling in the regulation of neuropeptidergic cell remodeling during metamorphosis (T. GU, T. ZHAO, R. S. HEWES, UNPUBLISHED OBSERVATIONS).

In addition to insulin signaling, the epidermal growth factor receptor (EGFR) signaling pathway is a critical regulator of axon growth and guidance and neuronal cell survival (DOMINGUEZ *et al.* 1998; DOROQUEZ and REBAY 2006). In this screen, we found two genes with known roles in EGFR signaling during neuronal development, the *pnt* ETS domain transcription factor and the *spen* nuclear co-repressor (CHEN and REBAY 2000; KUANG *et al.* 2000). Both *pnt* and *spen* elicited robust head eversion and

wing expansion defects when expressed in the *386Y-Gal4* and *CCAP-Gal4* patterns (Appendix 1, Supplemental Table S1-3), and *spen* overexpression resulted in the loss of most of the CCAP/bursicon neuron arbor and the disappearance of many abdominal CCAP/bursicon neuron somata (Appendix 1, Supplemental Table S1-4). Interestingly, reduced activity of *pnt* can suppress *spen* overexpression-mediated phenotypes (T. ZHAO, T. GU, R. S. HEWES, UNPUBLISHED OBSERVATIONS), which is consistent with a previous report that *spen* functions synergistically with *pnt* in regulation of the EGFR pathway (CHEN and REBAY 2000). These results suggest that EGFR signaling controls aspects of neurite outgrowth and neuropeptidergic cell survival during metamorphosis. Alternatively, *pnt* and *spen* may each influence different signaling pathways that contribute to the development or maintenance of adult CCAP/bursicon projections. In the GOF screen, we also obtained *spitz* (*spi*), which encodes a ligand of the Drosophila EGFR. When expressed in the *386Y-Gal4* pattern, *spi* produced pharate adult lethality, presumably due to actions of this ligand on neighboring cells.

Myb proto-oncoprotein-like transcription factors: Of the 14 genes that produced loss of adult-specific neurite projections, two appear to be involved in signaling by Myb-like protein complexes. The *mip120* gene encodes one of five components of the Drosophila Myb complex (BEALL *et al.* 2002), and *stonewall* (*stwl*) encodes a Myb-like transcription factor (CLARK and MCKEARIN 1996). In mammals, the apoptotic loss of post-mitotic neurons following the loss of trophic support from nerve growth factor (NGF) requires the de-repression of multiple transcriptional pathways. These include the FoxO pathway, the c-Jun and c-Jun N-terminal kinase

pathway (JNK), and the cell cycle pathway, which involves phosphorylation of retinoblastoma (Rb) proteins as well as the de-repression of Myb proteins (BRUNET *et al.* 2001; LIU *et al.* 2004). All three of these pathways converge on Bim, a pro-apoptotic protein that is activated in response to NGF deprivation. Overexpression of either FOXO or Myb family proteins (including STWL) can result in apoptotic cell death (BRUN *et al.* 2006; GILLEY *et al.* 2003; LIU and GREENE 2001). However, the apoptotic response to NGF under physiological conditions may require the combined de-repression of all three of these pathways (BISWAS *et al.* 2007). In this screen, *foxo* expression led to loss of CCAP/bursicon cell neurites and somata, while overexpression of *mip120* and *stwl* both led to loss of neurites alone (Appendix 1, Supplemental Table S1-4). In the case of *mip120*, the GOF phenotype appears to have resulted from overexpression, rather than misexpression, since we found that MIP120 was ubiquitously expressed in the larval CNS (Appendix 1, Supplemental Results and Discussion, and T. GU, T. ZHAO, R. S. HEWES, UNPUBLISHED OBSERVATIONS). Likewise, *stwl* was previously shown to be expressed ubiquitously in embryos (TOMANCAK *et al.* 2007). It will be of interest to determine whether these factors function together under physiological conditions to regulate nerve cell growth and survival in this system.

Ecdysteroid signaling: Studies on a variety of cell types in Drosophila and *M. sexta* have shown that the metamorphic remodeling of larval neurons is mediated by ecdysteroids. These steroid actions are mediated largely cell autonomously (BROWN *et al.* 2006; WILLIAMS and TRUMAN 2005) through ecdysteroid receptors, which are heterodimers consisting of Ultraspiracle along with one of three isoforms of the

ecdysteroid receptor (EcR), EcR-B1, -B2, or -A (KOELLE *et al.* 1991; TALBOT *et al.* 1993; THOMAS *et al.* 1993; YAO *et al.* 1993; YAO *et al.* 1992). In Drosophila neuroendocrine cells as well as in other neuronal cell types, loss of the EcR-B isoforms leads to pruning defects. In contrast, EcR-A is thought to regulate the outgrowth of the adult-specific neurites (BROWN *et al.* 2006; LEE *et al.* 2000; SANTOS *et al.* 2006; SCHUBIGER *et al.* 1998; TRUMAN 1996; TRUMAN *et al.* 1994).

GOF of several of the loci identified in this screen (*cbt*, *CG14438*, *faf*, *foxo*, *klar*, *mip120*, *miR-279*, *spen, stwl*, and the genes under the control of *EY(2)04392*, *XP(2)d07339*, *XP(3)d00809*, *XP(3)d02595*, and *XP(3)d04253*), produced defects consistent with the disruption of ecdysteroid-dependent remodeling of the CCAP/bursicon neurons. For *cbt*, we observed pruning on schedule, but formation of the adult central and peripheral adult arbor was retarded, and outgrowth appeared to cease after completion of an initial phase (Figure 2-6). Interestingly, *cbt* encodes a C2H2 zinc finger transcription factor (MUNOZ-DESCALZO *et al.* 2005) that functions as a primary ecdysteroid response gene (BECKSTEAD *et al.* 2005). Thus, EcR may directly regulate *cbt* expression, which in turn may regulate the expression of genes involved in controlling neuronal outgrowth.

Ubiquitin-proteasome system: Finally, we identified several genes that have previously been shown to regulate axonal pathfinding or synapse formation in other cell types (cf., KRAUT *et al.* 2001). One of these, *faf*, encodes a deubiquitinating protease that contributes to synaptic growth control at the neuromuscular junction (NMJ). The ubiquitin-proteosome system plays a crucial role in axon guidance and synaptogenesis

in diverse species (HEGDE 2004). In Drosophila, *faf* overexpression at the NMJ produces synapse overgrowth in third instar larvae (DIANTONIO *et al.* 2001). Similarly, we found that *faf* overexpression produced modest overgrowth, including enlarged varicosities, of larval CCAP/bursicon neurites within the CNS. In contrast, during metamorphosis, *faf* overexpression produced degenerative phenotypes (Appendix 1, Supplemental Table S1-4), accompanied by loss of neurite arbor and CCAP/bursicon cell somata. Thus, the contribution of ubiquitin-proteasome system components to the development of CCAP/bursicon neurons, or in the balance of regulated proteolysis in different subcellular domains, may change as a function of developmental stage.

Taken together, these results provide several molecular clues into how the complex processes of neuronal differentiation, ecdysteroid-dependent regulation of neuronal remodeling, and neuronal growth and maintenance may be coordinated in a single cell type, the CCAP/bursicon cells. The challenge for the future will be to define the biological functions of the factors identified in this screen and their roles in neuronal remodeling.

We thank David McCauley for assistance with *in situ* imaging, Adam Diehl, Adrienne Emel, Kendal Hopkins, Brett Kirkconnell, Matthew Mote, Rahul Patel, Elizabeth Pearsall, Edward Spencer, and Ryan Wilkes for assistance with EP crosses, insertion mapping, or immunostaining, Bryce Jones, Kim Krittenbrink, David McCauley, Jeremiah Smith, and Audrey Kennedy for technical assistance, Frédéric Bantignies, Mariann Bienz, Gabrielle Boulianne, John Ewer, Sue McNabb, Paul Taghert, Marc Tatar, and the Szeged and Bloomington Drosophila stock centers for fly stocks, and Bing Zhang for comments on the manuscript. This work was supported by grants to R.H. from the National Science Foundation (IBN0344018 and EPSCoR 0132534), the Oklahoma Center for the Advancement of Science and Technology (HR03-048S), the Oklahoma Research Council/University of Oklahoma Vice President for Research, and the Oklahoma State Regents for Higher Education.

Figure 2-1.—Head eversion and wing expansion phenotypes produced by gene GOF in peptidergic neurons. (A) Oregon R (wild type) adult female. (B) Examples of *y, w; CCAP-Gal4/EY(2)04392* females with normal wings (normal), partially expanded wings (PEW), and unexpanded wings (UEW). The PEW and UEW phenotypes were scored as described (LUAN *et al.* 2006a). Arrows indicate folds due to incomplete wing expansion in the PEW animal. (C-D) Dorsal (C) and ventral (D) views of an Oregon R (wild type) pupa and two *y, w/w; 386Y-Gal4/EY(3)10546* pupae displaying weak and strong microcephalic (mc) phenotypes (cf., HADORN and GLOOR 1943; HEWES *et al.* 2000). Cryptocephalic pupae are very similar to the strong microcephalic pupae, except that the head structures are found entirely within the thorax (CHADFIELD and SPARROW 1985; HADORN and GLOOR 1943; HEWES *et al.* 2000; PARK *et al.* 2003). The pronged bars in (C) indicate the anterior edges of the head and thorax and the posterior edge of the thorax. The solid and dashed lines in (D) indicate the posterior edges of the legs and wings, respectively. Asterisks, pupal abdomen lacking external bristles; b, posterior gas bubble due to failed anterior translocation of the gas bubble during head eversion. D, dorsal thorax dimpled; N, tanning incomplete; P, ptilinum permanently soft and partially extended; S, scutellum wrinkled and scutellar bristles crossed and directed toward anterior; T, darkened cuticle in shape of trident on dorsal thorax; X, non-glossy cuticle surface.

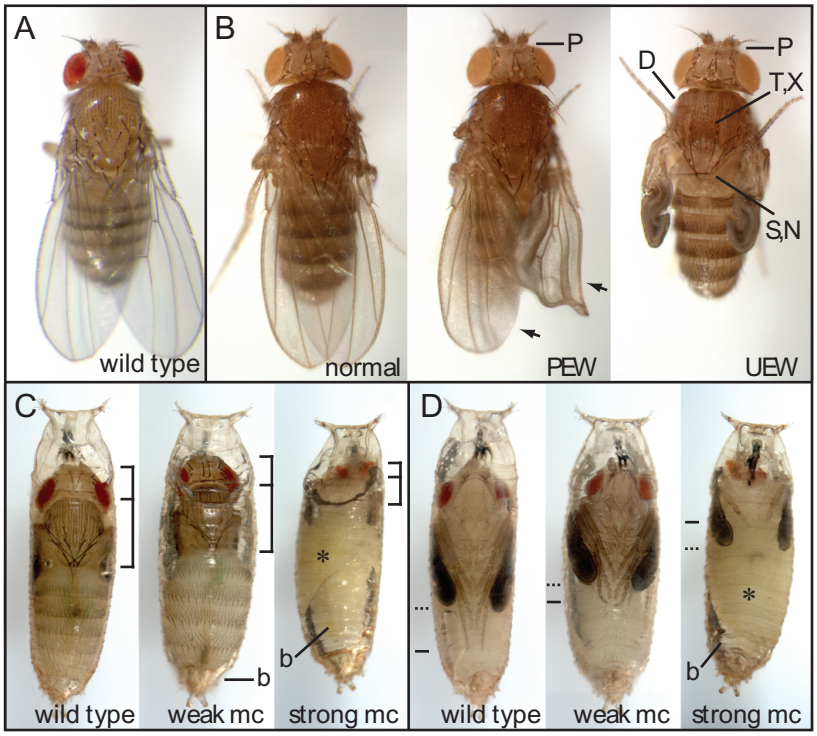
A
wild type
B
normal
P
PEW
P
D
T,X
S,N
UEW
C
wild type
b
weak mc
b
strong mc
D
wild type
weak mc
b
strong mc

Figure 2-2.—Scatter plot of target element insertion site distances from the nearest promoter or exon. The distance for each target element to the 5′ end of the nearest promoter (black) or exon (magenta) was plotted on the *y* axis. Negative values represent insertions located upstream of the respective promoter or exon splice acceptor site, and positive values refer to insertions that were located 3′ of these landmarks (while still 5′ of significant portions of the transcript). Only the first locus within 30 kb and in the same orientation as the direction of Gal4-directed transcription off of each *EP*, *EY*, or *WH* element (unidirectional) or *XP* element (bidirectional) was included, and the distances to putative LOF (antisense) transcripts (Appendix 1, Supplemental Table S1-3) are not shown. Insertions within the predicted coding sequence (CDS) of a transcript, and insertions located in introns located downstream of an exon containing CDS, are indicated with open symbols.

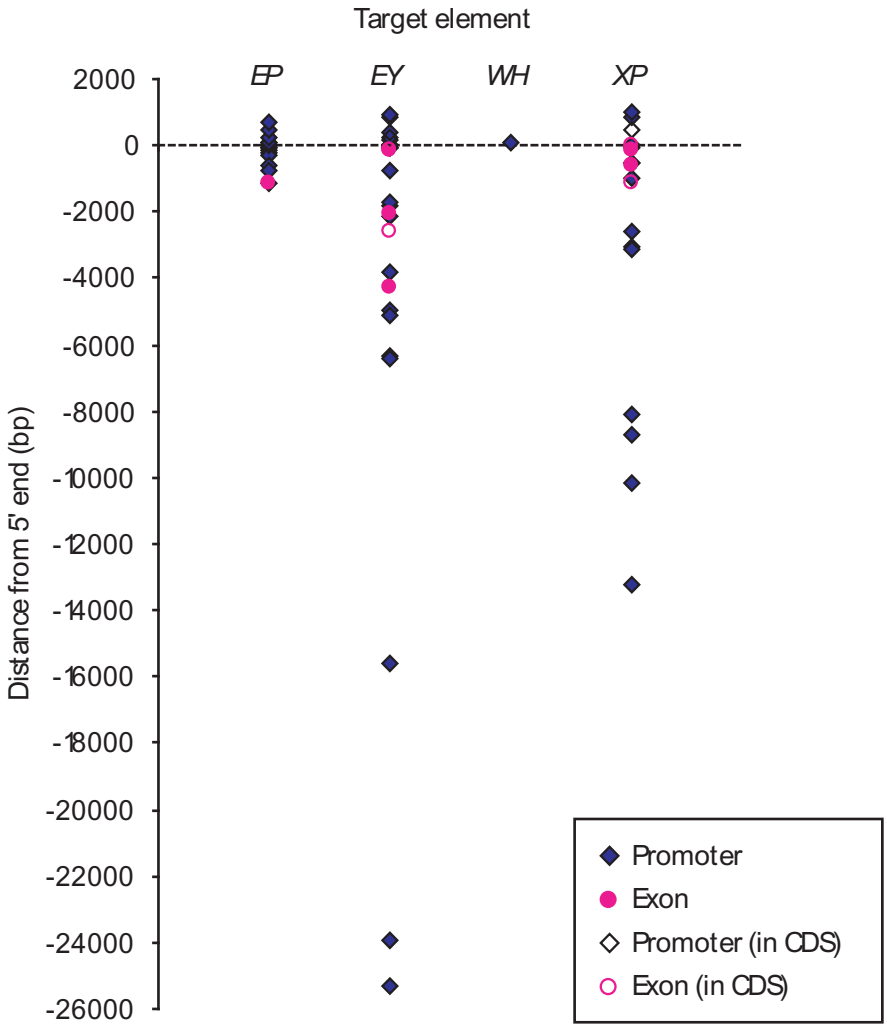
Target element
EP
EY
WH
XP
2000
0
-2000
-4000
-6000
-8000
-10000
-12000
-14000
-16000
-18000
-20000
-22000
-24000
-26000
Distance from 5' end (bp)
Promoter
Exon
Promoter (in CDS)
Exon (in CDS)

Figure 2-3.—Staining patterns and morphologies of the CCAP/bursicon neurons. (A) Anti-bursicon (BURS) and (B) anti-CCAP (CCAP) immunostaining in wandering third instar larval CNS (*CCAP-Gal4/+*). Anti-bursicon immunostaining was also observed in a cluster of neurites located over the corpora cardiaca (not shown). (C) mCD8::GFP (CD8::GFP) fluorescence in a wandering third instar CNS (*CCAP-Gal4, UAS-mCD8::GFP/+*). (D) Anti-bursicon immunostaining in a stage P14 pharate adult CNS (*CCAP-Gal4/+*). A midline protocerebral brain arbor was also bursicon immunoreactive (MPB; not shown, see Figure 2-5C). Abbreviations: AA, abdominal arbor; B_{AG}^{a}, eight neurons located toward the anterior of the abdominal ganglia; B_{AG}^{p}, six neurons located in the posterior abdominal ganglia; DP, dorsal protocerebral neuron (weakly bursicon-positive and CCAP-negative); CTA, circum-neuropilar (ventral) thoracic arbor; DTA, dorsal thoracic arbor; LB(S, T1-3, A1-A7), lateral branch (leading from LLT to MA) in the subesophageal region and segments T1-T3 and A1-A7; LLT, lateral longitudinal tract; LSE(1-3), lateral subesophageal neurons; MA(S, T1-3, A1-A7), midline arbor in the indicated segments; MLT, midline longitudinal tract; MP, midline protocerebral neurons; MPA, midline protocerebral arbor; PA, protocerebral arbor; PAA, posterior abdominal arbor; SA, subesophageal arbor; TA, tritocerebral arbor; VA, ventral abdominal neuron. Scale bar, 50 μm.

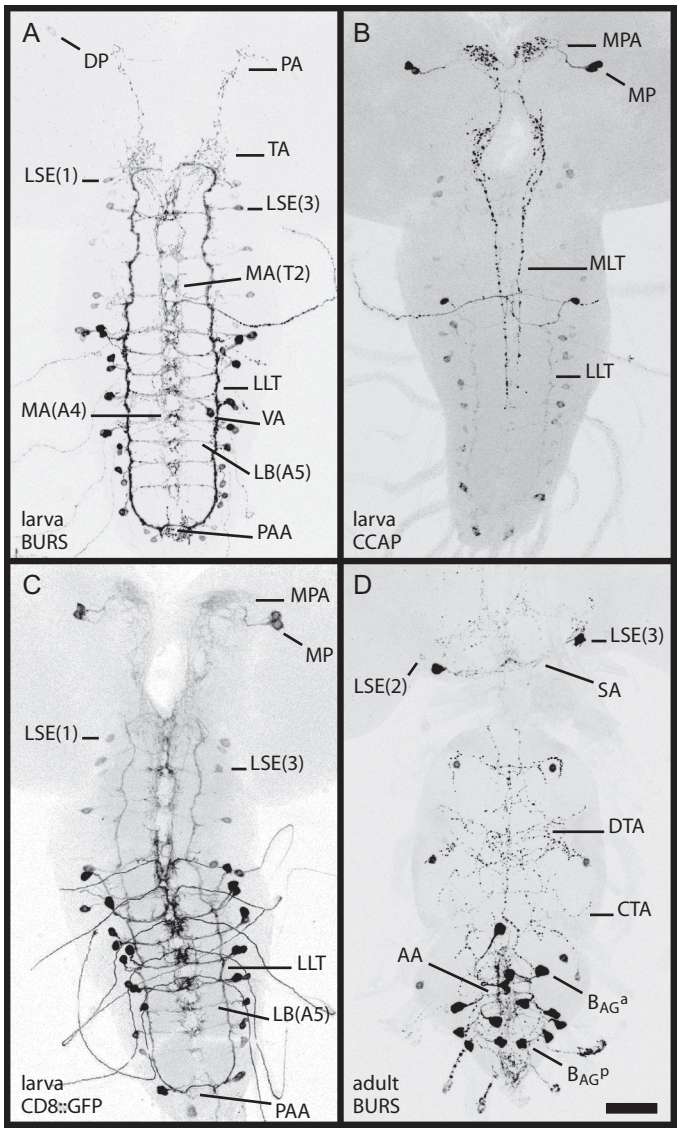
A
DP
PA
TA
LSE(1)
LSE(3)
MA(T2)
LLT
MA(A4)
VA
LB(A5)
larva
BURS
PAA
B
MPA
MP
MLT
LLT
larva
CCAP
C
MPA
MP
LSE(1)
LSE(3)
LLT
LB(A5)
larva
CD8::GFP
PAA
D
LSE(3)
LSE(2)
SA
DTA
CTA
AA
BAGa
BAGp
adult
BURS

Figure 2-4.—Remodeling of the CCAP/bursicon neurons during metamorphosis. (A) Anti-bursicon immunostaining of the ventral nerve cord (VNC) at 0, 12, 36, and 60 hr after puparium formation (APF) (*n*=6-19). Additional time points are shown in supplemental Figure S1-1. (B) mCD8::GFP fluorescence in the same preparations as in (A) (*CCAP-Gal4, UAS-mCD8::GFP/+*). (C) Time courses for pruning and outgrowth of the neuritic arborizations in the thoracic and abdominal ganglia. The relative extent of pruning and outgrowth (indicated by the relative height, along the *y* axis, of the horizontal shapes) was quantified for each of the time points represented with tick marks on the *x* axis. The images in (A) and (B) are representative of the changes at the selected times. Arrows, thoracic neurites that were pruned back by the next stage shown in the figure; arrowheads, new adult-specific thoracic neurites; double feathered arrows; abdominal neurites that were pruned back by the next stage shown; double feathered arrowheads, new adult-specific abdominal neurites. Scale bar, 50 μm.

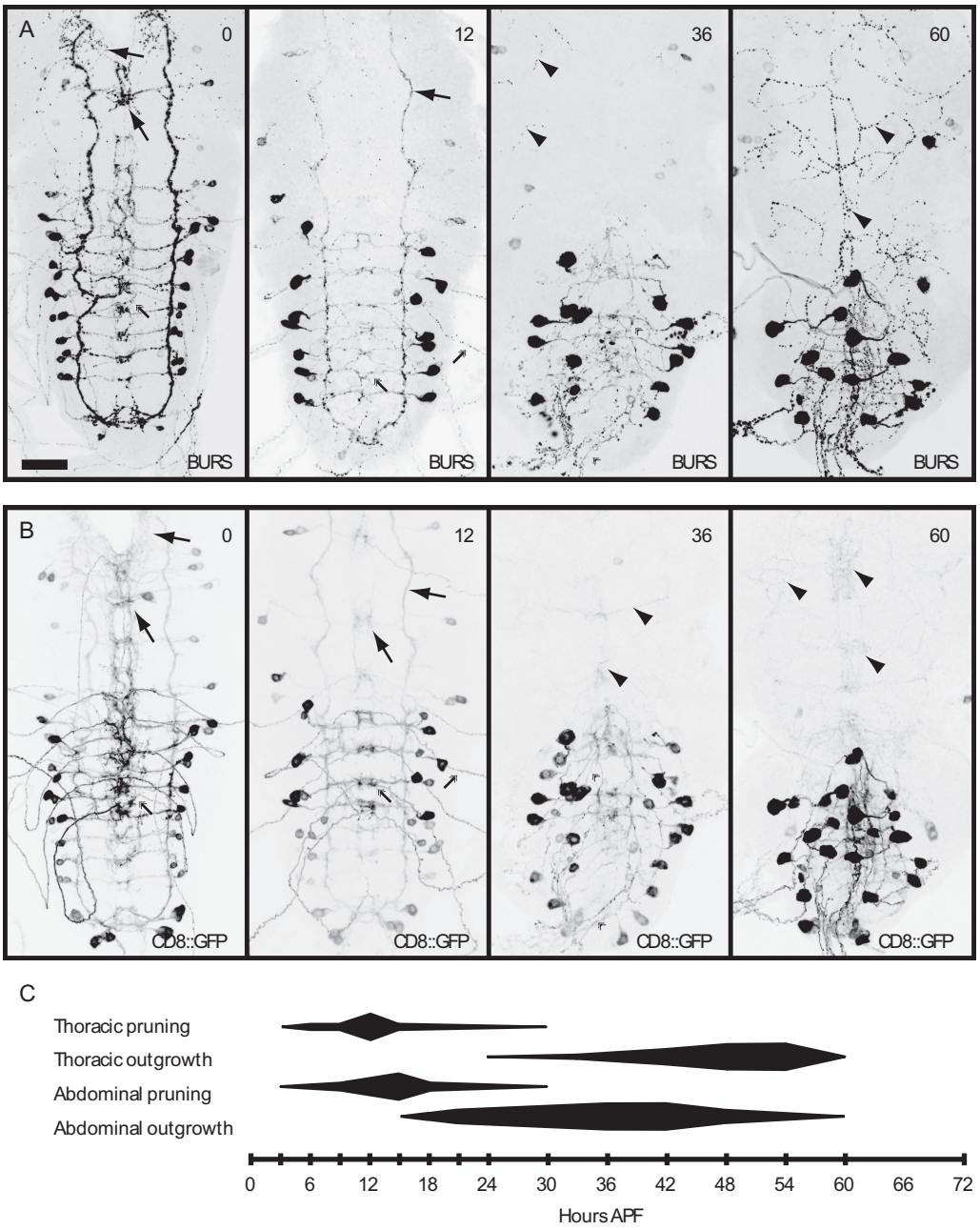
A
0
12
36
60
BURS
BURS
BURS
BURS
B
0
12
36
60
CD8::GFP
CD8::GFP
CD8::GFP
CD8::GFP
C
Thoracic pruning
Thoracic outgrowth
Abdominal pruning
Abdominal outgrowth
0
6
12
18
24
30
36
42
48
54
60
66
72
Hours APF

Figure 2-5.—GOF of *Ptr* produced neurite pathfinding defects in larval CCAP/bursicon neurons. In both larvae (A-B) and pharate adults (C), misexpression of *Ptr* (A′, B′, and C′) led to the loss of some somata and neurites (labels with dashed lines). Ectopic or mistargeted neurites were also observed (arrows). (A) mCD8::GFP (*UAS-mCD8::GFP*) expressed under the control of *CCAP-Gal4* either with (A′) or without (A) *EP(2)*2003, which is inserted just 5′ of the *Ptr* gene (Appendix 1, Supplemental Table S1-3). CNS dissections were performed at the wandering third instar stage (*n*=8). (B) Anti-CCAP immunostaining in a *CCAP-Gal4/EP(2)2003* wandering third instar larval CNS (B′) and a *CCAP-Gal4*/+ control (B) (*n*=5). In a second *CCAP-Gal4/EP(2)2003* CNS (B′ inset), MLT was missing on one side. (C) Anti-bursicon immunostaining in the CNS from two *CCAP-Gal4/EP(2)2003* P14 stage pharate adults (C′, C″) and a *CCAP-Gal4*/+ control (C) (*n*=7). The labels are defined in the legend for Figure 2-3. Arrowheads, thicker neurites with larger than normal varicosities; feathered arrows, small diameter somata. Scale bars: (A-C) 50 μm; (B′ inset) 100 μm.

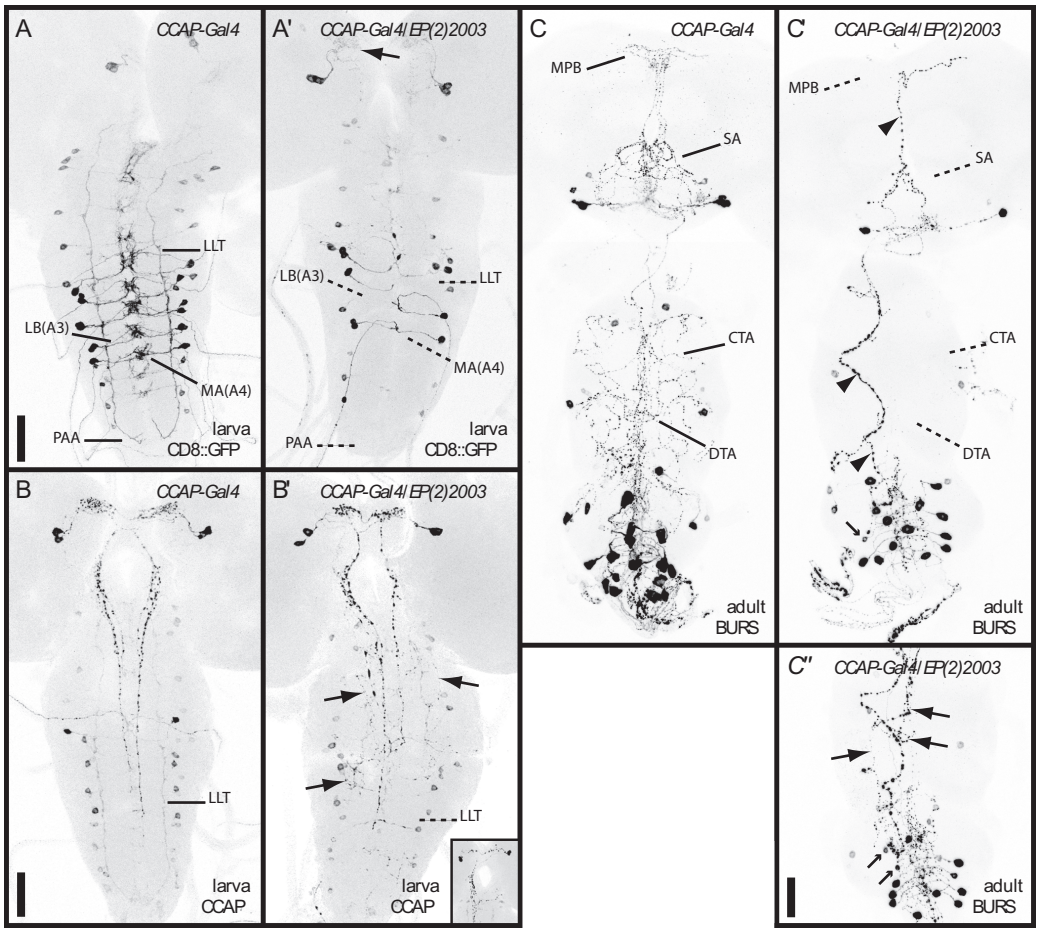
A
CCAP-Gal4
LLT
LB(A3)
MA(A4)
PAA
larva
CD8::GFP
A'
CCAP-Gal4/ EP(2)2003
LB(A3)
LLT
MA(A4)
PAA
larva
CD8::GFP
C
CCAP-Gal4
MPB
SA
CTA
DTA
adult
BURS
C'
CCAP-Gal4/ EP(2)2003
MPB
SA
CTA
DTA
adult
BURS
B
CCAP-Gal4
LLT
larva
CCAP
B'
CCAP-Gal4/ EP(2)2003
LLT
larva
CCAP
C''
CCAP-Gal4/ EP(2)2003
adult
BURS

Figure 2-6.—GOF of *cbt* prevented the outgrowth of adult-specific bursicon-immunoreactive neurites and the increase in diameter of the CCAP/bursicon cell somata during metamorphosis. (A-D) Anti-bursicon immunostaining in the CNS (A, C) and peripheral neurites (B, D). The staining was performed on tissue dissected at the wandering third instar larval stage (A-B) and P14 pharate adult stage (C-D) from *CCAP-Gal4/EP(2)2237* animals (A′-D′) and *CCAP-Gal4/+* controls (A-D) (*n*=5-7). Note that the morphology of the CCAP/bursicon neurons was largely unaffected following *cbt* GOF in larvae. In contrast, the pharate adult morphology of the cells was severely disrupted. (E-H) Anti-GFP immunostaining in the CNS (E-F) and peripheral neurites (G-H) at 18 hr APF (E), 30 hr APF (G), or 54 hr APF (F, H). Membrane-associated mCD8::GFP (*UAS-mGFP*) was expressed in *CCAP-Gal4/+* (E, G, F, H) and *CCAP-Gal4/EP(2)2237* (E′, F′, G′, H′) animals. In the CNS, *cbt* GOF caused the neurite projections to remain short, thick, and with few branches (F′), similar to the appearance of control animals 36 hr earlier (E). In the periphery, the efferents displayed some initial outgrowth, but they failed to form a complete adult arbor (H′). Asterisk, fine neuritic arbor; bi-color (black/white) arrows, non-branching efferent projections; black arrows, traces of remaining neurites; black arrowheads, smaller somata; black double feathered arrows, strongly immunoreactive axon terminals; black double feathered arrowheads, weakly immunoreactive axons; white arrows, adult-specific longitudinal axon tracts (forming or completed); white arrowheads, developing neurite branches; white double feathered arrows, persistent larval projections after muscle detachment and before pruning completed; white double feathered arrowheads, adult

efferents near points of exit from the CNS. Scale bars: (A, C) 50 μm; (B, D, G-H) 100 μm; (E-F) 10 μm.

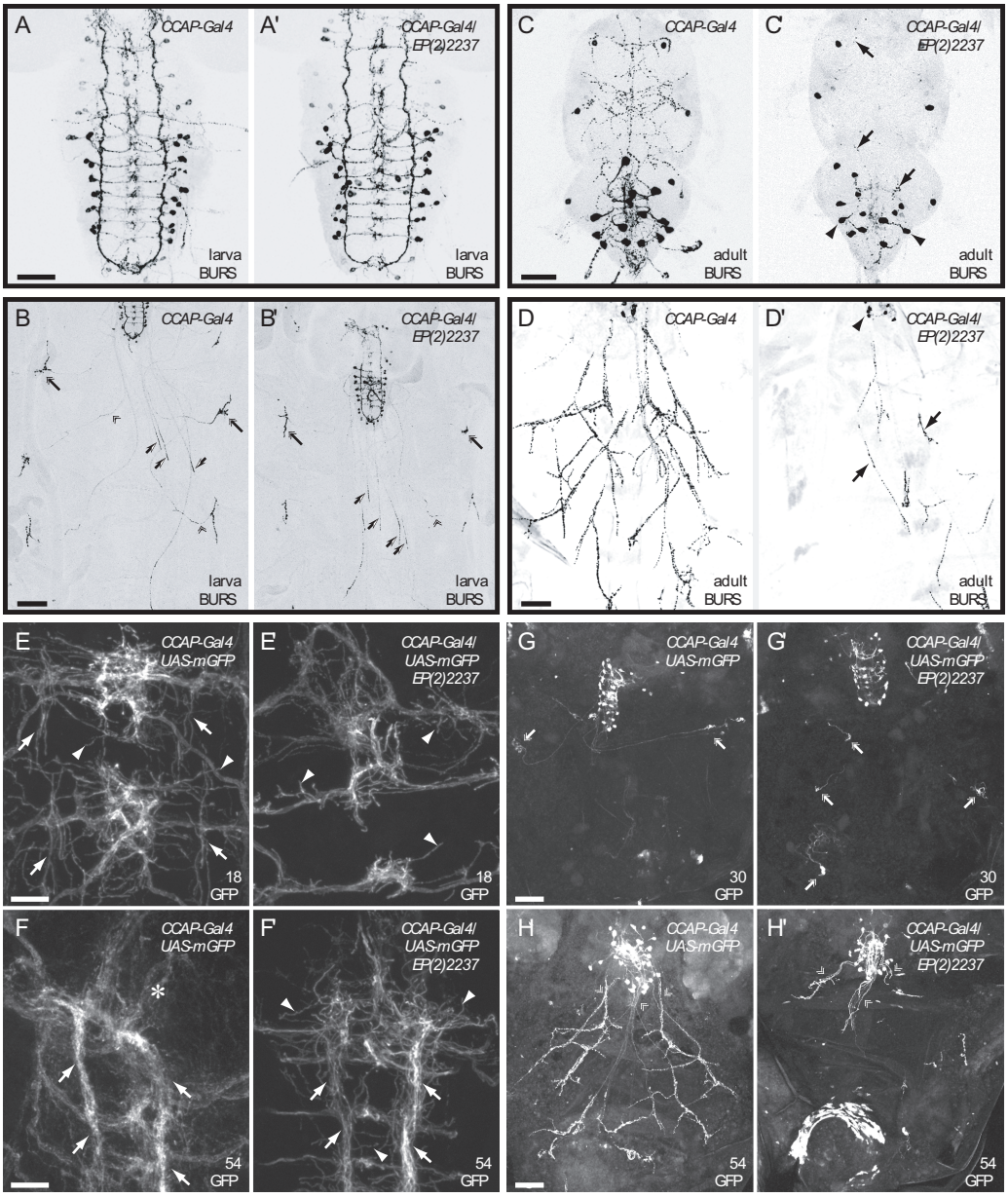
A
CCAP-Gal4
larva
BURS
A'
CCAP-Gal4/
EP(2)2237
larva
BURS
C
CCAP-Gal4
adult
BURS
C'
CCAP-Gal4/
EP(2)2237
adult
BURS
B
CCAP-Gal4
larva
BURS
B'
CCAP-Gal4/
EP(2)2237
larva
BURS
D
CCAP-Gal4
adult
BURS
D'
CCAP-Gal4/
EP(2)2237
adult
BURS
E
CCAP-Gal4
UAS-mGFP
18
GFP
E'
CCAP-Gal4/
UAS-mGFP
EP(2)2237
18
GFP
G
CCAP-Gal4
UAS-mGFP
30
GFP
G'
CCAP-Gal4/
UAS-mGFP
EP(2)2237
30
GFP
F
CCAP-Gal4
UAS-mGFP
54
GFP
F'
CCAP-Gal4/
UAS-mGFP
EP(2)2237
54
GFP
H
CCAP-Gal4
UAS-mGFP
54
GFP
H'
CCAP-Gal4/
UAS-mGFP
EP(2)2237
54
GFP

Figure 2-7.—GOF of *klar* resulted in specific loss of adult-specific bursicon-immunoreactive neurites and loss of 6-8 CCAP/bursicon cell somata. (A-B) Anti-bursicon immunostaining in wandering third instar (A) and P14 pharate adult (B) stage CNS from *CCAP-Gal4/EY(3)00559* animals (A′, B′) and *CCAP-Gal4/+* controls (A, B) (*n*=6-8). Most elements of the CCAP/bursicon cell projection pattern were retained in the larval CNS (A′), but there was a dramatic reduction of central neurites and B_{AG} somata number in the pharate adult (B′). Arrows, traces of remaining neurites; arrowhead, atrophied soma. Scale bars, 50 μm.

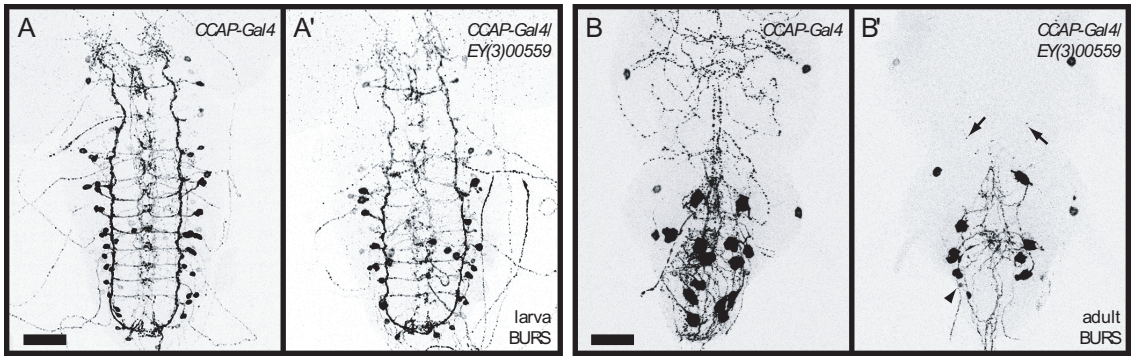
A
CCAP-Gal4
A'
CCAP-Gal4/
EY(3)00559
larva
BURS
B
CCAP-Gal4
B'
CCAP-Gal4/
EY(3)00559
adult
BURS

Figure 2-8.—GOF of the *miR-310-miR-313* microRNA cluster during an early-mid metamorphosis critical period prevented bursicon secretion in adults. (A) *In situ* hybridization (magenta) for *miR-310* (antisense LNA probe) in a wandering third instar larval CNS. Autofluorescence (green) was detected using an FITC/GFP filter set. *EP(2)2587* was expressed under the control of *CCAP-Gal4*. Comparable staining was observed with LNA probes for *miR-312* and *miR-313* (not shown; *miR-311* was not tested). (B) Anti-bursicon staining immediately after eclosion (0 hr AE) and 1 hr after eclosion (1 hr AE) in control flies (*CCAP-Gal4/+*) and flies with *miR-310-miR-313* GOF [*CCAP-Gal4/EP(2)2587*]. (C) Quantification of bursicon levels for the treatments shown in (B) (n=5-6). *, P<0.05; NS, not significant (P=0.000224, 1-Way ANOVA; Tukey-Kramer Multiple-Comparison *post hoc* test). The differences in staining intensities were confirmed by blind scoring. (D) Percentage of adult flies with unexpanded wings (UEW) or partially expanded wings (PEW) following *miR-310-miR-313* GOF at different developmental stages [n=7-119 (41.0±1.1) per point]. All animals had one copy each of *386Y-Gal4*, *EP(2)2587*, and *tubulinP-Gal80^{ts}*. The shift up group (black squares, solid line) was collected as embryos at the permissive temperature (19°) and then shifted at the times shown on the *x* axis to the restrictive temperature (30°). The shift down group (open circles, dashed line) was collected as embryos at the restrictive temperature and then shifted at the times shown to the permissive temperature. The curves are 5th order polynomials—only the center portions of the curves are shown. The gray bar indicates the critical window for the *EP(2)2587* effect on wing expansion: It begins at the shift time that produced wing expansion defects in ~50% of the shift down animals, and it ends at the shift time that produced displayed

wing expansion defects in ~50% of the shift up animals. Scale bars: (A) 50 μm; (B) 100 μm.

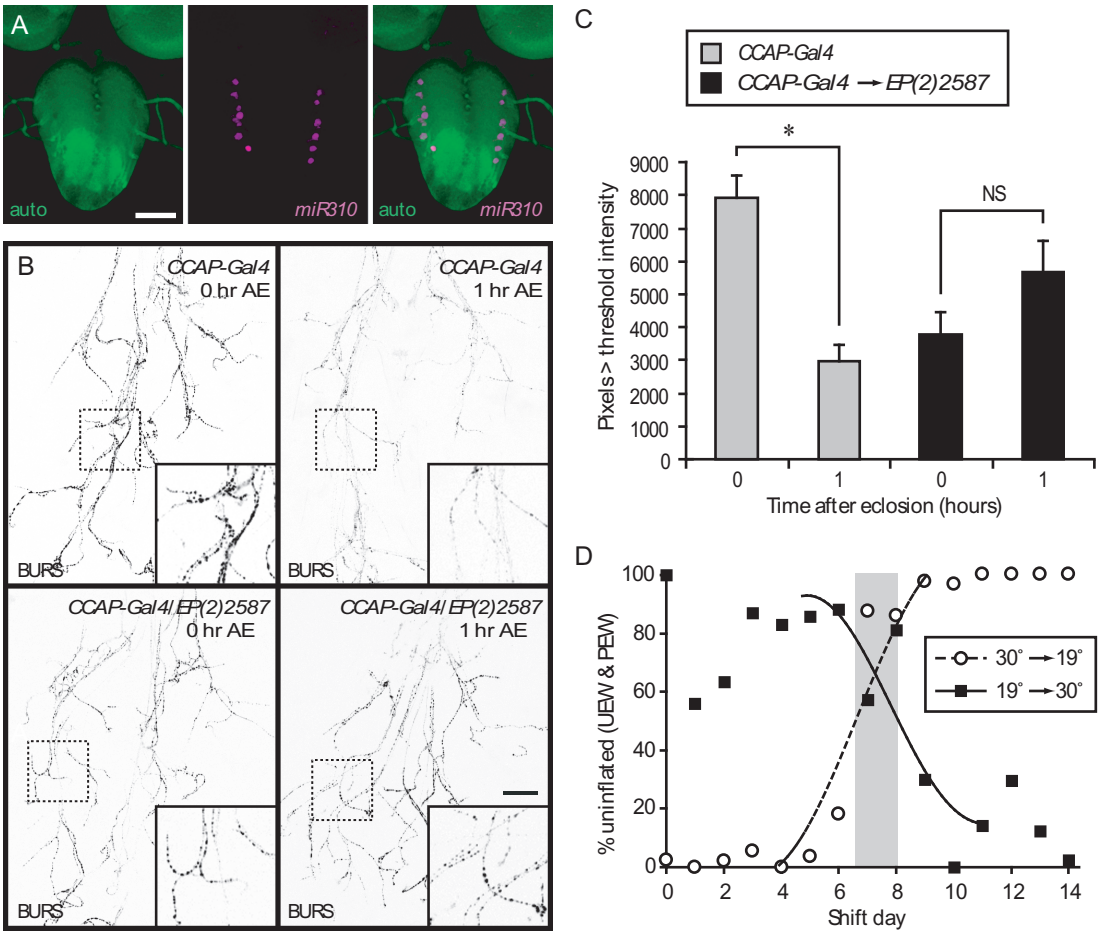
A
auto
miR310
auto
miR310
B
CCAP-Gal4
0 hr AE
CCAP-Gal4
1 hr AE
BURS
BURS
CCAP-Gal4/EP(2)2587
0 hr AE
CCAP-Gal4/EP(2)2587
1 hr AE
BURS
BURS
C
CCAP-Gal4
CCAP-Gal4 → EP(2)2587
*
NS
Pixels > threshold intensity
9000
8000
7000
6000
5000
4000
3000
2000
1000
0
0
1
0
1
Time after eclosion (hours)
D
% uninflated (UEW & PEW)
100
80
60
40
20
0
0
2
4
6
8
10
12
14
Shift day
30° → 19°
19° → 30°

TABLE 2-1

Lines with head eversion, pharate adult lethal, or wing expansion phenotypes with each Gal4 driver

			386Y-Gal4 phenotypes				*c929-Gal4* phenotypes				*CCAP-Gal4* phenotypes			
Symbol	Transposon	Lines[a]	HE	WE	P	Total (%)[b]	HE	WE	P	Total (%)[b]	HE	WE	P	Total (%)[b]
EP	*P(ABDELILAH-SEYFRIED et al.)*	2010	8	13	5	16 (0.8)	1			1 (0.05)	3	12		12 (0.6)
EY	*P{EPgy2}*	3044	9	16	12	31 (1.0)	2	2	1	4 (0.1)	6	12	1	16 (0.5)
WH	*PBac{WH}*	829	1			1 (0.1)	1			1 (0.1)				
XP	*P{XP}*	214	6	4	2	9 (4.2)	2			2 (0.9)	2	6	1	6 (2.8)
Total		6097	24	33	19	57	6	2	1	8	11	30	2	34

Only phenotypes that were visible in at least 5% of the progeny of a cross with *c929-Gal4* or *CCAP-Gal4* were counted. For *386Y-Gal4*, the cutoff was 10% (see Results). HE, head eversion-defective; P, pharate adult lethal; WE, wing expansion-defective.

[a]Total number of lines screened that produced pupae when crossed to *386Y-Gal4*.

[b]Total lines displaying head-eversion, pharate adult lethal, or wing expansion phenotypes.

CHAPTER 3

A Drosophila deficiency screen for modifiers of *split ends*-dependent effects on nerve cell remodeling.

INTRODUCTION

After terminal differentiation, mature neurons display substantial morphological plasticity in support of adaptive changes in the nervous system, such as during learning, puberty, and changes in reproductive status (CHKLOVSKII *et al.* 2004; GARCIA-SEGURA *et al.* 1994; ZEHR *et al.* 2006), or in response to traumatic injury or chronic stress (KADISH and VAN GROEN 2002; SOUSA *et al.* 2008; STEWARD 1982). Numerous external and internal cues must contribute to the regulation of morphological plasticity in mature neurons. However, only a few of these signals have been characterized, and the downstream mechanisms that mediate neuron morphological plasticity remain poorly understood.

Several of the most thoroughly studied examples of morphological plasticity in mature neurons are in holometabolous insects. These species are completely transformed through metamorphosis from vermiform, feeding larvae into highly mobile and reproductively-competent adults. During the metamorphic transition, most larval tissues undergo histolysis, and adult tissues are formed *de novo* from nests of undifferentiated cells that are set aside in the embryo or larva. Within the nervous system, however, many larval neurons are retained through metamorphosis and undergo

extensive remodeling. The larval axons and dendrites are pruned back, and this is followed by the elaboration of morphologically and functionally distinct adult-specific arborizations (TRUMAN 1992a). These changes in morphology are triggered and coordinated globally by circulating steroid hormones, the ecdysteroids, of which the principle active form is 20-hydroxyecdysone (hereafter referred to as ecdysone) (WEEKS 2003).

Intensive research in the fruit fly *Drosophila melanogaster* and tobacco hornworm *Manduca sexta* has focused on the role of ecdysone in directing neurite pruning and subsequent outgrowth in several neuronal cell types, including mushroom body neurons, olfactory neurons, peripheral sensory neurons, motorneurons, serotonergic interneurons, and peptidergic neurosecretory cells (CONSOULAS *et al.* 2000; KUO *et al.* 2006; LEE *et al.* 1999; MARIN *et al.* 2005; ROY *et al.* 2007; SANTOS *et al.* 2006; SCHUBIGER *et al.* 1998; WILLIAMS and TRUMAN 2005; ZHAO *et al.* 2008). More recent work, primarily in Drosophila, has revealed distinct roles for the three ecdysone receptor (EcR) isoforms, EcR-A, -B1, and -B2, in the regulation of pruning versus outgrowth (BROWN *et al.* 2006; HOOPFER *et al.* 2008; KUO *et al.* 2005; LEE *et al.* 2000; ROY *et al.* 2007; SCHUBIGER *et al.* 1998; ZHENG *et al.* 2003). Other signals and cellular processes that are important for pruning include the ubiquitin-proteasome system, extracellular matrix metalloproteases, glial engulfment, and cell adhesion molecules (AWASAKI *et al.* 2006; HEBBAR and FERNANDES 2005; KUO *et al.* 2005; KUO *et al.* 2006; LEE *et al.* 2009; WATTS *et al.* 2003; WATTS *et al.* 2004). A few studies have explored the contributions of different EcR isoforms and ecdysone-response genes to outgrowth (BROWN *et al.* 2006; CONSOULAS *et al.* 2005) and the importance of

pruning and electrical activity in the establishment of the adult arbor (HEBBAR and FERNANDES 2004; WILLIAMS and TRUMAN 2004). However, relatively little attention has been devoted toward understanding the molecular mechanisms underlying metamorphic outgrowth of adult neurites. Here, and in a prior study (ZHAO *et al.* 2008), we have begun to address these questions through genetic studies on remodeling of Drosophila neurosecretory cells.

The CCAP/bursicon neurosecretory cells produce multiple neuropeptides, including crustacean cardioactive peptide (CCAP) and bursicon, that play important roles in the coordination of molting behaviors (BAKER *et al.* 1999; CLARK *et al.* 2004a; DEWEY *et al.* 2004; KIM *et al.* 2006; LUAN *et al.* 2006a; PARK *et al.* 2003). During larval development, the CCAP/bursicon neurons play only a minor role, and their ablation results in subtle, quantitative effects on the timing of behaviors that lead to shedding of the old cuticle at the end of each molt (ecdysis). At the onset of metamorphosis, however, the CCAP/bursicon neurons are essential for events that are associated with pupal ecdysis, including eversion of the pupal head and elongation of the developing adult wings and legs (PARK *et al.* 2003). After the completion of metamorphosis, the CCAP/bursicon neurons are required for the execution of wing expansion behaviors and for plasticization and subsequent tanning of the adult cuticle (PARK *et al.* 2003; PEABODY *et al.* 2009). These changes in the role of the CCAP/bursicon neurons for pupal and adult ecdysis are associated with extensive metamorphic remodeling (ZHAO *et al.* 2008). Pruning of the larval CCAP/bursicon cell dendrites and axons begins soon after the onset of metamorphosis and is completed 24-30 hr after puparium formation (APF). During this period, a subset of the neurons in

the abdominal ganglia also ceases to express bursicon. Outgrowth of new, adult-specific neurites begins as pruning wanes and is completed by about 60 hr APF. During this phase, the diameters of the CCAP/bursicon cell somata within the abdominal ganglia are increased by more than twofold.

Although head eversion and wing expansion behaviors last for only a few minutes, the morphological defects that result from their disruption can be scored readily for several days afterwards. Therefore, the phenotypes are well suited for large-scale genetic screens (BANTIGNIES *et al.* 2000; ZHAO *et al.* 2008). In addition, since head eversion behavior occurs at the onset of CCAP/bursicon cell remodeling, and wing expansion behavior occurs after the reorganization of these neurons is completed, these phenotypes can be used to identify factors that specifically regulate metamorphic remodeling of the CCAP/bursicon cells without affecting their embryonic or larval development. With this goal, we previously conducted a gain-of-function screen by targeting gene misexpression to the CCAP/bursicon neurons (ZHAO *et al.* 2008). We identified 14 loci that perturbed the development of adult-specific neurites without major effects on larval CCAP/bursicon cell morphology. One of the genes, *split ends* (*spen*), encodes the founding member of an extended family of large proteins containing multiple N-terminal RNA-binding (RRM) motifs and a highly conserved C-terminal SPOC (SPEN paralog and ortholog C-terminal) domain that may interact with other transcriptional regulatory proteins (ARIYOSHI and SCHWABE 2003). The SPEN protein family is further subdivided in two subclasses based primarily on size. In *Drosophila*, there are two members of the family, with SPEN representing the large class and

Spenito (NITO) representing the smaller (JEMC and REBAY 2006). Both *spen* and *nito* are ubiquitously expressed in flies (CHANG *et al.* 2008).

Here, we found that SPEN is expressed in the CCAP/bursicon neurons and is required in an additive or synergistic fashion with NITO for normal metamorphic outgrowth of adult neurites. SPEN also acts in a manner that is antagonistic to signaling by the epidermal growth factor receptor (EGFR) and its effector, the monomeric G protein Ras. To identify additional interacting genes, we conducted a deficiency-based screen for modifiers of the SPEN overexpression phenotype in the CCAP/bursicon neurons. A total of 12 of the deficiencies were confirmed as suppressors of SPEN, and six were confirmed as enhancers. After mapping the modifiers for selected deficiencies to individual loci, we found that effects of SPEN on neuronal outgrowth are suppressed by elevated insulin/insulin-like growth factor signaling (IIS) and by reduced expression of subunits of the general transcription factor $TF_{II}D$. In addition, we characterized genetic interactions between SPEN and the Rho GTPases, Rho1 and Rac1, and their effectors Myosin binding subunit (MBS) and PAK-kinase (PAK). These studies indicate a role for SPEN in maintaining proper levels of myosin II activity for axon branching and peripheral accumulation of neuropeptides.

MATERIALS AND METHODS

Stocks and scoring: Flies (*Drosophila melanogaster*) were cultured on standard cornmeal-yeast-agar media at 22-25°. We obtained 449 lines containing Exelixis deficiencies (PARKS *et al.* 2004) on the 1st, 2nd and 3rd chromosomes, covering ~56% of the eukaryotic genome, from the Bloomington Drosophila Stock Center (BDSC). *CCAP-Gal4* (*y* w*; P{Ccap-GAL4.P}16*; FBti0037998) was used to target transgene expression in the CCAP/bursicon neurons (PARK *et al.* 2003), which are a subset of the CCAP neurons that express bursicon. All other alleles were obtained from the BDSC, the Harvard Exelixis Collection (THIBAULT *et al.* 2004), or individual laboratories.

Unless stated otherwise, experimental crosses were performed at an elevated temperature of 29° to increase the strength of Gal4-mediated transgene expression. Defects in wing expansion were scored as described by Luan *et al.* (2006a). Three classes of adult phenotypes were recorded: unexpanded wings (UEW), partially expanded wings (PEW), and expanded wings. Defects in pupal head eversion were classified as cryptocephal or microcephal as described by Zhao *et al.* (2008).

Immunochemistry and staining quantification: Immunostaining was performed as previously described (ZHAO *et al.* 2008). Briefly, central nervous system (CNS) or whole animal fillet preparations were obtained from wandering larvae and staged pupae (BAINBRIDGE and BOWNES 1981), dissected in calcium-free saline, fixed in either 4% paraformaldehyde (PFA) or 4% paraformaldehyde/7% picric acid (PFA-PA), incubated with different antisera overnight at 4˚, and then washed and incubated

with the secondary antisera overnight at 4˚. We used antisera directed against the following proteins: CCAP (1:4000, PFA/PA) (PARK *et al.* 2003), Bursicon α-subunit (1:5000, PFA/PA) (LUAN *et al.* 2006a), Green fluorescent protein (GFP) (1:500, PFA) (Invitrogen, Carlsbad, CA), and Split ends (SPEN) (1:50, PFA) (CHEN and REBAY 2000).

Image quantification was performed as described (ZHAO *et al.* 2008) on confocal *z*-series projections obtained with an Olympus FluoView FV500 microscope (Olympus, Center Valley, PA). For better visualization of the fine cellular processes, grayscale images were inverted in Adobe Photoshop (San Jose, CA). Except where indicated, test and control preparations, and preparations in each developmental time series, were stained in parallel and imaged and quantified using identical settings.

Modifier screen: Screening for modifiers on the second chromosome was performed by crossing *w^{1118}; CCAP-Gal4, EP(2)2583/CyO, Ubi-GFP; +/+* virgin females to Oregon R males (controls) and males from each stock containing a second chromosome Exelixis deficiency. These crosses were performed at 18° to increase the chances of observing suppression of the *spen* GOF phenotype. Most of the second chromosome deficiencies were maintained as balanced stocks with *CyO*. The *Curly*-winged adult progeny of these crosses (*Df/CyO, Ubi-GFP* and some of the *CCAP-Gal4, EP(2)2583*/*CyO* adults) were discarded. The remaining straight-winged, PEW, or UEW progeny were therefore of the genotypes *CCAP-Gal4, EP(2)2583*/*Df* or *CCAP-Gal4, EP(2)2583*/*CyO*. Prior to February 2007, the UEW rate in the control crosses was close to 100%, and suppression of the *spen* GOF phenotype was therefore indicated by the

presence of PEW progeny. Enhancement of the *spen* GOF phenotype was scored through the appearance of pupal head eversion defects.

For screening on the third chromosome, we crossed w^{1118}*; CCAP-Gal4, EP(2)2583/CyO, Ubi-GFP; +/+* virgin females to Oregon R (control) and Exelixis deficiency males at 18°. Most of the third chromosome deficiencies were balanced over *TM6B,* Tb^1. During our screening of the third chromosome, the control crosses began to produce some PEW progeny. Therefore, the third chromosome screening was conducted in two phases, with phase one generally before the appearance of PEW in the controls, and phase two after that time. In phase one, the *Curly*-winged adult progeny of these crosses (*CyO, Ubi-GFP/+; Df/+* or *CyO, Ubi-GFP/+; TM6,* Tb^1*/+*) were discarded, and the remaining adults (*CCAP-Gal4, EP(2)2583/+; Df/+* or *CCAP-Gal4, EP(2)2583/+; TM6,* Tb^1*/+*) were scored for wing expansion. As for the second chromosome, suppression of the *spen* GOF phenotype was indicated by the presence of straight-winged progeny, and enhancement was detected through scoring of pupal head eversion. In phase two, all *Tubby* pupae (*CyO, Ubi-GFP/+; TM6,* Tb^1*/+* or *CCAP-Gal4, EP(2)2583/+; TM6,* Tb^1*/+*) were removed daily from the vials. The *Curly*-winged adult progeny of these crosses (*CyO, Ubi-GFP/+; Df/+*) were discarded, and all remaining progeny (*CCAP-Gal4, EP(2)2583/+; Df/+*) were scored for wing expansion. For these crosses, either suppression or enhancement was detectable through changes in the percentage of UEW adults, but pupal head eversion was also monitored to detect strong enhancers.

For the first chromosome deficiencies (balanced over *FM7c* or *Binsinscy*), the sexes of the parental flies were reversed, and crosses were again performed at 18°. All

Bar-eyed and *Curly*-winged adult progeny were discarded, and only the *Df, w^{1118}/+; CCAP-Gal4, EP(2)2583/+; +/+* progeny were scored for wing expansion.

For each cross, we calculated an enhancement or suppression index, using values from the test cross and pooled values for all control crosses conducted during a similar time period. For enhancement, the index was calculated as (percentage $UEW_{test\ cross}$ - percentage $UEW_{control\ cross}$/1 - percentage $UEW_{control\ cross}$), and we set arbitrary thresholds of >75%, >85%, and no adults for classification of weak, moderate, and strong enhancers, respectively. For suppression, the index was calculated as (percentage $UEW_{control\ cross}$ - percentage $UEW_{test\ cross}$/percentage $UEW_{control\ cross}$), and we set arbitrary thresholds of >15%, >21%, and >35% for classification of weak, moderate, and strong suppressors. After repeating crosses to confirm modifier activity (or when the number of adult progeny was <10), some of the confirmed, strongest modifiers (mostly suppressors) were selected for mapping to single genes. Most of the Exelixis deficiencies contained fewer than 25 completely or partially deleted genes. We identified representative alleles for these genes by selecting known loss-of-function mutations or transposon insertions likely to disrupt transcripts, and tested these alleles for modifier activity using crosses similar to those used for each of the deficiencies. When these alleles displayed modifier activity, we repeated the crosses for confirmation.

RESULTS

Targeted expression of *EP(2)2583* interfered with CCAP/bursicon neuron remodeling: We previously reported that forced misexpression of the *EP(2)2583* element in the CCAP/bursicon neurons led to the loss of adult-specific neurites during metamorphosis (ZHAO *et al.* 2008). We repeated and extended these results here by performing anti-bursicon immunostaining on *CCAP>EP(2)2583* (*CCAP-Gal4/EP(2)2583*) animals at the wandering third instar larval stage, near the onset of metamorphosis, and at the P14 pharate adult stage, after metamorphosis was completed (Figures 3-1 and 3-2). In wandering larvae, the CCAP/bursicon neuron somata and efferent projections in *CCAP>EP(2)2583* were close to indistinguishable from those of *CCAP-Gal4/+* controls (Figures 3-1A, 3-1B, 3-2A, and 3-2B). In contrast, the adult CCAP/bursicon neurons were profoundly altered by *EP(2)2583* expression. In the CNS, most of the adult CCAP/bursicon cell somata were still visible, but they were reduced in diameter and more weakly bursicon immunoreactive (Figure 3-1D). The lateral subesophageal LSE neurons in particular were often either undetectable or very weakly labeled, as were most of the neurite projections in the brain lobes and ventral nerve cord. In the periphery, most of the adult axonal arbor was either absent or very weakly labeled, although we often observed a few axons along the ventral midline (Figure 3-2D). The midline axons arise from the B_{AG}^{p} neurons and exit the CNS via the medial abdominal nerve trunk. Consistent with the peripheral phenotype, the B_{AG}^{p} somata were larger and more strongly immunoreactive for bursicon than the B_{AG}^{a} somata (Figure 3-1D) and therefore appeared to be less sensitive to *EP(2)2583* expression.

All of these observations were confirmed in animals in which *CCAP-Gal4* was used to co-express *UAS-mCD8::GFP*, a fluorescent membrane marker, and *EP(2)2583* (data not shown). Although it is also possible that these phenotypes were due to the cessation of CCAP (*CCAP-Gal4*) and bursicon expression, this does not appear to be the sole cause, since reduced CCAP and bursicon expression alone would not account for the reduced size and extent of the remaining neuritic arbor. Thus, our initial results showed that *EP(2)2583* expression selectively disrupted either the metamorphosis of the CCAP/bursicon neurons or led to the loss of adult features after they were formed.

To determine whether the strength of these phenotypes could be moderated at lower temperatures, we evaluated the effects of *EP(2)2583* expression in the CCAP/bursicon neurons on pupal ecdysis and wing expansion at 29°, 25°, and 18°. At 29°, 100% of the adults had unexpanded wings (UEW; n=124). In addition, 20% of these pupae (n=48) displayed a microcephal phenotype, consistent with partial disruption of head eversion. At 25°, 98% of the adults were UEW (n=88), and all of the pupae completed head eversion normally. We observed a further reduction in the penetrance of the wing expansion defects at 18°, with 81% UEW and 19% PEW among the adult progeny (n=74). Reduced temperatures also led to less severe defects in the adult morphology of the CCAP/bursicon neurons. At 25° (versus 29°), many more axons were present, although there were fewer fine branches, the expression of the *UAS-mCD8::GFP* reporter was reduced, and axonal varicosities were smaller in diameter (Figure 3-3).

***EP(2)2583* drives SPEN overexpression:** The *EP(2)2583* insertion site was mapped to an intron of the *spen* gene, 1127 bp upstream of exon 2 (ZHAO *et al.* 2008). Exon 2 contains the translation initiation site, indicating that *EP(2)2583* drives the expression of functional *spen* transcripts. This was confirmed through anti-SPEN immunostaining on the CNS of third instar larvae (Figure 3-4). In controls (*CCAP-Gal4, UAS-CD8::GFP/+*), SPEN was expressed in most if not all CNS neurons, including the CCAP/bursicon neurons (Figure 3-4A) . SPEN protein was mostly localized in nuclei, consistent with reports that it may function as a transcriptional regulator (CHEN and REBAY 2000; KUANG *et al.* 2000; WIELLETTE *et al.* 1999). When *CCAP-Gal4* was used to drive *EP(2)2583* (*CCAP-Gal4, UAS-CD8::GFP/EP(2)2583*), we observed elevated nuclear SPEN immunostaining in the CCAP/bursicon neurons (Figure 3-4B). These results demonstrate that SPEN was normally expressed in the CCAP/bursicon neurons, and targeted expression of *EP(2)2583* led to a cell-autonomous increase in SPEN levels. Therefore, the mutant phenotypes produced by *EP(2)2583* reflected overexpression rather than ectopic expression of SPEN in the CCAP/bursicon neurons.

SPEN overexpression blocks axon outgrowth: The loss of peripheral CCAP/bursicon cell peripheral axons may have arisen due to inhibition of axon outgrowth or cellular atrophy later during metamorphosis. To distinguish between these alternatives, we examined the temporal changes in the peripheral projections of the CCAP/bursicon neurons following SPEN overexpression either with or without *EP(2)2583* misexpression at 25° during metamorphosis. We used mCD8::GFP

(combined with anti-GFP immunostaining) to label the peripheral projections of the CCAP/bursicon neurons at 0, 12, 18, 48, and 60 hr after puparium formation (APF). In control animals, most of the pruning back of the larval axon arbor is completed within the first 18 hr APF, and outgrowth of the adult arbor is observed between 18 hr and 60 hr APF (ZHAO *et al.* 2008). During the first 18 hr APF, the extent and time course of pruning did not appear to be altered by SPEN overexpression (Appendix 2, Supplemental Figure S1-1). However, once pruning was completed, subsequent outgrowth of the CCAP/bursicon axons was attenuated (Figure 3-5). At 48 hr APF, most of the initial axonal processes were present in the wild type animals (Figure 3-5A), although the arbor had not yet extended to the full adult size. Over the course of the next 12 hr, the arbor continued to extend to form an adult-like network (Figure 3-5B). Following SPEN overexpression, only a few peripheral axons were visible at 48 hr (Figure 3-5C), and little further extension was observed by 60 hr (Figure 3-5D). However, by stage P14, which occurs 87-103 hr APF (BAINBRIDGE and BOWNES 1981), the longest axons reached a similar distance from the CNS as controls, although fewer higher order branches were formed (Figure 3-3 and data not shown). Therefore, SPEN overexpression slowed axon outgrowth and partially blocked axon branching during metamorphic remodeling of the CCAP/bursicon cell peripheral axons.

SPEN promotes axon branch and bouton formation: The above results were based on SPEN overexpression. If SPEN is normally involved in regulating neuronal remodeling during metamorphosis, then we expected that loss of SPEN would also alter axonal outgrowth during remodeling of the CCAP/bursicon neurons. In embryos, loss

of *spen* produces axon fasciculation defects (KOLODZIEJ *et al.* 1995). However, *spen* null mutations are recessive embryonic lethal (CHEN and REBAY 2000). Therefore, we used *CCAP-Gal4* to drive cell-targeted expression of two dominant negative *spen* constructs (*spen-ΔC* and *spen-ΔN*) to test the hypothesis that SPEN is required for CCAP/bursicon cell axonal remodeling. The encoded proteins, SPEN-ΔC and SPEN-ΔN, lack the C-terminal SPOC domain and N-terminal RRM motifs, respectively. When expressed in other tissues, either *spen-ΔC* or *spen-ΔN* can phenocopy loss-of-function *spen* alleles (CHEN and REBAY 2000; LIN *et al.* 2003).

The *spen-ΔC* construct behaved as a weaker dominant negative allele, and *CCAP-Gal4/+; UAS-spen-ΔC/+* flies had normal wings at 25°. With two copies of the *CCAP-Gal4* driver and UAS element (*CCAP-Gal4; UAS-spen-ΔC*), 65% of the flies displayed UEW (n=195). In contrast, expression of one copy of *spen-ΔN* in the CCAP/bursicon neurons (*CCAP-Gal4/UAS-spen-ΔN;+/+*) resulted in 100% UEW adults at 25° (n=45). Therefore, we used *spen-ΔN* to look for effects on metamorphic remodeling of the CCAP/bursicon neurons (Figure 3-6A). In pharate adult animals, the peripheral axons were present, in the same abdominal nerves, and they extended a normal distance from the CNS. However, we noted three differences. First, fewer higher order, distal branches were formed in the peripheral axonal arbor. Second, in their place there were accumulations of bursicon immunoreactive material in club-shaped endings at the distal axon tips. Finally, there were fewer bursicon-immunoreactive boutons along the more proximal portions of each axon (Figure 3-6A′). These observations reveal a role for SPEN activity in the formation of distal axon

branches and proximal boutons during outgrowth of the CCAP/bursicon peripheral axon arbor.

As shown above, SPEN dominant negative (*spen-ΔN*) and SPEN overexpression (*EP(2)2583*) constructs produced similar defects in axon outgrowth and branching. If the truncated SPEN-ΔN and SPEN-ΔC proteins were simply adding to overall levels of SPEN, then expression of *spen-ΔN* or *spen-ΔC* together with *EP(2)2583* would be expected to result in an additive effect. However, if SPEN-ΔN and SPEN-ΔC each block SPEN activity by inhibiting its ability to interact properly with its targets, then additional SPEN expression would be expected to counteract the effects of the dominant negatives. Both *spen-ΔN* and *spen-ΔC* substantially reduced the percentage of UEW flies in the *EP(2)2583* background (Table 2-1). This result provides additional confirmation that *spen-ΔN* and *spen-ΔC* acted as dominant negatives in the CCAP/bursicon neurons.

To further confirm the necessity of SPEN activity for axon outgrowth in the CCAP/bursicon neurons, we expressed two independent *spen* RNAi constructs: *spen^{RNAi}-7* (CHANG *et al.* 2008) and *spen^{RNAi}-49543* (*P{GD16317}v49543*) (DIETZL *et al.* 2007) in these cells. The two RNAi constructs target distinct segments of the *spen* mRNA coding sequence that are shared by all known *spen* mRNA isoforms. When we crossed these constructs to *CCAP-Gal4*, neither produced wing expansion defects among the adult progeny. Therefore, we added *UAS-dicer-2* to the crosses, since Dicer-2 increases the strength of RNAi for many target genes (DIETZL *et al.* 2007). With Dicer-2, both constructs produced 100% UEW adults at 29°, 25° and 18° (n = 45-104). The *spen* RNAi also reduced expression of SPEN protein (Appendix 2, Supplemental

Figure 3-2) and produced defects in the adult peripheral arbor that closely resembled the *spenΔN* phenotype, including fewer distal branches, fewer proximal boutons, and club-shaped, strongly bursicon-immunoreactive distal axon endings (Figure 3-6B). Taken together with our observation that SPEN is normally expressed ubiquitously in the pupal CNS (Figure 3-4A), these results demonstrate that SPEN function is required in the CCAP/bursicon neurons for outgrowth of the adult axon arbor.

Additive or synergistic interactions between NITO and SPEN: The two members of the SPOC protein family in Drosophila, SPEN and NITO, display functional antagonism during eye development (JEMC and REBAY 2006). However, SPEN and NITO act synergistically in regulating Wingless signaling in the wing imaginal disc and cultured Kc cells, and several studies in vertebrates also suggest that the relationship between these two proteins is context dependent (CHANG *et al.* 2008). Similar to SPEN, NITO is broadly expressed in Drosophila tissues (CHANG *et al.* 2008). Therefore, we investigated the function of NITO and its possible interactions with SPEN in the context of remodeling of the CCAP/bursicon neurons.

We used *CCAP-Gal4* to drive NITO overexpression (*UAS-myc.nito*) (JEMC and REBAY 2006). At 18° and at 29°, the adult progeny of this cross displayed 100% UEW (n=150, n=11). NITO overexpression in the CCAP/bursicon neurons (at 18°) also produced markedly decreased somata sizes, reduced cell number, and a severely diminished peripheral arbor (Appendix 2, Supplemental Figure S2-3). These cellular defects closely resemble the effects of SPEN overexpression at 29° (Figure 3-1). At lower rearing temperatures (18° or 25°), SPEN overexpression produced much milder

phenotypes (Figure 3-3, and data not shown). Therefore, the defects resulting from NITO overexpression were similar to but more severe than those observed in response to SPEN overexpression.

We then asked whether NITO and SPEN act additively or synergistically to regulate CCAP/bursicon cell remodeling. To test this hypothesis, we used *CCAP-Gal4* to drive co-expression of a *nito* RNAi construct, *UAS-nito^{RNAi}-20942* (*P{GD9850}v20942*), and *dicer-2*. We observed 23% UEW (n=148) among the adult progeny of this cross (*UAS-dicer2, w^{1118}/+; CCAP-Gal4*), consistent with a requirement for NITO during metamorphosis of the CCAP/bursicon neurons. A second, independent *nito* RNAi line, *UAS-nito^{RNAi}-R* (JEMC and REBAY 2006), produced straight-winged adult progeny when crossed to *CCAP-Gal4* without *UAS-dicer-2* (data not shown). Despite the absence of an effect on wing expansion alone, *UAS-nito^{RNAi}-R* (without Dicer-2) was able to strongly suppress the UEW phenotype observed with *EP(2)2583* (Table 3-1). Thus, SPEN and NITO appear to function additively or synergistically in the CCAP/bursicon neurons.

SPEN interactions with EGFR signaling: In developing adult photoreceptor neurons, imaginal discs, and midline glial cells in the embryonic CNS, SPEN is a context-dependent regulator of signaling by epidermal growth factor (EGRF) and its downstream effector, the monomeric GTPase Ras (CHEN and REBAY 2000; DICKSON *et al.* 1996; DOROQUEZ *et al.* 2007; KUANG *et al.* 2000; REBAY *et al.* 2000; THERRIEN *et al.* 2000). Therefore, we investigated whether manipulation of EGFR/Ras signaling could modify wing expansion defects produced by SPEN overexpression in the

CCAP/bursicon neurons. When we co-expressed SPEN together with dominant negative EGFR (*Egfr*^{DN}) (BUFF *et al.* 1998), the UEW rate was enhanced from 85% to 100% (Table 3-1). In contrast, the wing expansion phenotype was partially suppressed when *EP(2)2583* was coexpressed with positively-acting components of the EGFR pathway (Table 3-1): EGFR (*UAS-Egfr*^{B}) (BUFF *et al.* 1998), Ras [*Ras oncogene at 85D* (*Ras85D*); *UAS-Ras*^{WT}] (KARIM and RUBIN 1998), and a constitutively active mutant form of Ras (*UAS-Ras*^{v12}) (KARIM and RUBIN 1998; SEEBURG *et al.* 1984). When *UAS-spen* was omitted from the crosses, expression of EGFR^{B} or Ras^{v12} did not produce wing expansion defects (data not shown). In addition, the suppression observed with wild type Ras was much less pronounced than with Ras^{v12}, consistent with previous observations that Ras^{v12} is much stronger enhancer of EGFR signaling (FORTINI *et al.* 1992; KARIM and RUBIN 1998; SEEBURG *et al.* 1984).

The one apparent exception to the general trend of these results was with dominant negative Ras (*UAS-Ras*^{N17}) (FEIG 1999; LEE *et al.* 1996), which showed weak suppression of SPEN. In the regulation of Drosophila prothoracic gland growth, Ras^{N17} was an ineffective allele while Ras^{v12} was a strong allele (CALDWELL *et al.* 2005). Ras^{N17} has a decreased affinity for GTP, and it may compete with endogenous Ras for common cellular sites, with their ratio determining the degree of signaling in the cell (FEIG and COOPER 1988). Therefore, the expression of *UAS-Ras*^{N17} may not be sufficiently strong to inhibit Ras in this context. Alternatively, there may be downstream targets of EGFR and SPEN that can be activated by Ras (e.g., by Ras^{v12}) but are normally activated by Ras-independent mechanisms. Taken together, the above genetic interactions suggest that SPEN negatively regulates EGFR/Ras signaling in the

CCAP/bursicon neurons. However, these results are based primarily on effects of SPEN/EGFR/Ras overexpression, and confirmation of this genetic interaction will require further investigation with loss-of-function alleles.

Deficiency screen for SPEN modifiers: The above genetic interaction experiments between *spen*, *nito*, and *Egfr*/*Ras* indicated that these phenotypes are sensitive to epistatic interactions. Therefore, to identify genes that interact with SPEN in controlling CCAP/bursicon cell remodeling, we conducted a genetic screen for modifiers of the UEW phenotype produced by SPEN overexpression.

We performed the modifier screen with 449 Exelixis, DrosDel, and Bloomington Stock Center (BSC) deficiencies with isogenic backgrounds and sequence-defined breakpoints (Appendix 2, Supplemental Table S2-1). Together, these deficiencies covered ~56% of the euchromatic genome. Based on changes in the ratio of UEW adult progeny relative to control crosses without a deficiency, we calculated an enhancement or suppression index for each cross (see Materials and Methods) to identify candidate modifiers. Initially, the percentage of UEW adults in *CCAP-Gal4, EP(2)2583/+* control flies was close to 100%, and we focused on identifying candidate suppressors—these crosses produced elevated numbers of PEW adults. In addition, we were able to identify two enhancers, *Df(3L)Exel6135* and *Df(3R)Exel6263*, that produced no adults in the cross and pupal head eversion defects. Over a period of several months, however, the control UEW percentage drifted (presumably due to selective forces within the control stock), with gradually increasing numbers of PEW progeny. This allowed the easier identification of both enhancers and suppressors. For

subsequent analysis, we focused primarily on suppressors in order to favor isolation of factors involved in direct molecular interactions with SPEN.

We identified a total of 13 suppressors and 6 enhancers that were confirmed as modifiers in repeated crosses (Table 3-2). All of the confirmed modifier deficiencies were located on the third chromosome, with a majority on 3R. The most likely reason for this was the shift in control UEW rates, which may have produced a more sensitized background for detection of modifiers. Most of the crosses performed later in the screen were with deficiencies on the third chromosome, and deficiencies on the right arm of the third chromosome were tested last.

Identification of single-gene modifiers: In order to identify genes responsible for the modification produced by deficiencies, we tested representative or candidate mutant alleles for all genes, for which stocks were available, contained within the genomic regions defined by five of the stronger suppressors. We performed similar mapping, though not to completion, for two enhancers (Appendix 2, Supplemental Table S2-1). In each case, we successfully identified dominant, single-gene modifiers (Table 3-2). Generally, with the exception of *Df(3R)Exel6148*, we identified multiple (2-7) modifier genes for each deficiency. For *Df(3L)Exel6123*, *Df(3R)Exel6144*, *Df(3R)Exel6148*, and *Df(3R)Exel6265*, the modifiers were the same sign (enhancer or suppressor) as the deficiency and of equal or lesser strength. With two of the other suppressor deficiencies [*Df(3L)Exel6127* and *Df(3R)Exel6216*], we obtained a mixture of single-gene suppressors and enhancers, although the balance in the number and/or strength of the modifiers appeared to be in favor of the suppressors. Therefore, in most

cases, the combined effects of the disruption of two or more genes contributed to the modifier activity displayed by the deficiencies isolated in our screen.

For nine of the genes in Table 3-2, the initially available alleles for mapping were transposon insertions with the potential to drive *CCAP-Gal4*-dependent misexpression of flanking promoters. For two of the suppressors in this group, *N-methyl-D-aspartate-type glutamate NMDA receptor 1* (*Nmdar1*), and *Invadolysin*, we later confirmed that the suppressor activity was due to a dominant, loss-of-function effect in crosses with additional alleles (Table 3-2). However, for three other genes [*HGTX*, *Ras homology enriched in brain* (*Rheb*), and *meiosis I arrest* (*mia*)], our results with multiple alleles suggest that these genes function as suppressors of SPEN only when they are overexpressed (Table 3-2 and Appendix 2, Supplemental Table 3-2). For the other four genes in this group (*CG12746*, *CG6744*, *CG12054*, and *CG31005*), it will be necessary to test additional alleles when they become available to determine whether the epistasis results from loss- or gain-of-function mutations.

Insulin/insulin-like growth factor signaling (IIS) suppressed the SPEN overexpression phenotype: *Rheb* functions as a component of the IIS pathway in the regulation of cellular growth (WULLSCHLEGER *et al.* 2006). Therefore, stimulation of the IIS pathway may suppress the SPEN overexpression phenotype through positive effects on cell growth. To test this hypothesis, we investigated whether other components of the IIS pathway could also modify the defects produced by SPEN overexpression (Table 3-1). Co-overexpression of *Insulin-like receptor* (*InR*) with *spen* in the CCAP neurons led to strong suppression of the UEW phenotype, as compared to

control preparations with expression of *EP(2)2583* alone. We also tested the effects of three *InR* mutants (InR^{R418P}, InR^{A1325D} and InR^{del}), each of which is thought to be constitutively active, based on conserved mutations that produce constitutively active InR in vertebrate cells (FLYBASE_CONSORTIUM 2003; WU *et al.* 2005). Two of the three constitutively active *InR* mutants, InR^{R418P} and InR^{A1325D}, showed robust suppression, although the third one, InR^{del} (which has not yet been confirmed to display constitutive activity in Drosophila cells) did not. In contrast, a loss-of-function allele of *InR* (InR^{E19}) produced dominant enhancement of the wing expansion defects produced by SPEN overexpression. The percentage of UEW adults was also increased by co-expression of dominant negative InR (InR^{K1409A}) with *EP(2)2583* (Table 3-1). Finally, we tested for effects of Pi3K (Pi3K92E), a downstream effector in the IIS pathway (YENUSH *et al.* 1996), on the SPEN overexpression phenotype. We used *CCAP-Gal4* to co-express *EP(2)2583* with either wild type or mutant Pi3K in the CCAP/bursicon neurons. Wild type and constitutively active Pi3K ($Pi3K92E^{CAAX}$) each suppressed the wing expansion defects produced by SPEN overexpression. In contrast, expression of the dominant negative form of Pi3K ($Pi3K92E^{A2860C}$) showed enhancement. Therefore, the IIS pathway attenuates the effects of SPEN overexpression on CCAP/bursicon cell outgrowth during metamorphosis.

SPEN interactions with the general transcription factor $TF_{II}D$: Among the dominant modifiers of SPEN overexpression, we identified *TBP-associated factor 4* (*Taf4*) and *meiosis I arrest* (*mia*, *Taf6*) as strong suppressors that were uncovered by *Df(3L)Exel6127* and *Df(3R)Exel6144*, respectively (Table 3-2). Taf4 and Mia/Taf6 are

two essential components of a large protein complex and general transcription factor, $TF_{II}D$ (MICHEL *et al.* 1998; WEINZIERL *et al.* 1993; WRIGHT *et al.* 2006). After binding to promoters during the early stages of transcription, $TF_{II}D$ recruits other complexes, including RNA polymerase II (ORPHANIDES *et al.* 1996). When crossed into the *CCAP>EP(2)2583* background, the EMS allele $Taf4^{1}$ suppressed the effects of SPEN overexpression on neurite and soma growth in the CNS (Appendix 2, Supplemental Figure S2-4), although growth of the peripheral axon arbor was not affected (data not shown). Therefore, SPEN may function as a transcriptional coactivator for genes involved in dendrite development through interactions with $TF_{II}D$. These findings are consistent with another recent study, which implicated Taf4 in the morphogenesis of dendrites in embryonic *Drosophila* peripheral sensory neurons (KOLODZIEJ *et al.* 1995).

Rho1 and MBS interact with SPEN to regulate axonal outgrowth: In addition to *Taf4*, we identified a second suppressor, *Myosin binding subunit* (*Mbs*), within *Df(3L)Exel6127*. MBS negatively regulates myosin II activity (HARTSHORNE *et al.* 1998b; MIZUNO *et al.* 2002). The Mbs^{3} allele is a strong loss-of-function mutation that can promote myosin II activity and suppress phenotypes produced by myosin down-regulation (MIZUNO *et al.* 2002). In our wing expansion assay, Mbs^{3} produced dominant, moderate-strength suppression of the wing expansion defects produced by SPEN overexpression (Table 3-2). Mbs^{3} also produced dominant, partial suppression of the CCAP/bursicon axon branching defects observed in the peripheral projections (Figure 3-7). The effects of MBS and SPEN on axonal outgrowth were not simply additive (or subtractive), since the CCAP/bursicon neurons of Mbs^{3}/+ animals without

SPEN overexpression developed a normal peripheral arbor (data not shown). This interaction led us to hypothesize that SPEN regulates outgrowth by affecting actin dynamics or by inhibiting myosin II, perhaps through stimulation of MBS activity.

To test this hypothesis, we first looked for genetic interactions with mutant alleles of genes encoding three known regulators of F-actin dynamics in Drosophila neurons, Wiskott-Aldrich syndrome protein (WASp), LIM-kinase 1 (LIMK1), and the Drosophila cofilin/actin depolymerisation factor, Twinstar (TSR) (BOGDAN *et al.* 2004; COYLE *et al.* 2004; MENZEL *et al.* 2007; NG 2008; NG and LUO 2004; RODAL *et al.* 2008). WASp promotes *de novo* actin polymerization, TSR promotes actin de-polymerization, and LIMK1 inhibits TSR to inhibit actin de-polyerization (LUO 2002). Single copies of two putative *WASp* null alleles, $WASp^{1}$ and $WASp^{3}$ (BEN-YAACOV *et al.* 2001; COYLE *et al.* 2004), failed to modify the severity of the wing expansion defects produced by SPEN overexpression (data not shown). We also saw no modification of the wing expansion phenotype following co-misexpression of SPEN with HA-tagged LIMK1 ($UAS\text{-}LIMK1^{Scer\backslash UAS.T:Ivir\backslash HA1}$) (NIWA *et al.* 2002), wild-type TSR ($UAS\text{-}Tsr^{N}$) (NG and LUO 2004), or constitutively active TSR ($UAS\text{-}TSR^{S3A}$) (ANG *et al.* 2006). RNAi to *LIMK1* ($UAS\text{-}LIMK^{IR}$) (NG and LUO 2004) also had no effect (data not shown). Therefore, we found no evidence for genetic interactions between *spen* and regulators of F-actin.

MBS is a component of myosin light chain phosphatase (MLCP), which dephosphorylates the myosin regulatory light chain (MRLC) to inactivate Myosin II. MLCP is negatively regulated through phosphorylation of MBS by Rho-associated kinase (RHOK), and RHOK is stimulated by Rho1 (KIMURA *et al.* 1996b; LEE and

TREISMAN 2004b; NAKAI *et al.* 1997). Therefore, we reasoned that enhanced Rho1 signaling should suppress the defects induced by SPEN overexpression. To test this hypothesis, we co-overexpressed SPEN and Rho1 under the control of the *CCAP-Gal4* driver. In control animals at 29°, expression of Rho1 alone did not affect wing expansion (data not shown). At a lower temperature of 18°, where overexpression of SPEN alone produced 61% UEW, co-expression of Rho1 with SPEN yielded 100% suppression of the severe wing expansion phenotype (0% UEW, n=75). At a cellular level, Rho1 also produced modest suppression of the CCAP/bursicon axon branching defects observed in the peripheral arbor (Data not shown). This effect was comparable to the suppression seen in Mbs^{3}/+ animals (Figure 3-7A, B). Reduced Rho1 function enhanced the UEW phenotypes induced by *spen* overexpression. Two LOF alleles, $Rho1^{72O}$ and $Rho1^{72F}$ (STRUTT *et al.* 1997), both increased the UEW rate from 35% (n= 100) to 100% (n = 23 and 29 females, respectively). Co-expression of dominant negative Rho1, $Rho1^{N19}$ (*P{UAS-*$Rho1^{N19}$*}2.1*) (STRUTT *et al.* 1997), also produced strong enhancement of the SPEN wing expansion phenotype (data not shown). Therefore, the genetic interactions above indicate that SPEN inhibits Myosin II-dependent axonal outgrowth during CCAP/bursicon neuron remodeling.

Interactions between SPEN and Rac1: There are two other Rho family GTPases, Cdc42 and Rac1, that have been extensively characterized and that regulate process outgrowth in Drosophila and vertebrate neurons (LUO 2000). In different contexts, Cdc42 and Rac1 both can stimulate MRLC phosphorylation in neurons. Since our above experiments suggested that SPEN inhibits myosin II, we reasoned that Cdc42

or Rac1 activity might suppress the defects induced by SPEN overexpression. To test this hypothesis, we first expressed constitutively active Cdc42 (*UAS-Cdc42^{V12}*) (LUO *et al.* 1994) under the control of the *CCAP-Gal4* driver. We examined adult females only in this case, because the severity of the wing expansion phenotype in the *CCAP-Gal4, EP(2)2583* stock had decreased by the time that these crosses were performed, presumably due to the accumulation of unidentified suppressors, and males displayed almost normal wing expansion. At 18°, expression of Cdc42^{V12} alone in the CCAP/bursicon neurons led to an UEW phenotype in 98% of adult female progeny (n=77), whereas expression of SPEN alone [*EP(2)2583*] produced 60% UEW (n=92). When both Cdc42^{V12} and SPEN were expressed together, the proportion of adult females with UEW was the same (96%, n=28) as with Cdc42^{V12} alone. Because there was no evidence of suppression in these crosses, we did not investigate Cdc42 further.

In contrast to Cdc42, Rac1 partially suppressed the effects of SPEN on wing expansion. At 18°, wild type Rac1 (*UAS-Rac1^{L}*) (LUO *et al.* 1994) had no effect on wing expansion when it was expressed alone under control of the *CCAP-Gal4* driver (n=47). However, when Rac1 was expressed together with SPEN at 18°, the number of adult UEW progeny was reduced to 54% (n=132) from the parallel control percentage of 90% (n=84) with SPEN alone. Co-expression of dominant negative Rac1, Rac1^{N17} (Luo et al. 1994), enhanced the SPEN wing expansion phenotype (data not shown), although expression of Rac1^{N17} alone also produced some UEW adults (see below).

Based on the partial suppression of the wing expansion phenotype, we predicted that Rac1 would also partially suppress the effects of SPEN overexpression on growth of the adult CCAP/bursicon peripheral arbor. As expected, co-overexpression of Rac1

with SPEN (Figure 3-8) produced a modest increase in the number and length of axon branches and stronger anti-bursicon immunostaining throughout the arbor (Figure 3-8C). However, the arbor was not completely restored back to the wild type morphology (Figure 3-8A).

The relatively strong genetic interaction between *spen* and *Rac1*, and the similar phenotypes obtained with both SPEN overexpression and also SPEN dominant negative manipulations, suggested that SPEN and Rac1 may both be important for maintaining myosin II activity within a specific operating range in order to sustain outgrowth of the CCAP/bursicon cell arbor. One prediction of this model is that *CCAP-Gal4*-driven Rac1 dominant negative constructs should suppress the phenotypic effects of the SPEN dominant negatives. To examine this possibility, we first asked whether Rac1 signaling was required for the normal development and function of the CCAP/bursicon neurons. When *CCAP-Gal4* was used to drive the expression of $Rac1^{N17}$ at 18°, 38% of adults displayed the UEW phenotype (n=48). A second dominant negative Rac1 (*UAS-$Rac1^{L89}$*) (LUO *et al.* 1994) produced a similar, but weaker effect, with 26% UEW adults at 18° (n=144). Anti-bursicon immunostaining of the stage P14 pharate adult CCAP/bursicon cell arbor (Figure 3-9) revealed that expression of $Rac1^{N17}$ lead to fewer branches and accumulation of immunoreactive material near the distal ends of the axonal branches (Figure 3-9C). We observed a qualitatively similar reduction of branching and distal accumulation of bursicon immunoreactive material with two independent dominant negative SPEN constructs, SPEN-ΔC and -ΔN, and *spen* RNAi (Figures 3-6 and 3-9B). However, when SPEN-ΔC was expressed together with $Rac1^{N17}$, we observed greater bursicon immunoreactivity and more branching

throughout the CCAP/bursicon axon arbor (Figure 3-9D) than with either of the dominant negative constructs alone (Figures 3-9B and 3-9C). The cellular data were supported by wing expansion data. Expression of $Rac1^{N17}$ at 25° gave rise to progeny that were mostly in the PEW class, with 0-1% UEW and only 5% with normal wings (n=39). Co-expression of $Rac1^{N17}$ and spen-ΔC produced progeny with 90% normal wings (n=48). These results suggest that a balance of SPEN and Rac1 signaling is required to maintain myosin II activity within a narrow range for the normal extent of axon branching and peripheral accumulation of neuropeptides during development of the adult CCAP/bursicon axon arbor.

Interactions between SPEN and PAK: Rac1 regulates multiple effectors to control F-actin structure and myosin II activity. One of the best studied Rac1 effectors in neurons is PAK-Kinase (PAK), which stimulates both LIMK1 and myosin II (LUO 2002). Therefore, we looked for interactions between PAK and SPEN during outgrowth of the CCAP/bursicon adult axon arbor. Adult flies that were heterozygous for the amorphic Pak^6 allele (HING *et al.* 1999) displayed normal wings (data not shown). Nevertheless, Pak^6 behaved as a very strong enhancer of the SPEN overexpression phenotypes. At 18°, the number of UEW adults was increased from 29% with *EP(2)2583* alone (n=105) to 97% in a Pak^6/+ mutant background (n=95). At 25°, we also observed much more severe defects in the growth of the adult CCAP/bursicon cell axons, with marked reductions in the number of branches and accumulation of bursicon-immunoreactive material throughout the peripheral arbor

(Figure 3-10A). Thus, wild type expression of Pak served to lessen the severity of the SPEN overexpression in the CCAP/bursicon neurons.

Persistent PAK over-activity in the CCAP/bursicon neurons, induced by *CCAP-Gal4*-targeted expression of a constitutively active PAK mutant protein, PAK^{myr} (FAN *et al.* 2003; HING *et al.* 1999), resulted in 100% UEW at 18° (n = 120). Overexpression of SPEN together with PAK^{myr} reduced the UEW rate to 83% (n=157). Cellular immunostaining showed results that were consistent with these effects on wing expansion. Even at 18°, expression of PAK^{myr} under the control of *CCAP-Gal4* driver almost completely eliminated branches within the peripheral CCAP/bursicon axon arbor (Figure 3-10B). Overexpression of SPEN together with PAK^{myr} led to the partial restoration of peripheral axon branches (Figure 3-10B′). Therefore, Rac1 and its effector PAK both acted antagonistically to SPEN during formation of the adult CCAP/bursicon peripheral arbor.

DISCUSSION

SPEN regulates outgrowth of adult-specific neurites: Several previous studies have examined the role of SPEN during neuronal differentiation. In embryos, SPEN contributes to neuronal cell fate specification and regulates the growth, pathfinding, and fasciculation of PNS and CNS axons (KOLODZIEJ *et al.* 1995; KUANG *et al.* 2000; MINDORFF *et al.* 2007). SPEN also regulates proliferation and differentiation of Drosophila photoreceptor neurons (BRUMBY *et al.* 2004; DOROQUEZ *et al.* 2007; JEMC and REBAY 2006; LANE *et al.* 2000; LIN *et al.* 2003; MINDORFF *et al.* 2007; REBAY *et al.* 2000; STAEHLING-HAMPTON *et al.* 1999; THERRIEN *et al.* 2000), and it modifies the extent of late-onset, progressive neurodegeneration resulting from expression of human Spinocerebellar Ataxia 8 noncoding RNA in the mature Drosophila retina (MUTSUDDI *et al.* 2004). Here, we report that SPEN also regulates developmental plasticity in mature neurons, specifically through the regulation of metamorphic remodeling of neurite projections, and we identified novel and important interactions between SPEN and multiple regulators of actinomyosin-based components of axon outgrowth (see below). Consistent with this function, SPEN is expressed ubiquitously in neurons throughout larval and pupal development (Figure 3-4, and data not shown). These findings suggest that SPEN expression may continue in many mature neurons to support morphological plasticity and perhaps neuronal maintenance and survival.

SPEN overexpression specifically inhibited neurite outgrowth during metamorphic remodeling of the CCAP/bursicon cells (Figures 3-1, 3-2 and 3-5), with

little or no effect on the larval morphology of these neurons (Figures 3-1 and 3-2). The reasons for the stage-dependence of SPEN activity in these cells are unknown, but it suggests a direct or indirect link to the ecdysone titer during metamorphosis. Work on the human SPEN ortholog, SHARP, provides further support for this hypothesis. SHARP expression is steroid-inducible, and it potently inhibits steroid receptor transcriptional activity (SHI *et al.* 2001). In future studies, it will be important to examine interactions between SPEN and ecdysone signaling during steroid-dependent neuronal remodeling.

SPEN inhibits myosin II-based movements: Our identification of *Mbs* as a dominant modifier of the SPEN overexpression phenotype provides the first evidence that SPEN regulates neurite development through actinomyosin-dependent mechanisms. *Mbs* encodes a subunit of the myosin light chain phosphatase (MLCP), which targets MLCP to its substrates to dephosphorylate the myosin regulatory light chain (MRLC) (HARTSHORNE *et al.* 1998b; LEE and TREISMAN 2004b). Dephosphorylation of MRLC leads to reduced myosin II assembly and motor activity.

The actions of MLCP are opposed by factors that promote MRLC phosphorylation, including the Rho GTPases Rho1, Rac1, and Cdc42. Here, we found that Rho1 and Rac1, through regulation of their respective downstream targets MBS and PAK, promote actinomyosin-based axon branching and peripheral accumulation of bursicon in the CCAP/bursicon cell peripheral arbor. The effects of SPEN and the Rho GTPases on axon branching and peripheral accumulation of bursicon were antagonistic. Furthermore, while our experiments do not exclude the possibility of earlier

developmental actions, the growing CCAP/bursicon cell axons were particularly sensitive to regulation by Rho1/MBS, Rac1/PAK, and SPEN during the outgrowth phase of metamorphic remodeling. Taken together, these results support a model in which SPEN either directly or indirectly inhibits myosin II-dependent axon outgrowth, axon branching, and neuropeptide accumulation during steroid-dependent neuronal remodeling.

This model is supported by the following five lines of evidence. First, through a genetic modifier screen, we identified the loss-of-function allele of *Mbs*, Mbs^{3}, as a dominant suppressor of the wing expansion and cellular defects produced by SPEN overexpression. This allele had no effect on wing expansion or CCAP/bursicon cell morphology in the context of normal SPEN expression levels. Second, Rho1 and SPEN were antagonistic. Although overexpression of Rho1 in the CCAP/bursicon neurons alone had no effect on wing expansion and axon branching, the effects of SPEN on these features were suppressed by Rho1, and they were enhanced by dominant negative Rho1 and heterozygous loss-of-function Rho1 alleles. Third, Rac1 and SPEN were antagonistic. Overexpression of Rac1 alone had no apparent effects on the CCAP/bursicon neurons, but Rac1 was a relatively strong suppressor of the wing expansion, axon branching, and peptide accumulation defects resulting from SPEN overexpression. Expression of either dominant negative Rac1 or dominant negative SPEN produced defects in wing expansion and in CCAP/bursicon neuron branching and peptide accumulation, but expression of both dominant negative proteins together led to suppression of these mutant phenotypes. Fourth, the Rac1 effector, PAK, was also antagonistic to SPEN. Although animals that were heterozygous for an amorphic *Pak*

allele appeared to be normal, this allele dominantly enhanced the effects of SPEN on wing expansion, axon branching, and peripheral accumulation of bursicon. Expression of constitutively active PAK, however, led to suppression of these SPEN overexpression phenotypes. Finally, we found no evidence for genetic interactions between *spen* and a third Rho GTPase, *Cdc42*, or three regulators (*WASp*, *LIMK1*, *Tsr*) of actin polymerization. We conclude that the regulation of axon branching and peptide accumulation during metamorphic outgrowth of the CCAP/bursicon cell axons is regulated by myosin II, which is inhibited by SPEN and stimulated by Rho1/MBS and Rac1/PAK signaling.

Outgrowth may require balanced myosin II activity: We observed reduced neurite outgrowth in the CCAP/bursicon neurons following SPEN overexpression (Figure 3-1) as well as in response to cell-targeted *spen* RNAi or expression of dominant negative SPEN (Figure 3-6). The similar effects of loss-of-function and gain-of-function manipulations on the CCAP/bursicon neurons indicate that SPEN may need to be maintained at a specific level, or within an expression window, to regulate outgrowth of neuronal projections. The precise mechanisms underlying these similar phenotypes are unknown. However, this may be explained in part by the genetic interaction between *spen* and two Rho GTPases, Rho1 and Rac1, and their downstream effectors in the regulation of myosin II activity.

Local changes in actinomyosin-based movements govern axon initiation, growth cone extension, growth cone turning, and axon branching (BRADKE and DOTTI 1999; LIN and FORSCHER 1995; LUO 2002; ZHOU *et al.* 2002), and Rho GTPases are critical

regulators of each of these processes. However, depending on the assays employed, Rho GTPases can either promote or prevent axon growth, and loss-of-function and gain-of-function manipulations can produce similar responses. For example, downregulation of Rac1 or PAK activity produces extensive defects in axon growth, pathfinding, and branching (LUO *et al.* 1994; NG *et al.* 2002), whereas expression of constitutively active *Rac1* or PAK leads to similar cellular phenotypes (FAN *et al.* 2003; LUO *et al.* 1994; SCHENCK *et al.* 2003). The similar cellular responses to these opposite manipulations of Rho GTPase signaling likely stem from the fact that opposing or cyclic myosin II-dependent processes, such as filopodia extension and retraction in growth cones, are required for neurite outgrowth (LUO 2000). The effects of SPEN on axon outgrowth may be similarly dependent on the delicate orchestration of myosin II activity.

The conventional view is that myosin II is mainly involved in the retrograde flow of F-actin and thus the retraction of neurites (GOVEK *et al.* 2005; LUO 2000). However, there is accumulating evidence to indicate that myosin II is indispensible for normal neurite outgrowth. For example, treatment with antisense oligodeoxyribonucleotides directed against myosins IIB and IIC in cultured mouse neuroblastoma cells led to defects in outgrowth and reduced growth cone sizes (WYLIE and CHANTLER 2008; WYLIE *et al.* 1998). Similar findings were obtained from cultured superior cervical ganglion neurons isolated from myosin IIB knock-out mice (BRIDGMAN *et al.* 2001; TULLIO *et al.* 2001). The precise molecular mechanisms responsible for these phenotypes remain obscure, although it has been suggested that the depletion of myosin IIB disrupts the cross-linking between myosin II filaments and

actin bundles in an organized network (DIEFENBACH *et al.* 2002). These discoveries on mammalian neurons lend support to our model that myosin II activity is important for neurite outgrowth in the remodeling CCAP/bursicon neurons.

SPEN and myosin II regulation of peripheral neuropeptide accumulation: Extensive studies on a wide variety of neuroendocrine cell types have revealed common mechanisms for the production and transport of secretory granules (EICHLER *et al.* 2006; MALACOMBE *et al.* 2006). Immature secretory granules bud from the trans-Golgi network, from which they are transported along microtubules to the cell periphery. There they are transferred to the F-actin-rich cell cortex, where they undergo maturation processes before undergoing Ca^{++}-dependent secretion. In adrenal chromaffin cells, PC12 cells, pancreatic MIN6 β cells, and other neuroendocrine cell types, late transport events such as the transfer of secretory granules from microtubules to the cortex require myosin Va (EICHLER *et al.* 2006; VARADI *et al.* 2005). Myosin Va has also been shown to contribute to retrograde movements of large dense core vesicles in cultured hippocampal neurons (BITTINS *et al.* 2009), and other myosins, in particular myosin II, have also been implicated in later exocytosis events (MALACOMBE *et al.* 2006).

Most of this work has been done using non-neuronal cells, raising the question of whether peptidergic neurons or other neurosecretory cells also utilize actinomyosin to control secretory granule trafficking or secretion. At the Drosophila neuromuscular junction, depolymerization of F-actin had no effect on basal or stimulus-induced secretory granule mobilization within type Ib boutons (SHAKIRYANOVA *et al.* 2005). However, this does not preclude a role for actinomyosin at earlier steps in the regulated

secretory pathway. The CCAP/bursicon cell axons contain dense, strongly bursicon-immunoreactive varicosities. Because bursicon can be rapidly depleted along the length of these axons (ZHAO *et al.* 2008), these varicosities are presumed to be neurosecretory boutons. Following SPEN overexpression, the level of bursicon present throughout the CCAP/bursicon cell axonal arbor was markedly reduced (Figure 3-2 C, D). This effect was attenuated by co-overexpression of Rac1 (Figure 3-8C), and it was enhanced by a mutation in *Pak* (Figure 3-10A). In contrast, RNAi and dominant negative SPEN constructs drove accumulation of bursicon in distal, enlarged axon endings and the proximal loss of boutons (Figure 3-6). These findings suggest that 1) the effects on bursicon levels are not strictly due to the regulation of neuropeptide expression, 2) myosin II supports peripheral accumulation of neuropeptides, perhaps through participation in the capture of immature secretory granules at neurosecretory boutons, and 3) SPEN regulates this process through the inhibition of myosin II.

TABLE 3-1

Selected modifiers of the wing expansion defects induced by *spen* overexpression

Cellular pathway	Gene	Allele	Mode of action	% UEW with modifier (% UEW for control)	Extent of enhancement/suppression (%)
SPEN	*spen*	*UAS-spen-ΔC* [a]	Dominant negative	2 (90)	↓98 [f]
		UAS-spen-ΔN [a]	Dominant negative	19 (68)	↓32
	spenito (*nito*)	*UAS-myc.nito* [a]	Wild type	100 (88) [b]	PL; $HE^{30/22}$ [b]
		$UAS\text{-}nito^{RNAi}\text{-}R$	RNAi	0 (68)	↓53
Epithelial growth factor receptor (EGFR)	*Epidermal growth factor receptor* (*Egfr*)	$UAS\text{-}Egfr^{B}$	Wild type	42 (88)	↓53

signaling					
		UAS-Egfr$^{DN\ c}$	Dominant negative	100 (85)	↑100^{f}
	Ras oncogene at 85D (*Ras85D*)	*UAS-Ras*^{WT}	Wild type	61 (90)	↓32
		UAS-Ras$^{v12\ d}$	Constitutively active	5 (40)	↓88^{f}
		UAS-Ras$^{N17\ e}$	Dominant negative	74 (90)	↓19
Insulin/insulin-like growth factor signaling	*Insulin-like receptor* (*InR*)	*UAS-InR*	Wild type	43 (90)	↓52
		UAS-InR^{R418P}	Constitutively	46 (90)	↓50

		active		
	UAS-InR^{A1325D}	Constitutively active	52 (90)	↓42
	UAS-InR^{del}	Constitutively active	54 (41)	↑21[f]
	UAS-InR^{K1409A} *(2nd chromosome)*	Dominant negative	100 (41)	↑100[f]
	UAS-InR^{K1409A} *(1st chromosome)*	Dominant negative	100 (71)	↑100[f]
	InR^{E19}	LOF	100 (50)	↑100[f]
phosphatidylinositol 3-kinase (*Pi3K92E*)	*UAS-Pi3K92E*^{Exel}	Wild type	59 (41)	↑30[f]

	UAS-Pi3K92E^{CAAX}	Constitutively active	39 (26)	↑51[f]
	UAS-Pi3K92E^{A2860C}	Dominant negative	100 (86)	↑100[f]
Ras homology enriched in brain (*Rheb*)	*UAS-Rheb*	Wild type	24 (88)	↓73

Extent of enhancement = (%UEW$_{test\ cross}$ – %UEW$_{control\ cross}$)/(100 - %UEW$_{control\ cross}$). Extent of suppression = (%UEW$_{control\ cross}$ – %UEW$_{test\ cross}$)/(%UEW$_{control\ cross}$). Most crosses were repeated, and these values therefore represent the average extent of enhancement/suppression. HE$^{x/x}$, head eversion defects observed in pupae (the numbers in superscript represent the percentage of pupae with uneverted/partially everted heads); PL, pupal lethal (no adults obtained), LOF, loss of function.

[a] (CHEN and REBAY 2000; LIN *et al.* 2003).

[b] 100% UEW and some head eversion defects were also observed with *UAS-myc.nito* alone [without *EP(2)2583*].

[c] (BUFF *et al.* 1998).

[d] (KARIM and RUBIN 1998).

[e] (LEE *et al.* 1996).

[f] Measured for females only. The control males in this cross had normal wings.

TABLE 3-2

Deficiency and single gene modifiers of the *spen* GOF wing expansion phenotype

Deficiency	Class	Extent of enhancement/ suppression (%)	Responsible gene(s)	Class (allele)	Extent of enhancement /suppression (%)
Df(3L)Exel6084	Suppressor	↓31			
Df(3L)Exel6112	Suppressor	↓26			
Df(3L)Exel6123	Enhancer	HE, PL	*big bang* (*bbg*)	Enhancer ($bbg^{EY02818}$, bbg^{e03261})	↑100
			Mitochondrial phosphate carrier protein (*Mpcp*)	Enhancer ($Mpcp^{00564}$)	↑100
			CG9238	Enhancer ($CG9238^{e03123}$)	↑100

			HGTX	Enhancer [b] (*HGTX*^{d00083})/Suppressor (*HGTX*^{e03190})	HE, PL/↓20
Df(3L)Exel6127	Suppressor	↓63	*Myosin binding subunit* (*Mbs*)	Suppressor (*Mbs*^{3})	↓31
			Zn72D	Enhancer (*Zn72D*^{BG02677})	↑100 [c]
			TBP-associated factor 4 (*Taf4*)	Suppressor (*Taf4*^{1}, *Taf4*^{e02502})	↓31-57
Df(3R)Exel6135	Enhancer	HE, PL			
Df(3R)Exel6144	Suppressor	↓47	*N-methyl-D-aspartate-type glutamate NMDA receptor 1* (*Nmdar1*)	Suppressor (*Nmdar1*$^{DG23512\ c}$, *Nmdar1*$^{EY02522\ b}$)	↓32-38
			CG2519	Suppressor (*CG2519*^{EY00928})	↓16
			meiosis I arrest (*mia*)	Suppressor (*mia*^{EY07883}) [b]	↓40

			Snm1	Suppressor (*Snm1*$^{ZIII\text{-}2589}$, *Snm1*$^{ZIII\text{-}4709}$)	↓40-63
			CG12746	Suppressor (*CG12746*^{EY10535}) [d]	↓26
			Ras homology enriched in brain (*Rheb*)	Suppressor (*Rheb*^{LA01053}) [e]	↓78
			asterless (*asl*)	Suppressor (*asl*^{c01524}) [a]	↓21
Df(3R)Exel6148	Enhancer	HE, PL	*CG9238*	Enhancer (*CG9238*^{e03123})	↑100
Df(3R)Exel6160	Suppressor	↓33	*prospero* (*pros*)	Suppressor (*l(3)rM060*) [f]/Enhancer (*pros*^{17})	↓38/↑75 [i]
			CG6744	Suppressor [b] (*CG6744*^{EY03872})	↓28
			CG17230	Suppressor (*CG17230*$^{tho\text{-}1}$)	↓32
			CG10898	Suppressor (*CG10898*^{c05103})	↓40
Df(3R)Exel6170	Suppressor	↓18			

Df(3R)Exel6218	Suppressor	↓45	*chaoptic* (*chp*)	Suppressor (*chp*^{KG05897})	↓66
			CG1746	Enhancer (*CG1746*^{KG01914})	↑100
			CG12054	Enhancer (*CG12054*^{EY01782}) [g]	↑75
			CG31005	Suppressor (*CG31005*^{EP984}) [h]	↓32
Df(3R)Exel6263	Enhancer	↑100			
Df(3R)Exel6265	Suppressor	↓48	*Fragile X mental retardation 1* (*Fmr1*)	Suppressor (*Fmr1*$^{\Delta 50m}$)	↓19
			Invadolysin	Suppressor (*Invadolysin*^{EY11299} [b], *Invadolysin*^{1})	↓19-21
Df(3R)Exel7312	Suppressor	↓50			
Df(3R)Exel7313	Suppressor	↓30			

Df(3R)Exel7315	Enhancer	↑100
Df(3R)Exel7316	Suppressor	↓27
Df(3R)Exel9013	Enhancer	↑100
Df(3R)Exel9030	Suppressor	↓18

Only alleles with confirmed >15% suppression or >75% enhancement are listed. The results for all other tested alleles are provided in Supplemental Tables 1 and 2. Except where indicated, the modifier activity for each of the listed deficiencies and other alleles was confirmed with at one additional test cross. The extent of enhancement/suppression was calculated as in Table 1. HE, head eversion defects observed in pupae; PL, pupal lethal (no adults obtained).

[a] Not confirmed with a second cross.

[b] May be gain-of-function (GOF) or loss-of-function (LOF).

[c] May also disrupt *Inositol 1,4,5,-tris-phosphate receptor* (*Itp-r83A*), an embedded gene. However, a potentially severe LOF allele of *Itp-r83A* (*Itp-r83A*^{05616}; intronic for *Nmdar1* and in the first exon of *Itp-r83A*) displayed no modification.

[d] Possible GOF of *CG14671*.

[e] Within first exon of *Rheb* and possible GOF of *Rheb*. No modification was observed with *Rheb*^{EY08085} (also within the 1st exon of *Rheb* but possible GOF of *CG2931*).

[f] Insertion in the first exon of *pros*, although not a confirmed *pros* LOF allele. A second insertion allele in this exon, *pros*^{10419}, did not show suppression.

[g] Insertion within the second exon of *CG12054*, but may be GOF for *CG1746*.

[h] Insertion within the first exon of *CG31005*, but may be GOF for *mRpL32*.

[i] Measured for females only. The control males in this cross had normal wings.

Figure 3-1.—CCAP/bursicon cell-targeted expression of *EP(2)2583* resulted in the absence of bursicon-immunoreactive neurites and the LSE cells in the pharate adult CNS. (A-D) Anti-bursicon immunostaining in the CNS of wandering third instar larvae (A and B) and stage P14 pharate adults (C and D) from either *CCAP-Gal4*/+ (A and C) or *CCAP-Gal4*/*EP(2)2583* (B and D) animals. Note that the morphology of the larval CCAP/bursicon neurons was essentially normal following *EP(2)2583* expression. In contrast, adult-specific neurites (arrows) were mostly absent, the LSE neurons (LSE) were either absent or very poorly immunostained, and the abdominal somata (B_{AG}^{a} and B_{AG}^{p}) were smaller in diameter, weakly immunostained, or absent. The B_{AG}^{a} are eight neurons located toward the anterior of the abdominal ganglia, and the B_{AG}^{p} are six neurons located in the posterior abdominal ganglia. Bars: A and B, 50μm; C and D, 100 μm.

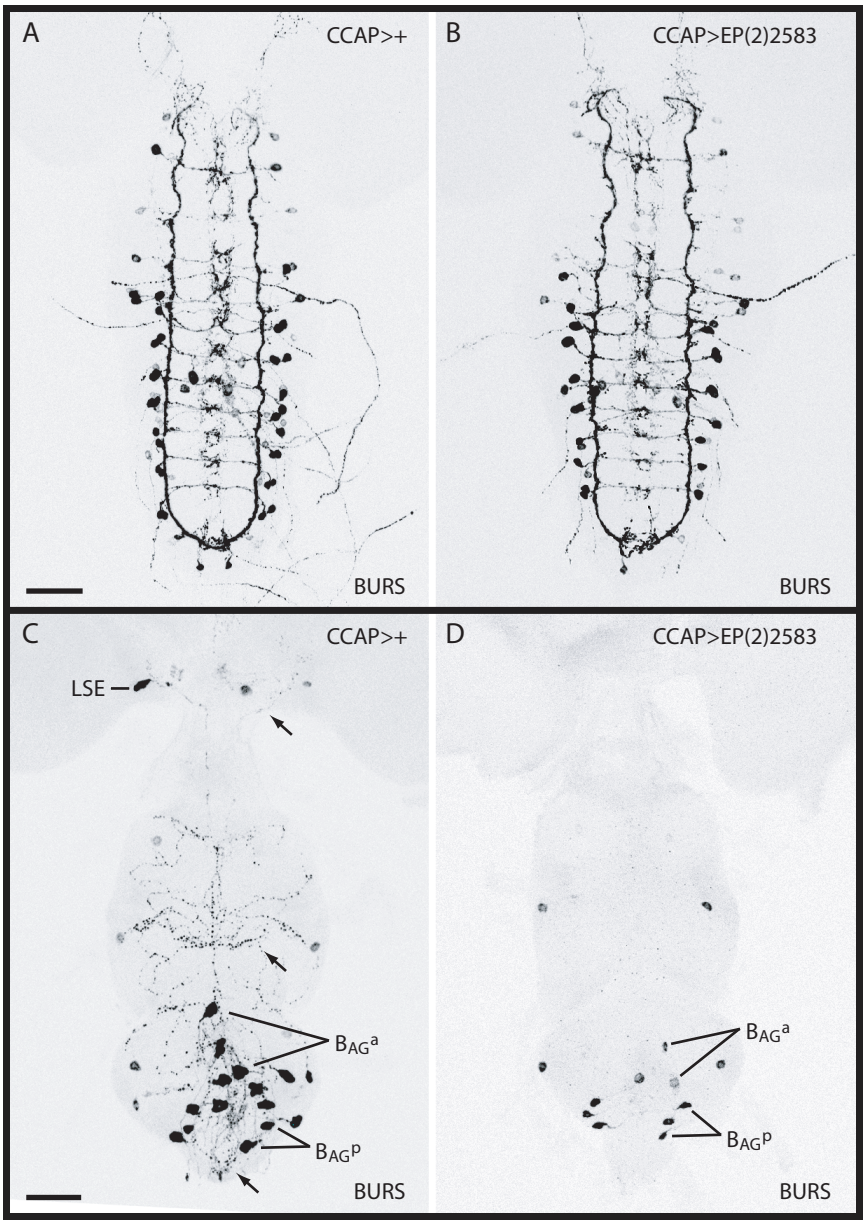
A
CCAP>+
BURS
B
CCAP>EP(2)2583
BURS
C
CCAP>+
LSE
BAGa
BAGp
BURS
D
CCAP>EP(2)2583
BAGa
BAGp
BURS

Figure 3-2.—CCAP/bursicon cell-targeted expression of *EP(2)2583* resulted in the absence of bursicon-immunoreactive peripheral axons in pharate adults. (A-D) Anti-bursicon immunostaining of the peripheral CCAP/bursicon cell axons in wandering third instar larvae (A and B) and P14 pharate adults (C and D). The genotypes are the same as in Figure 1. Feathered arrows, strongly immunoreactive axon terminals; feathered arrowheads, weakly immunoreactive axons; solid arrow, remaining peripheral axons. Bars: A and B, 50 μm; C and D, 100 μm.

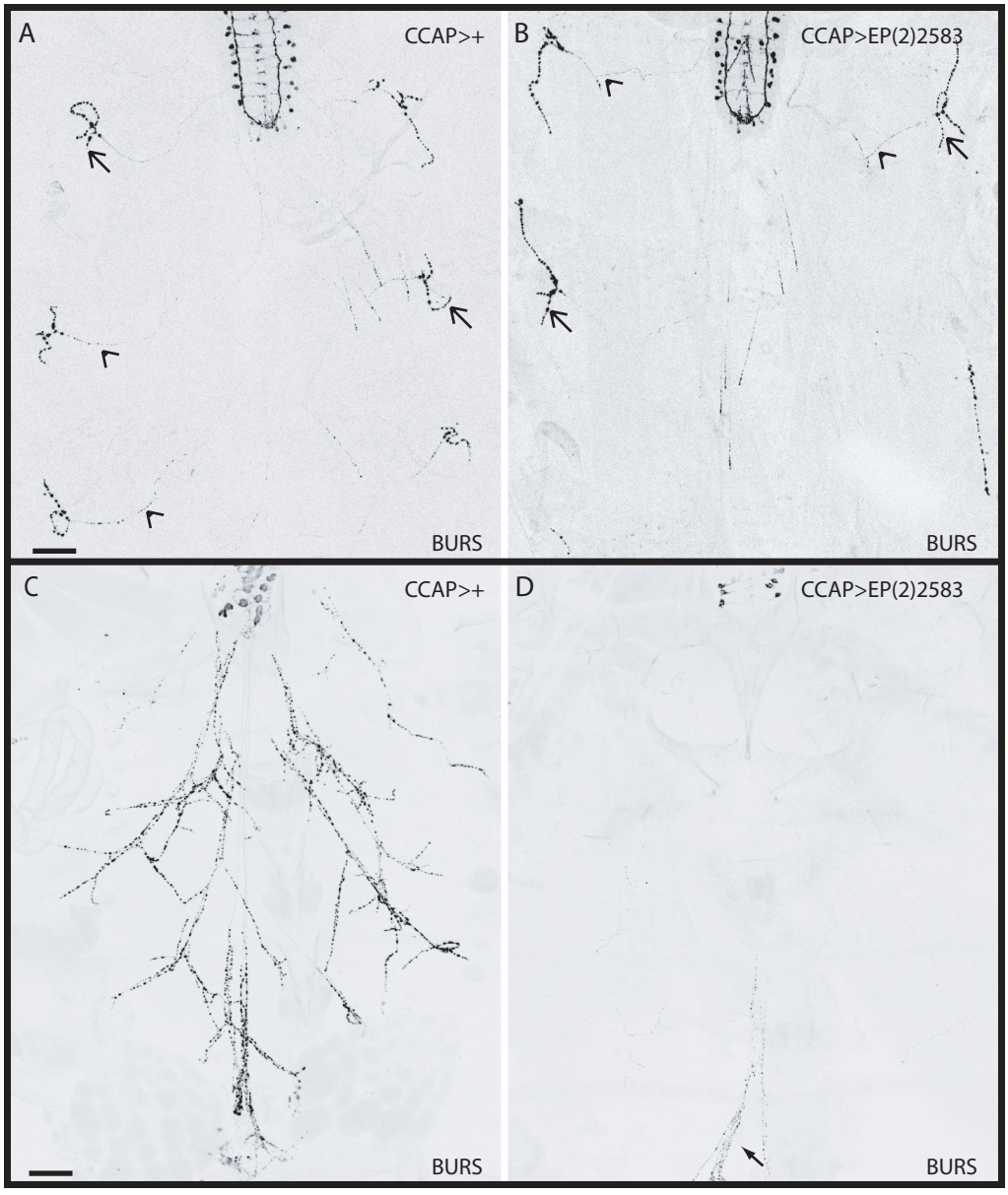
A
CCAP>+
BURS
B
CCAP>EP(2)2583
BURS
C
CCAP>+
BURS
D
CCAP>EP(2)2583
BURS

Figure 3-3.—At 25°, CCAP/bursicon cell-targeted expression of *EP(2)2583* led to fewer axonal branches and reduced bouton size and number. (A and B) Anti-GFP staining in CCAP/bursicon cell axons in either (A) *CCAP-Gal4, UAS-CD8::GFP/+* or (B) *CCAP-Gal4, UAS-CD8::GFP/EP(2)2583* stage P14 pharate adults. The culture temperature for this experiment was 25° instead of 29°, since very few axons were observed at 29° (Figure 2). Note in panel (A) the greater overall number of branches and the presence of long axonal swellings (arrows), possibly resulting from fusion of adjacent boutons. Individually identifiable boutons (arrowheads) were also more oblong and larger in (A). Bar: 25 μm.

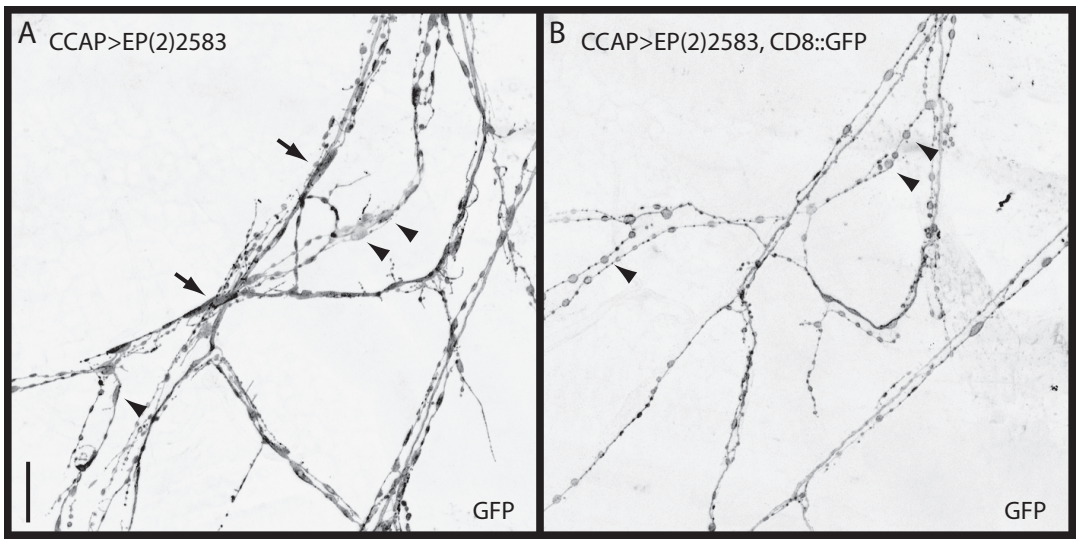
A
CCAP>EP(2)2583
GFP
B
CCAP>EP(2)2583, CD8::GFP
GFP

Figure 3-4.—SPEN expression was ubiquitous in the larval CNS and was elevated with *EP(2)2583*. (A-A") anti-SPEN immunostaining (magenta) was ubiquitous and nuclear in the wandering third instar larval CNS (genotype: *yw/w; CCAP-Gal4, UAS-CD8::GFP/+*). The regions indicated by the dashed boxes are shown as single confocal sections at higher magnification in the insets to illustrate co-expression of SPEN and *CCAP>CD8::GFP* (green) in the CCAP/bursicon neurons. (B-B") Elevated SPEN immunostaining was observed in the CCAP/bursicon neurons when *CCAP-Gal4* was used to drive co-expression of *UAS-CD8::GFP* and *EP(2)2583* in a wandering third instar CNS (genotype: *yw; CCAP-Gal4, UAS-CD8::GFP/EP(2)2583*). Note that the gain for imaging the anti-SPEN channel was set lower in (B) than in (A) to enable better visualization of the change in SPEN levels with *EP(2)2583*. Arrows, selected neurons with cytoplasmic CD8::GFP and elevated nuclear SPEN labeling. Bars: A, 25 μm; B, 50 μm.

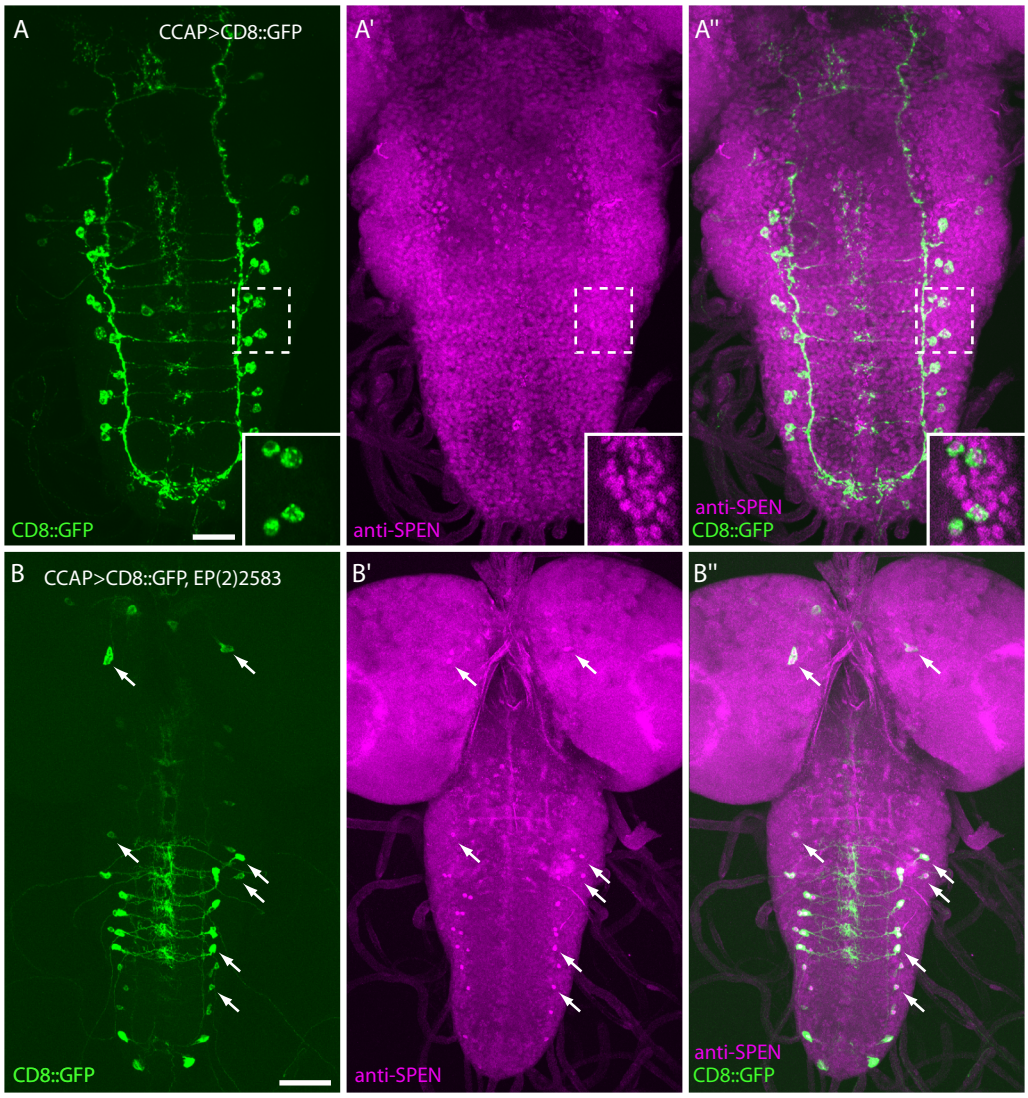
A
CCAP>CD8::GFP
CD8::GFP
A'
anti-SPEN
A''
anti-SPEN
CD8::GFP
B
CCAP>CD8::GFP, EP(2)2583
CD8::GFP
B'
anti-SPEN
B''
anti-SPEN
CD8::GFP

Figure 3-5.—SPEN overexpression inhibited outgrowth of the peripheral CCAP/bursicon axons during metamorphosis. (A-B) Anti-GFP immunostaining on abdominal body wall fillets from *CCAP-Gal4, UAS-mCD8::GFP/+* (A and A′) and *CCAP-Gal4, UAS-mCD8::GFP/EP(2)2583* (B and B′) animals at the indicated times APF (hr at 25°; *n*=5-9). Arrows, peripheral axon endings. Bar, 100 μm.

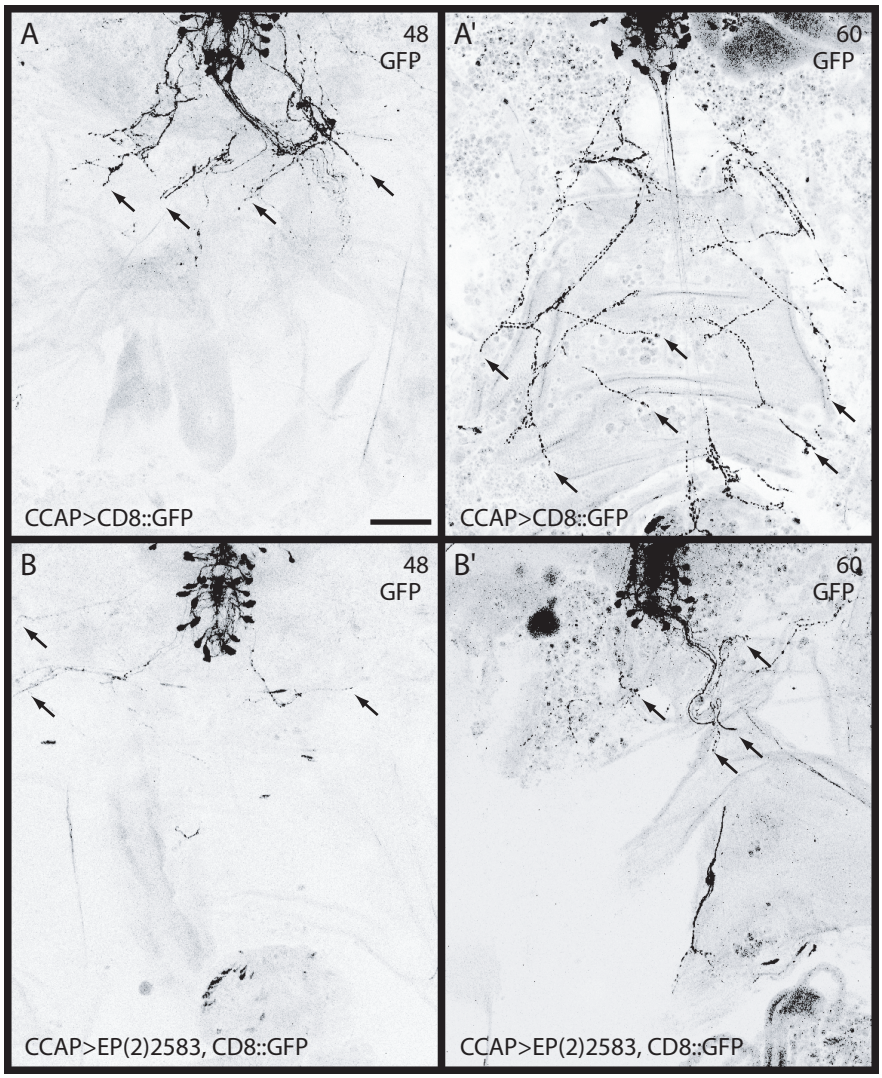
A
48
GFP
CCAP>CD8::GFP
A'
60
GFP
CCAP>CD8::GFP
B
48
GFP
CCAP>EP(2)2583, CD8::GFP
B'
60
GFP
CCAP>EP(2)2583, CD8::GFP

Figure 3-6.—SPEN activity is required for normal axon outgrowth during metamorphic remodeling of the CCAP/bursicon neurons. (A-B) Anti-bursicon immunostaining on abdominal body wall fillets from stage P14 pharate adults following CCAP/bursicon cell-targeted expression of dominant negative SPEN (A′) or spen RNAi (B′ and B″) at 25°. Genotypes: (A) *CCAP-Gal4/+*; (A′) *CCAP-Gal4/UAS-spen-ΔN*; (B) *UAS-dicer2/+; CCAP-Gal4/+*; (B′) *UAS-dicer2/+; CCAP-Gal4/UAS-spen-RNAi7*; (B″) *UAS-dicer2/+; CCAP-Gal4/UAS-spen-RNAi*^{49543}. Expression of dominant negative SPEN (A′) or *spen* RNAi (B′ and B″) resulted in reduced branching and the appearance of swollen, club-shaped axonal endings (arrows). The proximal portions of each axonal projection also displayed fewer strongly bursicon-immunoreactive boutons (arrowheads). Asterisk, artifact due to debris on the slide. Bars, 100 μm.

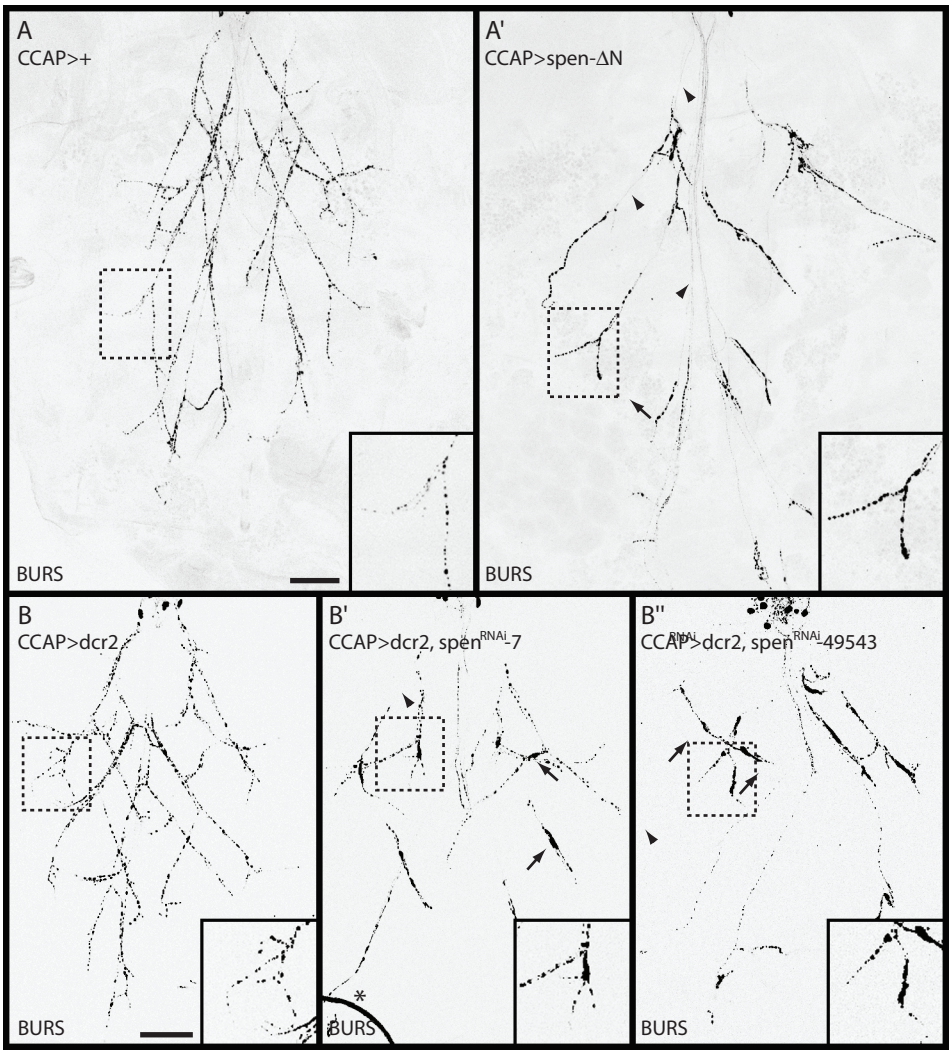
A
CCAP>+
BURS
A'
CCAP>spen-ΔN
BURS
B
CCAP>dcr2
BURS
B'
CCAP>dcr2, spen^RNAi-7
BURS
B''
CCAP>dcr2, spen^RNAi-49543
BURS

Figure 3-7.—An *Mbs* LOF mutation suppressed the growth defects induced by *spen* overexpression in the CCAP/bursicon cells. (A-B) Anti-bursicon immunostaining of the peripheral CCAP/bursicon cell axons in P14 pupae of *CCAP-Gal4,EP(2)2583/+* (A) and *CCAP-Gal4,EP(2)2583/+;Mbs^{3}/+* (B). The crosses were performed at 29°, and the confocal *z*-series images for each panel in this figure were obtained at settings that were optimal for showing the neurites. Bar: 100 μm.

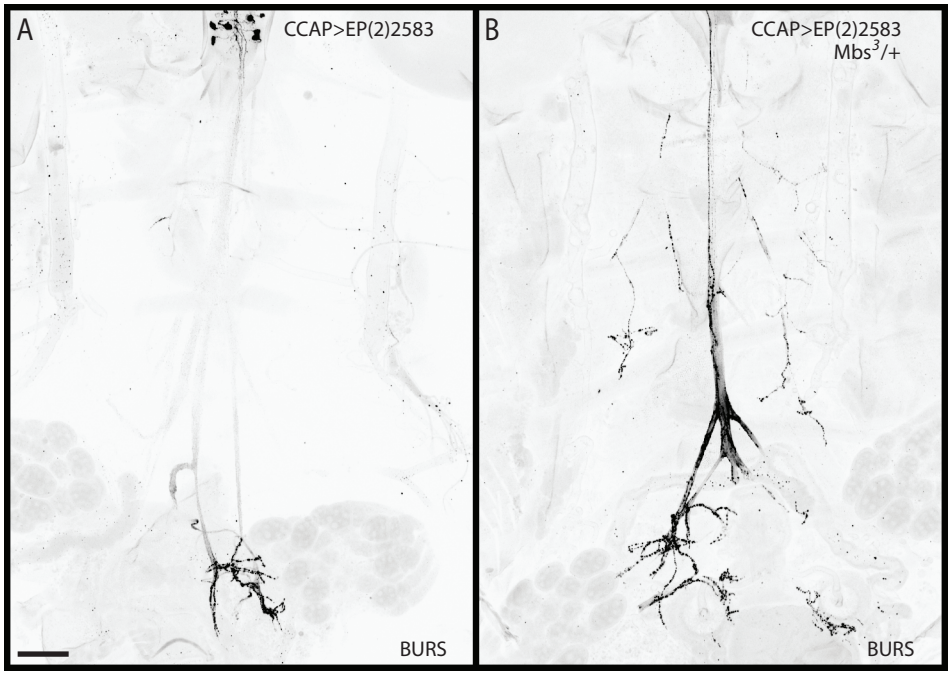
A
CCAP>EP(2)2583
BURS
B
CCAP>EP(2)2583
Mbs3/+
BURS

Figure 3-8.—Rac1 overexpression partially suppressed the growth defects induced by SPEN overexpression in the CCAP/bursicon cells. (A-C) Anti-bursicon immunostaining of the peripheral CCAP/bursicon cell axons in P14 stage pharate adults. (B) At 25°, SPEN overexpression (*CCAP-Gal4,EP(2)2583/+*) produced cells with fewer axonal branches. In addition, the boutons were reduced in size and number (Figure 3), and the intensity of the anti-bursicon immunostaining throughout the axonal arbor was reduced. (C) Co-overexpression of SPEN and Rac1 (*CCAP-Gal4,EP(2)2583/UAS-Rac1.L*) resulted in a partial restoration of branching, larger boutons, and stronger anti-SPEN immunoreactivity. Bar: 100 μm.

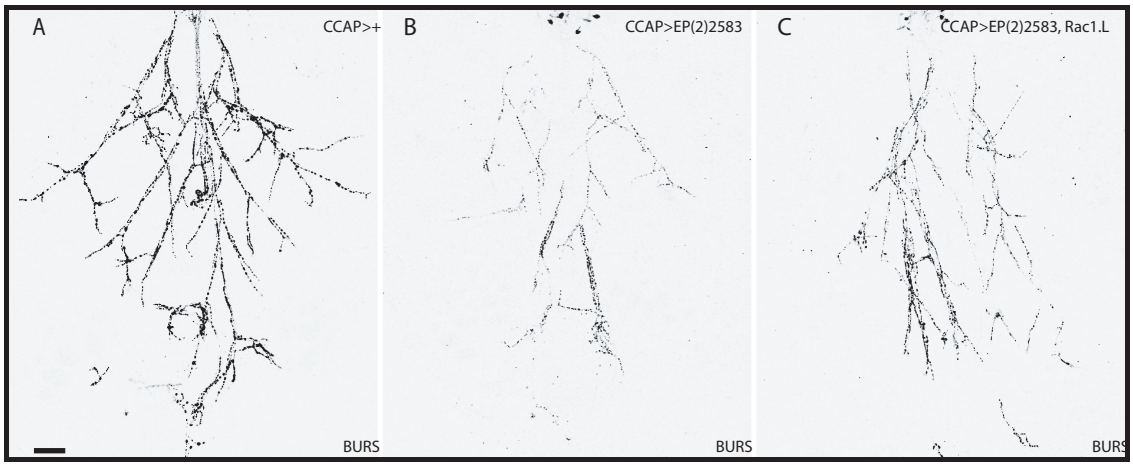
A
CCAP>+
BURS
B
CCAP>EP(2)2583
BURS
C
CCAP>EP(2)2583, Rac1.L
BURS

Figure 3-9.—Expression of dominant negative SPEN partially suppressed the remodeling defects produced by expression of dominant negative Rac1. (A-D) Anti-bursicon immunostaining of the CCAP/bursicon cell peripheral axons in stage P14 pharate adults (25°). (A) Control: *CCAP-Gal4/+*. (B) Expression of dominant negative SPEN (*CCAP-Gal4,UAS-spen-ΔC/+*) resulted in reduced branching and the appearance of swollen, club-shaped axonal endings (arrows). (C) Expression of dominant negative Rac1 (*CCAP-Gal4/UAS-Rac1*^{N17}) produced an arbor with fewer branches overall and clusters of short branches near the peripheral axon endings (arrowheads). (D) Co-expression of dominant negative SPEN and dominant negative Rac1 produced an arbor with longer branches, larger boutons, and greater accumulation of bursicon-immunoreactive material than with dominant negative Rac1 alone. The number of branches was intermediate between that shown in (A) and (C), and clusters of short branches near the peripheral axon endings (arrowheads) were still observed. Bar: 100μm.

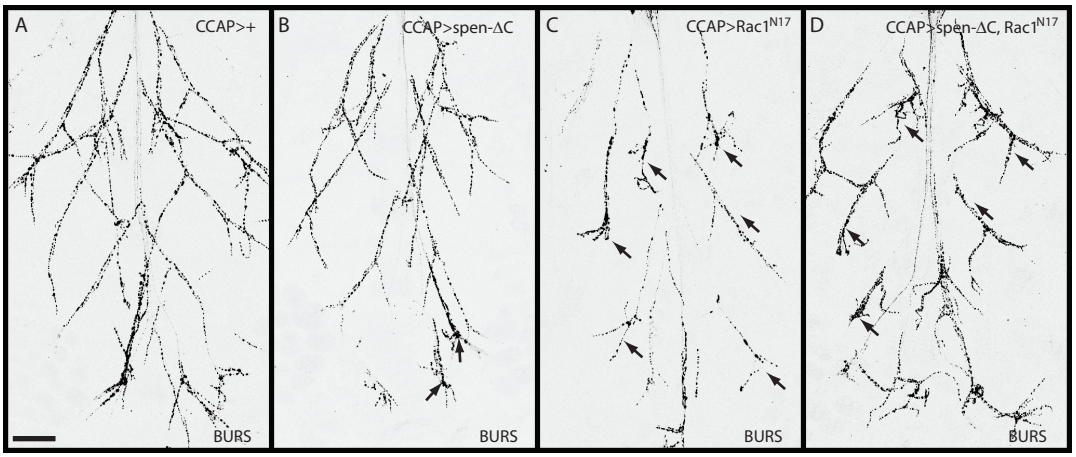
A
CCAP>+
BURS
B
CCAP>spen-ΔC
BURS
C
CCAP>Rac1N17
BURS
D
CCAP>spen-ΔC, Rac1N17
BURS

Figure 3-10.—Genetic interactions between *PAK* and *spen* in regulation of adult axon outgrowth. All images show the peripheral CCAP/bursicon cell axons in stage P14 pharate adults (reared at 25°) immunostained with anti-bursicon. (A-A″) Loss of *PAK* dominantly enhanced the defects in CCAP/bursicon cell axon outgrowth caused by SPEN overexpression. (A) Control: *CCAP-Gal4/+*. (A′) Reduced CCAP/bursicon cell arbor following SPEN overexpression (*CCAP-Gal4/EP(2)2583*). (A″) A mutation in *PAK* (PAK^{6}) dominantly enhanced the growth defects produced by SPEN overexpression. (B-B′) Overexpression of SPEN partially suppressed the branching defects produced in the CCAP/bursicon cell axons following expression of constitutively active PAK. (B) Expression of constitutively active PAK (*CCAP-Gal4/UAS-*PAK^{myr}) produced axonal projections with very few branches (arrow). (B′) Overexpression of SPEN together with constitutively active PAK (*CCAP-Gal4,EP(2)2583/UAS-*PAK^{myr}) partially restored peripheral axon branching (arrowheads). Bars: 100 μm.

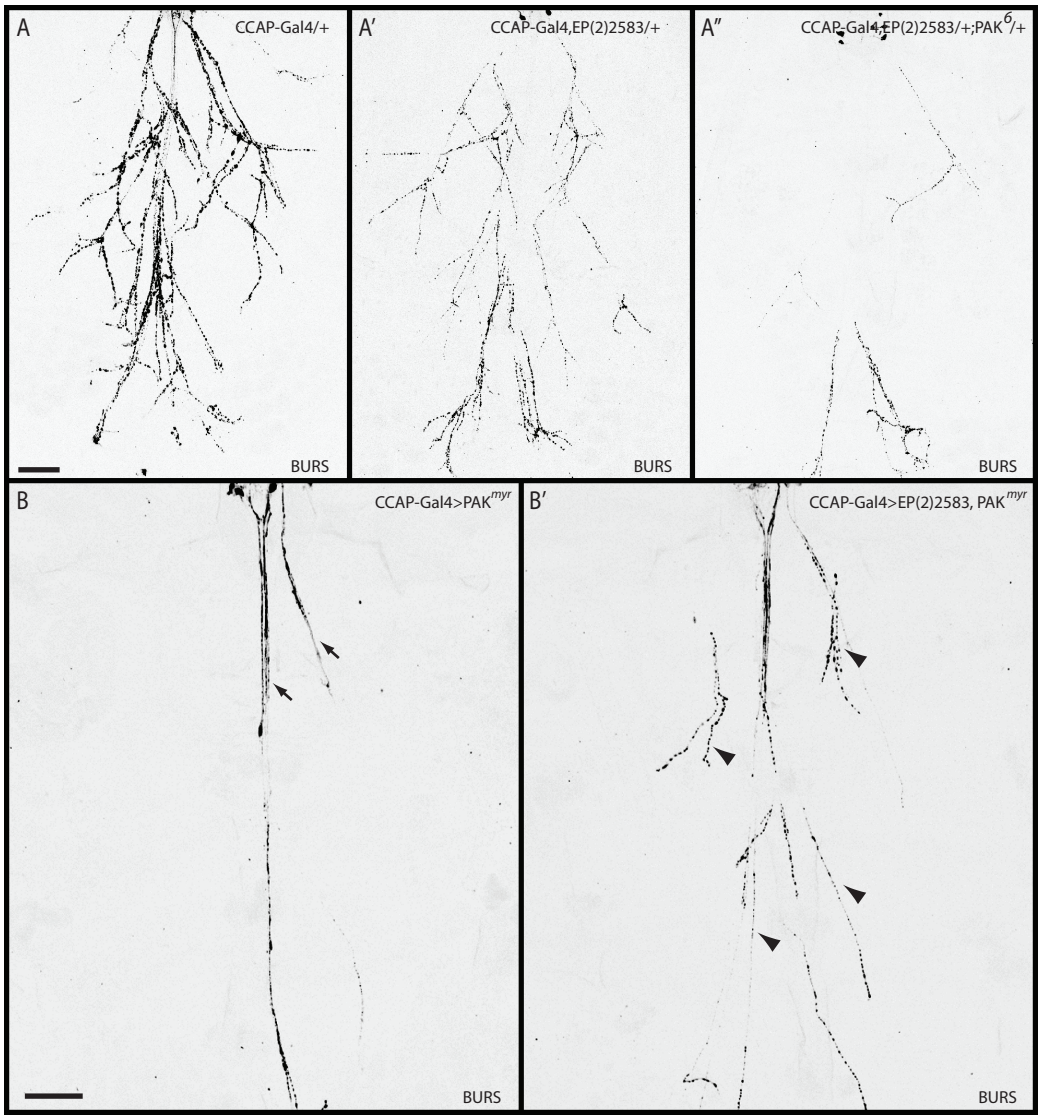
A
CCAP-Gal4/+
BURS
A′
CCAP-Gal4,EP(2)2583/+
BURS
A″
CCAP-Gal4,EP(2)2583/+;PAK6/+
BURS
B
CCAP-Gal4>PAKmyr
BURS
B′
CCAP-Gal4>EP(2)2583, PAKmyr
BURS

Appendix 1: A Drosophila gain-of-function screen for candidate genes involved in steroid-dependent neuroendocrine cell remodeling.

Table of Contents

SUPPLEMENTAL MATERIALS AND METHODS

***In situ* hybridization with locked nucleic acid (LNA) probes:** We used the following digoxigenin (DIG)-labeled LNA probes and calculated melting temperatures (Tm):

miR-276a (5′-AGAGCACGGTATGAAGTTCCTA-3′; Tm=75°)

miR-279 (5′-TTAATGAGTGTGGATCTAGTCA-3′; Tm=70°)

miR-310 (5′-AAAGGCCGGGAAGTGTGCAATA-3′; Tm=79°)

miR-312 (5′-TCAGGCCGTCTCAAGTGCAATA-3′; Tm=77°)

miR-313 (5′-TCGGGCTGTGAAAAGTGCAATA-3′; Tm=77°).

We diluted each probe in hybridization solution [50% formamide, 5X sodium choride/sodium citrate (SSC), 0.5 mg/ml yeast tRNA, 50 μg/ml Heparin, 0.1% Tween-20, 9 mM citric acid, pH 6.0] at 1 nM (*miR-279*) or 10 nM (all other probes) prior to use. We dissected the tissues in ice cold calcium-free saline, fixed in 4% PFA for 30 min at RT, washed in PBS + 0.1% Tween20 (PBS-TW) (3 x 5 min, RT), and treated in 10 μg/ml Proteinase K (2 min, RT). We stopped the enzyme by washing in PBS-TW containing mg/ml glycine (2 x 2 min, RT), followed by washes in PBS-TW (2 x 2 min, RT), postfixation in 4% PFA (30 min, RT), and washes in PBS-TW (3 x 5 min, RT), freshly prepared 0.1 M triethanolamine (TEA; 2 x 5 min, RT), and PBS-TW (2 x 5 min, RT). After rinses in 50% PBS-TW/50% hybridization solution (5 min, RT) and 100% hybridization solution (5 min, RT), we pre-hybridized in hybridization solution for 1 hr at 20° below the calculated Tm. Each probe was preheated (2 min, 95°), snap cooled,

and then diluted in hybridization solution. The probes were warmed to the hybridization temperature (20° below the calculated Tm) before use.

After hybridization overnight, the probe was removed, and the tissues were washed at 20° below the calculated Tm in hybridization solution (20 min), a dilution series containing hybridization solution/2X SSC (75%/25%, 50%/50%, 25%/75%, 0%/100%, 15 min each), and 0.2X SSC (2 x 30 min). Then, the tissues were washed in a RT dilution series of 0.2X SSC/PBS-TW (75%/25%, 50%/50%, 25%/75%, 0%/100%, 10 min each) and PBS-TW with 4 mg/ml BSA (RT, several hr) before performing immunostaining with 1:2000 pre-absorbed anti-DIG (HEWES *et al.* 2003; TAUTZ and PFEIFLE 1989). Tissues were post-fixed again in 4% PFA and washed in PBS before mounting in 90% glycerol/10% PBS.

SUPPLEMENTAL RESULTS AND DISCUSSION

Identification of loci responsible for GOF phenotypes: Our isolation of multiple insertions upstream of five genes (*CG11966*, *faf*, *headcase*, *miR-276a*, *miR-310-miR313*) provided indirect support for the correct identification of the genes responsible for the observed phenotypes. In addition, of the two genes potentially targeted by *XP(2)d07339*, the gene responsible for the phenotypes observed in this screen appears to be *saliva* (*slv*), since a unidirectional GOF insertion (*UY1770*) located -731 bp upstream of *slv* (NICOLAI *et al.* 2003) also produced flies with 100% UEW when crossed to *CCAP-Gal4*. Consistent with our observation that *XP(2)d07339* expression produced loss of neurites in the CCAP/bursicon cells, *UY1770* GOF in the mushroom bodies produced axonal growth and guidance defects (NICOLAI *et al.* 2003). Thus, *slv* may regulate neurite outgrowth in diverse neurons during metamorphosis.

We used three methods to independently validate the identification of the misexpressed genes for selected gain-of-function lines. In particular, we focused on obtaining positive identifications for the loci included in the cellular analysis. First, for *foxo*, we phenocopied the molting defects and cellular phenotypes elicited with *EY(3)11248* by using *CCAP-Gal4* to direct expression of a UAS transgene containing wild-type *foxo*. Likewise, UAS transgenes containing the two known wild-type isoforms of *pnt* (*pnt-1* and *pnt-2*), the nearest gene downstream of *EY(3)03254*, both produced adults with 100% UEW (in addition, with *pnt-2*, 35% of the pupae displayed head eversion defects and 45% died as pharate adults). Other groups have confirmed the GOF of *cbt* by *EP(2)2237* (see Results) and *faf* by *EP(3)3520* (DIANTONIO *et al.*

2001). Second, we confirmed overexpression of *spen* and *mip120* by *EP(2)2583* and *EY(2)05304*, respectively, by immunostaining with antisera specific to the products of these two genes; in wild type CNS, we observed ubiquitous immunostaining for SPEN and MIP120 (data not shown). Third, we performed *in situ* hybridization with LNA probes to confirm the GOF of the *miR-310-miR-313* cluster, *miR-276a*, and *miR-279* by *EP(2)2587*, *EP(3)3523*, and *EP(3)3140*, respectively (Figure 8, and data not shown). Thus, for seven of the 17 loci included in the cellular analysis, and two additional loci in supplemental Table 3, we or others have obtained independent confirmation of the identity of the target gene.

Hit rates with different Gal4 drivers: We used three different Gal4 drivers to conduct phase II of the screen (crosses to 2010 second and third chromosome *EP* insertions), and each produced a different percentage of crosses with molting-related phenotypes: 0.8% with *386Y-Gal4*, 0.05% with *c929-Gal4*, and 0% with *EH-Gal4*. In follow-up crosses, *CCAP-Gal4* produced phenotypes with 12 of the 16 lines isolated with *386Y-Gal4*—by extrapolation, we calculate that the hit rate with this driver was therefore at least 0.6%. In contrast, most other *EP* screens have produced hit rates in the range of 2-9% (ABDELILAH-SEYFRIED *et al.* 2000; BIDET *et al.* 2003; KRAUT *et al.* 2001; PENA-RANGEL *et al.* 2002; RØRTH *et al.* 1998; TSENG and HARIHARAN 2002), although lower hit rates of 0.4% (MCGOVERN *et al.* 2003) to 0.9% (SCHULZ *et al.* 2004) were also observed. Thus, the highest hit rates in this screen (with *386Y-Gal4* and *CCAP-Gal4*) were comparable to the lowest rates observed in other GOF screens, and *c929-Gal4* and *EH-Gal4* were much less effective. These differences appear to stem in

part from the size of the Gal4 patterns for each driver, with *386Y-Gal4* driving transgene expression in the most cells (a few hundred) and yielding the most hits in the screen, and *EH-Gal4* driving transgene expression in just two cells and producing no hits. In addition, only a subset of the cells in the *386Y-Gal4* pattern is likely to control molting behaviors.

The results with *c929-Gal4* did not follow this trend. Although *c929-Gal4* produces transgene expression in a large subset of the cells in the *386Y-Gal4* pattern, including two cells types involved in the control of molting behaviors, the Inka cells and some of the CCAP/bursicon neurons, very few lines produced molting defects when crossed to this driver. The fact that a large proportion of the lines that produced phenotypes with *386Y-Gal4* also did so with *CCAP-Gal4* (Table 1) suggests that the disruption of a small number of specific cell types was responsible for a majority of the observed molting defects. The CCAP/bursicon neurons are essential for head eversion and wing expansion (PARK *et al.* 2003), yet only some of the CCAP/bursicon cells are in the *c929-Gal4* pattern in adults (LUAN *et al.* 2006a), and fewer cells express both *c929-Gal4* and *CCAP-Gal4* at pupal ecdysis (HEWES *et al.* 2003; C. Qu and R. S. Hewes, unpublished observations). Thus, *c929-Gal4* may not drive transgene expression in enough of the CCAP/bursicon neurons, or in the correct CCAP/bursicon neurons, to disrupt molting behaviors (cf., LUAN *et al.* 2006a).

The CCAP/bursicon neurons are a heterogeneous population of cells. This conclusion is based on three lines of evidence: differential activation by ETH, co-expression of different peptides, and functional mapping with genetic mosaics (KIM *et al.* 2006; LUAN *et al.* 2006a). Therefore, differential effects of some of the genes

isolated in this screen on selected CCAP/bursicon cells may account for some of the variation in the types of molting defects (e.g., disruption of head eversion versus wing expansion) that we observed. Alternatively, the variation in cellular phenotypes produced by GOF of different genes (supplemental Table 4) may account for some of the differential effects of these genes on molting behaviors. These two models are not mutually exclusive, and the observed molting defects may result from multiple independent actions of these genes within the CCAP/bursicon neuron population.

Additional cell types involved in molting behavior: Three cell types have confirmed roles in the peptidergic control of Drosophila ecdysis behaviors: the CCAP/bursicon neurons, the EH neurons, and the endocrine Inka cells (McNabb *et al.* 1997; Park *et al.* 2003). Imaging of transient Ca^{2+} signals suggested the involvement of two other neuropeptidergic cell types, the *FMRFamide-related*-expressing thoracic ventral (Tv) neurons and lateral abdominal neurons that produce leucokinin-like peptides, although targeted ablation of the Tv neurons produced only a subtle weakening of pre-ecdysis behaviors (Kim *et al.* 2006). Finally, there is indirect evidence for the involvement of 28 *apterous*-expressing cells (which include the Tv neurons) (Park *et al.* 2004) and corazonin-producing neurons (Kim *et al.* 2004) in the control of Drosophila ecdysis. Our identification of several loci that produced molting defects when expressed with *386Y-Gal4* but not *CCAP-Gal4* (or *c929-Gal4*) provides evidence for one or more undefined neuropeptidergic cell types in the *386Y-Gal4* pattern with important roles in the control of head eversion, eclosion, and wing expansion behaviors. Future genetic mosaic experiments with additional Gal4 drivers may enable the identification of these cells.

Interestingly, Luan *et al*. (2006a) found that expression of a dominant negative form of the regulatory subunit of protein kinase A (PKA^{inh}) had no effect on wing expansion when it was expressed with *c929-Gal4*, although PKA^{inh} produced severe wing expansion defects when expressed with *CCAP-Gal4*. Therefore, only c929-negative cells in the *CCAP-Gal4* pattern appear to require PKA function in order to regulate wing expansion behavior. On first inspection, our results with overexpression of the cAMP-specific phosphodiesterase encoded by *dnc* appear different. Although *dnc* and PKA^{inh} expression both inhibit cAMP signaling, albeit at different points in the pathway, we found that *dnc* blocked wing expansion when expressed with either the *CCAP-Gal4* or the *c929-Gal4* driver (supplemental Table 2). Three observations indicate that this apparent discrepancy with the earlier results of Luan et al. (2006a) may simply reflect dosage effects. First, when we crossed *c929-Gal4* to *UAS-dnc.*C^{X}, we observed modest wing expansion defects with a single copy of each transgene (supplemental Table 2) and much stronger defects with two copies (data not shown). Second, PKA^{inh} expression with *c929-Gal4* produced a significant reduction in bursicon secretion into the hemolymph, even though this reduction was not as severe as with *CCAP-Gal4* and was not sufficient to perturb wing expansion (LUAN *et al.* 2006a). Third, Luan *et al.* also reported that suppression of electrical excitability with *c929-Gal4* completely blocked bursicon secretion into the hemolymph. These animals displayed wing expansion defects that were only seen when electrical activity was blocked in the CCAP cell subset of the *c929-Gal4* pattern. Nevertheless, we cannot yet exclude the possibility that wing expansion requires PKA-dependent functions of cAMP

in c929-negative, CCAP-positive cells and PKA-independent functions of cAMP in cells that express either both drivers or *c929-Gal4* alone.

TABLE S1-1

Additional fly lines used in the forced misexpression screen and follow-up analysis

Name	Genotype	FlyBase ID	Reference
tubulinP-Gal80^{ts}	*w*;; P{w^{+mC}=tubP-GAL80^{ts}}2*	FBti0027797	(MCGUIRE *et al.* 2003)
UY1770	*y^{1} w^{67c23}; P{Mae-UAS.6.11}slv^{UY1770}*	FBti0040304	(NICOLAI *et al.* 2003)
UAS-Cam.B12Q	*y^{1} w*; Cam^{n339}/CyO, y^{+}; P{w^{+mC}=UAS-Cam.B12Q}3*	FBti0026954	(WANG *et al.* 2002)
UAS-Cam.B34Q	*y^{1} w*; Cam^{n339}/CyO, y^{+}; P{w^{+mC}=UAS-Cam.B34Q}3*	FBti0026952	
UAS-Cam.V91G	*y^{1} w*; Cam^{n339}/CyO, y^{+}; P{w^{+mC}=UAS-Cam.V91G}3*	FBti0026953	
UAS-Cam.W	*y^{1} w*; Cam^{n339}/CyO, y^{+}; P{w^{+mC}=UAS-Cam.W}3*	FBti0026955	
UAS-CrebB-17A.DN	*y* w*; P{Cbz}4/TM3*	FBti0038047	(ERESH *et al.* 1997)
UAS-dnc.C^{X}	*w^{1}, P{UAS-dnc.C}*	FBtp0011209	(CHEUNG *et al.* 1999)
UAS-dnc.C^{X},	*w^{1}, P{UAS-dnc.C}; P{UAS-dnc.C}/TM3, P{w^{+mC}=ActGFP}JMR2,*		
UAS-dnc.C^{3}	*Ser^{1}*		
UAS-dORKΔ-C1	*y^{1} w*; P{w^{+mC}=UAS-Ork1.Delta-C}1/TM3, Sb^{1}*	FBti0023687	(NITABACH *et al.* 2002)

UAS-dORKΔ-C2	*y^1 w*; P{w^{+mC}=UAS-Ork1.Delta-C}2*	FBti0023688	
UAS-dORKΔ-NC	*y^1 w*; P{w^{+mC}=UAS-Ork1.Delta-NC}1*	FBti0023689	
UAS-EcR.A	*w*; P{w^{+mC}=UAS-EcR.A}3a*	FBti0023087	(CHERBAS *et al.* 2003)
UAS-EcR.B1	*w*; P{w^{+mC}=UAS-EcR.B1}3b*	FBti0023086	
UAS-EcR.B2	*w*; P{w^{+mC}=UAS-EcR.B2}3a*	FBti0023085	
UAS-EcR.C	*w^{1118}; P{w^{+mC}=UAS-EcR.C}TP1-4*	FBti0026959	
UAS-EcR-B1-F645A	*w^{1118}; P{w^{+mC}=UAS-EcR.B1-DeltaC655.F645A}TP1*	FBti0026961	
UAS-EcR-B1-W650A	*w^{1118}; P{w^{+mC}=UAS-EcR.B1-DeltaC655.W650A}TP1-9*	FBti0026963	
UAS-foxo	*y* w*; P{UAS-foxo}m3-1*	FBgn0038197	(HWANGBO *et al.* 2004)
UAS-Fra.DN	*w^{1118}; P{UAS-Fra.Fbz}5*	FBti0038037	(ERESH *et al.* 1997)
UAS-GFP	*w*, P{UAS-GFP.Y}D1*	FBtp0001170	(YEH *et al.* 1995)
UAS-Jra.DN	*w^{1118}; P{w^{+mC}=Jbz}1*	FBti0038038	(ERESH *et al.* 1997)
UAS-mCD8::GFP	*y^1 w^*; P{w^{+mC}=UAS-mCD8::GFP.L}LL5*	FBti0012685	(LEE and LUO 1999)
UAS-shi.K44A$^{3-10}$	*w^*; TM3, P{w^{+mC}=UAS-shi.K44A}3-10/TM6B, Tb^1*	FBti0015791	(MOLINE *et al.* 1999)
UAS-shi.K44A$^{4-1}$;	*y^1 w^* P{w^{+mC}=UAS-shi.K44A}4-1; P{w^{+mC}=UAS-shi.K44A}3-7*	FBti0016096,	

UAS-shi.K44A$^{3-7}$	FBti0016097

TABLE S1-2

Phenotypes obtained through peptidergic cell-directed expression of target UAS elements

Gene	UAS line	Protein (Mode of Action)	*EH-Gal4* Phenotype	*c929-Gal4* Phenotype	*386Y-Gal4* Phenotype	*CCAP-Gal4* Phenotype
EcR	*UAS-EcR-B1-F645A*	Ecdysone receptor (DN) [a]	Pharate adult lethal[45]	Larval lethal[M]	Pupariation, early pupal lethal	Head eversion[0/5], pharate adult lethal[12], wing expansion[100/0 b]
	UAS-EcR-B1-W650A	Ecdysone receptor (DN) [a]	Larval lethal, pupariation, pharate adult lethal[33], wing expansion[56/44 c D]	Larval lethal[M], pupariation, early pupal lethal, head eversion	Larval lethal[M], pupariation, early pupal lethal, head eversion	18°: head eversion[39/57], pharate adult lethal, wing expansion[100/0 b]

			L N X S T			29°: head eversion, pharate adult lethal
	UAS-EcR.A	EcR-A (GOF) [a]	Normal	Normal	Normal	Normal
	UAS-EcR.B1	EcR-B1 (GOF) [a]	Normal	Wing expansion$^{4/96}$ D X	Pharate adult lethal^{100}	head eversion$^{0/10}$, Wing expansion$^{0/10}$
	UAS-EcR.B2	EcR-B2 (GOF) [a]	Normal	Normal	Normal	Normal
	UAS-EcR.C	EcR common region (GOF) [a]	Normal	Head eversion$^{4/0}$, pharate adult lethal[22]	Head eversion$^{0/35}$	Normal
dnc	*UAS-dnc.C^{X}*	cAMP-specific phosphodiesterase (1X GOF) [d]	Normal	Wing expansion$^{5/95}$ D L N S T X	ND	Wing expansion$^{98/2}$ D L N P S T X *c*
	UAS-dnc.C^{X}, *UAS-dnc.C^{3}*	cAMP-specific phosphodiesterase (2X GOF) [d]	Normal	ND	Wing expansion$^{100/0}$ D L N P S T X	Wing expansion$^{94/3}$ D L N P S T X *c*
shi	*UAS-shi.K44A$^{4-1}$;*	Dynamin (DN) [e]	Normal	Head eversion,	Pupariation, head	ND

	UAS-shi.K44A$^{3-7}$			pharate adult lethal^{95}, wing expansion$^{0/100\ X}$	eversion, pharate adult lethal	
	UAS-shi.K44A$^{3-10}$	Dynamin (DN) [e]	Head eversion$^{4/0}$, pharate adult lethal^{39}, wing expansion$^{36/64\ D\ L\ N\ P\ S\ X}$	100% lethal (no pupae)	100% lethal (no pupae)	ND
Ork1	*UAS-dORKΔ-C1*	Constitutively open K^+-selective leak channel (GOF) [f]	Normal	Pupariation, early pupal lethal, head eversion	Larval lethal	ND
	UAS-dORKΔ-C2	Constitutively open K^+-selective leak channel	Normal	Larval lethal, pupariation, early pupal lethal, pharate	Larval lethal	ND

		(GOF) [f]		adult lethal		
	UAS-dORKΔ-NC	Non-conducting pore mutant channel (GOF) [f]	Normal	Normal	Normal	ND
Cam	*UAS-Cam.B34Q*	CAM with Ca^{++}-binding sites 3 and 4 disabled (DN) [g]	Normal	Normal	Normal	ND
	UAS-Cam.V91G	V91G mutant CAM (GOF) [g]	Normal	Normal	Normal	ND
	UAS-Cam.B12Q	CAM with Ca^{++}-binding sites 1 and 2 disabled (GOF) [g]	Normal	Normal	Normal	ND
	UAS-Cam.W	Wild-type CAM	Normal	Normal	Normal	ND

		(GOF) [g]				
CrebB-17A	*UAS-CrebB-17A.DN*	Truncated bZIP fragment of CrebB-17A (DN)[h]	Normal	Normal	Normal	ND
Jra	*UAS-Jra.DN*	Truncated bZIP fragment of JRA (DN) [h]	Normal	Normal	Normal	ND
kay	*UAS-Fra.DN*	Truncated bZIP fragment of KAY (DN) [h]	Normal	Normal	pharate adult lethal[67]	ND

Pupal and adult phenotypes are summarized as follows (embryonic and larval phenotypes were not scored unless indicated): early pupal lethal, lethal with developmental arrest after pupariation and prior to head eversion; head eversion, defective in pupal head eversion [the numbers in superscript indicate the percentage of cryptocephalic/microcephalic pupae (HEWES *et al.* 2000)]; Larval

lethal, lethality during the larval stages (only scored when this was the predominant phenotype); pupariation, pupariation defects that were variable and included failure to fully shorten the pupal case and retention of other larval features, failure to evert anterior spiracles, and curving of the puparium to one side; pharate adult lethal^{x}, lethality in animals completing metamorphosis but failing to eclose (the number in superscript indicates the percentage of animals displaying pharate adult lethality); wing expansion$^{x/x}$, defective wing expansion (the numbers in superscript indicate the percentage of adults with completely unexpanded/partially expanded wings) (n>20). The counts of microcephal-like pupae may have been undersampled, since some animals with a weaker microcephal phenotype eclosed. Embryonic lethality was not scored. We examined representative adult animals for phenotypes associated with defects in tanning of the adult cuticle and expansion of adult structures (BAKER and TRUMAN 2002; MCNABB *et al.* 1997). These included: ^{D}, dimpling of the dorsal and anterior surfaces of the thorax; ^{L}, bent femur and tibia (highly variable); ^{N}, tanning delayed or incomplete; ^{P}, ptilinum remained soft and partially extended several hours to days after eclosion; ^{S}, scutellum wrinkled and scutellar bristles crossed and directed toward anterior; ^{T}, darkened cuticle in shape of trident forms on dorsal thorax (highly variable); ^{X}, loss of the glossy surface finish of the cuticle. Other abbreviations: DN, Dominant negative; GOF, gain-of-function; ^{M}, larvae with multiple mouthparts; ND, not done.

[a](CHERBAS *et al.* 2003).

[b]D, L, N, P, S, T, and X phenotypes not scored.

[c]Scoring performed at 24.5º (for *UAS-EcR-B1-W650A*, only the wing expansion phenotype was scored at 24.5º).

[d](CHEUNG *et al.* 1999).

[e]The *UAS-shi.K44A*$^{4-1}$*; UAS-shi.K44A*$^{3-7}$ double-insertion line expresses dominant negative *shi* at a moderate level, and the *UAS-shi.K44A*$^{3-10}$ insertion expresses dominant negative *shi* at a high level (FLYBASE_CONSORTIUM 2003; MOLINE *et al.* 1999).

[f]The *UAS-dORKΔ-C1* and *UAS-dORKΔ-NC* insertions are expressed at high levels, while the expression obtained with *UAS-dORKΔ-C2* is lower (NITABACH *et al.* 2002).

[g](WANG *et al.* 2002).

[h](ERESH *et al.* 1997).

TABLE S1-3

Summary of gain-of-function lines and mutant phenotypes detected with the *c929-Gal4*, *386Y-Gal4, and CCAP-Gal4* drivers

Insertion	Gene	Gene Product (Mode of Action)	Reference EST	Distance to EST 5′ end	*c929-Gal4* Phenotype	*386Y-Gal4* Phenotype	*CCAP-Gal4* Phenotype
EP(2)2003	*Ptc-related* (*Ptr*)	Patched-family membrane protein (GOF)	RE06080	-279 [a]	Normal	Head eversion$^{4/44}$, wing expansion$^{18/0\ b}$ D L N P S T X	Wing expansion$^{50/12}$ D L N P S T X
EP(2)2237	*cabut (cbt)*	C2H2 type zinc finger transcription factor (GOF)	RH55484	-15 [a]	Normal	Pupariation, head eversion$^{0/81}$, wing expansion$^{100/0}$ D L N P S T X	Pupariation, head eversion$^{11/53}$, wing expansion$^{100/0}$ D L N P S T X

EP(2)2356	*miR-313*	MicroRNA (GOF)	*miR-313*	-204 [a]	Normal	Pharate adult lethal[20], wing expansion[100/0]	ND
	miR-312		*miR-312*	-343 [a]			
	miR-311		*miR-311*	-504 [a]			
	miR-310		*miR-310*	-624 [a]			
EP(2)2586		(GOF)	*miR-313*	-76 [a]	Head eversion[2/0]	Wing expansion[100/0]	ND
			miR-312	-215 [a]			
			miR-311	-376 [a]			
			miR-310	-496 [a]			
EP(2)2587		(GOF)	*miR-313*	-76 [a]	Head eversion[4/3]	Pharate adult lethal[27], wing expansion[100/0 D L N P S T X]	Wing expansion[100/0 D L N P S T X]

			miR-312	-215 [a]			
			miR-311	-376 [a]			
			miR-310	-496 [a]			
EP(2)2583	*split ends* (*spen*)	Large RNA-binding protein (RRM superfamily) (GOF)	RE45577	+2425 [a] (-1127 of exon 2, which contains translational start site)	Normal	Head eversion$^{0/25}$, wing expansion$^{100/0\ c}$	Head eversion$^{0/20}$, wing expansion$^{100/0\ D\ L\ N\ P\ S\ T\ X}$
EP(3)0917	*BEST:RE29262*	CDS unknown (GOF)	RE29262	+442 [a]	Normal	Head eversion$^{0/91}$, wing expansion$^{100/0\ D\ L\ N\ P\ S\ T\ X}$	Wing expansion$^{24/40\ D\ L\ N\ P\ S\ T\ X}$
EP(3)3015	EP(3)3015a:	Novel (GOF)	SD16005	+705 [a]	Normal	Head	Head

	l(3)neo38					eversion[15/82], wing expansion[100/0 *b c* L]	eversion[0/32], wing expansion[8/79 *b* D N L P S T X]
	EP(3)3015b: *SNF4/AMP-activated protein kinase gamma subunit* (*SNF4Agamma*)	5′-AMP-activated serine/threonine protein kinase subunit (noncatalytic subunit of the SNF/AMPK complex) (GOF)	LD41424	-114 [a]			
EP(3)3121	*CG5585*	Similar to retinoblastoma binding protein 5	RE17089	-627 [a]	Normal	Head eversion[5/5]	Normal

		(WD40 repeat containing protein) (GOF)					
EP(3)3140	*miR-279*	microRNA (GOF)	EN05557	-724 [a]	Normal	Pupariation, head eversion$^{4/55}$, wing expansion$^{86/14}$ D L N P S X	Wing expansion$^{100/0}$ D L N P S T X
EP(3)3354	*jing interacting gene regulatory 1 (jigr1)*	ADH transcription factor 1-like protein (GOF)	RE50978	-5 [a]	Normal	Pupariation, head eversion$^{0/29}$, wing expansion$^{47/53}$ D L N P S T X	Wing expansion$^{53/40}$ D N P S T X
EP(3)3390	*EP3390*	CDS unknown (GOF)	CO26727 2	+70 [a]	Normal	Pupariation, pharate adult lethal [d], wing expansion$^{38/62}$ D L	Wing expansion$^{7/82}$ D N P S T X

						N P S T X	
EP(3)3415	*pebble* (*pbl*)	Rho guanyl-nucleotide exchange factor (GOF)	RE72229	+41 [a]	Normal	Pharate adult lethal[74 e]	Normal
EP(3)3520	*fat facets* (*faf*)	Ubiquitin-specific protease (GOF)	RE01547	+52 [a]	100% lethal (no pupae)	Wing expansion[97/3 D L N P S T X]	Wing expansion[100/0 D L N P S T X]
EP(3)0381			RE01547	+255	ND	Wing expansion[44/0 D L N P S T X]	Wing expansion[31/3 D L N P S T X]
EP(3)3523	*miR-276a* (*l(3)L0539*)	microRNA (GOF)	EP18729	-1138	Normal	Pharate adult lethal[100]	Wing expansion[14/38 D L P S T X]
EY(3)13010			EP18729	-23931	Normal	Pharate adult	Normal

						lethal[98]	
EY(X)10575	*CG14438*	Smad- and Olf-interacting Zn-finger-like (Zfp423) protein (GOF)	LP02916	+170	Normal	Pharate adult lethal[27]	Wing expansion[68/15 D L N P S X]
EY(X)14679	*CG11265*	Topoisomerase-related function protein 4-2 (TRF4-2)-like protein (GOF)	RE04457	+923	Normal	Wing expansion[0/10]	Wing expansion[39/6 D L N P S T X]
EY(2)03416	Unknown	Unknown			Normal	Wing expansion[31/69 D L P S T X]	Normal
EY(2)04392	*BEST:RH2476*	CDS unknown	RH24762	-3814	Normal	Wing	Wing

	2	(GOF)				expansion$^{21/76\ D\ L\ N\ P\ S\ T\ X}$	expansion$^{63/37\ D\ L\ N\ P\ S\ T\ X}$
EY(2)05304	*Myb-interacting protein 120* (*mip120*)	Putative transcriptional regulator (GOF)	RE01859	+3207 (-140 of exon 2 splice acceptor site; in CDS with most of the CDS 3′ of the insertion)	Wing expansion$^{10/17\ D\ L\ N\ P\ S\ T\ X\ f}$	Pharate adult lethal^{17}, wing expansion$^{92/8\ D\ L\ N\ P\ S\ T\ X}$	Wing expansion$^{100/0\ D\ L\ N\ P\ S\ T\ X}$
EY(2)06734	*CG3651*	Novel (GOF)	GH15431	-5121 ^{g}	Normal	Wing expansion$^{28/3\ D\ L\ N\ P\ S\ T\ X}$	Normal
EY(2)08136	*CG3363*	Similar to MAX-	CO30915	+818	Normal	Wing	Normal

		interacting protein isoform 1 (GOF)	7 (putative 5′ UTR of CG3363)			expansion$^{81/19\ D\ L\ N\ P\ S\ T\ X}$	
EY(2)08577	*CG8170*	Serine-type endopeptidase (GOF)	RE24424	-30	Normal	Wing expansion$^{100/0\ D\ L\ N\ P\ S\ X}$	Normal
EY(2)08937	*CG14471* (in an intron of *Src42A*)	Novel (GOF)		*CG14471-RA*: -2038	Normal	Wing expansion$^{88/12\ D\ L\ N\ P\ S\ T\ X\ h}$	Wing expansion$^{5/30\ D\ L\ N\ P\ S\ T\ X}$
	Src oncogene at 42A (*Src42A*)	Protein tyrosine kinase (GOF)		*Src42A*:near center of 20kb intron			
EY(2)11371	*Gonadotropin-releasing hormone*	Neuropeptide G-protein coupled receptor (GOF)	GH19447	+19	Normal	Pharate adult lethal^{26}, wing expansion$^{14/4\ D\ L\ N}$	Normal

	receptor (*GRHR*)					P S T X	
EY(2)12630	*CG31739*	Aspartyl-tRNA synthetase (GOF)	SD02215	+239 (-156 of exon 2)	Normal	Pharate adult lethal[29] [e]	Normal
EY(2)13709	*CG2808*	Homeobox transcription factor (GOF)	CO33169 6	-6306	Normal [i]	Larval lethal, pupariation, head eversion[0/100], wing expansion [j]	Wing expansion[2/98] D N P S T X
	foraging (for)	cGMP-dependent protein kinase (LOF)	NM_2059 04 [k]	-21			
EY(2)14184	*spitz (spi)*	EGF-like growth factor (GOF)	RH69567	+41	Normal	Pharate adult lethal[70] [e]	Normal
EY(3)00146	*stonewall* (*stwl*)	Similar to Myb and ADF-1 helix-	U41367 [k]	+272 (in CDS with	Normal	Head eversion[3/89], wing expansion [c]	Wing expansion[100/0] D

		turn-helix transcription factors (GOF)		most of the CDS 3′ of the insertion)			L N P S T X
EY(3)00559	*klarsicht* (*klar*)	Microtubule-associated protein (GOF)	LD36052	-2564 of *klar* exon 5 (in CDS with most of the CDS 3′ of the insertion)	Normal	Wing expansion$^{20/25\ D\ L\ N\ P\ S\ T\ X}$	Head eversion$^{5/5}$, wing expansion$^{44/39\ D\ L\ N\ P\ S\ T\ X}$
EY(3)00681	*Insulin-like receptor* (*InR*)	Insulin-like peptide receptor (GOF)	U28136 [k]	-25291	Normal	Pharate adult lethal$^{22\ e}$	Normal
EY(3)03118	*logjam* (*loj*)	EMP24/GP25	RE44409	+6	Normal	Pharate adult	Normal

		protein (transmembrane component of cytoplasmic vesicles) (GOF)				lethal[8], wing expansion[15/15 D L N P S T X]	
EY(3)03254	*pointed (pnt)*	ETS domain transcription factor (GOF)	SD17072	+375	Normal	Pharate adult lethal[94], wing expansion[75/0 D L N P S T X]	Pupariation, head eversion[4/9], wing expansion[8/22 L P T X]
EY(3)03808	*BEST:RH6416 1*	CDS unknown (GOF)	RH64161	-6437	Normal	Pharate adult lethal[100]	Normal
EY(3)03940	*headcase (hdc)*	Novel (GOF)	RE14371	-4978	Pupariation, head	Head eversion[5/95]	Early pupal lethal[11], head

					eversion$^{0/11}$		eversion$^{1/18}$
EY(3)08255		(GOF)	RE14371	-765	Early pupal lethal^{31}	Head eversion$^{0/100}$	Head eversion$^{31/53}$
EY(3)14615		(LOF? Flanking sequence in opposite orientation of *hdc* gene)	RE14371	-59	Normal	Head eversion$^{7/67}$	Head eversion$^{0/14}$
EY(3)05179	Unknown	Unknown			Normal	Wing expansion$^{27/21\ D\ L\ N\ P\ S\ T\ X}$	Normal
EY(3)06009	*CG11966*	C2H2 type zinc finger transcription factor (GOF)	RT01119	-1811 (position 16 of RT01119—	Head eversion$^{0/32}$	Larval lethal, pupariation, early pupal lethal, head eversion$^{0/57}$	Normal

				1st 15 bases could not be mapped to upstream sequence)			
EY(3)16110		(GOF)	RT01119	-1778 (position 16 of RT01119—1st 15 bases could not be mapped to upstream sequence)	Normal	Larval lethal, pupariation, early pupal lethal, head eversion$^{38/62}$	Wing expansion$^{0/10\ L\ P\ X}$
EY(3)08024	*CG11899*	Phosphoserine	RH42411	-37	Normal	Head eversion$^{0/37}$	Pupariation,

		transaminase (GOF)					early pupal lethal[21], head eversion[0/35], wing expansion[11/22 D N P S T X]
EY(3)09041	*BEST:RH64518*	CDS unknown (GOF)	RH64518	-2122	Normal	Pharate adult lethal[44 *e*]	Early pupal lethal[14]
EY(3)09825	*CG14060*	Putative component of snRNP U2, nuclear mRNA splicing (GOF)	LP16591	-4250 of exon 2	Pharate adult lethal[15 *e*], wing expansion[9/27 L N S T X *e*]	Pharate adult lethal[21 *e*]	Pharate adult lethal[16]
EY(3)10546	*BEST:SD07879*	CDS unknown (GOF)	SD07879	-15585	Normal	Head eversion[18/74]	Normal

EY(3)11248	*forkhead box, sub-group O* (*foxo*)	Forkhead transcription factor (GOF)	LD19191	-68	Normal	Wing expansion$^{16/42\ D\ L\ P\ S\ T\ X}$	Wing expansion$^{50/10\ D\ L\ N\ P\ S\ X}$
WH(2)f04134	*CG1441*	Oxidoreductase (GOF)	RE66242	+104	Head eversion$^{0/17}$	Pupariation, head eversion$^{0/70}$	Normal
XP(2)d03190	*CG9162*	Novel (GOF)	GH05093	+848	Normal	Wing expansion$^{17/12\ D\ L\ N\ P\ S\ T\ X}$	Normal
XP(2)d07339	*CG9154 sugar transporter 1* (*sut1*)	Novel (GOF) Facilitated glucose transporter (GOF)	GM04011 RE44635	-8683 -83	Head eversion$^{0/5}$	Pupariation, early pupal lethal, head eversion$^{6/77}$, wing expansion$^{100/0\ D\ L\ N\ P\ S\ T\ X}$	Wing expansion$^{100/0\ D\ L\ N\ P\ S\ T\ X}$

	saliva (*slv*)	Novel (GOF)	U70979 [k]	-524			
XP(3)d00809	*CG14290*	Novel (UniProtKB/Swiss-Prot family/domain classification: UPF0041 family) (GOF)	RE54918	+13	Normal	Head eversion$^{0/100}$	Head eversion$^{5/5}$, wing expansion$^{100/0\ D\ L\ N\ P\ S\ T\ X}$
	CG31295	Novel (GOF)	SD17750	-529			
XP(3)d02427	*Dichaete* (*D*)	HMG (high mobility group) box protein -- transcriptional activator (GOF)	AT02631	+1016 (in 5′ UTR)	Normal	Pupariation, head eversion$^{3/89}$, wing expansion$^{100/0\ b\ c}$	Normal

	nuclear fallout (*nuf*)	Rab11 family-interacting protein 4 (GOF)	RE36768	-13244			
XP(3)d02595	*CG6621*	TPR (tetratricopeptide repeat domain) protein (intracellular trafficking) (GOF/LOF)	LD24134	+888 (-5 from splice acceptor site of exon 3)	Normal	Larval lethal^{M}	Head eversion$^{18/55\ e}$, wing expansion$^{100/0\ D\ L\ N\ P\ S\ T\ X}$
	CG4674	Arrestin-domain protein (GOF/LOF)	RE18068	-1159 of exon 2 splice acceptor site			
XP(3)d02894	*n-*	v-SNARE (GOF)	GH04963	-608 of n-	Normal	Wing	Wing

	synaptobrevin (*n-syb*)			syn-RB exon 2 (5′ of translational start site)		expansion$^{0/35\ D\ L\ N\ P\ S\ T\ X}$	expansion$^{0/18\ D\ L\ N\ P\ S\ T\ X}$
	methyltransferase-like (*metl*)	Methyltransferase (LOF)	RE19309	+2181			
	Big brother (*Bgb*)	Core binding factor β subunit (GOF)	SD08175	-3090			
XP(3)d04253	*CG14701*	CSL zinc finger (LOF)	IP03582	+918 (+285 of 3′ end of transcript)	Pupariation, head eversion$^{38/31}$	Pupariation, head eversion$^{24/42\ l}$	Pharate adult lethal^{16}, wing expansion$^{100/0\ D\ L\ N\ P\ S\ T\ X}$
	CG17187	Heat shock protein DnaJ (Hsp40)	RE47242	-973			

		(GOF)					
	CG17184	Arfaptin-like protein (LOF)	LD44124	+2161 (in 3′ UTR)			
	CG17721	RING-finger domain protein (GOF)	LP09251	-2553			
XP(3)d07058	*CG6149*	Related to hamster androgen-induced FAR-17a protein, and its human homologue, the AIG1 protein (GOF/LOF)	None	+467 (downstream of predicted splice acceptor site for exon 2; in CDS)	Normal	Head eversion$^{0/5}$, pharate adult lethal[93]	Males: Wing expansion$^{53/0\ D\ L\ N\ P\ S\ T\ X\ f}$ Females: Normal
	CG7557	Similar to MoxR-	GH07076	-10147			

		like ATPase (GOF)					
XP(3)d07478	*Lnk*	Similar to Lnk cytokine receptor signaling adaptor protein (GOF)	RH23441	+969 (in intron, -143 bp 5′ of exon containing predicted start ATG)	Normal	Pharate adult lethal[52 c]	Normal
	CG17370	Signal peptide peptidase-like 3 (LOF)	GM06145	+7497 (+1947 from 3′ end of gene)			
	Tetraspanin 96F (*Tsp96F*)	Tetraspanin, CD82 antigen	RE46458	-8117			

		(Metastasis suppressor homolog) (GOF)					
XP(3)d11470	*CG4476*	Similar to cation/neurotransmitter symporters (GOF)	RE33779	+3	Normal	Pupariation, head eversion$^{0/67}$	Normal
	CG4484	Major Facilitator Superfamily (MFS_1) transporter, sucrose:hydrogen symporter (GOF)	LP09277	-3033			

Only lines with mutant phenotypes in at least 10% of the pupae or adults are listed. The descriptions for the larval, pupal, and adult phenotypes are summarized as in supplemental Table 2 (n>20). The genes listed for each insertion were identified as described in the Materials and Methods. CDS, coding sequence; GOF, gain-of-function (sense); LOF, loss-of-function (antisense); ND, not done.

[a]Insertion site verified by PCR analysis and gel electrophoresis (to test for products of the expected sizes) using gene-specific primers flanking the insertion site and a primer targeting the inverted repeat sequence at each end of the EP element.

[b]Leg defects unusually severe, often with large and distended tarsal segments and strongly bent femurs.

[c]Most adults die while stuck to the food with unexpanding wings.

[d]Pharate adult lethality was the predominant phenotype when this line was first tested. Several months later, when this line was retested, wing expansion defects were the primary phenotype.

[e]Adult labrum transformed into paired larval-like mouthparts (with melanization and serration) (cf., COLOMBANI *et al.* 2005).

[f]At 24.5º. Adults were normal at 29º. [Note: We tested 10 of 17 of the lines analyzed in supplemental Table 4 in crosses to *c929-Gal4* at 24.5º, and *EY(2)05304* was the only line that produced wing expansion defects].

[g]This insertion site is unclear due to insertion into a *Doc* transposable element (R. W. Levis, personal communication).

[h]D L N T all weak in this cross (i.e., tanning defects were mild).

[i]Behaviorally abnormal: adults fly very little, even when disturbed, and pupae all in food.

[j]Too few adults to score frequency of PEW versus UEW.

[k]GenBank accession number.

[l]Severity of head eversion defects strongly positively correlated with severity of pupariation defects.

SUPPLEMENTAL TABLE S1-4

Cellular phenotypes for insertions that produced strong wing expansion defects in combination with *CCAP-Gal4*

		CCAP/bursicon neuron morphology			
		Wandering third instar larvae		Pharate adults	
Insertion	External phenotype class	CNS	Periphery (Type III neuromuscular endings) [a]	CNS [a]	Periphery [a]
		Class I—Neurite pathfinding defects			
EP(2)2003	SI	Most neurites mistargeted to ectopic locations in VNC and to lesser extent in brain lobes; some neurites	0-40% of endings visible; fewer boutons.	Neurites thicker, more intensely immunostained, bilaterally asymmetric and with larger	50% of efferents visible, with fewer higher order branches and >50% reduction in extent of distal efferent

with large swellings near normal branch sites; many efferents and abdominal somata absent.[abc]	varicosities; midline longitudinal thoracic tracts and DTA usually missing; MPB missing or with few branches and extending further laterally; AA, CTA and SA incomplete, but with ectopic projections; most B_{AG} somata rounded with 70-80% smaller diameters, while 1-3 B_{AG} somata weakly stained with thin ring	branches bearing larger varicosities.

				of cytoplasm surrounding nucleus.	
Class II—Defective bursicon secretion without gross changes in adult cell morphology					
EP(2)2587	SF	LB(T1-A7) defasciculated and branching from LLT at ectopic anterior-posterior positions (or missing); elevated bursicon immunoreactivity in PA, TA, and MA(S-A7); ectopic (<50 μm-long) primary neurites from MP somata;	Normal.	Normal.	Normal.

		projections in LLT often turn to join LB.[abc]			
EP(3)3354	MF	Posterior LLT (near PAA) defasciculated.[abc]	Normal.	Normal.	Normal.
		Class III—Loss of adult-specific neurites			
EP(2)2237	P, HE[1], SF	Normal.[abc]	Fewer, smaller boutons.	Markedly reduced LSE immunoreactivity; 7-13 B_{AG} somata visible, with 50% smaller diameters; some B_{AG} with increased immunoreactivity and others very weakly immunostained; most neurites present but	Fewer than 50% of efferents visible; smaller varicosities.

				only weakly immunopositive; DTA missing.	
EP(2)2583	HE[2], SF	CCAP immunoreactivity reduced by 95% in MLT; somata diameters (except VA) smaller; LLT wavy and defasciculated.[abc]	Smaller boutons.	Markedly reduced LSE immunoreactivity; 6-13 B_{AG} somata visible, with 50% smaller diameters; AA weakly immunostained, and most other neurites missing.	Fewer than 50% of efferents visible; smaller varicosities.
EP(3)3140	SF	Ectopic (<50 μm-long) primary neurites from MP somata.[abc]	Normal.	B_{AG}^{p} somata diameters 50% smaller; B_{AG}^{a} somata with very little cytoplasm and	50-75% normal number of efferents visible, most lacking branches and *en passant*

				condensed, or fragmented; CNS arbor less profuse.	varicosities but with strongly immunoreactive, club-shaped endings.
EP(3)3520	SF	MLT extends further posteriorly to terminate near PAA; ectopic arborization between MPA and MP somata and (with enlarged varicosities) in PA, TA, PAA, and from LLT.[abc]	Normal.	MPB missing or weakly immunostained; AA and SA less profuse, with large, strongly immunoreactive varicosities and club-shaped endings in SA; 10-13 B_{AG} somata visible, and 1-4 very weakly stained with	50-70% of efferents visible; fewer, shorter higher order branches, with smaller, more sparsely distributed varicosities; some efferents missing branches and large varicosities.

				thin ring of cytoplasm surrounding nucleus while others rounded with 20-50% smaller diameters.	
EY(X)10575	SI	Normal.[a]	Normal.	Portions of MPB, SA, DTA, CTA, and longitudinal thoracic tracts missing; AA less profuse; 11-14 B_{AG} somata visible; LSE and B_{AG} somata rounded with 50% smaller diameters.	50-70% of efferents visible, with smaller varicosities; 30-50% reduction in extent of distal efferent branches bearing larger varicosities.
EY(2)04392	MF	PA reduced or not	Smaller boutons.	MPB missing or	Normal.

		visible and arborization in TA reduced; neurites (particularly LLT) punctate; short ectopic neurites from LLT or initial processes of cells throughout VNC.[a]		weakly immunostained, and SA, DTA, and CTA weakly immunostained.	
EY(2)05304	SF	CD8::GFP fluorescence stronger in MP somata and arbor, LSE(1-3), and TA.[abc]	Normal.	MPB and DTA absent or weakly immunostained; SA less profuse and/or weakly immunostained; immunostaining in CTA and AA reduced by 50-75%, and AA	50-70% of efferents visible (lateral efferents missing); efferents with fewer branches and small, weakly stained varicosities throughout (comparable to varicosities located in

				more punctate; B_{AG} somata rounded, more strongly immunopositive, and with 50% smaller diameters or very weakly stained with thin ring of cytoplasm surrounding nucleus.	the proximal portion of wild type efferents).
EY(3)00146	SF	Normal.[abc]	Smaller boutons.	MPB, SA, DTA, and CTA weakly immunostained, and MPB and SA often missing; B_{AG}^{p} somata with 50% smaller	50 of efferents visible (most lateral efferents missing); remaining efferents with fewer branches and fewer varicosities.

				diameters; B_{AG}[a] somata increased in number (to ~18) with 80-90% smaller somata diameters and very weak immunostaining; AA punctate and anterior portion less profuse.	
EY(3)00559	HE[2], SI	Normal.[ab]	Normal.	MPB, SA, DTA, and CTA absent or very weakly immunostained; 0-1 LSE visible with 50% reduced immunostaining and	50% of efferents visible.

				soma diameters; 6-8 B_{AG} somata visible with 50% smaller diameters and large, poorly immunostained cytoplasmic inclusions, or very small and weakly immunoreactive; AA smaller and more weakly immunostained.	
UAS-foxo [d]	SF (25°)	Normal.[a]	Smaller boutons.	Most neurites absent or unstained; 0-1 LSE and 1-5 B_{AG} somata visible and small, rounded, and	Most efferents missing.

				weakly immunoreactive.	
XP(2)d07339	SF	MA(A1-A7) less profusely branched.[abc]	Bouton size and number markedly reduced, particularly in more posterior segments (often fewer than 10 visible).	MPB, SA, DTA, and CTA less profuse and weakly immunostained; AA less profuse, with a few large varicosities; B_{AG} somata smaller and rounded, with smaller, with irregularly shaped protrusions.	Only 60-80% normal number of efferents visible, most with fewer higher order branches and fewer varicosities.
XP(3)d00809	HE[2], SF	Bursicon levels elevated in DPs; somata diameters (except VA) 30-50%	Fewer boutons, particularly in posterior segments, where many terminals have only 0-15	MPB, SA, DTA, and CTA missing; AA reduced, with anterior portions more severely	Most efferents present but very weakly immunopositive near point of CNS exit;

		smaller.[ab]	boutons.	affected; 10-14 B_{AG} somata visible and small, rounded, and weakly immunopositive (B_{AG}^{p} somata less severely affected).	fewer large varicosities that are restricted to distal portions of neurite branches; reduced neurite branching.
XP(3)d02595	HE[1], SF	Normal.[ab]	Fewer, smaller boutons.	Most CNS neurites and LSE missing; 0-4 B_{AG} somata visible and small, rounded, and weakly immunopositive.	Efferents missing.
XP(3)d04253	SF	Posterior LLT (near PAA) defasciculated.[a]	Fewer, smaller boutons.	Most CNS neurites missing, except 0-30%	Efferents often missing, but when present,

of AA visible; most LSE missing; 10-14 B_{AG} somata visible and small, rounded, and weakly immunopositive.	visible as short, isolated, weakly immunostained stretches of axon in the normal branching pattern.

Only insertions that produced strong wing expansion defects in combination with *CCAP-Gal4* are listed (all refer to phenotypes observed at 29° unless noted). The abbreviations for cellular structures are defined in Figure 3, and each phenotype description is based on analysis of 3-27 preparations (n>5 for 82 out of 91 total phenotypic analyses). More detailed descriptions of the phenotypes are presented in supplemental Table 3. Wing expansion defects were classified as: SF, strong and fully penetrant wing expansion defects with ≥90% UEW; MF, moderate and fully penetrant wing expansion defects with 50-90% UEW and 90-100% total (UEW + PEW); SI, strong and incompletely penetrant with >40% UEW and <90% total. When head eversion defects were also observed, these were classified as: HE^1, strong head eversion defect with >10% cryptocephal and >50% microcephal pupae; HE^2, weak to moderate head eversion defect with <10% cryptocephal and <36% microcephal pupae. Unless noted, all genotypes displayed

20-50% general reductions in bursicon immunoreactivity, CCAP immunoreactivity, and mCD8::GFP fluorescence. P, pupariation defects. ND, not done.

[a]Visualized with anti-bursicon immunocytochemistry (ICC).

[b]Visualized with anti-CCAP ICC.

[c]Visualized with *CCAP-Gal4* → *UAS-mCD8::GFP*.

[d]*UAS-foxo* was substituted for *EY(3)11248*. Both insertions displayed similar wing expansion and cellular defects, although these phenotypes were more severe with *UAS-foxo*.

Figure S1-1.—Remodeling in the CNS of the CCAP/bursicon neurons during metamorphosis. The panels show anti-bursicon immunostaining of the VNC at the indicated times (in hr) after puparium formation (APF). All images are confocal *z*-series projections that were obtained with the same scan settings, and most of the staining was performed in parallel. The images are representative of 5-19 preparations for each time point. Arrows, large swellings in retracting axons (not always observed). Scale bar, 50 μm.

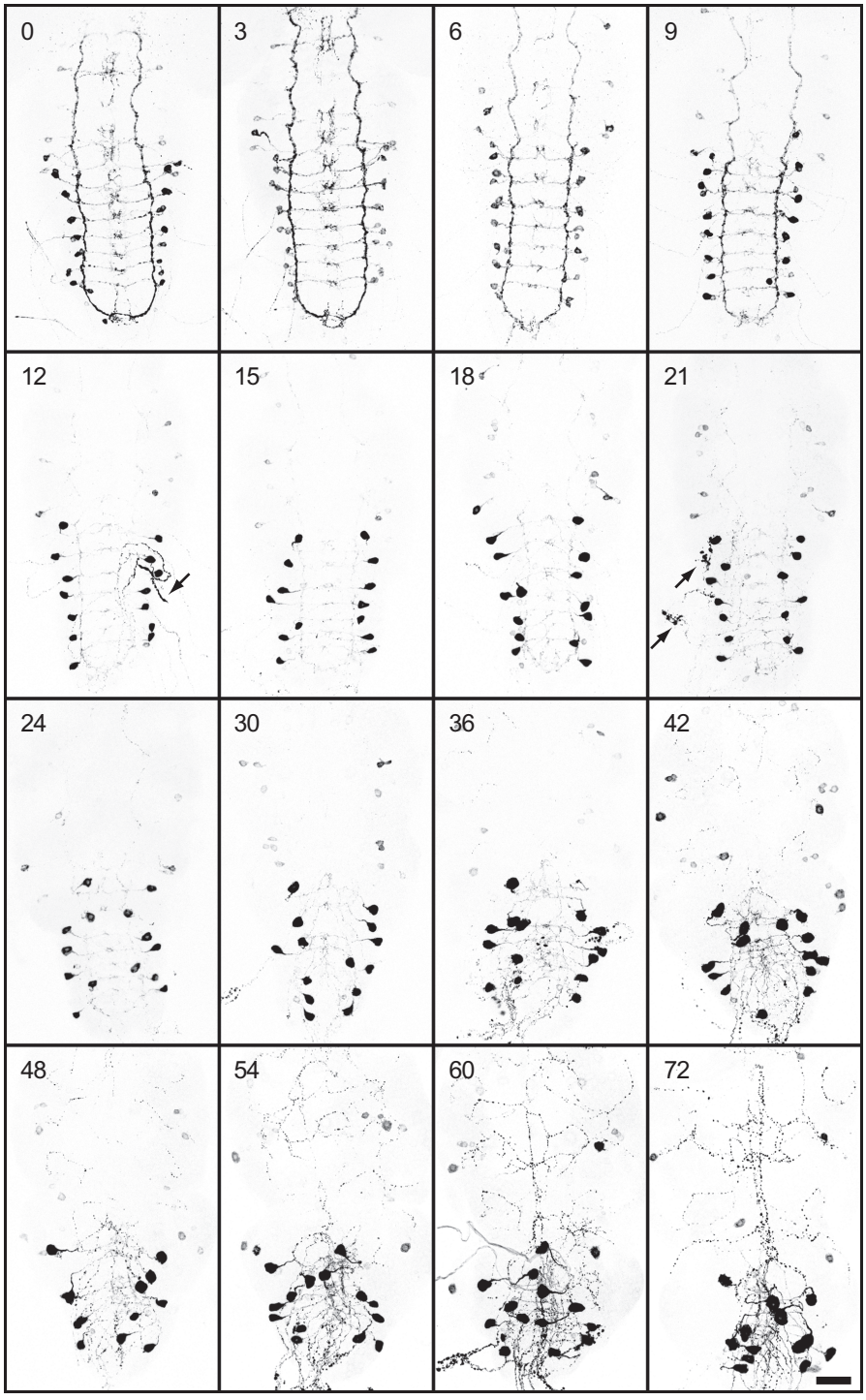
0
3
6
9
12
15
18
21
24
30
36
42
48
54
60
72

Supplemental Figure S1-2.—Remodeling of the CCAP/bursicon neuron efferent projections during metamorphosis. The panels show representative images of anti-GFP immunostaining of the body wall and ventral nerve cord from *CCAP-Gal4, UAS-mCD8::GFP/+* animals at the indicated times APF (in hr; *n*=6-9). All images are confocal *z*-series projections that were obtained with the same scan settings, and most of the staining was performed in parallel. The 54 hr image is also shown in Figure 6H. Asterisk, axonal fragment; arrows, type III boutons at neuromuscular endings; arrowheads, unbranched axons with few varicosities; double feathered arrows, material accumulated at distal ends of retracting axons; double feathered arrowheads, newly formed axonal processes. Scale bar, 100 μm.

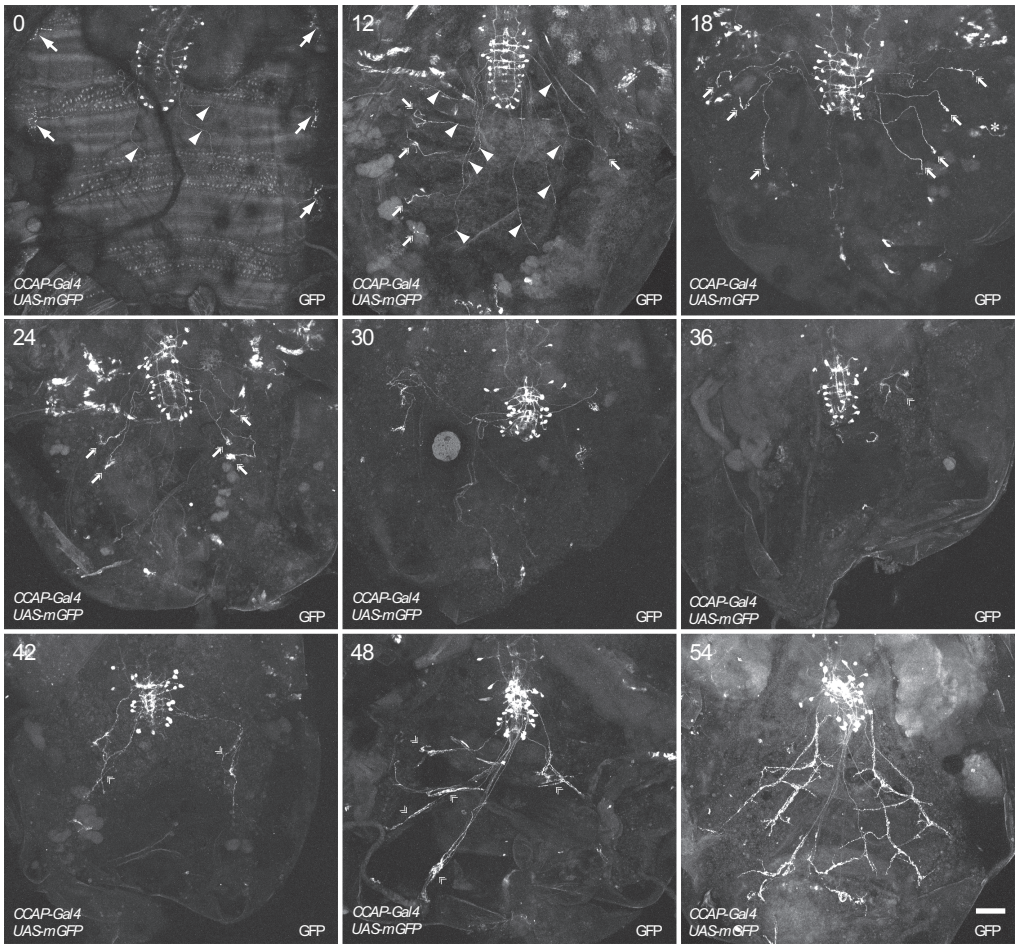
0
12
18
24
30
36
42
48
54
CCAP-Gal4
UAS-mGFP
GFP

Appendix 2: A Drosophila deficiency screen for modifiers of *split ends*-dependent effects on nerve cell remodeling.

SUPPLEMENTAL MATERIAL

Table of Contents

SUPPLEMENTAL TABLE S2-1

Deficiencies screened for modification of the wing expansion phenotype produced by *spen* overexpression

		Trial 1					Trial 2				Trial 3				
			%UEW				%UEW				%UEW				
Deficiency	Breakpoints	Date	Test	Ctrl	Mod.	Class	Test	Ctrl	Mod.	Class	Test	Ctrl	Mod.	Class	Final Status
Df(1)Exel6223	664015; 803283	Jan-07	92.0	100.0	SUP (8)										
Df(1)Exel6225	880096; 1028960--1029014	Aug-07	95.5	83.8	ENH (71.9)										
Df(1)Exel6226	891664; 1079814	Nov-06	100.0	100.0	--										
Df(1)Exel6227	1216410; 1372852	Aug-07	100.0	83.8	ENH (100)	M									Unconfirmed enhancer
Df(1)Exel8196	1372852; 1563281--1563287	Dec-06	100.0	100.0	--										
Df(1)Exel6231	2144526; 2226073	Aug-06	93.3	100.0	SUP (6.7)										
Df(1)Exel6233	3131399; 3244124	Nov-06	100.0	100.0	--										
Df(1)Exel6290	5105146; 5169157	Nov-06	100.0	100.0	--										
Df(1)Exel6234	5322576;	Dec-06	96.4	100.0	SUP										

	5410644				(3.6)						
Df(1)Exel6235	5410644; 5487999	Jan-07	100.0	100.0	--						
Df(1)Exel6236	5574020; 5664594	Dec-06	100.0	100.0	--						
Df(1)Exel6237	5664594; 5786823	Nov-06	100.0	100.0	--						
Df(1)Exel6238	5963027; 6162626	Nov-06	88.9	100.0	SUP (11.1)						
Df(1)Exel6239	6084709; ?	Nov-06	100.0	100.0	--						
Df(1)Exel6240	6437996; 6563890--6563891	Nov-06	100.0	100.0	--						
Df(1)Exel6241	8603854; 8700609	Nov-06	100.0	100.0	--						
Df(1)Exel9049	9141146; 9146198--9146199	Nov-06	100.0	100.0	--						
Df(1)Exel6242	11356858(R4); 11450275	Dec-06	100.0	100.0	--						
Df(1)Exel9050	11429473; 11441214	Nov-06	100.0	100.0	--						
Df(1)Exel9053	11429473; 11441214	Dec-06	96.0	100.0	SUP (4)						
Df(1)Exel6244	12194252(R4);	Aug-07	66.7	83.8	SUP (20.5)	W	27.0	41.2	SUP (34.5)	M	Confirmed W to M suppressor

	12278611						
Df(1)Exel6245	13213906; 13305677--13305678	Nov-06	100.0	100.0	--		
Df(1)Exel6248	14557007; 14654681	Nov-06	100.0	100.0	--		
Df(1)Exel6251	15535368(R4); 15598856	Nov-06	100.0	100.0	--		
Df(1)Exel7463	18428598; 18635466	Nov-06	100.0	100.0	--		
Df(1)Exel9051	18586964; 18635466	Aug-07	94.4	83.8	ENH (65.7)		
Df(1)Exel9054	18586964; 18635466	Aug-07	94.0	83.8	ENH (62.9)		
Df(1)Exel7464	18586964; 18725228	Aug-07	100.0	83.8	ENH (100)	M	Unconfirmed enhancer
Df(1)Exel9067	18520229; 18543242	Dec-06	100.0	100.0	--		
Df(1)Exel7465	18694300; 18793206--18793210	Dec-06	100.0	100.0	--		
Df(1)Exel9068	19136043; 19154050	Nov-06	96.8	100.0	SUP (3.2)		
Df(1)Exel7468	19158545; 19403670	Nov-06	100.0	100.0	--		
Df(1)Exel6253	19393976;	Nov-06	100.0	100.0	--		

Df(1)Exel6254	19519673 20201559; 20339410	Nov-06	88.0	100.0	SUP (12)			
Df(1)Exel6255	21390230; 21919501	Nov-06	100.0	100.0	--			
Df(2L)Exel6001	67166(R4); 129261	Dec-06	100.0	100.0	--			
Df(2L)Exel7002	203089; ?	Dec-06	100.0	100.0	--			
Df(2L)Exel8003	560804; 716750	Dec-06	100.0	100.0	--			
Df(2L)Exel7005	778813; 870038	Jan-07	100.0	100.0	--			
Df(2L)Exel6003	827838; 1075745	Dec-06	100.0	100.0	--			
Df(2L)Exel6002	715084; 826285	Dec-06	100.0	100.0	--			
Df(2L)Exel6004	1074079; 1158137	Dec-06	100.0	100.0	--			
Df(2L)Exel7006	1158197; 1311170--1311516	Dec-06	94.1	100.0	SUP (5.9)	87.5	100.0	SUP (12.5)
Df(2L)Exel6005	1556764(R4); 1738914	Dec-06	100.0	100.0	--			
Df(2L)Exel7007	1716977; 1909976	Dec-06	100.0	100.0	--			
Df(2L)Exel8005	1739625; 2011801	Dec-06	100.0	100.0	--			

Df(2L)Exel6006	1913292; 2168166	Dec-06	96.9	100.0	SUP (3.1)
Df(2L)Exel7008	1989057--1989058; 2152458	Dec-06	97.6	100.0	SUP (2.4)
Df(2L)Exel6007	2168174; 2355484	Dec-06	100.0	100.0	--
Df(2L)Exel7010	2221020; 2362808	Dec-06	100.0	100.0	--
Df(2L)Exel7011	2355484; 2485014	Dec-06	100.0	100.0	--
Df(2L)Exel6008	2494660; 2755377	Jan-07	100.0	100.0	--
Df(2L)Exel6277	2670261; 2800669	Dec-06	100.0	100.0	--
Df(2L)Exel7014	2979654; 3056809	Dec-06	100.0	100.0	--
Df(2L)Exel7015	3039204; 3302818(R4)	Dec-06	100.0	100.0	--
Df(2L)Exel8008	3302636--3302646; 3354856--3	Dec-06	100.0	100.0	--
Df(2L)Exel7016	3466059; 3473493	Dec-06	100.0	100.0	--
Df(2L)Exel7018	3595211; 3722749	Dec-06	100.0	100.0	--

Df(2L)Exel6009	3763937; 3881546	Dec-06	94.4	100.0	SUP (5.6)
Df(2L)Exel8010	3887981; 4031325	Dec-06	94.1	100.0	SUP (5.9)
Df(2L)Exel6010	4813316(R4); 4880335	Dec-06	100.0	100.0	--
Df(2L)Exel9062	4839530; 4880335	Dec-06	100.0	100.0	--
Df(2L)Exel8012	4846961; 4977638	Dec-06	100.0	100.0	--
Df(2L)Exel7021	4908197; 4971870	Dec-06	100.0	100.0	--
Df(2L)Exel8013	4975605; 5000943	Dec-06	97.2	100.0	SUP (2.8)
Df(2L)Exel7022	5000837--5000838; 5058522	Dec-06	100.0	100.0	--
Df(2L)Exel6011	5139829; 5298217	Dec-06	93.8	100.0	SUP (6.3)
Df(2L)Exel6012	5305646; 5555049	Dec-06	97.2	100.0	SUP (2.8)
Df(2L)Exel7023	5524375--5524385; 5594234	Dec-06	100.0	100.0	--
Df(2L)Exel6256	5547264; 5650844	Dec-06	100.0	100.0	--
Df(2L)Exel8016	5555049;	Dec-06	100.0	100.0	--

	5659285				
Df(2L)Exel6013	5658629; 5805324	Dec-06	100.0	100.0	--
Df(2L)Exel6014	5805324; 5944680	Dec-06	100.0	100.0	--
Df(2L)Exel7024	5890506; 5972368	Dec-06	100.0	100.0	--
Df(2L)Exel6015	6080576; ?	Dec-06	100.0	100.0	--
Df(2L)Exel6016	6245225; 6403707	Dec-06	100.0	100.0	--
Df(2L)Exel9038	6285110; 6331070	Dec-06	100.0	100.0	--
Df(2L)Exel7027	6657034; 6779122	Dec-06	100.0	100.0	--
Df(2L)Exel7029	6922143; 7022660— 7022707	Dec-06	100.0	100.0	--
Df(2L)Exel8019	7140259-- 7140502; 7202317	Dec-06	100.0	100.0	--
Df(2L)Exel6017	7202317; 7418003-- 7418128	Dec-06	100.0	100.0	--
Df(2L)Exel7031	7364976; 7495492	Dec-06	100.0	100.0	--
Df(2L)Exel6018	7568861; 7695111	Dec-06	100.0	100.0	--

Df(2L)Exel9031	7637689; 7660390	Dec-06	100.0	100.0	--
Df(2L)Exel7034	8071311; 8205166	Dec-06	100.0	100.0	--
Df(2L)Exel7038	8438123; 8528528	Dec-06	100.0	100.0	--
Df(2L)Exel7039	8521355; 8793889(R4)	Dec-06	100.0	100.0	--
Df(2L)Exel7040	8797995; 8984993	Dec-06	100.0	100.0	--
Df(2L)Exel6021	8981539; 9168395	Dec-06	100.0	100.0	--
Df(2L)Exel8022	9388129; 9448660-- 9448833	Dec-06	100.0	100.0	--
Df(2L)Exel9064	9415663; 9431473	Dec-06	100.0	100.0	--
Df(2L)Exel6022	9439878; 9552718	Dec-06	100.0	100.0	--
Df(2L)Exel7042	9515175; 9615216	Dec-06	100.0	100.0	--
Df(2L)Exel9040	9605894; 9614757	Dec-06	100.0	100.0	--
Df(2L)Exel6024	9613611; 9782218	Dec-06	100.0	100.0	--
Df(2L)Exel6025	9782218;	Dec-06	96.8	100.0	SUP

	9897536				(3.2)				
Df(2L)Exel7043	9860016; 9940209	Dec-06	100.0	100.0	--				
Df(2L)Exel8024	10056941; 10239844	Dec-06	100.0	100.0	--				
Df(2L)Exel9032	10134181; 10198945--10198992	Dec-06	100.0	100.0	--				
Df(2L)Exel7046	10269280; 10326113	Dec-06	100.0	100.0	--				
Df(2L)Exel7048	10443323; 10544859	Jan-07	100.0	100.0	--				
Df(2L)Exel8026	10516675; 10861982	Dec-06	100.0	100.0	--				
Df(2L)Exel7049	10853446--10853462; 10975285	Jan-07	100.0	100.0	--				
Df(2L)Exel6027	11059438(R4); 11148234	Dec-06	77.5	100.0	SUP (22.5)	M	81.4	55.3	ENH (58.3)
Df(2L)Exel6028	11148234; 11347474	Dec-06	100.0	100.0	--				
Df(2L)Exel6029	11347474; 11434633	Dec-06	100.0	100.0	--				
Df(2L)Exel6030	11796280; 11959952	Dec-06	100.0	100.0	--				
Df(2L)Exel6031	11959952;	Dec-06	100.0	100.0	--				

Df(2L)Exel6032	12055718 12066846--12066969; 12270844	Dec-06	100.0	100.0	--
Df(2L)Exel6033	12423459; 12655793	Dec-06	100.0	100.0	--
Df(2L)Exel6034	12655793; 12854729	Dec-06	100.0	100.0	--
Df(2L)Exel8028	12832803; 12896409	Dec-06	100.0	100.0	--
Df(2L)Exel7055	12861487; 13154806	Jan-07	100.0	100.0	--
Df(2L)Exel7059	13782981; 13860340	Jan-07	100.0	100.0	--
Df(2L)Exel6035	14283121; 14452399	Dec-06	100.0	100.0	--
Df(2L)Exel6036	14409711; 14490657	Dec-06	100.0	100.0	--
Df(2L)Exel8033	14455715--14455716; 14997588	Jan-07	100.0	100.0	--
Df(2L)Exel8034	15264714; 15439965	Jan-07	97.8	100.0	SUP (2.2)
Df(2L)Exel7063	15404136; 15722529	Jan-07	100.0	100.0	--
Df(2L)Exel6038	15912343; 16042754	Dec-06	97.7	100.0	SUP (2.3)

Df(2L)Exel7066	16457328; 16727482	Jan-07	100.0	100.0	--						
Df(2L)Exel6039	16663295; 16864641	Dec-06	100.0	100.0	--						
Df(2L)Exel7067	16728375; 16824908	Jan-07	100.0	100.0	--						
Df(2L)Exel8036	16769571; 17428338	Jan-07	100.0	100.0	--		100.0	87.0	ENH (100)	M	Unconfirmed enhancer
Df(2L)Exel7068	17361071; 17474075	Jan-07	100.0	100.0	--						
Df(2L)Exel9044	17502487--17502514; 17604760	Jan-07	100.0	100.0	--						
Df(2L)Exel7069	17482011; 17773525	Jan-07	94.4	100.0	SUP (5.6)						
Df(2L)Exel7070	17903087--17903187; 18161791	Jan-07	100.0	100.0	--						
Df(2L)Exel8038	18123514; 18455586	Jan-07	100.0	100.0	--	HE					Unconfirmed enhancer
Df(2L)Exel9033	18294845; 18299279	Jan-07	97.4	100.0	SUP (2.6)						
Df(2L)Exel6041	18571864--18571867; 18732675	Dec-06	100.0	100.0	--						
Df(2L)Exel7071	18689053; 18795820	Jan-07	100.0	100.0	--						

Df(2L)Exel7072	18753432--18753444; 18943942	Jan-07	100.0	100.0	--					
Df(2L)Exel7073	18859186; 19022139	Jan-07	100.0	100.0	--					
Df(2L)Exel8039	18995784; 19044446	Jan-07	100.0	100.0	--	100.0	87.0	ENH (100)	M	Unconfirmed enhancer
Df(2L)Exel6042	18952025; 19139810	Dec-06	100.0	100.0	--					
Df(2L)Exel8040	19088224; 19139791	Jan-07	100.0	100.0	--					
Df(2L)Exel6043	19161727; 19423559--19423709	Dec-06	100.0	100.0	--					
Df(2L)Exel7075	19320414--19320415; 19452918	Jan-07	100.0	100.0	--	86.8	90.6	SUP (4.2)		
Df(2L)Exel8041	19404542; 19564458	Jan-07	100.0	100.0	--					
Df(2L)Exel9043	19438065; 19452918	Jan-07	100.0	100.0	--					
Df(2L)Exel6044	19576108--19576133; 19764726	Dec-06	97.7	100.0	SUP (2.3)					
Df(2L)Exel6045	19764726; 19935139	Dec-06	100.0	100.0	--					
Df(2L)Exel7077	19918015;	Jan-07	97.4	100.0	SUP					

	20072236				(2.6)		
Df(2L)Exel6046	20205107; 20449190--20458307	Dec-06	100.0	100.0	--		
Df(2L)Exel7078	20449190--20458307; 20680624	Jan-07	100.0	100.0	--		
Df(2L)Exel7079	20770538; 20874804	Jan-07	97.5	100.0	SUP (2.5)		
Df(2L)Exel7080	20861544; 21102742	Jan-07	96.8	100.0	SUP (3.2)		
Df(2L)Exel6047	21102742; 21244119	Dec-06	100.0	100.0	--		
Df(2L)Exel6048	21207015; 21279263	Dec-06	100.0	100.0	--		
Df(2L)Exel7081	21279263; 21496059	Jan-07	100.0	100.0	--	HE (M)	Unconfirmed enhancer
Df(2L)Exel6049	21661374(R4); 21852372	Dec-06	100.0	100.0	--		
Df(2R)Exel6050	2628314; 2760146	Dec-06	100.0	100.0	--		
Df(2R)Exel6051	2760146; 2880531	Dec-06	100.0	100.0	--		
Df(2R)Exel6283	2100923; 2207951	Dec-06	100.0	100.0	--		
Df(2R)Exel7092	2683473;	Jan-07	100.0	100.0	--		

Df(2R)Exel6052	3220520 2554098; 2683984(R4)	Dec-06	100.0	100.0	--				
Df(2R)Exel6053	2594454; 2726696	Dec-06	100.0	100.0	--				
Df(2R)Exel6054	2726696; 2873373	Dec-06	100.0	100.0	--				
Df(2R)Exel6055	3773849; 3948670	Dec-06	82.9	100.0	SUP (17.1)	W	100.0	100.0	--
Df(2R)Exel7094	3948670; 4019248	Jan-07	100.0	100.0	--				
Df(2R)Exel6056	3948670; 4119961	Dec-06	87.1	100.0	SUP (12.9)				
Df(2R)Exel7095	4012164; 4119968	Jan-07	100.0	100.0	--				
Df(2R)Exel6057	4062156; 4214936	Dec-06	100.0	100.0	--				
Df(2R)Exel6058	3388275; 3505491	Dec-06	100.0	100.0	--				
Df(2R)Exel7096	4321177; 4460278	Jan-07	100.0	100.0	--				
Df(2R)Exel8047	4487805; 4536994	Jan-07	100.0	100.0	--				
Df(2R)Exel7098	4536987; 4621135	Jan-07	94.9	100.0	SUP (5.1)				
Df(2R)Exel9016	4773434;	Jan-07	93.8	100.0	SUP				

	4780731(R4)				(6.2)						
Df(2R)Exel6059	6761890; 7073443--7073552	Dec-06	100.0	100.0	--	100.0	87.0	ENH (100)	M		Unconfirmed enhancer
Df(2R)Exel6060	7073443--7073552; 7285333	Jan-07	100.0	100.0	--						
Df(2R)Exel6061	8149005; 8324950	Dec-06	93.6	100.0	SUP (6.4)						
Df(2R)Exel7121	8458192; 8567258	Jan-07	100.0	100.0	--	100.0	87.0	ENH (100)	M		Unconfirmed enhancer
Df(2R)Exel8056	8630644--8630724; 8781610--8	Jan-07	100.0	100.0	--						
Df(2R)Exel7124	8345964; 8797160	Jan-07	97.4	100.0	SUP (2.6)						
Df(2R)Exel7123	8749715; 8868687	Jan-07	94.6	100.0	SUP (5.4)						
Df(2R)Exel6062	8868689; 8922684	Dec-06	96.1	100.0	SUP (3.9)						
Df(2R)Exel8057	8922352; 9106852--9106854	Jan-07	97.7	100.0	SUP (2.3)						
Df(2R)Exel7128	8866670; 8962541	Jan-07	87.9	100.0	SUP (12.1)						
Df(2R)Exel7130	9960585;	Jan-07	100.0	100.0	--						

	10100288								
	10118170--								
Df(2R)Exel7131	10118172;	Jan-07	100.0	100.0	--				
	10247930								
Df(2R)Exel8059	?; 9639309	Jan-07	100.0	100.0	--				
	10462255;								
Df(2R)Exel6284	10653073--	Dec-06	100.0	100.0	--				
	10653275								
Df(2R)Exel7135	11017461; 11150447	Jan-07	100.0	100.0	--				
Df(2R)Exel9015	10438901; 10450049	Jan-07	97.1	100.0	SUP (2.9)				
Df(2R)Exel6285	11371023; 11563707	Dec-06	100.0	100.0	--				
Df(2R)Exel9026	11456133; 11463121-- 11463338	Aug-07	88.2	83.8	ENH (27.3)	100.0	83.8	ENH (100)	M
Df(2R)Exel7137	?; 10922973	Jan-07	100.0	100.0	--				
Df(2R)Exel7138	11805928; 11895238	Jan-07	90.5	100.0	SUP (9.5)				
	12030362--								
Df(2R)Exel9060	12030372; 12046356	Jan-07	100.0	100.0	--				
Df(2R)Exel6063	11251613; 11450240	Dec-06	100.0	100.0	--				
Df(2R)Exel7142	12176759; 12312794	Jan-07	100.0	100.0	--				

Df(2R)Exel6064	11675358; 11892799	Jan-07	100.0	100.0	--
Df(2R)Exel6066	12161229(R 4); 12458367	Dec-06	100.0	100.0	--
Df(2R)Exel7145	12618999; 12734126	Jan-07	100.0	100.0	--
Df(2R)Exel6065	12744683; 12985001	Dec-06	96.6	100.0	SUP (3.4)
Df(2R)Exel7149	13469001; 13579292	Dec-06	100.0	100.0	--
Df(2R)Exel7150	13603767-- 13603976; 13669537	Dec-06	100.0	100.0	--
Df(2R)Exel7153	14038949; 14118059	Dec-06	100.0	100.0	--
Df(2R)Exel7157	14509027; 14618276	Dec-06	100.0	100.0	--
Df(2R)Exel7158	14593031; 14717233	Dec-06	98.2	100.0	SUP (1.8)
Df(2R)Exel6067	14745547; 14834784	Dec-06	100.0	100.0	--
Df(2R)Exel6068	14011006; 14205669	Dec-06	100.0	100.0	--
Df(2R)Exel6069	14205669; 14389343	Dec-06	100.0	100.0	--
Df(2R)Exel7162	16132691--	Dec-06	100.0	100.0	--

	16132995; 16201140				
Df(2R)Exel7163	15487656; 15646458	Dec-06	100.0	100.0	--
Df(2R)Exel7164	15645883; 15730562	Dec-06	100.0	100.0	--
Df(2R)Exel6070	15646492; 15879577	Dec-06	100.0	100.0	--
Df(2R)Exel7166	16758362; 16887668	Dec-06	100.0	100.0	--
Df(2R)Exel6071	16723538; 16944303	Dec-06	100.0	100.0	--
Df(2R)Exel6072	16100342; 16294396	Dec-06	100.0	100.0	--
Df(2R)Exel6076	16423078; 16650632	Dec-06	100.0	100.0	--
Df(2R)Exel6077	16757519; 16915579	Dec-06	100.0	100.0	--
Df(2R)Exel7169	17749738--17749756; 17927135	Dec-06	100.0	100.0	--
Df(2R)Exel6078	17083091; 17241017(R4)	Dec-06	100.0	100.0	--
Df(2R)Exel7170	17927146; 18023434	Dec-06	91.2	100.0	SUP (8.8)
Df(2R)Exel7171	18023507;	Dec-06	100.0	100.0	--

	18130755											
Df(2R)Exel7173	17424002; 17557688	Dec-06	100.0	100.0	--							
Df(2R)Exel6079	17772917; 17841872	Dec-06	97.4	100.0	SUP (2.6)							
Df(2R)Exel7177	18956207; 19091521	Dec-06	100.0	100.0	--							
Df(2R)Exel7178	19179008; 19283437	Dec-06	100.0	100.0	--							
Df(2R)Exel7180	19431599; 19573869	Dec-06	100.0	100.0	--							
Df(2R)Exel7184	20026902; 20145426	Dec-06	97.0	100.0	SUP (3)							
Df(2R)Exel6082	20145420; 20257300	Dec-06	89.3	100.0	SUP (10.7)		85.4	90.6	SUP (5.7)			
Df(2R)Exel7185	20298585--20298685; 20403180	Dec-06	100.0	100.0	--							
Df(3L)Exel6083	104350; 180193	Dec-06	100.0	100.0	--		67.9 %	83.8 %	SUP (19)	W	SUP (9.1)	
Df(3L)Exel6084	180193; 346863	Dec-06	82.1	100.0	SUP (17.9)	W			SUP (43.6)	S		Confirmed W to S suppressor
Df(3L)Exel9057	306168; 319594--319595	Dec-06	100.0	100.0	--							
Df(3L)Exel6085	529157; 729932	Dec-06	90.0	100.0	SUP (10)		100.0	100.0	--			

Df(3L)Exel6086	729971(R4); 940280	Dec-06	100.0	100.0	--			
Df(3L)Exel6087	1459303; 1567510	Dec-06	90.0	100.0	SUP (10)	94.4	100.0	SUP (5.6)
Df(3L)Exel6088	1774992; 1857014	Dec-06	94.7	100.0	SUP (5.3)			
Df(3L)Exel6089	2151744; 2256098	Dec-06	88.5	100.0	SUP (11.5)	85.7	100.0	SUP (14.3)
Df(3L)Exel6091	2656263; 2821245	Dec-06	100.0	100.0	--			
Df(3L)Exel6092	2821245; 3047162	Dec-06	100.0	100.0	--			
Df(3L)Exel6093	3231085; 3398761(R4)	Dec-06	100.0	100.0	--			
Df(3L)Exel6094	3359142; 3460609	Dec-06	100.0	100.0	--			
Df(3L)Exel6095	3460609; 3545153	Dec-06	100.0	100.0	--			
Df(3L)Exel6096	3542583; 3593857--3593973	Dec-06	100.0	100.0	--			
Df(3L)Exel6097	3525789(R4); 3805762	Dec-06	100.0	100.0	--			
Df(3L)Exel6098	3805762; 3906112	Dec-06	97.0	100.0	SUP (3)			
Df(3L)Exel6099	3906112;	Dec-06	100.0	100.0	--			

	4054622											
Df(3L)Exel9000	4227243; 4284262	Dec-06	100.0	100.0	--							
Df(3L)Exel8098	4259429; 4407036	Dec-06	100.0	100.0	--							
Df(3L)Exel9001	4341239; 4407036	Dec-06	100.0	100.0	--							
Df(3L)Exel6101	4364118; 4520041	Dec-06	100.0	100.0	--							
Df(3L)Exel9028	4510281; 4528197--4528199	Dec-06	90.3	100.0	SUP (9.7)							
Df(3L)Exel9058	4542105; 4554415	Dec-06	100.0	100.0	--							
Df(3L)Exel6102	4670346; 4954252	Dec-06	96.2	100.0	SUP (3.8)							
Df(3L)Exel6103	4954344; 5144105	Dec-06	100.0	100.0	--							
Df(3L)Exel6104	5144349(R4); 5325370	Dec-06	100.0	100.0	--		100.0	100.0	--			
Df(3L)Exel6105	5325370; 5567583	Dec-06	100.0	100.0	--	HE (M)						Unconfirmed enhancer
Df(3L)Exel6106	5567583; 5650310	Dec-06	100.0	100.0	--							
Df(3L)Exel6107	5746110; 5895644	Dec-06	100.0	100.0	--		100.0	87.0	ENH (100)	M		Unconfirmed enhancer
Df(3L)Exel7210	5919748;	Dec-06	100.0	100.0	--							

	6058752							
Df(3L)Exel8101	6002150(R4); 6177581	Dec-06	100.0	100.0	--			
Df(3L)Exel6108	6177691(R4); 6223459	Dec-06	97.4	100.0	SUP (2.6)			
Df(3L)Exel6109	6736213; 6936639	Dec-06	96.2	100.0	SUP (3.8)			
Df(3L)Exel6110	7087906; 7149284	Dec-06	100.0	100.0	--			
Df(3L)Exel8104	7353086; 7522363	Dec-06	100.0	100.0	--	100.0	100.0	--
Df(3L)Exel6114	9466175; 9652180	Dec-06	100.0	100.0	--			
Df(3L)Exel9048	9896122; 9957205	Dec-06	100.0	100.0	--			
Df(3L)Exel6115	11815104; 12074906	Dec-06	96.4	100.0	SUP (3.6)			
Df(3L)Exel6116	12039402; 12161528	Dec-06	100.0	100.0	--			
Df(3L)Exel6117	12620934; 12783033	Dec-06	93.8	100.0	SUP (6.3)			
Df(3L)Exel6118	13186202(R4); 13304190	Dec-06	96.8	100.0	SUP (3.2)			
Df(3L)Exel6119	13434803; 13624373	Dec-06	90.0	100.0	SUP (10)			
Df(3L)Exel6120	14052761;	Dec-06	100.0	100.0	--			

Df(3L)Exel6121	14183963 14139743; 14221933(R4)	Dec-06	100.0	100.0	--	HE (M)	100.0	100.0	--						
Df(3L)Exel6122	14266160; 14402934	Dec-06	100.0	100.0	--										
Df(3L)Exel6123	14358721; 14563315	Dec-06	100.0	100.0	--	HE (M)				HE (S)					Confirmed M to S enhancer
Df(3L)Exel6125	14917302; 15044925	Dec-06	100.0	100.0	--										
Df(3L)Exel6126	14961558; 15072766	Dec-06	100.0	100.0	--										
Df(3L)Exel6262	15028352; 15183406	Dec-06	100.0	100.0	--										
Df(3L)Exel6127	15995819; 16078526(R4)	Dec-06	40.0	100.0	SUP (60)	S	27.3	100.0	SUP (72.7)	S	44.4	100.0	SUP (55.6)	S	Confirmed S suppressor
Df(3L)Exel6128	16122754; 16210428	Dec-06	100.0	100.0	--										
Df(3L)Exel6129	16360572; 16432436	Dec-06	100.0	100.0	--										
Df(3L)Exel6130	16654391; 16799748	Dec-06	96.7	100.0	SUP (3.3)										
Df(3L)Exel9003	16799740--16799741; 16864660	Jan-07	95.8	100.0	SUP (4.2)										
Df(3L)Exel7253	16842928;	Dec-06	100.0	100.0	--										

Df(3L)Exel6131	16981186 17231345; 17414638	Dec-06	100.0	100.0	--									
Df(3L)Exel6132	17370461; 17481906	Dec-06	100.0	100.0	--	HE	100.0	100.0	--					
Df(3L)Exel6133	17965582; 18088200	Dec-06	95.8	100.0	SUP (4.2)									
Df(3L)Exel6134	18456353; 18615556	Dec-06	92.3	100.0	SUP (7.7)		100.0	87.0	ENH (100)	M				
Df(3L)Exel6090	2417381; 2490163	Dec-06	100.0	100.0	--		90.9	90.6	ENH (3.4)		100.0	83.8	ENH (100)	M	Unconfirmed enhancer
Df(3L)Exel9001	4341239; 4407036	Dec-06	100.0	100.0	--									
Df(3L)Exel9028	4510281; 4528197--4528199	Dec-06	90.3	100.0	SUP (9.7)									
Df(3L)Exel7208	?; 4670012	Dec-06	100.0	100.0	--									
Df(3L)Exel6279	7828555(R4); 8055183	Dec-06	100.0	100.0	--									
Df(3L)Exel9034	7974043--7974423; 8048609	Dec-06	96.0	100.0	SUP (4)									
Df(3L)Exel6112	8089573; 8351924	Dec-06	100.0	100.0	--		56.5	87.0	SUP (35)	S	76.9	90.6	SUP (15.1)	W	Confirmed W to S suppressor
Df(3L)Exel9017	13451177; 13470342	Dec-06	100.0	100.0	--									
Df(3L)Exel9002	16799740--	Dec-06	100.0	100.0	--									

Df(3L)Exel9004	16799741; 16837972 16775136; 16844490	Dec-06	93.8	100.0	SUP (6.3)						
Df(3L)Exel9006	17816959; 17834548	Dec-06	90.9	100.0	SUP (9.1)		87.5	87.0	ENH (3.8)		
Df(3L)Exel9046	19284479; 19323668	Feb-07	100.0	100.0	--						
Df(3L)Exel9007	19373570; 19585752	Feb-07	100.0	100.0	--						
Df(3L)Exel9008	?; 19585752	Feb-07	100.0	100.0	--						
Df(3L)Exel9009	19459595; 19585752	Feb-07	92.3	100.0	SUP (7.7)						
Df(3L)Exel9011	19532970; 19585752	Feb-07	100.0	100.0	--						
Df(3L)Exel6135	19585788; 19709627	Jan-07	no adults	100.0	E, no adults	S			HE (S)		Confirmed S enhancer
Df(3L)Exel9061	19712909--19712962; 19754145	Feb-07	100.0	100.0	--						
Df(3L)Exel9045	19839162; 19857021	Feb-07	100.0	100.0	--						
Df(3L)Exel6136	20303330; 20486308	Jan-07	100.0	100.0	--						
Df(3L)Exel9065	21434299; 21440359(R4)	Feb-07	100.0	100.0	--						

Df(3L)Exel9066	21533338; 21548247	Feb-07	100.0	100.0	--						
Df(3L)Exel6137	21836682; 21948191	Jan-07	100.0	100.0	--						
Df(3L)Exel6138	22260871; 22401054	Jan-07	100.0	100.0	--						
Df(3R)Exel6140	107401; 186686	Jan-07	100.0	100.0	--						
Df(3R)Exel6141	288185; 425461--425532	Jan-07	100.0	100.0	--						
Df(3R)Exel6142	540172; 632614	Jan-07	100.0	100.0	--						
Df(3R)Exel6143	776723; 912501	Jan-07	100.0	100.0	--						
Df(3R)Exel9029	1229919--1229920; 1263319	Feb-07	85.0	100.0	SUP (15)						
Df(3R)Exel6144	1328532; 1438438	Jan-07	45.5	100.0	SUP (54.5)	S	46.2	87.0	SUP (47)	S	Confirmed S suppressor
Df(3R)Exel7283	1474080; 1572399	Feb-07	100.0	100.0	--						
Df(3R)Exel6145	1542490; 1638975	Jan-07	100.0	100.0	--						
Df(3R)Exel7284	1641741; 1833508	Mar-07	88.9	87.0	ENH (14.4)						
Df(3R)Exel6146	2988428;	Jan-07	100.0	100.0	--						

Df(3R)Exel6263	3317338 3792892--3792893; 3945737	Feb-07	no adults	100.0	E, no adults	S			ENH (100)	HE (M)	Confirmed M to S enhancer
Df(3R)Exel6147	4076136; 4166717	Jan-07	100.0	100.0	--						
Df(3R)Exel6148	4159500; 4303404--4303405	Jan-07	100.0	100.0	--	HE	no adults	87.0	E, no adults	S	Confirmed S enhancer
Df(3R)Exel6149	4303405; 4495198	Jan-07	95.2	100.0	SUP (4.8)						
Df(3R)Exel8143	4495318; ?	Feb-07	100.0	100.0	--						
Df(3R)Exel6150	4495369; 4753498	Jan-07	100.0	100.0	--		82.4	87.0	SUP (5.4)		
Df(3R)Exel6151	4878567; 4983814	Jan-07	100.0	100.0	--						
Df(3R)Exel6152	4983814; 5073219	Jan-07	93.8	100.0	SUP (6.3)						
Df(3R)Exel9036	5153013; 5165744	Feb-07	100.0	100.0	--						
Df(3R)Exel6153	5338758; 5457662	Jan-07	100.0	100.0	--						
Df(3R)Exel6264	5376443; 5530688	Jan-07	94.4	100.0	SUP (5.6)						
Df(3R)Exel6154	5619087; 5754513	Jan-07	100.0	100.0	--		100.0	87.0	ENH (100)	M	Unconfirmed enhancer
Df(3R)Exel6155	5754513;	Feb-07	100.0	100.0	--						

Df(3R)Exel6265	5915190 5915198; 6015388	Jan-07	67.9	100.0	SUP (32.1)	M	25.0	100.0	SUP (75)	S	52.3	83.8	SUP (37.6)	S	Confirmed M to S suppressor
Df(3R)Exel6156	6015370; 6175936	Jan-07	100.0	100.0	--										
Df(3R)Exel6157	6175936; 6209759-- 6213369	Jan-07	100.0	100.0	--										
Df(3R)Exel6158	6399658; 6464616— 6464617	Jan-07	100.0	100.0	--										
Df(3R)Exel6159	6464635; 6715093	Jan-07	100.0	100.0	--										
Df(3R)Exel7305	6606276; 6697983	Feb-07	100.0	100.0	--										
Df(3R)Exel7306	6696729; 6982551	Feb-07	85.7	100.0	SUP (14.3)										
Df(3R)Exel8152	6979890; 7026020	Feb-07	100.0	100.0	--		85.7	100.0	SUP (14.3)						
Df(3R)Exel7308	7069685; 7264869	Feb-07	100.0	100.0	--										
Df(3R)Exel9018	7103606; 7178879	Feb-07	95.8	100.0	SUP (4.2)										
Df(3R)Exel6160	7179003; 7394944(R4)	Jan-07	78.3	100.0	SUP (21.7)	M	68.2	87.0	SUP (21.6)	M	39.3	90.6	SUP (56.6)	S	Confirmed M to S suppressor
Df(3R)Exel8153	7261649;	Feb-07	94.1	100.0	SUP										

	7394911				(5.9)						
Df(3R)Exel6276	7394893; 7495390	Feb-07	100.0	100.0	--						
Df(3R)Exel7309	7472850--7472851; 7541866	Jul-07	100.0	90.6	ENH (100)	M					Unconfirmed enhancer
Df(3R)Exel8154	7472850--7472851; 7585211	Jul-07	88.2	90.6	SUP (2.6)						
Df(3R)Exel6161	7394952; 7495415	Jan-07	100.0	100.0	--						
Df(3R)Exel9019	7575265; 7590145	Feb-07	93.3	100.0	SUP (6.7)						
Df(3R)Exel7310	7584303; 7712814	Feb-07	95.0	100.0	SUP (5)						
Df(3R)Exel6163	7712905; 7824974	Jan-07	93.3	100.0	SUP (6.7)						
Df(3R)Exel6162	7713484; 8106824	Jan-07	96.2	100.0	SUP (3.8)						
Df(3R)Exel7312	7803596; 7905868	Feb-07	72.7	100.0	SUP (27.3)	M			SUP (73.8)	S	Confirmed M to S suppressor
Df(3R)Exel8155	7819266; 7939447	Feb-07	100.0	100.0	--		100.0	90.6	ENH (100)	M	Unconfirmed enhancer
Df(3R)Exel7313	7933857; 8106601	Feb-07	77.8	100.0	SUP (22.2)	M	56.5	90.6	SUP (37.6)	S	Confirmed M to S suppressor
Df(3R)Exel7314	8061009; 8198770	Feb-07	95.7	100.0	SUP (4.3)						

Df(3R)Exel6164	8106805; 8268847	Jan-07	100.0	100.0	--		100.0	87.0	ENH (100)	M			Unconfirmed enhancer
Df(3R)Exel6165	8106824; 8268866	Jan-07	90.5	100.0	SUP (9.5)		100.0	87.0	ENH (100)	M			
Df(3R)Exel7315	8194980; 8239608	Jul-07	100.0	90.6	ENH (100)	M			ENH (100)	M			Confirmed M enhancer
Df(3R)Exel7316	8231988; 8274830	Feb-07	100.0	100.0	--		81.0	100.0	SUP (19)	W	SUP (35)	M	Confirmed W to M suppressor
Df(3R)Exel7317	8267098; 8456321--8456331	Feb-07	100.0	100.0	--								
Df(3R)Exel6166	8504772; ?	Jan-07	94.1	100.0	SUP (5.9)								
Df(3R)Exel7318	8549596; ?	Feb-07	95.8	100.0	SUP (4.2)								
Df(3R)Exel8157	8838454; 8877526	Feb-07	94.7	100.0	SUP (5.3)								
Df(3R)Exel6167	8877179; 9085101	Jan-07	94.4	100.0	SUP (5.6)								
Df(3R)Exel8158	9067483; 9190062	Jul-07	81.8	90.6	SUP (9.7)		80.0	83.8	SUP (4.6)				
Df(3R)Exel6168	9105453; 9205505--9205506	Jan-07	73.7	100.0	SUP (26.3)	M	95.2	100.0	SUP (4.8)				
Df(3R)Exel7320	9207130; 9369382	Mar-07	70.0	87.0	SUP (19.6)	W	83.3	90.6	SUP (8)				
Df(3R)Exel6169	9369382;	Jan-07	100.0	100.0	--		73.0	87.0	SUP	W			

	9509691(R4)								(16.1)				
Df(3R)Exel6170	9509964--9509965; 9638552	Jan-07	72.7	100.0	SUP (27.3)	M	80.0	100.0	SUP (20)	W	80.0	87.0	SUP (8.1)	Confirmed W to M suppressor
Df(3R)Exel6288	9638571; 9809255	Feb-07	100.0	100.0	--									
Df(3R)Exel6171	9638627; 9809182	Jan-07	100.0	100.0	--									
Df(3R)Exel8159	9809255; 10085668	Jul-07	100.0	90.6	ENH (100)	M								Unconfirmed enhancer
Df(3R)Exel7321	9951211; 10103926	Feb-07	100.0	100.0	--									
Df(3R)Exel6267	10103684(R4); 10307581	Feb-07	100.0	100.0	--									
Df(3R)Exel8160	10475129; 10701715	Feb-07	100.0	100.0	--									
Df(3R)Exel6275	10549505; 10744000	Feb-07	100.0	100.0	--									
Df(3R)Exel6172	10643968; 10744000	Jan-07	100.0	100.0	--									
Df(3R)Exel6173	10744000; 10920182	Jan-07	100.0	100.0	--									
Df(3R)Exel6174	11154443--11154444; 11363188	Jan-07	100.0	100.0	--									

Df(3R)Exel7326	11363141; ?	Feb-07	85.7	100.0	SUP (14.3)		100.0	90.6	ENH (100)	M		
Df(3R)Exel8162	11618140--11618265; 11727190	Feb-07	100.0	100.0	--							
Df(3R)Exel7327	11727155--11727156; 11867284	Feb-07	100.0	100.0	--							
Df(3R)Exel7328	11835140; 11983178	Feb-07	100.0	100.0	--							
Df(3R)Exel7330	12177448; 12298844	Feb-07	100.0	100.0	--		72.4	90.6	SUP (20.1)	W	SUP (1.8)	
Df(3R)Exel7329	12067151; 12184534	Jul-07	100.0	90.6	ENH (100)	M	87.5	83.8	ENH (22.7)			
Df(3R)Exel9055	12274994; 12279419--12279615	Mar-07	87.5	87.0	ENH (3.8)							
Df(3R)Exel6269	12131453; 12328470(R4)	Feb-07	100.0	100.0	--							
Df(3R)Exel8163	12298768; 12328332	Jul-07	82.1	90.6	SUP (9.3)							
Df(3R)Exel6270	12328472; 12528639	Feb-07	100.0	100.0	--							
Df(3R)Exel8165	12838655; 12879706	Mar-07	100.0	87.0	ENH (100)	M						Unconfirmed enhancer
Df(3R)Exel6176	12879384--	Jan-07	100.0	100.0	--							

Df(3R)Exel6178	12879395; 12974829 13992164; 14223094	Jan-07	95.2	100.0	SUP (4.8)									
Df(3R)Exel6179	14223249; 14410113	Jan-07	100.0	100.0	--		69.2	100.0	SUP (30.8)	M	84.0	87.0	SUP (3.5)	
Df(3R)Exel9030	14420735; 14448184	Mar-07	100.0	87.0	ENH (100)	M	70.6	87.0	SUP (18.9)	W	72.4	90.6	SUP (20.1)	W	Confirmed W suppressor
Df(3R)Exel6180	14410136; 14566207	Jan-07	100.0	100.0	--									
Df(3R)Exel6181	14566207(R 4); 14749762	Jan-07	100.0	100.0	--									
Df(3R)Exel6182	14749762; 14853135	Jan-07	100.0	100.0	--									
Df(3R)Exel6183	14853118; 14989771	Jan-07	92.3	100.0	SUP (7.7)									
Df(3R)Exel6184	15289202; 15467055	Jan-07	100.0	100.0	--									
Df(3R)Exel6185	16135245; 16376386	Jan-07	96.3	100.0	SUP (3.7)									
Df(3R)Exel6272	16783442; 16938073	Feb-07	100.0	100.0	--									
Df(3R)Exel6186	17444144; 17545495	Jan-07	91.7	100.0	SUP (8.3)									
Df(3R)Exel6187	17545502; 17700988	Jan-07	100.0	100.0	--									

Df(3R)Exel6188	17700995; 17868467	Jan-07	100.0	100.0	--		
Df(3R)Exel6189	17859431; 17950482	Jan-07	100.0	100.0	--		
Df(3R)Exel6190	17950472; 18184659	Jul-07	98.2	90.6	ENH (81.4)	W	Unconfirmed enhancer
Df(3R)Exel6191	18184659; 18347158	Jan-07	100.0	100.0	--		
Df(3R)Exel6273	18347158; 18483028	Feb-07	100.0	100.0	--	HE	Unconfirmed enhancer
Df(3R)Exel6192	18492372; 18724923	Jan-07	88.2	100.0	SUP (11.8)		
Df(3R)Exel6193	18715609; 18991826	Aug-07	94.1	83.8	ENH (63.6)		
Df(3R)Exel6274	19001169; 19121235--19121356	Feb-07	92.3	100.0	SUP (7.7)		
Df(3R)Exel6280	19017039; 19121235--19121356	Feb-07	100.0	100.0	--		
Df(3R)Exel9012	19096137; 19162766	Aug-07	75.0	83.8	SUP (10.5)		
Df(3R)Exel6194	19201557; 19457785	Feb-07	100.0	100.0	--		
Df(3R)Exel6195	19457692(R4); 19540279	Jan-07	94.4	100.0	SUP (5.6)		

Df(3R)Exel9013	19548559; 19610564	Mar-07	100.0	87.0	ENH (100)	M	100.0	87.0	ENH (100)	M	Confirmed W enhancer
Df(3R)Exel9014	19589500; 19759383	Mar-07	100.0	87.0	ENH (100)	M					Unconfirmed enhancer
Df(3R)Exel6196	19747854--19747855; 19857149	Jan-07	100.0	100.0	--						
Df(3R)Exel6197	19857149; 19967091	Jan-07	100.0	100.0	--						
Df(3R)Exel6198	19967091; 20096927	Jan-07	95.8	100.0	SUP (4.2)						
Df(3R)Exel6199	20096927; 20275677	Jan-07	100.0	100.0	--						
Df(3R)Exel8178	20096927; 20353553	Mar-07	100.0	87.0	ENH (100)	M	85.7	87.0	SUP (1.5)		Unconfirmed enhancer
Df(3R)Exel7357	20275677; 20476746	Feb-07	100.0	100.0	--						
Df(3R)Exel6200	20595064; 20720429	Jan-07	95.2	100.0	SUP (4.8)						
Df(3R)Exel6201	20954218; 21013378(R4)	Jan-07	85.7	100.0	SUP (14.3)		98.1	90.6	ENH (79.6)	W	Unconfirmed enhancer
Df(3R)Exel9056	21022721; 21035008--21035010	Mar-07	88.2	87.0	ENH (9.4)						
Df(3R)Exel6202	21118719; 21341395	Jan-07	100.0	100.0	--		100.0	87.0	ENH (100)	M	Unconfirmed enhancer

Df(3R)Exel6203	21330985; 21452963	Jan-07	94.7	100.0	SUP (5.3)							
Df(3R)Exel6204	21832109; 22087161	Jan-07	100.0	100.0	--	83.9	90.6	SUP (7.4)				
Df(3R)Exel6205	?; 22885211	Jan-07	100.0	100.0	--	100.0	90.6	ENH (100)	M	92.0	90.6	ENH (15)
Df(3R)Exel6206	22885211; 22972573	Jan-07	87.1	100.0	SUP (12.9)							
Df(3R)Exel6208	22983208; 23079244	Jan-07	100.0	100.0	--							
Df(3R)Exel6259	24141831; 24416263	Jan-07	100.0	100.0	--							
Df(3R)Exel6209	24416263; 24490049	Jan-07	100.0	100.0	--							
Df(3R)Exel6210	24490049; 24806106	Feb-07	100.0	100.0	--							
Df(3R)Exel6211	24816740; 24889986	Jan-07	93.8	100.0	SUP (6.3)							
Df(3R)Exel6212	25040897; 25113953	Jan-07	100.0	100.0	--							
Df(3R)Exel9025	25570975; 25585907	Mar-07	81.3	87.0	SUP (6.6)							
Df(3R)Exel6213	25692182; 25827836	Jan-07	100.0	100.0	--							
Df(3R)Exel6214	25914470; 26018056(R4)	Jan-07	88.2	100.0	SUP (11.8)							

Df(3R)Exel6216	26291754; 26358290	Jan-07	100.0	100.0	--										
Df(3R)Exel6215	?; 26378570	Jan-07	90.9	100.0	SUP (9.1)		64.0	90.6	SUP (29.4)	M					
Df(3R)Exel7378	26378312; 26610043	Jul-07	80.0	90.6	SUP (11.7)		93.3	83.8	ENH (58.8)						
Df(3R)Exel9020	26582110--26582237; 26620677	Feb-07	100.0	100.0	--										
Df(3R)Exel8194	26571483; 26703333	Feb-07	100.0	100.0	--										
Df(3R)Exel6217	26635749; 26703333	Jan-07	100.0	100.0	--										
Df(3R)Exel7379	26917412; ?	Feb-07	100.0	100.0	--		66.7	83.8	SUP (20.5)	W					
Df(3R)Exel6219	27126307; 27277252	Jan-07	100.0	100.0	--										
Df(3R)Exel6218	26994861; 27126217	Jan-07	63.6	100.0	SUP (36.4)	S	57.1	87.0	SUP (34.3)	M	29.3	83.8	SUP (65.1)	S	Confirmed M to S suppressor

SUPPLEMENTAL TABLE S2-2

Alleles tested for mapping modifiers of the wing expansion defect induced by *spen* overexpression

Deficiency	Deleted genes	Alleles tested (notes)	Extent of enhancement/ suppression (%)
Df(3L)Exel6123	*CG3919*	$CG3919^{EY00986}$ (insertion within exon 1)	No modification detected [a]
	big bang (*bbg*)	$bbg^{EY02818}$ (insertion within exon 3)	↑100
		bbg^{e03261} (insertion within exon 7)	↑100
	Mitochondrial phosphate carrier protein (*Mpcp*)	$Mpcp^{00564}$ (insertion within exon 1) [b]	↑100
		$Mpcp^{EY08330}$ (insertion within exon 1)	No modification detected [a]
	CG9238	$CG9238^{BG02516}$ (insertion within exon1)	No modification detected [a]
		$CG9238^{e03123}$(insertion within exon 1)	↑100
	HGTX	$HGTX^{d00083}$ (insertion between exons 1 and 2 of *HGTX-RB*; potential *HGTX* GOF)	PL, HE
		$HGTX^{e03190}$(insertion within exon 5)	↓20
Df(3L)Exel6127	*Myosin binding*	Mbs^{3}	↓31

	subunit (*Mbs*)		
	CG5222	*CG5222*^{e03477}(insertion 5′, within 100 bp of transcriptional start)	↓14
	Zn72D	*Zn72D*^{c00611} (insertion within exon 3)	↓8
		Zn72D^{BG02677}(insertion within exon 1)	↑83 [c]
	TBP-associated factor 4 (*Taf4*)	*Taf4*^{1}	↓ 57
		Taf4^{e02502} (insertion within the last exon)	↓31
Df(3R)Exel6144	*N-methyl-D-aspartate-type glutamate NMDA receptor 1* (*Nmdar1*)	*Nmdar1*^{DG23512} (insertion between exons 1 and 2 of *Nmdar1*; also within 100 bp 5′ of *Itp-r83A*)	↓38
		Itp-r83A^{EY02522} (insertion within 100 bp 5′ of *Nmdar1*, potential *Nmdar1* GOF; between exons 1 and 2 of *Itp-r83A*)	↓32
	Inositol 1,4,5,-	*Itp-r83A*^{05616}, *Nmdar1*^{05616} (insertion within	↑10

tris-phosphate receptor (*Itp-r83A*)	exon 1 of *Itp-r83A*, and between exons 1 and 2 of *Nmdar1*) [b]	
CG2519	$CG2519^{EY00928}$ (insertion within exon 1)	↓16
meiosis I arrest (*mia*)	mia^{B560} (insertion between exons 2 and 3)	↑33
	$mia^{EY07883}$ (insertion within exon 1)	↓40 [c]
Protein-L-isoaspartate (*D-aspartate*) *O-methyltransferase* (*Pcmt*)	$Pcmt^{f00979}$ (insertion within 200 bp 5′ of *Pcmt* and within 700 bp 5′ *Snm1*; possible GOF for *Snm1*)	↑40
Snm1	$Snm1^{ZIII-2589}$ [d]	↓63
	$Snm1^{ZIII-4709}$ [d]	↓40
Pi4KIIα	$Pi4KIIalpha^{c02099}$ (insertion within 400 bp 5′ *Pi4KIIα*)	↑70
CG12746	$CG12746^{EY10535}$ (insertion within exon 1 of	↓26

	transcript *CG12746-RE*; may be GOF for *CG14671*)	
Ras homology enriched in brain (*Rheb*)	$Rheb^{EY08085}$ (insertion within exon 1 of *Rheb*; possible GOF of *CG2931*)	↓12
	$Rheb^{LA01053}$ (insertion within exon 1, and possible GOF, of *Rheb*)	↓78
Collapsin Response Mediator Protein (*CRMP*)	$CRMP^{KG02006}$ (insertion within exon 1) [b]	↓12
	$CRMP^{EY04380}$ (insertion within exon 1, and possible GOF, of *CRMP*)	↓3
rev7	$CG2926^{e01499}$ (insertion within 600 bp 5′ of *CG2926* and within 100 bp 5′ of *rev7*)	↓9
noisette (*noi*)	noi^{f05442} (insertion within exon 1)	↑70
Vacuolar H^+-	$Vha26^{j3E7}$ (insertion within exon 1)	↓4

	ATPase 26kD E subunit (*Vha26*)		
	extra bases (*exba*)	*exba*^{03022} (insertion within exon 1 of transcript *exba-RC*) [b]	↑70
	CG1427		
	asterless (*asl*)	*asl*^{c01524} (insertion within 100 bp 5′ of *asl*)	↓21
Df(3R)Exel6148	*ADP ribosylation factor 84F* (*Arf84F*)	*Arf84F*^{f00424} (insertion within exon 1; possible GOF for *CG9603*)	N/A
	CG9601	*CG9601*^{c06901} (insertion within exon 1)	N/A
	steamer duck (*stck*)	*stck*^{e01454} (insertion between exons 1 and 2)	N/A
		stck^{f01146} (insertion between exons 1 and 2)	N/A
Df(3R)Exel6160	*prospero* (*pros*)	*pros*^{10419} (insertion within exon 1) [b]	↑63
		l(3)rM060 (insertion within exon 1)	↓38
		pros^{17}	↑75 [c]
	CG6719	*CG6719*^{e00315} (insertion within 100 bp 5′ of	0

		CG6719 and within 200 bp 5′ of *Irp*)	
	Ranbp9	*Ranbp9*^{KG05068} (insertion within 100 bp 5′ of *Ranbp9*) [b]	↓2
	ninaG	*ninaG*^{e00313} (insertion within 100 bp 5′ of *ninaG* and within 400 bp 5′ of *CG5270*)	↑69
	CG5276	*CG5276*^{e03505} (insertion within exon 1)	↑38
	CG6744	*CG6744*^{EY03872} (insertion within exon 1 and possible GOF of *CG6744*)	↓28
	CG17230	*tho*^{1}, *CG17230*$^{tho\text{-}1}$ (insertion within 100 bp 5′ of *CG31374* and between exons 1 and 2 of *CG17230*) [b]	↓32
	CG10898	*CG10898*^{c05103} (insertion within 300 bp 5′ of *CG10898*)	↓40
Df(3R)Exel6218	*CG1544*	*CG1544*^{f06723} (insertion between exons 4 and 5)	↓4
	zwilch	*zwilch*^{PL00428} (insertion within the last exon)	↓13 [c]
		zwilch^{c04101} (insertion within exon 1)	0

	CG1746	*CG1746*^{KG01914} (insertion within exon 1)	↑100
		CG1746^{KG05897} (insertion within 200 bp 5′ of *CG1746* and within 1 kb 5′ of *CG12054*) [b]	↓66
	CG12054	*CG12054*^{EY01782} (insertion within exon 2 of *CG12054*; possible GOF for *CG1746*)	↑75 [c]
	CG31005	*CG31005*^{C04819} (insertion within 200 bp 5′ of *CG31005* and within 200 bp 5′ of *mRpL32*)	↑6
		CG31005^{EP984} (insertion within exon 1; potential GOF for *mRpL32*)	↓32 [c]
Df(3R)Exel6265	*Fragile X mental retardation 1* (*Fmr1*)	*Fmr1*$^{\Delta 113m}$	↓12
		Fmr1$^{\Delta 50m}$	↓19
		Fmr1^{KG00715} (insertion between exons 1 and 2) [b]	↓6
		Fmr1^{EP3517} (insertion in exon 1 and possible GOF of *Fmr1*)	↓11

CG31477	*CG6208*^{f06990} (insertion within 100 bp 5′ of *CG31477* and within 400 bp 5′ of *CG6208*)	↑11
knickkopf (*knk*)	*knk*^{f01902} (insertion within exon 2)	↓13
twins (*tws*)	*tws*^{02414} (insertion within exon 2 of transcript *tws-RC*) [b]	↑19
Invadolysin	*Invadolysin*^{c128} (insertion between exons 1 and 2)	↓3
	Invadolysin^{EY11299} (overexpressing within 100 bp 5′ and potential GOF of *Invadolysin*)	↓21
	Invadolysin^{1} [e]	↓19
CG12814	*EY08208* (insertion within 100 bp 5′ of *Best1*)	↓1
	KG02257 (insertion within 100 bp 5′ of *Best1*) [b]	↓10

See Table 1 for explanation of values and abbreviations.

[a] The percentage of UEW in the controls was 100% at this time, so no enhancement of wing expansion was detectable. No enhancement of head eversion defects was observed.

[b] Stock contained ry^{506}.

[c] Measured for females only. The control males in this cross had normal wings.

[d] Stock contained bw^1, st^1. No modification was observed in test crosses with bw^1, st^1 alone.

[e] Stock contained mwh^1, e^1.

Supplemental Figure S2-1.—Overexpression of SPEN in the CCAP/bursicon cells at 25° did not affect pruning of the peripheral axons during early metamorphosis. The panels show representative images of anti-GFP immunostaining of the body wall and ventral nerve cord from *CCAP-Gal4, UAS-mCD8::GFP/+* (A-A″) and *CCAP-Gal4, UAS-mCD8::GFP/EP(2)2583* (B-B″) animals at the indicated times APF (in hr; *n*=5-9). Arrows, type III boutons at neuromuscular endings; arrowheads, unbranched axons with few varicosities; feathered arrows, distal ends of retracting axons. Bar, 100 μm.

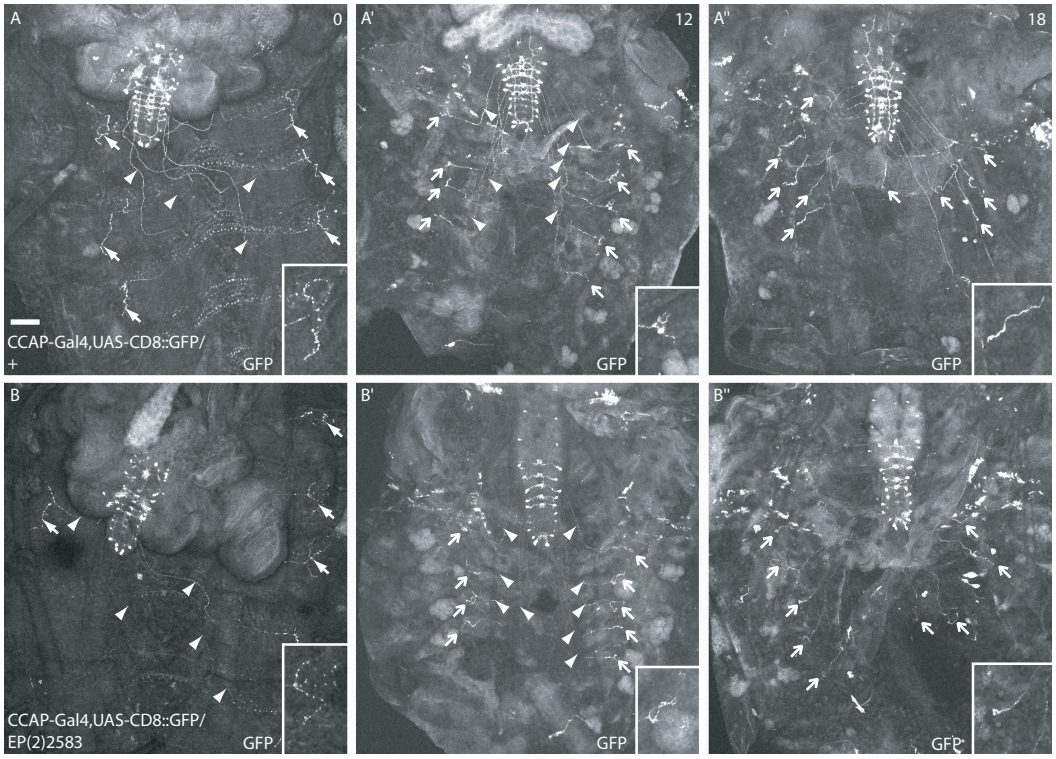
A
0
A'
12
A''
18
CCAP-Gal4,UAS-CD8::GFP/
+
GFP
GFP
GFP
B
B'
B''
CCAP-Gal4,UAS-CD8::GFP/
EP(2)2583
GFP
GFP
GFP

Supplemental Figure S2-2.—CCAP/bursicon cell-targeted *spen* RNAi cell autonomously reduced the levels of SPEN protein. (A-A") Anti-SPEN immunostaining in the wandering third instar CNS (genotype: *UAS-dicer2, yw/w; CCAP-Gal4, UAS-CD8::GFP/+*). SPEN expression (magenta, monoclonal anti-SPEN) was detected in cells with the CCAP-Gal4 reporter (CD8::GFP, green). (B-B") *CCAP-Gal4* was used to drive co-expression of *UAS-CD8::GFP* and *spen-RNAi*^{49543} in a wandering third instar CNS (genotype: *UAS-dicer2, yw/w; CCAP-Gal4, UAS-CD8::GFP/UAS-spen-RNAi*^{49543}). Note the reduced level of nuclear SPEN in the CCAP/bursicon neurons in B-B". Arrows, in-focus CCAP/bursicon neurons with cytoplasmic CD8::GFP. The confocal images are from single confocal scans, and the nuclei of additional CD8::GFP-labeled CCAP/bursicon neurons (green, but not labeled with arrows) were not visible within the scanned focal planes. Bar, 5 μm.

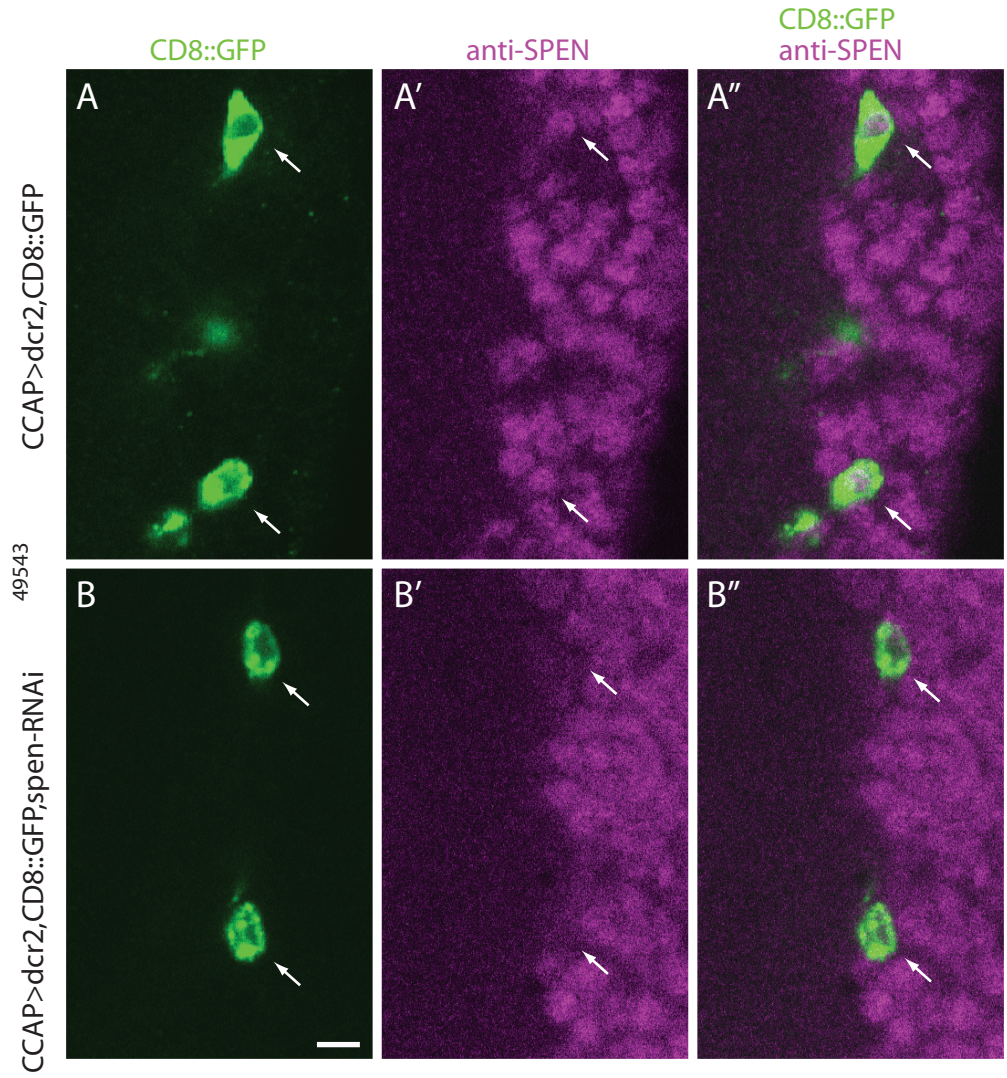
CD8::GFP
anti-SPEN
CD8::GFP
anti-SPEN
A
A′
A″
B
B′
B″
CCAP>dcr2,CD8::GFP
49543
CCAP>dcr2,CD8::GFP,spen-RNAi

Supplemental Figure S2-3.—NITO overexpression blocked adult-specific growth of the CCAP/bursicon neurons. (A and B) Anti-bursicon immunostaining of the posterior VNC and peripheral CCAP/bursicon cell axons in either *CCAP-Gal4*/+ (A) or *CCAP-Gal4*/*UAS-Myc.nito* (B) P14 pharate adults. Arrows, B_{AG} somata. Bar, 100 μm.

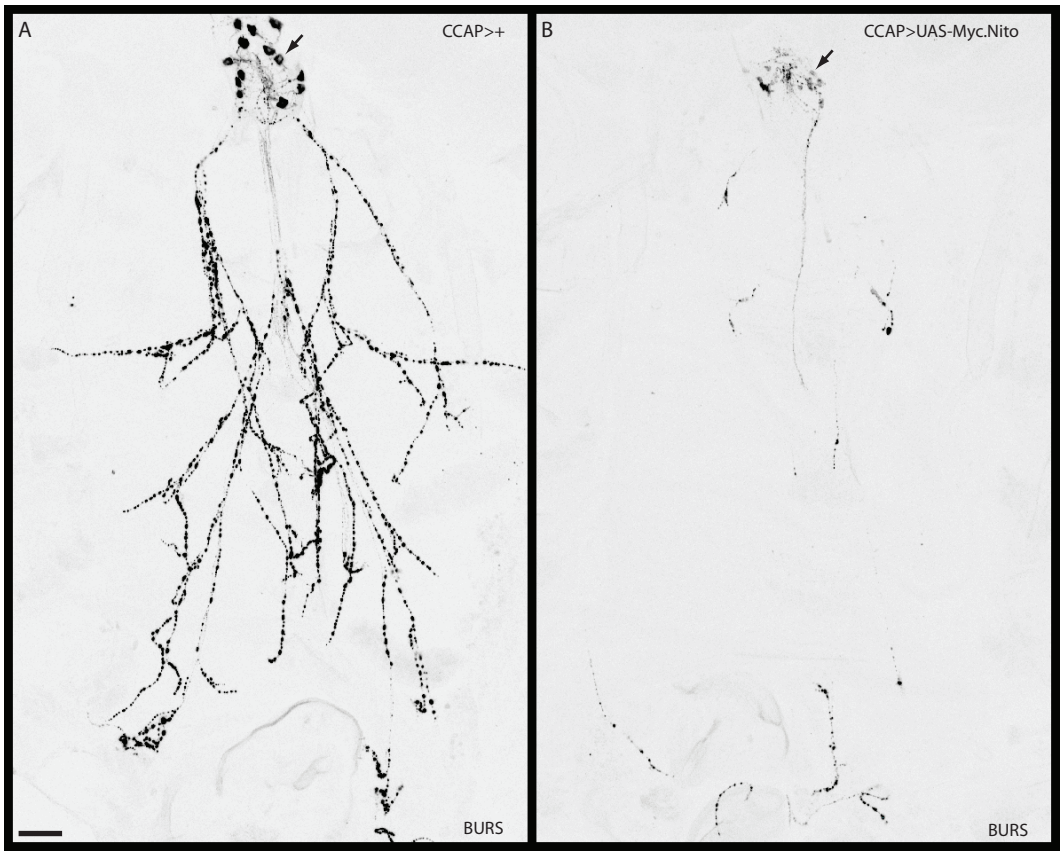
A
CCAP>+
BURS
B
CCAP>UAS-Myc.Nito
BURS

Supplemental Figure S2-4.—Loss of *Taf4* dominantly and partially suppressed the CCAP/bursicon cell remodeling defects observed in the abdominal ganglia following SPEN overexpression. (A) Anti-bursicon immunostaining in stage P14 pharate adult CNS following SPEN overexpression. (B) The effects of SPEN overexpressed were suppressed by one copy of the $Taf4^{1}$ allele. Bursicon immunoreactivity was stronger in the somata and neurites, and varicosities along the neurites (feathered arrows) were larger. Note that the confocal *z*-series images for this figure were taken at settings that were optimal for showing the neurites. However, this tended to saturate the signal in the somata, and the difference in staining intensity in the somata was greater than shown. Bar: 50 μm.

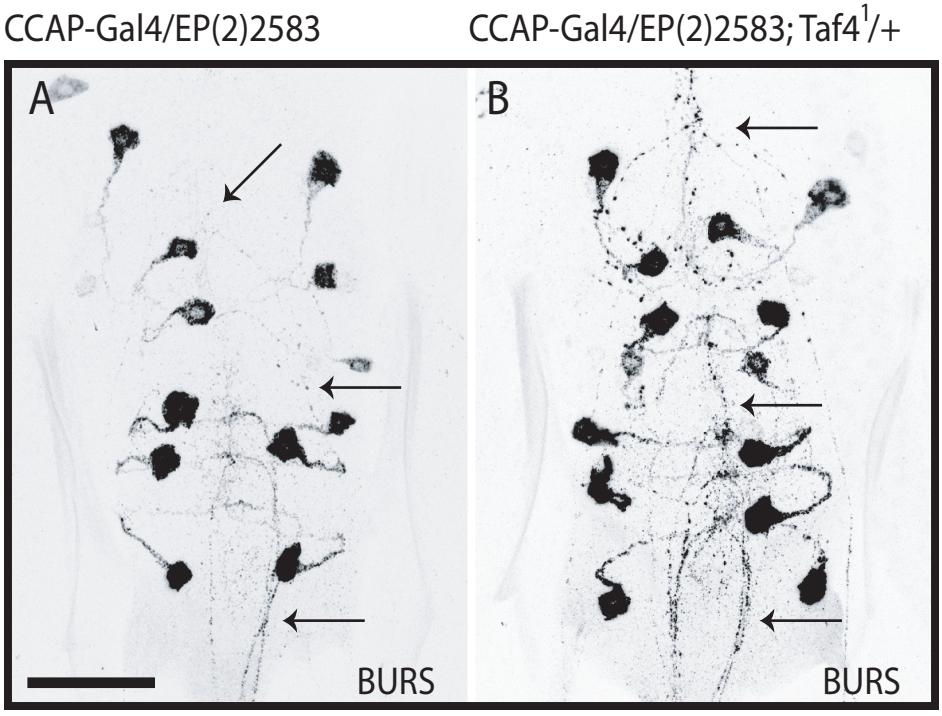
CCAP-Gal4/EP(2)2583
CCAP-Gal4/EP(2)2583; Taf4[1]/+
A
B
BURS
BURS

Bibliography:

ABDELILAH-SEYFRIED, S., Y. M. CHAN, C. ZENG, N. J. JUSTICE, S. YOUNGER-SHEPHERD *et al.*, 2000 A gain-of-function screen for genes that affect the development of the Drosophila adult external sensory organ. Genetics **155:** 733-752.

ALESSI, D., L. K. MACDOUGALL, M. M. SOLA, M. IKEBE and P. COHEN, 1992 The control of protein phosphatase-1 by targetting subunits. The major myosin phosphatase in avian smooth muscle is a novel form of protein phosphatase-1. Eur J Biochem **210:** 1023-1035.

ALLAN, D. W., S. E. PIERRE, I. MIGUEL-ALIAGA and S. THOR, 2003 Specification of neuropeptide cell identity by the integration of retrograde BMP signaling and a combinatorial transcription factor code. Cell **113:** 73-86.

AMANO, M., M. ITO, K. KIMURA, Y. FUKATA, K. CHIHARA *et al.*, 1996 Phosphorylation and activation of myosin by Rho-associated kinase (Rho-kinase). J Biol Chem **271:** 20246-20249.

ABDELILAH-SEYFRIED, S., Y. M. CHAN, C. ZENG, N. J. JUSTICE, S. YOUNGER-SHEPHERD *et al.*, 2000 A gain-of-function screen for genes that affect the development of the Drosophila adult external sensory organ. Genetics **155:** 733-752.

ALESSI, D., L. K. MACDOUGALL, M. M. SOLA, M. IKEBE and P. COHEN, 1992 The control of protein phosphatase-1 by targetting subunits. The major myosin phosphatase in avian smooth muscle is a novel form of protein phosphatase-1. Eur J Biochem **210:** 1023-1035.

ALLAN, D. W., S. E. PIERRE, I. MIGUEL-ALIAGA and S. THOR, 2003 Specification of neuropeptide cell identity by the integration of retrograde BMP signaling and a combinatorial transcription factor code. Cell **113:** 73-86.

AMANO, M., M. ITO, K. KIMURA, Y. FUKATA, K. CHIHARA *et al.*, 1996 Phosphorylation and activation of myosin by Rho-associated kinase (Rho-kinase). J Biol Chem **271:** 20246-20249.

ANG, L. H., W. CHEN, Y. YAO, R. OZAWA, E. TAO *et al.*, 2006 Lim kinase regulates the development of olfactory and neuromuscular synapses. Dev Biol **293:** 178-190.

ARANCIO, O., and M. V. CHAO, 2007 Neurotrophins, synaptic plasticity and dementia. Curr Opin Neurobiol **17:** 325-330.

ARAVIN, A. A., M. LAGOS-QUINTANA, A. YALCIN, M. ZAVOLAN, D. MARKS *et al.*, 2003 The small RNA profile during *Drosophila melanogaster* development. Dev Cell **5:** 337-350.

ARIYOSHI, M., and J. W. SCHWABE, 2003 A conserved structural motif reveals the essential transcriptional repression function of Spen proteins and their role in developmental signaling. Genes Dev **17:** 1909-1920.

AWASAKI, T., and K. ITO, 2004 Engulfing action of glial cells is required for programmed axon pruning during Drosophila metamorphosis. Curr Biol **14:** 668-677.

AWASAKI, T., R. TATSUMI, K. TAKAHASHI, K. ARAI, Y. NAKANISHI *et al.*, 2006 Essential role of the apoptotic cell engulfment genes draper and ced-6 in programmed axon pruning during Drosophila metamorphosis. Neuron **50:** 855-867.

BAINBRIDGE, S. P., and M. BOWNES, 1981 Staging the metamorphosis of *Drosophila melanogaster*. J Embryol Exp Morphol **66:** 57-80.

BAKER, J. D., S. L. MCNABB and J. W. TRUMAN, 1999 The hormonal coordination of behavior and physiology at adult ecdysis in Drosophila melanogaster. J Exp Biol **202:** 3037-3048.

BAKER, J. D., and J. W. TRUMAN, 2002 Mutations in the Drosophila glycoprotein hormone receptor, *rickets*, eliminate neuropeptide-induced tanning and selectively block a stereotyped behavioral program. J Exp Biol **205:** 2555-2565.

BANTIGNIES, F., R. H. GOODMAN and S. M. SMOLIK, 2000 Functional interaction between the coactivator Drosophila CREB-binding protein and ASH1, a member of the trithorax group of chromatin modifiers. Mol Cell Biol **20:** 9317-9330.

BARTHELEMY, C., C. E. HENDERSON and B. PETTMANN, 2004 Foxo3a induces motoneuron death through the Fas pathway in cooperation with JNK. BMC Neurosci **5:** 48.

BEALL, E. L., J. R. MANAK, S. ZHOU, M. BELL, J. S. LIPSICK *et al.*, 2002 Role for a Drosophila Myb-containing protein complex in site-specific DNA replication. Nature **420:** 833-837.

BECK, Y., C. DAUER and G. RICHARDS, 2005 Dynamic localisation of KR-H during an ecdysone response in Drosophila. Gene Expr Patterns **5:** 403-409.

BECKSTEAD, R. B., G. LAM and C. S. THUMMEL, 2005 The genomic response to 20-hydroxyecdysone at the onset of Drosophila metamorphosis. Genome Biol **6:** R99.

BELLEN, H. J., R. W. LEVIS, G. LIAO, Y. HE, J. W. CARLSON *et al.*, 2004 The BDGP gene disruption project: single transposon insertions associated with 40% of Drosophila genes. Genetics **167:** 761-781.

BEN-YAACOV, S., R. LE BORGNE, I. ABRAMSON, F. SCHWEISGUTH and E. D. SCHEJTER, 2001 *Wasp*, the Drosophila Wiskott-Aldrich syndrome gene homologue, is required for cell fate decisions mediated by *Notch* signaling. J Cell Biol **152:** 1-13.

BENDER, M., F. B. IMAM, W. S. TALBOT, B. GANETZKY and D. S. HOGNESS, 1997 Drosophila ecdysone receptor mutations reveal functional differences among receptor isoforms. Cell **91:** 777-788.

BEREZIKOV, E., E. CUPPEN and R. H. PLASTERK, 2006 Approaches to microRNA discovery. Nat Genet **38 Suppl:** S2-7.

BIDET, Y., T. JAGLA, J. P. DA PONTE, B. DASTUGUE and K. JAGLA, 2003 Modifiers of muscle and heart cell fate specification identified by gain-of-function screen in Drosophila. Mech Dev **120:** 991-1007.

BISWAS, S. C., Y. SHI, A. SPROUL and L. A. GREENE, 2007 Pro-apoptotic Bim induction in response to NGF deprivation requires simultaneous activation of three different death signaling pathways. J Biol Chem **282:** 29368-29374.

BITTINS, C. M., T. W. EICHLER, J. A. HAMMER, 3RD and H. H. GERDES, 2009 Dominant-Negative Myosin Va Impairs Retrograde but Not Anterograde Axonal Transport of Large Dense Core Vesicles. Cell Mol Neurobiol.

BOGDAN, S., O. GREWE, M. STRUNK, A. MERTENS and C. KLAMBT, 2004 Sra-1 interacts with Kette and Wasp and is required for neuronal and bristle development in Drosophila. Development **131:** 3981-3989.

BRADKE, F., and C. G. DOTTI, 1999 The role of local actin instability in axon formation. Science **283:** 1931-1934.

BRENNECKE, J., D. R. HIPFNER, A. STARK, R. B. RUSSELL and S. M. COHEN, 2003 *bantam* encodes a developmentally regulated microRNA that controls cell proliferation and regulates the proapoptotic gene *hid* in Drosophila. Cell **113:** 25-36.

BRIDGMAN, P. C., S. DAVE, C. F. ASNES, A. N. TULLIO and R. S. ADELSTEIN, 2001 Myosin IIB is required for growth cone motility. J Neurosci **21:** 6159-6169.

BROWN, H. L., L. CHERBAS, P. CHERBAS and J. W. TRUMAN, 2006 Use of time-lapse imaging and dominant negative receptors to dissect the steroid receptor control of neuronal remodeling in Drosophila. Development **133:** 275-285.

BROWN, M. E., and P. C. BRIDGMAN, 2004 Myosin function in nervous and sensory systems. J Neurobiol **58:** 118-130.

BRUMBY, A., J. SECOMBE, J. HORSFIELD, M. COOMBE, N. AMIN *et al.*, 2004 A genetic screen for dominant modifiers of a cyclin E hypomorphic mutation identifies novel regulators of S-phase entry in Drosophila. Genetics **168:** 227-251.

BRUN, S., A. RINCHEVAL-ARNOLD, J. COLIN, Y. RISLER, B. MIGNOTTE *et al.*, 2006 The myb-related gene *stonewall* induces both hyperplasia and cell death in Drosophila: rescue of fly lethality by coexpression of apoptosis inducers. Cell Death Differ **13:** 1752-1762.

BRUNET, A., S. R. DATTA and M. E. GREENBERG, 2001 Transcription-dependent and -independent control of neuronal survival by the PI3K-Akt signaling pathway. Curr Opin Neurobiol **11:** 297-305.

BUFF, E., A. CARMENA, S. GISSELBRECHT, F. JIMENEZ and A. M. MICHELSON, 1998 Signalling by the Drosophila epidermal growth factor receptor is required for the specification and diversification of embryonic muscle progenitors. Development **125:** 2075-2086.

BURBACH, J. P., S. M. LUCKMAN, D. MURPHY and H. GAINER, 2001 Gene regulation in the magnocellular hypothalamo-neurohypophysial system. Physiol. Rev. **81:** 1197-1267.

CALDWELL, P. E., M. WALKIEWICZ and M. STERN, 2005 Ras activity in the Drosophila prothoracic gland regulates body size and developmental rate via ecdysone release. Curr Biol **15:** 1785-1795.

CHADFIELD, C. G., and J. C. SPARROW, 1985 Pupation in *Drosophila melanogaster* and the effect of the *lethalcryptocephal* mutation. Dev Genet **5:** 103-114.

CHANG, J. L., H. V. LIN, T. A. BLAUWKAMP and K. M. CADIGAN, 2008 Spenito and Split ends act redundantly to promote Wingless signaling. Dev Biol **314:** 100-111.

CHEN, F., and I. REBAY, 2000 split ends, a new component of the Drosophila EGF receptor pathway, regulates development of midline glial cells. Curr Biol **10:** 943-946.

CHEN, S. Y., Z. Y. WANG and X. L. CAI, 2007 OsRRM, a Spen-like rice gene expressed specifically in the endosperm. Cell Res **17:** 713-721.

CHERBAS, L., X. HU, I. ZHIMULEV, E. BELYAEVA and P. CHERBAS, 2003 EcR isoforms in *Drosophila*: testing tissue-specific requirements by targeted blockade and rescue. Development **130:** 271-284.

CHEUNG, U. S., A. J. SHAYAN, G. L. BOULIANNE and H. L. ATWOOD, 1999 Drosophila larval neuromuscular junction's responses to reduction of cAMP in the nervous system. J Neurobiol **40:** 1-13.

CHKLOVSKII, D. B., B. W. MEL and K. SVOBODA, 2004 Cortical rewiring and information storage. Nature **431:** 782-788.

CHOI, Y. J., G. LEE and J. H. PARK, 2006 Programmed cell death mechanisms of identifiable peptidergic neurons in Drosophila melanogaster. Development **133:** 2223-2232.

CLARK, A. C., M. L. DEL CAMPO and J. EWER, 2004a Neuroendocrine control of larval ecdysis behavior in Drosophila: complex regulation by partially redundant neuropeptides. J Neurosci **24:** 4283-4292.

CLARK, A. C., M. L. DEL CAMPO and J. EWER, 2004b Neuroendocrine control of larval ecdysis behavior in *Drosophila*: complex regulation by partially redundant neuropeptides. J Neurosci **24:** 4283-4292.

CLARK, K. A., and D. M. MCKEARIN, 1996 The Drosophila *stonewall* gene encodes a putative transcription factor essential for germ cell development. Development **122:** 937-950.

COLOMBANI, J., L. BIANCHINI, S. LAYALLE, E. PONDEVILLE, C. DAUPHIN-VILLEMANT *et al.*, 2005 Antagonistic actions of ecdysone and insulins determine final size in Drosophila. Science **310:** 667-670.

CONSOULAS, C., C. DUCH, R. J. BAYLINE and R. B. LEVINE, 2000 Behavioral transformations during metamorphosis: remodeling of neural and motor systems. Brain Res Bull **53:** 571-583.

CONSOULAS, C., R. B. LEVINE and L. L. RESTIFO, 2005 The steroid hormone-regulated gene Broad Complex is required for dendritic growth of motoneurons during metamorphosis of Drosophila. Journal of Comparative Neurology **485:** 321-337.

COOKE, B., C. D. HEGSTROM, L. S. VILLENEUVE and S. M. BREEDLOVE, 1998 Sexual differentiation of the vertebrate brain: principles and mechanisms. Front Neuroendocrinol **19:** 323-362.

COYLE, I. P., Y. H. KOH, W. C. LEE, J. SLIND, T. FERGESTAD *et al.*, 2004 Nervous wreck, an SH3 adaptor protein that interacts with Wsp, regulates synaptic growth in Drosophila. Neuron **41:** 521-534.

DEMEREC, M., 1994 *Biology of Drosophila*. Cold Spring Harbor Laboratory Press, Cold Spring Harbor, NY.

DEWEY, E. M., S. L. MCNABB, J. EWER, G. R. KUO, C. L. TAKANISHI *et al.*, 2004 Identification of the gene encoding bursicon, an insect neuropeptide responsible for cuticle sclerotization and wing spreading. Curr Biol **14:** 1208-1213.

DIANTONIO, A., A. P. HAGHIGHI, S. L. PORTMAN, J. D. LEE, A. M. AMARANTO *et al.*, 2001 Ubiquitination-dependent mechanisms regulate synaptic growth and function. Nature **412:** 449-452.

DICKSON, B. J., A. VAN DER STRATEN, M. DOMINGUEZ and E. HAFEN, 1996 Mutations Modulating Raf signaling in Drosophila eye development. Genetics **142:** 163-171.

DIEFENBACH, T. J., V. M. LATHAM, D. YIMLAMAI, C. A. LIU, I. M. HERMAN *et al.*, 2002 Myosin 1c and myosin IIB serve opposing roles in lamellipodial dynamics of the neuronal growth cone. J Cell Biol **158:** 1207-1217.

DIETZL, G., D. CHEN, F. SCHNORRER, K. C. SU, Y. BARINOVA *et al.*, 2007 A genome-wide transgenic RNAi library for conditional gene inactivation in Drosophila. Nature **448:** 151-156.

DOMINGUEZ, M., J. D. WASSERMAN and M. FREEMAN, 1998 Multiple functions of the EGF receptor in Drosophila eye development. Curr Biol **8:** 1039-1048.

DOROQUEZ, D. B., T. L. ORR-WEAVER and I. REBAY, 2007 Split ends antagonizes the Notch and potentiates the EGFR signaling pathways during Drosophila eye development. Mech Dev **124:** 792-806.

DOROQUEZ, D. B., and I. REBAY, 2006 Signal integration during development: mechanisms of EGFR and Notch pathway function and cross-talk. Crit Rev Biochem Mol Biol **41:** 339-385.

DRAIZEN, T. A., J. EWER and S. ROBINOW, 1999 Genetic and hormonal regulation of the death of peptidergic neurons in the Drosophila central nervous system. J Neurobiol **38:** 455-465.

EICHLER, T. W., T. KOGEL, N. V. BUKORESHTLIEV and H. H. GERDES, 2006 The role of myosin Va in secretory granule trafficking and exocytosis. Biochem Soc Trans **34:** 671-674.

ENRIGHT, A. J., B. JOHN, U. GAUL, T. TUSCHL, C. SANDER *et al.*, 2003 MicroRNA targets in Drosophila. Genome Biol **5:** R1.

ERESH, S., J. RIESE, D. B. JACKSON, D. BOHMANN and M. BIENZ, 1997 A CREB-binding site as a target for decapentaplegic signalling during Drosophila endoderm induction. Embo J **16:** 2014-2022.

EWER, J., S. C. GAMMIE and J. W. TRUMAN, 1997 Control of insect ecdysis by a positive-feedback endocrine system: roles of eclosion hormone and ecdysis triggering hormone. J Exp Biol **200 (Pt 5):** 869-881.

EWER, J., and S. E. REYNOLDS, 2002 Neuropeptide control of molting in insects, pp. 1-92 in *Hormones, brain and behavior in invertebrates*, edited by D. W. PFAFF, A. P. ARNOLD, A. M. ETGEN, S. E. FAHRBACH and R. T. RUBIN. Academic Press, New York.

FAN, X., J. P. LABRADOR, H. HING and G. J. BASHAW, 2003 Slit stimulation recruits Dock and Pak to the roundabout receptor and increases Rac activity to regulate axon repulsion at the CNS midline.[see comment]. Neuron **40:** 113-127.

FEIG, L. A., 1999 Tools of the trade: use of dominant-inhibitory mutants of Ras-family GTPases. Nat Cell Biol **1:** E25-27.

FEIG, L. A., and G. M. COOPER, 1988 Inhibition of NIH 3T3 cell proliferation by a mutant ras protein with preferential affinity for GDP. Mol Cell Biol **8:** 3235-3243.

FLYBASE_CONSORTIUM, 2003 The FlyBase database of the Drosophila genome projects and community literature. http://flybase.org. Nucleic Acids Res **31:** 172-175.

FORTINI, M. E., M. A. SIMON and G. M. RUBIN, 1992 Signalling by the sevenless protein tyrosine kinase is mimicked by Ras1 activation.[see comment]. Nature **355:** 559-561.

FRAENKEL, G., and C. HSIAO, 1965 Bursicon, a hormone which mediates tanning of the cuticle in the adult fly and other insects. J Insect Physiol **11:** 513-556.

GARCIA-SEGURA, L. M., J. A. CHOWEN, A. PARDUCZ and F. NAFTOLIN, 1994 Gonadal hormones as promoters of structural synaptic plasticity: cellular mechanisms. Prog Neurobiol **44:** 279-307.

GILLEY, J., P. J. COFFER and J. HAM, 2003 FOXO transcription factors directly activate bim gene expression and promote apoptosis in sympathetic neurons. J Cell Biol **162:** 613-622.

GOVEK, E. E., S. E. NEWEY and L. VAN AELST, 2005 The role of the Rho GTPases in neuronal development. Genes Dev **19:** 1-49.

GRUMBLING, G., V. STRELETS and T. F. CONSORTIUM, 2006 FlyBase: anatomical data, images and queries. Nucleic Acids Research **34:** D484-D488.

GRUN, D., Y. L. WANG, D. LANGENBERGER, K. C. GUNSALUS and N. RAJEWSKY, 2005 microRNA target predictions across seven Drosophila species and comparison to mammalian targets. PLoS Comput Biol **1:** e13.

HADORN, E., and H. GLOOR, 1943 *Cryptocephal* ein spat wirkender Letalfaktor bei *Drosophila melanogaster*. Revue suisse Zool **50:** 256-261.

HARTSHORNE, D. J., M. ITO and F. ERDODI, 1998a Myosin light chain phosphatase: subunit composition, interactions and regulation. J Muscle Res Cell Motil **19:** 325-341.

HARTSHORNE, D. J., M. ITO and F. ERDODI, 1998b Myosin light chain phosphatase: subunit composition, interactions and regulation. Journal of Muscle Research & Cell Motility **19:** 325-341.

HEBBAR, S., and J. J. FERNANDES, 2004 Pruning of motor neuron branches establishes the DLM innervation pattern in Drosophila. J Neurobiol **60:** 499-516.

HEBBAR, S., and J. J. FERNANDES, 2005 A role for Fas II in the stabilization of motor neuron branches during pruning in Drosophila. Dev Biol **285:** 185-199.

HEGDE, A. N., 2004 Ubiquitin-proteasome-mediated local protein degradation and synaptic plasticity. Prog Neurobiol **73:** 311-357.

HEWES, R. S., 2008 The buzz on fly neuronal remodeling. Trends Endocrinol Metab **19:** 317-323.

HEWES, R. S., T. GU, J. A. BREWSTER, C. QU and T. ZHAO, 2006 Regulation of secretory protein expression in mature cells by DIMM, a bHLH neuroendocrine differentiation factor. J Neurosci **26:** 7860-7869.

HEWES, R. S., D. PARK, S. A. GAUTHIER, A. M. SCHAEFER and P. H. TAGHERT, 2003 The bHLH protein Dimmed controls neuroendocrine cell differentiation in Drosophila. Development **130:** 1771-1781.

HEWES, R. S., A. M. SCHAEFER and P. H. TAGHERT, 2000 The *cryptocephal* gene (ATF4) encodes multiple basic-leucine zipper proteins controlling molting and metamorphosis in Drosophila. Genetics **155:** 1711-1723.

HEWES, R. S., and J. W. TRUMAN, 1991 The roles of central and peripheral eclosion hormone release in the control of ecdysis behavior in *Manduca sexta*. J Comp Physiol [A] **168:** 697-707.

HING, H., J. XIAO, N. HARDEN, L. LIM and S. L. ZIPURSKY, 1999 Pak functions downstream of Dock to regulate photoreceptor axon guidance in Drosophila. Cell **97:** 853-863.

HODGE, J. J., J. C. CHOI, C. J. O'KANE and L. C. GRIFFITH, 2005 Shaw potassium channel genes in Drosophila. J Neurobiol **63:** 235-254.

HOLTMAAT, A., and K. SVOBODA, 2009 Experience-dependent structural synaptic plasticity in the mammalian brain. Nat Rev Neurosci **10:** 647-658.

HOOPFER, E. D., T. MCLAUGHLIN, R. J. WATTS, O. SCHULDINER, D. D. O'LEARY *et al.*, 2006 Wld^s protection distinguishes axon degeneration following injury from naturally occurring developmental pruning. Neuron **50:** 883-895.

HOOPFER, E. D., A. PENTON, R. J. WATTS and L. LUO, 2008 Genomic analysis of Drosophila neuronal remodeling: a role for the RNA-binding protein Boule as a negative regulator of axon pruning. J Neurosci **28:** 6092-6103.

HU, X., L. CHERBAS and P. CHERBAS, 2003 Transcription activation by the ecdysone receptor (EcR/USP): identification of activation functions. Mol Endocrinol **17:** 716-731.

HUBER, A. B., A. L. KOLODKIN, D. D. GINTY and J. F. CLOUTIER, 2003 Signaling at the growth cone: ligand-receptor complexes and the control of axon growth and guidance. Annu Rev Neurosci **26:** 509-563.

HWANGBO, D. S., B. GERSHMAN, M. P. TU, M. PALMER and M. TATAR, 2004 *Drosophila* dFOXO controls lifespan and regulates insulin signalling in brain and fat body. Nature **429:** 562-566.

JEMC, J., and I. REBAY, 2006 Characterization of the split ends-like gene spenito reveals functional antagonism between SPOC family members during Drosophila eye development. Genetics **173:** 279-286.

JIN, L. H., J. K. CHOI, B. KIM, H. S. CHO, J. KIM *et al.*, 2009 Requirement of Split ends for epigenetic regulation of Notch signal-dependent genes during infection-induced hemocyte differentiation. Mol Cell Biol **29:** 1515-1525.

JIN, L. H., J. SHIM, J. S. YOON, B. KIM, J. KIM *et al.*, 2008 Identification and functional analysis of antifungal immune response genes in Drosophila. PLoS Pathog **4:** e1000168.

KADISH, I., and T. VAN GROEN, 2002 Low levels of estrogen significantly diminish axonal sprouting after entorhinal cortex lesions in the mouse. J Neurosci **22:** 4095-4102.

KARIM, F. D., and G. M. RUBIN, 1998 Ectopic expression of activated Ras1 induces hyperplastic growth and increased cell death in Drosophila imaginal tissues. Development **125:** 1-9.

KARMARKAR, U. R., and Y. DAN, 2006 Experience-dependent plasticity in adult visual cortex. Neuron **52:** 577-585.

KAROLCHIK, D., R. BAERTSCH, M. DIEKHANS, T. S. FUREY, A. HINRICHS *et al.*, 2003 The UCSC Genome Browser Database. Nucleic Acids Res **31:** 51-54.

KAWANO, Y., Y. FUKATA, N. OSHIRO, M. AMANO, T. NAKAMURA *et al.*, 1999 Phosphorylation of myosin-binding subunit (MBS) of myosin phosphatase by Rho-kinase in vivo. J Cell Biol **147:** 1023-1038.

KIM, Y. J., I. SPALOVSKA-VALACHOVA, K. H. CHO, I. ZITNANOVA, Y. PARK *et al.*, 2004 Corazonin receptor signaling in ecdysis initiation. Proc Natl Acad Sci U S A **101:** 6704-6709.

KIM, Y. J., D. ZITNAN, C. G. GALIZIA, K. H. CHO and M. E. ADAMS, 2006 A command chemical triggers an innate behavior by sequential activation of multiple peptidergic ensembles. Curr Biol **16:** 1395-1407.

KIMURA, K., M. ITO, M. AMANO, K. CHIHARA, Y. FUKATA *et al.*, 1996a Regulation of myosin phosphatase by Rho and Rho-associated kinase (Rho-kinase). Science **273:** 245-248.

KIMURA, K., M. ITO, M. AMANO, K. CHIHARA, Y. FUKATA *et al.*, 1996b Regulation of myosin phosphatase by Rho and Rho-associated kinase (Rho-kinase)[see comment]. Science **273:** 245-248.

KINCH, G., K. L. HOFFMAN, E. M. RODRIGUES, M. C. ZEE and J. C. WEEKS, 2003 Steroid-triggered programmed cell death of a motoneuron is autophagic and involves structural changes in mitochondria. J Comp Neurol **457:** 384-403.

KLOOSTERMAN, W. P., and R. H. PLASTERK, 2006 The diverse functions of microRNAs in animal development and disease. Dev Cell **11:** 441-450.

KOELLE, M. R., W. S. TALBOT, W. A. SEGRAVES, M. T. BENDER, P. CHERBAS *et al.*, 1991 The Drosophila *EcR* gene encodes an ecdysone receptor, a new member of the steroid receptor superfamily. Cell **67:** 59-77.

KOLODZIEJ, P. A., L. Y. JAN and Y. N. JAN, 1995 Mutations that affect the length, fasciculation, or ventral orientation of specific sensory axons in the Drosophila embryo. Neuron **15:** 273-286.

KORN, E. D., and J. A. HAMMER, 3RD, 1988 Myosins of nonmuscle cells. Annu Rev Biophys Biophys Chem **17:** 23-45.

KOZLOVA, T., and C. S. THUMMEL, 2003 Essential roles for ecdysone signaling during Drosophila mid-embryonic development. Science **301:** 1911-1914.

KRAUT, R., K. MENON and K. ZINN, 2001 A gain-of-function screen for genes controlling motor axon guidance and synaptogenesis in Drosophila. Curr Biol **11:** 417-430.

KUANG, B., S. C. WU, Y. SHIN, L. LUO and P. KOLODZIEJ, 2000 split ends encodes large nuclear proteins that regulate neuronal cell fate and axon extension in the Drosophila embryo. Development **127:** 1517-1529.

KUO, C. T., L. Y. JAN and Y. N. JAN, 2005 Dendrite-specific remodeling of Drosophila sensory neurons requires matrix metalloproteases, ubiquitin-proteasome, and ecdysone signaling. Proc Natl Acad Sci U S A **102:** 15230-15235.

KUO, C. T., S. ZHU, S. YOUNGER, L. Y. JAN and Y. N. JAN, 2006 Identification of E2/E3 ubiquitinating enzymes and caspase activity regulating Drosophila sensory neuron dendrite pruning. Neuron **51:** 283-290.

LANE, M. E., M. ELEND, D. HEIDMANN, A. HERR, S. MARZODKO *et al.*, 2000 A screen for modifiers of cyclin E function in *Drosophila melanogaster* identifies *Cdk2* mutations, revealing the insignificance of putative phosphorylation sites in *Cdk2*. Genetics **155:** 233-244.

LEAMAN, D., P. Y. CHEN, J. FAK, A. YALCIN, M. PEARCE *et al.*, 2005 Antisense-mediated depletion reveals essential and specific functions of microRNAs in Drosophila development. Cell **121:** 1097-1108.

LEE, A., and J. E. TREISMAN, 2004a Excessive Myosin activity in mbs mutants causes photoreceptor movement out of the Drosophila eye disc epithelium. Mol Biol Cell **15:** 3285-3295.

LEE, A., and J. E. TREISMAN, 2004b Excessive Myosin activity in mbs mutants causes photoreceptor movement out of the Drosophila eye disc epithelium. Molecular Biology of the Cell **15:** 3285-3295.

LEE, H. H., L. Y. JAN and Y. N. JAN, 2009 Drosophila IKK-related kinase Ik2 and Katanin p60-like 1 regulate dendrite pruning of sensory neuron during metamorphosis. Proc Natl Acad Sci U S A **106:** 6363-6368.

LEE, T., L. FEIG and D. J. MONTELL, 1996 Two distinct roles for Ras in a developmentally regulated cell migration. Development **122:** 409-418.

LEE, T., A. LEE and L. LUO, 1999 Development of the Drosophila mushroom bodies: sequential generation of three distinct types of neurons from a neuroblast. Development **126:** 4065-4076.

LEE, T., and L. LUO, 1999 Mosaic analysis with a repressible cell marker for studies of gene function in neuronal morphogenesis. Neuron **22:** 451-461.

LEE, T., S. MARTICKE, C. SUNG, S. ROBINOW and L. LUO, 2000 Cell-autonomous requirement of the USP/EcR-B ecdysone receptor for mushroom body neuronal remodeling in Drosophila. Neuron **28:** 807-818.

LEVINE, R. B., and J. W. TRUMAN, 1982 Metamorphosis of the insect nervous system: changes in morphology and synaptic interactions of identified neurones. Nature **299:** 250-252.

LEWIS, P. W., E. L. BEALL, T. C. FLEISCHER, D. GEORLETTE, A. J. LINK *et al.*, 2004 Identification of a Drosophila Myb-E2F2/RBF transcriptional repressor complex. Genes Dev **18:** 2929-2940.

LI, T., and M. BENDER, 2000 A conditional rescue system reveals essential functions for the ecdysone receptor (EcR) gene during molting and metamorphosis in Drosophila. Development **127:** 2897-2905.

LI, X., and R. W. CARTHEW, 2005 A microRNA mediates EGF receptor signaling and promotes photoreceptor differentiation in the Drosophila eye. Cell **123:** 1267-1277.

LIN, C. H., E. M. ESPREAFICO, M. S. MOOSEKER and P. FORSCHER, 1996 Myosin drives retrograde F-actin flow in neuronal growth cones. Neuron **16:** 769-782.

LIN, C. H., and P. FORSCHER, 1995 Growth cone advance is inversely proportional to retrograde F-actin flow. Neuron **14:** 763-771.

LIN, H. V., D. B. DOROQUEZ, S. CHO, F. CHEN, I. REBAY *et al.*, 2003 Splits ends is a tissue/promoter specific regulator of Wingless signaling. Development **130:** 3125-3135.

LIU, D. X., S. C. BISWAS and L. A. GREENE, 2004 B-myb and C-myb play required roles in neuronal apoptosis evoked by nerve growth factor deprivation and DNA damage. J Neurosci **24:** 8720-8725.

LIU, D. X., and L. A. GREENE, 2001 Regulation of neuronal survival and death by E2F-dependent gene repression and derepression. Neuron **32:** 425-438.

LUAN, H., W. C. LEMON, N. C. PEABODY, J. B. POHL, P. K. ZELENSKY *et al.*, 2006a Functional dissection of a neuronal network required for cuticle tanning and wing expansion in Drosophila. J Neurosci **26:** 573-584.

LUAN, H., W. C. LEMON, N. C. PEABODY, J. B. POHL, P. K. ZELENSKY *et al.*, 2006b Functional dissection of a neuronal network required for cuticle tanning and wing expansion in Drosophila. Journal of Neuroscience **26:** 573-584.

LUDEWIG, A. H., C. KOBER-EISERMANN, C. WEITZEL, A. BETHKE, K. NEUBERT *et al.*, 2004 A novel nuclear receptor/coregulator complex controls C. elegans lipid metabolism, larval development, and aging. Genes Dev **18:** 2120-2133.

LUO, C. W., E. M. DEWEY, S. SUDO, J. EWER, S. Y. HSU *et al.*, 2005 Bursicon, the insect cuticle-hardening hormone, is a heterodimeric cystine knot protein that activates G protein-coupled receptor LGR2. Proc Natl Acad Sci U S A **102:** 2820-2825.

LUO, L., 2000 Rho GTPases in neuronal morphogenesis. Nat Rev Neurosci **1:** 173-180.

LUO, L., 2002 Actin cytoskeleton regulation in neuronal morphogenesis and structural plasticity. Annu Rev Cell Dev Biol **18:** 601-635.

LUO, L., Y. J. LIAO, L. Y. JAN and Y. N. JAN, 1994 Distinct morphogenetic functions of similar small GTPases: Drosophila Drac1 is involved in axonal outgrowth and myoblast fusion. Genes Dev **8:** 1787-1802.

LUO, X., O. PUIG, J. HYUN, D. BOHMANN and H. JASPER, 2007 Foxo and Fos regulate the decision between cell death and survival in response to UV irradiation. Embo J **26:** 380-390.

MALACOMBE, M., M. F. BADER and S. GASMAN, 2006 Exocytosis in neuroendocrine cells: new tasks for actin. Biochim Biophys Acta **1763:** 1175-1183.

MARIN, E. C., R. J. WATTS, N. K. TANAKA, K. ITO and L. LUO, 2005 Developmentally programmed remodeling of the Drosophila olfactory circuit. Development **132:** 725-737.

MCCAULEY, D. W., and M. BRONNER-FRASER, 2006 Importance of SoxE in neural crest development and the evolution of the pharynx. Nature **441:** 750-752.

MCGOVERN, V. L., C. A. PACAK, S. T. SEWELL, M. L. TURSKI and M. A. SEEGER, 2003 A targeted gain of function screen in the embryonic CNS of Drosophila. Mech Dev **120:** 1193-1207.

MCGUIRE, S. E., P. T. LE, A. J. OSBORN, K. MATSUMOTO and R. L. DAVIS, 2003 Spatiotemporal rescue of memory dysfunction in Drosophila. Science **302:** 1765-1768.

MCGUIRE, S. E., Z. MAO and R. L. DAVIS, 2004 Spatiotemporal gene expression targeting with the TARGET and gene-switch systems in Drosophila. Sci STKE **2004:** pl6.

MCNABB, S. L., J. D. BAKER, J. AGAPITE, H. STELLER, L. M. RIDDIFORD *et al.*, 1997 Disruption of a behavioral sequence by targeted death of peptidergic neurons in Drosophila. Neuron **19:** 813-823.

MENZEL, N., D. SCHNEEBERGER and T. RAABE, 2007 The Drosophila p21 activated kinase Mbt regulates the actin cytoskeleton and adherens junctions to control photoreceptor cell morphogenesis. Mech Dev **124:** 78-90.

MICHEL, B., P. KOMARNITSKY and S. BURATOWSKI, 1998 Histone-like TAFs are essential for transcription in vivo. Mol Cell **2:** 663-673.

MINDORFF, E. N., D. D. O'KEEFE, A. LABBE, J. P. YANG, Y. OU *et al.*, 2007 A gain-of-function screen for genes that influence axon guidance identifies the NF-kappaB protein dorsal and reveals a requirement for the kinase Pelle in Drosophila photoreceptor axon targeting. Genetics **176:** 2247-2263.

MIZUNO, T., M. AMANO, K. KAIBUCHI and Y. NISHIDA, 1999 Identification and characterization of Drosophila homolog of Rho-kinase. Gene **238:** 437-444.

MIZUNO, T., K. TSUTSUI and Y. NISHIDA, 2002 Drosophila myosin phosphatase and its role in dorsal closure. Development **129:** 1215-1223.

MOLINE, M. M., C. SOUTHERN and A. BEJSOVEC, 1999 Directionality of wingless protein transport influences epidermal patterning in the Drosophila embryo. Development **126:** 4375-4384.

MULLER, D., S. J. KUGLER, A. PREISS, D. MAIER and A. C. NAGEL, 2005 Genetic modifier screens on Hairless gain-of-function phenotypes reveal genes involved in cell differentiation, cell growth and apoptosis in *Drosophila melanogaster*. Genetics **171:** 1137-1152.

MUNOZ-DESCALZO, S., J. TEROL and N. PARICIO, 2005 Cabut, a C2H2 zinc finger transcription factor, is required during Drosophila dorsal closure downstream of JNK signaling. Dev Biol **287:** 168-179.

MUTSUDDI, M., C. M. MARSHALL, K. A. BENZOW, M. D. KOOB and I. REBAY, 2004 The spinocerebellar ataxia 8 noncoding RNA causes neurodegeneration and associates with staufen in Drosophila. Curr Biol **14:** 302-308.

NAKAI, K., Y. SUZUKI, H. KIHIRA, H. WADA, M. FUJIOKA *et al.*, 1997 Regulation of myosin phosphatase through phosphorylation of the myosin-binding subunit in platelet activation. Blood **90:** 3936-3942.

NAVARRO, X., M. VIVO and A. VALERO-CABRE, 2007 Neural plasticity after peripheral nerve injury and regeneration. Prog Neurobiol **82:** 163-201.

NEWBERRY, E. P., T. LATIFI and D. A. TOWLER, 1999 The RRM domain of MINT, a novel Msx2 binding protein, recognizes and regulates the rat osteocalcin promoter. Biochemistry **38:** 10678-10690.

NG, J., 2008 TGF-beta signals regulate axonal development through distinct Smad-independent mechanisms. Development **135:** 4025-4035.

NG, J., and L. LUO, 2004 Rho GTPases regulate axon growth through convergent and divergent signaling pathways. Neuron **44:** 779-793.

NG, J., T. NARDINE, M. HARMS, J. TZU, A. GOLDSTEIN *et al.*, 2002 Rac GTPases control axon growth, guidance and branching. Nature **416:** 442-447.

NICOLAI, M., C. LASBLEIZ and J. M. DURA, 2003 Gain-of-function screen identifies a role of the Src64 oncogene in Drosophila mushroom body development. J Neurobiol **57:** 291-302.

NIJHOUT, H. F., 1994 *Insect hormones*. Princeton University Press, Princeton, NJ.

NIKOLIC, M., 2008 The Pak1 kinase: an important regulator of neuronal morphology and function in the developing forebrain. Mol Neurobiol **37:** 187-202.

NITABACH, M. N., J. BLAU and T. C. HOLMES, 2002 Electrical silencing of Drosophila pacemaker neurons stops the free-running circadian clock. Cell **109:** 485-495.

NIWA, R., K. NAGATA-OHASHI, M. TAKEICHI, K. MIZUNO and T. UEMURA, 2002 Control of actin reorganization by Slingshot, a family of phosphatases that dephosphorylate ADF/cofilin. Cell **108:** 233-246.

O'BRIEN, M. A., and P. H. TAGHERT, 1998 A peritracheal neuropeptide system in insects: release of myomodulin-like peptides at ecdysis. J Exp Biol **201 (Pt 2):** 193-209.

ORPHANIDES, G., T. LAGRANGE and D. REINBERG, 1996 The general transcription factors of RNA polymerase II. Genes Dev **10:** 2657-2683.

PARK, D., M. HAN, Y. C. KIM, K. A. HAN and P. H. TAGHERT, 2004 Ap-let neurons--a peptidergic circuit potentially controlling ecdysial behavior in *Drosophila*. Dev. Biol. **269:** 95-108.

PARK, J. H., A. J. SCHROEDER, C. HELFRICH-FORSTER, F. R. JACKSON and J. EWER, 2003 Targeted ablation of CCAP neuropeptide-containing neurons of Drosophila causes specific defects in execution and circadian timing of ecdysis behavior. Development **130:** 2645-2656.

PARKS, A. L., K. R. COOK, M. BELVIN, N. A. DOMPE, R. FAWCETT *et al.*, 2004 Systematic generation of high-resolution deletion coverage of the Drosophila melanogaster genome. Nat Genet **36:** 288-292.

PEABODY, N. C., J. B. POHL, F. DIAO, A. P. VREEDE, D. J. SANDSTROM *et al.*, 2009 Characterization of the decision network for wing expansion in Drosophila using targeted expression of the TRPM8 channel. J Neurosci **29:** 3343-3353.

PECASSE, F., Y. BECK, C. RUIZ and G. RICHARDS, 2000 Kruppel-homolog, a stage-specific modulator of the prepupal ecdysone response, is essential for Drosophila metamorphosis. Dev Biol **221:** 53-67.

PENA-RANGEL, M. T., I. RODRIGUEZ and J. R. RIESGO-ESCOVAR, 2002 A misexpression study examining dorsal thorax formation in *Drosophila melanogaster*. Genetics **160:** 1035-1050.

RAJEWSKY, N., and N. D. SOCCI, 2004 Computational identification of microRNA targets. Dev Biol **267:** 529-535.

REBAY, I., F. CHEN, F. HSIAO, P. A. KOLODZIEJ, B. H. KUANG *et al.*, 2000 A genetic screen for novel components of the Ras/Mitogen-activated protein kinase signaling pathway that interact with the yan gene of Drosophila identifies split ends, a new RNA recognition motif-containing protein. Genetics **154:** 695-712.

REYNOLDS, S. E., P. H. TAGHERT and J. W. TRUMAN, 1979 Eclosion hormone and bursicon titers and the onset of hormonal responsiveness during the last day of adult development in *Manduca sexta* (L.). J Exp Biol **78:** 77-86.

RIDDIFORD, L. M., R. S. HEWES and J. W. TRUMAN, 1994 Dynamics and metamorphosis of an identifiable peptidergic neuron in an insect. J Neurobiol **25:** 819-830.

ROBINOW, S., W. S. TALBOT, D. S. HOGNESS and J. W. TRUMAN, 1993 Programmed cell death in the Drosophila CNS is ecdysone-regulated and coupled with a specific ecdysone receptor isoform. Development **119:** 1251-1259.

RODAL, A. A., R. N. MOTOLA-BARNES and J. T. LITTLETON, 2008 Nervous wreck and Cdc42 cooperate to regulate endocytic actin assembly during synaptic growth. J Neurosci **28:** 8316-8325.

ROMEO, R. D., and B. S. MCEWEN, 2006 Stress and the adolescent brain. Ann N Y Acad Sci **1094:** 202-214.

RØRTH, P., 1996 A modular misexpression screen in Drosophila detecting tissue-specific phenotypes. Proc Natl Acad Sci U S A **93:** 12418-12422.

RØRTH, P., K. SZABO, A. BAILEY, T. LAVERTY, J. REHM *et al.*, 1998 Systematic gain-of-function genetics in Drosophila. Development **125:** 1049-1057.

ROY, B., A. P. SINGH, C. SHETTY, V. CHAUDHARY, A. NORTH *et al.*, 2007 Metamorphosis of an identified serotonergic neuron in the Drosophila olfactory system. Neural Dev **2:** 20.

RYOO, H. D., and H. STELLER, 2007 Unfolded protein response in Drosophila: why another model can make it fly. Cell Cycle **6:** 830-835.

SANCHEZ-PULIDO, L., A. M. ROJAS, K. H. VAN WELY, A. C. MARTINEZ and A. VALENCIA, 2004 SPOC: a widely distributed domain associated with cancer, apoptosis and transcription. BMC Bioinformatics **5:** 91.

SANTOS, J. G., E. POLLAK, K. H. REXER, L. MOLNAR and C. WEGENER, 2006 Morphology and metamorphosis of the peptidergic Va neurons and the median nerve system of the fruit fly, *Drosophila melanogaster*. Cell Tissue Res **326:** 187-199.

SCHENCK, A., B. BARDONI, C. LANGMANN, N. HARDEN, J. L. MANDEL *et al.*, 2003 CYFIP/Sra-1 controls neuronal connectivity in Drosophila and links the Rac1 GTPase pathway to the fragile X protein.[see comment]. Neuron **38:** 887-898.

SCHUBIGER, M., S. TOMITA, C. SUNG, S. ROBINOW and J. W. TRUMAN, 2003 Isoform specific control of gene activity in vivo by the Drosophila ecdysone receptor. Mech Dev **120:** 909-918.

SCHUBIGER, M., A. A. WADE, G. E. CARNEY, J. W. TRUMAN and M. BENDER, 1998 Drosophila EcR-B ecdysone receptor isoforms are required for larval molting and for neuron remodeling during metamorphosis. Development **125:** 2053-2062.

SCHULZ, C., A. A. KIGER, S. I. TAZUKE, Y. M. YAMASHITA, L. C. PANTALENA-FILHO *et al.*, 2004 A misexpression screen reveals effects of *bag-of-marbles* and TGF beta class signaling on the Drosophila male germ-line stem cell lineage. Genetics **167:** 707-723.

SEEBURG, P. H., W. W. COLBY, D. J. CAPON, D. V. GOEDDEL and A. D. LEVINSON, 1984 Biological properties of human c-Ha-ras1 genes mutated at codon 12. Nature **312:** 71-75.

SEMPERE, L. F., N. S. SOKOL, E. B. DUBROVSKY, E. M. BERGER and V. AMBROS, 2003 Temporal regulation of microRNA expression in *Drosophila melanogaster* mediated by hormonal signals and *broad-Complex* gene activity. Dev Biol **259:** 9-18.

SHAKIRYANOVA, D., A. TULLY, R. S. HEWES, D. L. DEITCHER and E. S. LEVITAN, 2005 Activity-dependent liberation of synaptic neuropeptide vesicles. Nat Neurosci **8:** 173-178.

SHERWOOD, N. T., Q. SUN, M. XUE, B. ZHANG and K. ZINN, 2004 Drosophila spastin regulates synaptic microtubule networks and is required for normal motor function. PLoS Biol **2:** e429.

SHI, L., S. LIN, Y. GRINBERG, Y. BECK, C. M. GROZINGER *et al.*, 2007 Roles of Drosophila Kruppel-homolog 1 in neuronal morphogenesis. Dev Neurobiol **67:** 1614-1626.

SHI, Y., M. DOWNES, W. XIE, H. Y. KAO, P. ORDENTLICH *et al.*, 2001 Sharp, an inducible cofactor that integrates nuclear receptor repression and activation. Genes Dev **15:** 1140-1151.

SORIANO, F. X., S. PAPADIA, F. HOFMANN, N. R. HARDINGHAM, H. BADING *et al.*, 2006 Preconditioning doses of NMDA promote neuroprotection by enhancing neuronal excitability. J Neurosci **26:** 4509-4518.

SOUSA, N., J. J. CERQUEIRA and O. F. ALMEIDA, 2008 Corticosteroid receptors and neuroplasticity. Brain Research Reviews **57:** 561-570.

SRIVASTAVA, D. P., K. M. WOOLFREY, K. A. JONES, C. Y. SHUM, L. L. LASH *et al.*, 2008 Rapid enhancement of two-step wiring plasticity by estrogen and NMDA receptor activity. Proc Natl Acad Sci U S A **105:** 14650-14655.

STAEHLING-HAMPTON, K., P. J. CIAMPA, A. BROOK and N. DYSON, 1999 A genetic screen for modifiers of *E2F* in *Drosophila melanogaster*. Genetics **153:** 275-287.

STARK, A., J. BRENNECKE, R. B. RUSSELL and S. M. COHEN, 2003 Identification of Drosophila MicroRNA targets. PLoS Biol **1:** E60.

STEWARD, O., 1982 Assessing the functional significance of lesion-induced neuronal plasticity. Int Rev Neurobiol **23:** 197-254.

STRUTT, D. I., U. WEBER and M. MLODZIK, 1997 The role of RhoA in tissue polarity and Frizzled signalling. Nature **387:** 292-295.

TAGHERT, P. H., R. S. HEWES, J. H. PARK, M. A. O'BRIEN, M. HAN *et al.*, 2001 Multiple amidated neuropeptides are required for normal circadian locomotor rhythms in Drosophila. J. Neurosci. **21:** 6673-6686.

TAGHERT, P. H., and J. W. TRUMAN, 1982 Identification of the bursicon-containing neurones in abdominal ganglia of the tobacco hornworm, *Manduca sexta*. J Exp Biol **98:** 385-401.

TALBOT, W. S., E. A. SWYRYD and D. S. HOGNESS, 1993 Drosophila tissues with different metamorphic responses to ecdysone express different ecdysone receptor isoforms. Cell **73:** 1323-1337.

TAN, C., B. STRONACH and N. PERRIMON, 2003 Roles of myosin phosphatase during Drosophila development. Development **130:** 671-681.

TAUTZ, D., and C. PFEIFLE, 1989 A non-radioactive in situ hybridization method for the localization of specific RNAs in Drosophila embryos reveals translational control of the segmentation gene *hunchback*. Chromosoma **98:** 81-85.

TELEMAN, A. A., Y. W. CHEN and S. M. COHEN, 2005 Drosophila Melted modulates FOXO and TOR activity. Dev Cell **9:** 271-281.

TELEMAN, A. A., S. MAITRA and S. M. COHEN, 2006 Drosophila lacking microRNA miR-278 are defective in energy homeostasis. Genes Dev **20:** 417-422.

THERRIEN, M., D. K. MORRISON, A. M. WONG and G. M. RUBIN, 2000 A genetic screen for modifiers of a kinase suppressor of Ras-dependent rough eye phenotype in Drosophila. Genetics **156:** 1231-1242.

THIBAULT, S. T., M. A. SINGER, W. Y. MIYAZAKI, B. MILASH, N. A. DOMPE *et al.*, 2004 A complementary transposon tool kit for *Drosophila melanogaster* using *P* and *piggyBac*. Nat Genet **36:** 283-287.

THIERY, J. C., P. CHEMINEAU, X. HERNANDEZ, M. MIGAUD and B. MALPAUX, 2002 Neuroendocrine interactions and seasonality. Domest Anim Endocrinol **23:** 87-100.

THOMAS, H. E., H. G. STUNNENBERG and A. F. STEWART, 1993 Heterodimerization of the Drosophila ecdysone receptor with retinoid X receptor and ultraspiracle. Nature **362:** 471-475.

THUMMEL, C. S., 2001 Molecular mechanisms of developmental timing in C. elegans and Drosophila. Dev Cell **1:** 453-465.

TOMANCAK, P., B. P. BERMAN, A. BEATON, R. WEISZMANN, E. KWAN *et al.*, 2007 Global analysis of patterns of gene expression during Drosophila embryogenesis. Genome Biol **8:** R145.

TRINH, L. A., M. D. MCCUTCHEN, M. BONNER-FRASER, S. E. FRASER, L. A. BUMM *et al.*, 2007 Fluorescent in situ hybridization employing the conventional NBT/BCIP chromogenic stain. Biotechniques **42:** 756-759.

TRUMAN, J. W., 1973 Physiology of insect ecdysis. III. Relationship between the hormonal control of eclosion and tanning in the tobacco hornworm, *Manduca sexta*. J Exp Biol **57:** 805-820.

TRUMAN, J. W., 1984 Cell death in invertebrate nervous systems. Annu Rev Neurosci **7:** 171-188.

TRUMAN, J. W., 1992a Developmental neuroethology of insect metamorphosis. Journal of Neurobiology **23:** 1404-1422.

TRUMAN, J. W., 1992b Developmental neuroethology of insect metamorphosis. J Neurobiol **23:** 1404-1422.

TRUMAN, J. W., 1996 Steroid receptors and nervous system metamorphosis in insects. Dev Neurosci **18:** 87-101.

TRUMAN, J. W., W. S. TALBOT, S. E. FAHRBACH and D. S. HOGNESS, 1994 Ecdysone receptor expression in the CNS correlates with stage-specific responses to ecdysteroids during Drosophila and Manduca development. Development **120:** 219-234.

TSENG, A. S., and I. K. HARIHARAN, 2002 An overexpression screen in Drosophila for genes that restrict growth or cell-cycle progression in the developing eye. Genetics **162:** 229-243.

TULLIO, A. N., P. C. BRIDGMAN, N. J. TRESSER, C. C. CHAN, M. A. CONTI *et al.*, 2001 Structural abnormalities develop in the brain after ablation of the gene encoding nonmuscle myosin II-B heavy chain. J Comp Neurol **433:** 62-74.

VARADI, A., T. TSUBOI and G. A. RUTTER, 2005 Myosin Va transports dense core secretory vesicles in pancreatic MIN6 beta-cells. Mol Biol Cell **16:** 2670-2680.

VIAU, V., 2002 Functional cross-talk between the hypothalamic-pituitary-gonadal and -adrenal axes. J Neuroendocrinol **14:** 506-513.

WANG, B., C. BOLDUC and K. BECKINGHAM, 2002 Calmodulin UAS-constructs and the in vivo roles of calmodulin: analysis of a muscle-specific phenotype. Genesis **34:** 86-90.

WATTS, R. J., E. D. HOOPFER and L. LUO, 2003 Axon pruning during Drosophila metamorphosis: evidence for local degeneration and requirement of the ubiquitin-proteasome system. Neuron **38:** 871-885.

WATTS, R. J., O. SCHULDINER, J. PERRINO, C. LARSEN and L. LUO, 2004 Glia engulf degenerating axons during developmental axon pruning. Curr Biol **14:** 678-684.

WEEKS, J. C., 2003 Thinking globally, acting locally: steroid hormone regulation of the dendritic architecture, synaptic connectivity and death of an individual neuron. Prog Neurobiol **70:** 421-442.

WEINZIERL, R. O., S. RUPPERT, B. D. DYNLACHT, N. TANESE and R. TJIAN, 1993 Cloning and expression of Drosophila TAFII60 and human TAFII70 reveal conserved interactions with other subunits of TFIID. Embo J **12:** 5303-5309.

WIELLETTE, E. L., K. W. HARDING, K. A. MACE, M. R. RONSHAUGEN, F. Y. WANG *et al.*, 1999 *spen* encodes an RNP motif protein that interacts with Hox pathways to repress the development of head-like sclerites in the Drosophila trunk. Development **126:** 5373-5385.

WILLIAMS, D. W., and J. W. TRUMAN, 2004 Mechanisms of dendritic elaboration of sensory neurons in Drosophila: insights from in vivo time lapse. Journal of Neuroscience **24:** 1541-1550.

WILLIAMS, D. W., and J. W. TRUMAN, 2005 Cellular mechanisms of dendrite pruning in Drosophila: insights from in vivo time-lapse of remodeling dendritic arborizing sensory neurons. Development **132:** 3631-3642.

WINTER, C. G., B. WANG, A. BALLEW, A. ROYOU, R. KARESS *et al.*, 2001 Drosophila Rho-associated kinase (Drok) links Frizzled-mediated planar cell polarity signaling to the actin cytoskeleton. Cell **105:** 81-91.

WRIGHT, K. J., M. T. MARR, 2ND and R. TJIAN, 2006 TAF4 nucleates a core subcomplex of TFIID and mediates activated transcription from a TATA-less promoter. Proceedings of the National Academy of Sciences of the United States of America **103:** 12347-12352.

WU, Q., Y. ZHANG, J. XU and P. SHEN, 2005 Regulation of hunger-driven behaviors by neural ribosomal S6 kinase in Drosophila. Proc Natl Acad Sci U S A **102:** 13289-13294.

WULLSCHLEGER, S., R. LOEWITH and M. N. HALL, 2006 TOR signaling in growth and metabolism. Cell **124:** 471-484.

WYLIE, S. R., and P. D. CHANTLER, 2008 Myosin IIC: a third molecular motor driving neuronal dynamics. Mol Biol Cell **19:** 3956-3968.

WYLIE, S. R., P. J. WU, H. PATEL and P. D. CHANTLER, 1998 A conventional myosin motor drives neurite outgrowth. Proc Natl Acad Sci U S A **95:** 12967-12972.

YAO, T. P., B. M. FORMAN, Z. JIANG, L. CHERBAS, J. D. CHEN *et al.*, 1993 Functional ecdysone receptor is the product of EcR and Ultraspiracle genes. Nature **366:** 476-479.

YAO, T. P., W. A. SEGRAVES, A. E. ORO, M. MCKEOWN and R. M. EVANS, 1992 Drosophila ultraspiracle modulates ecdysone receptor function via heterodimer formation. Cell **71:** 63-72.

YEH, E., K. GUSTAFSON and G. L. BOULIANNE, 1995 Green fluorescent protein as a vital marker and reporter of gene expression in Drosophila. Proc. Natl. Acad. Sci. U. S. A. **92:** 7036-7040.

YENUSH, L., R. FERNANDEZ, M. G. MYERS, JR., T. C. GRAMMER, X. J. SUN *et al.*, 1996 The Drosophila insulin receptor activates multiple signaling pathways but requires insulin receptor substrate proteins for DNA synthesis. Molecular & Cellular Biology **16:** 2509-2517.

ZEHR, J. L., B. J. TODD, K. M. SCHULZ, M. M. MCCARTHY and C. L. SISK, 2006 Dendritic pruning of the medial amygdala during pubertal development of the male Syrian hamster. J Neurobiol **66:** 578-590.

ZHAO, T., T. GU, H. C. RICE, K. L. MCADAMS, K. M. ROARK *et al.*, 2008 A Drosophila gain-of-function screen for candidate genes involved in steroid-dependent neuroendocrine cell remodeling. Genetics **178:** 883-901.

ZHENG, X., J. WANG, T. E. HAERRY, A. Y. WU, J. MARTIN *et al.*, 2003 TGF-beta signaling activates steroid hormone receptor expression during neuronal remodeling in the Drosophila brain. Cell **112:** 303-315.

ZHONG, Y., and C. F. WU, 2004 Neuronal activity and adenylyl cyclase in environment-dependent plasticity of axonal outgrowth in Drosophila. J Neurosci **24:** 1439-1445.

ZHOU, F. Q., C. M. WATERMAN-STORER and C. S. COHAN, 2002 Focal loss of actin bundles causes microtubule redistribution and growth cone turning. J Cell Biol **157:** 839-849.

ZITNANOVA, I., M. E. ADAMS and D. ZITNAN, 2001 Dual ecdysteroid action on the epitracheal glands and central nervous system preceding ecdysis of *Manduca sexta*. J Exp Biol **204:** 3483-3495.